Roles of neuro-exocytotic proteins at the neuromuscular junction

Sons-Michel, M.S.

Roles of neuro-exocytotic proteins at the neuromuscular junction

Michèle S. Sons

ISBN: 978-90-8891-339-6
Cover design: Evangelia Tantalaki
Printed by: Proefschriftmaken.nl
Published by: Uitgeverij BOXPress, Oisterwijk

Roles of neuro-exocytotic proteins at the neuromuscular junction

Proefschrift

ter verkrijging van
de graad van Doctor aan de Universiteit Leiden,
op gezag van de Rector Magnificus Prof. mr. P.F. van der Heijden,
volgens besluit van het College voor Promoties
te verdedigen op dinsdag 1 november 2011
klokke 13:45 uur

door

Michèle S. Sons-Michel
geboren te Amsterdam
in 1976

Promotiecommissie

Promotor
Prof. Dr. J.J.G.M. Verschuuren

Co-promotor
Dr. J.J. Plomp

Overige leden
Prof. Dr. R.A.C. Roos
Prof. Dr. J.N. Noordermeer
Prof. Dr. M. Missler

Most experiments described in this thesis were performed at the:
Leiden University Medical Centre
Department of Molecular Cell Biology
Neurophysiology Laboratory Dr. J.J. Plomp
Einthovenweg 20
P.O. box 9600
NL 2300RC Leiden
The Netherlands

The studies described in this thesis were supported by grants from the Netherlands Organisation for Scientific Research, NWO, (903-42-073), and the Deutsche Forschungsgemeinschaft, DFG (SFB 406-C9).

Voor mijn ouders

Contents

1

General Introduction

Preface

The neuromuscular junction (NMJ) connects the motor neuron and the skeletal muscle cell. In mammals, the neurotransmitter acetylcholine (ACh) is released from presynaptic terminals upon activation of the motor neuron. Subsequently, ACh will bind and activate postsynaptic ACh receptors (AChRs) leading to membrane depolarization and contraction of the muscle fiber. Proper function of the NMJ is of crucial importance for the survival of the organism. Several paralytic neuromuscular diseases are known to be caused by either post- or presynaptic NMJ dysfunction.

The NMJ has been of key importance in our understanding of chemical synaptic transmission. Since Katz and colleagues first measured synaptic events at the NMJ of frog some 60 years ago (Fatt and Katz, 1950) the NMJ has remained an important model system. It is technically easier to measure the synaptic signals in vitro at this peripheral synapse compared to synapses in the brain. Another advantage over central synapses is that it is a 'one-to-one synapse', in contrast to the central nervous system (CNS) where many presynaptic nerve terminals are present at one postsynaptic neuron. This allows for direct assessment of the physiological parameters of a single synapse.

Chemical transmission involves the highly controlled fusion of transmitter-filled vesicles with the presynaptic plasma membrane, leading to exocytosis of the transmitter into the synaptic cleft. Many presynaptic proteins important for the tight regulation of this process have been identified in the last two decades. This research has been greatly facilitated by the generation of transgenic mice lacking or over expressing specific proteins. The roles of neuro-exocytotic proteins hitherto have been experimentally characterized mainly in mouse brain slice preparations and cultured brain synapses.

This thesis investigates whether the neuro-exocytotic proteins identified in the CNS also serve this role at the presynaptic NMJ. Besides being of neurobiological importance, characterization of such roles might be relevant to primary and secondary presynaptic phenomena in diseases with NMJ dysfunction, such as (congenital forms) of presynaptic myasthenic syndromes and myasthenia gravis (MG)

The neuromuscular junction: a model-synapse

The NMJ is one of the most thoroughly studied synapses. Using the NMJ, Sir Henry Dale demonstrated the principle of chemical transmission of an electrical signal from one cell to another (Dale et al., 1936), for which he and Otto Loewi were awarded the Nobel Prize in Physiology or Medicine. In 1966 Katz reported the quantal and vesicular properties of ACh release (Katz, 1966). Since then, the cholinergic NMJ has proven a highly suitable experimental synapse model that has enabled detailed analysis of neurotransmission.

Cellular components

The NMJ comprises parts of the motor neuron, skeletal muscle fiber, and Schwann cell (Figure 1) (reviewed in Couteaux, 1973; Ogata, 1988; Engel, 1994). The motor axon, myelinated by Schwann cells, originates from the nerve cell body within the ventral horn of the spinal cord, and projects to the target muscle through the peripheral nerve. The terminal branches of the motor axon, which are each up to 100 μm long, can contact up to tens to hundreds of muscle fibers. The combination of a motor neuron and all of the muscle fibers it innervates is called a motor unit. The place of synaptic contact is at a site near to the middle of the muscle fiber, where invaginations in the postsynaptic membrane (primary clefts) harbor the axon terminals. The nerve terminal is covered by perisynaptic Schwann cells. They insulate the nerve terminal from the environment, support the long-term maintenance of the synapse and are capable to modulate neurotransmitter release. Schwann cells guide regeneration after injury as well and are play a crucial role during development (Sanes and Lichtman, 1999; reviewed by Feng and Ko, 2007).

The synaptic cleft between the nerve terminal and the postsynaptic membrane is about 50 nm wide and is lined with basal lamina, a thin layer of connective tissue that sheaths the muscle fiber. It consists of collagen IV, laminin, entactin, and heparan sulfate proteoglycans. The synaptic basal lamina also contains a collagen-tailed form of acetylcholinesterase, important for the degradation of ACh (Krejci et al., 1997).

The nerve terminal contains many mitochondria, microtubules and actin microfilaments. The most noticeable characteristic in electron microscopic images is the presence of many synaptic vesicles with a diameter of about 50 nm. Some of these are clustered at specialized sites at the presynaptic membrane, called 'active zones', appearing as electron-dense regions of the cytoplasm. Upon Ca^{2+} influx through voltage-gated Ca^{2+} channels ($Ca_v2.1$, also called P/Q type), these vesicles undergo exocytosis.

Localized opposite to the pre-synaptic membrane, the post-synaptic muscle membrane exhibits an eight-time increased surface area due to extensive folding

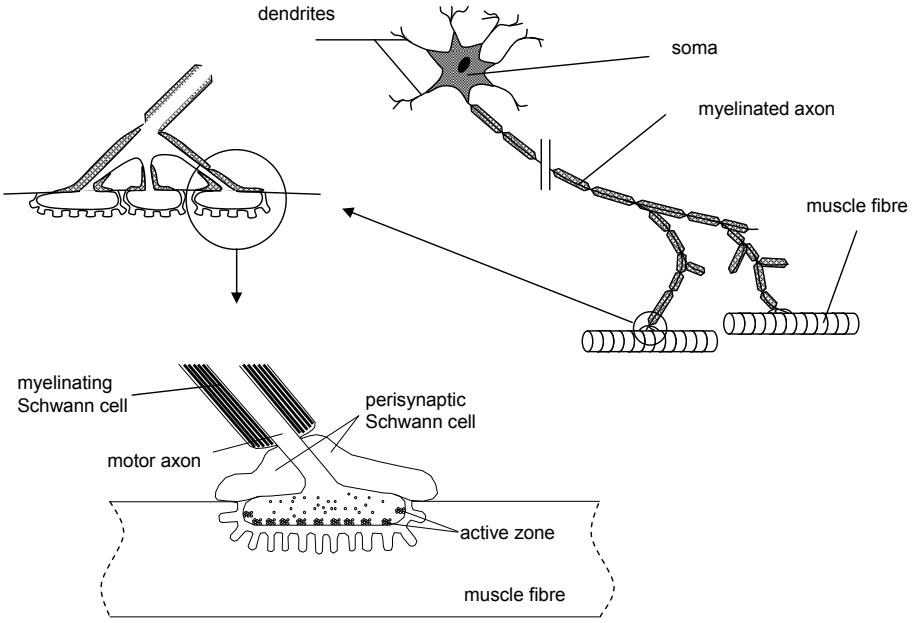

Figure 1. Motor neuron and NMJ
Schematic representation of the motor neuron, making synaptic contact with a number of muscle fibers, together forming the motor unit. The nerve endings are positioned in the primary folds of the muscle fiber membrane and are covered with perisynaptic Schwann cells. The nerve terminal contains synaptic vesicles filled with ACh. Upon arrival of a presynaptic action potential, the vesicles fuse with the presynaptic cell membrane at the active zones, thereby releasing ACh in the synaptic cleft. AChRs located on top of the secondary folds open after binding of ACh, permitting an ion current to flow which underlies a depolarization that activates voltage gated Na^+ channels located in the depths of the folds. This results in a muscle action potential that eventually induces contraction of the fiber. Modified from Plomp et al., 2003.

('secondary folds'). Voltage-gated Na^+ channels are localized in the depths of the folds. Several myonuclei with associated Golgi apparatus lie just beneath the post-synaptic membrane. On the surface of the secondary folds exposed to the synaptic cleft, large numbers of ACh-gated receptor-channels (AChRs) are present at high density (10000/μm^2). Upon binding of ACh, these channels open and cause a net inward ion current (see below). Extrasynaptically, the AChR density drops to 10/μm^2 (Fertuck and Salpeter, 1976).

The acetylcholine receptor

The endplate AChR is a ligand-gated ion channel of the nicotinic class. Binding of two ACh molecules results in a short opening of the pore, allowing influx of Na^+ and efflux of K^+ ions. This leads to a net inward electrical current. The discovery of α-bungarotoxin (α-BTx), a peptide component of the venom of the snake Bungarus multicinctus, enabled the purification and subsequent structural analysis of the AChR (reviewed in: Karlin, 2002). α-BTx is a highly specific irreversibly binding ligand that has been applied to extract AChRs from the Torpedo electric organ in large amounts. AChRs are heteromultimeric structures consisting of four different

polypeptides subunits: α, β, γ, and δ with a stoichiometry of α2βγδ. X-ray crystallography analysis shows a structure that resembles a chalice, with a large extracellular 'mouth' of 65 Å, and a smaller intracellular vestibule of 20 Å, connected by a 30 Å wide pore. The binding sites for ACh and α-BTx are located on the α-subunits. Embryonic mammalian NMJs possess AChRs with the same subunit composition as the Torpedo AChR; however, during the first postnatal week the γ-subunit is replaced by an ε-subunit. This yields a channel with a shorter opening duration and a larger electrical conductance (Mishina et al., 1986; Gu and Hall, 1988; Missias et al., 1996).

Function

The function of the NMJ is to transmit signals from the motor neuron to the muscle fiber, which is achieved by action potential-induced ACh release from the nerve terminal. ACh is synthesized from choline and acetyl coenzyme A (AcCoA) by the enzyme choline-acetyltransferase (ChAT) which transfers an acetyl group from AcCoA onto choline. In the synaptic cleft, ACh is rapidly hydrolyzed by acetylcholinesterase into choline and acetate, thereby terminating the ACh signal. Subsequently, choline is transported back into the nerve terminal and re-used for ACh synthesis. Cytoplasmic ACh is transported into synaptic vesicles by a vesicle specific proton pump (V-ATPase), packing about 10,000 molecules of ACh into one single vesicle.

Upon arrival of an action potential at the presynaptic terminal, voltage-gated Ca^{2+} channels open. These are $Ca_v2.1$ (P/Q-type) channels, also widely expressed in the CNS (Wheeler et al., 1995). In the PNS, $Ca_v2.1$ channels are mainly restricted to the NMJ (Uchitel et al., 1992). The opening of Ca^{2+} channels results in a short Ca^{2+} influx, causing a transient local elevation of the Ca^{2+} concentration, from 100 nM to 200-300 μM. The Ca^{2+} signal is transmitted to the exocytotic protein machinery and induces rapid fusion of vesicles from the readily-releasable pool (RRP) with the plasma membrane, thereby releasing ACh in the synaptic cleft. Vesicle fusion increases with $[Ca^{2+}]_n$, with n = 3-4, interpreted as three to four Ca^{2+} ions to work cooperatively in inducing fusion (reviewed by Meir et al., 1999).

ACh binds to the postsynaptic AChRs which in turn open and permit a net inward current of positive ions, the endplate current (EPC). The EPC underlies a depolarization, the endplate potential (EPP) (Fatt and Katz, 1951). Using electrophysiological techniques, EPPs can be measured in vitro (Figure 2, also see below). Next to the action-potential evoked EPPs, small depolarizations of ~1 mV can be observed at ~1/s, the miniature endplate potentials (MEPPs) (Fatt and Katz, 1952). MEPPs are the result of the spontaneous release of one single quantum of ACh. Typically, in the NMJ (depending on species, muscle-type and age), the quantal content of endplates (i.e., the number of vesicles that fuse upon a presynaptic action potential) varies between 25 and 100.

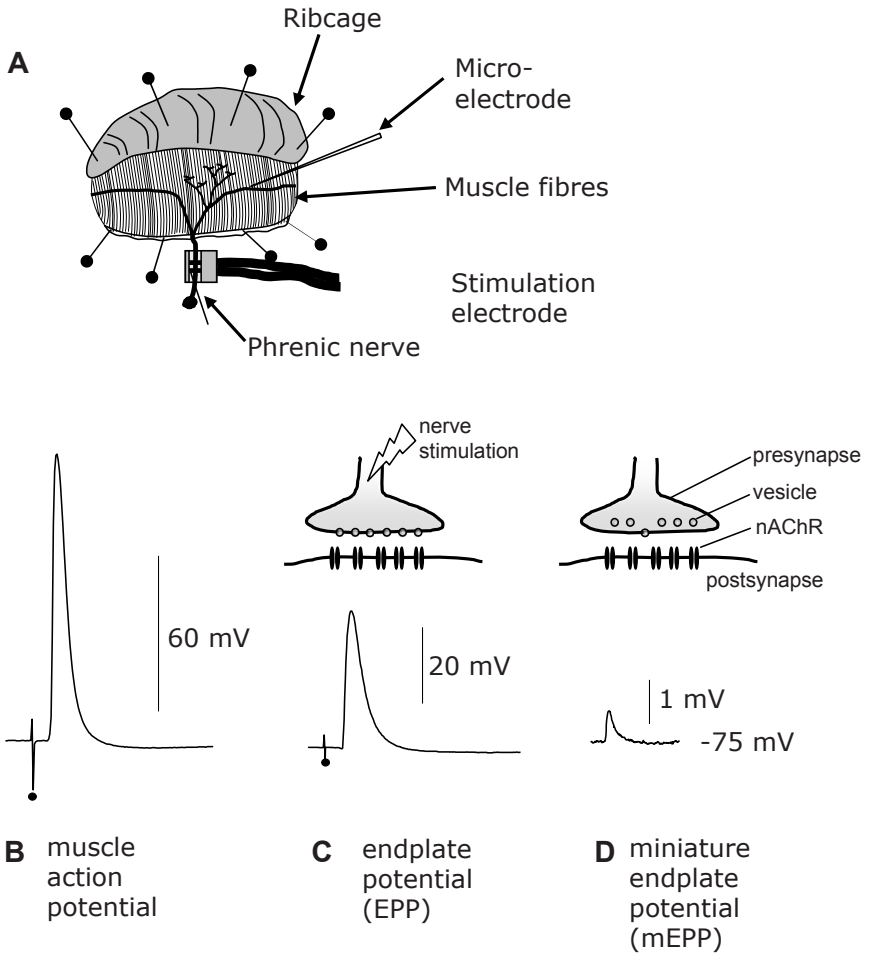

Figure 2. NMJ electrophysiology
Schematic representation of a hemidiaphragm, pinned out in a dish (A). The phrenic nerve has been placed on a bipolar stimulation electrode that delivers electrical pulses which trigger nerve-action potentials. Under microscopic inspection a muscle fiber is impaled with a microelectrode to monitor the membrane potential which typically is around -75 mV. Stimulation of the nerve (indicated with a black dot) will eventually result in a muscle action potential (B), which in most cases will disrupt the recording since it induces contraction of the muscle. μ-Conotoxin-GIIIB is used to block the muscle Na^+ channels in order to prevent muscle action potentials, enabling undisturbed measurement of the EPPs (C). Spontaneous release events can be monitored as MEPPs (D). The quantal content, which is the number of vesicles that have fused to give rise to an EPP is calculated by dividing the EPP amplitude by the MEPP amplitude. (Modified from (Kaja, 2007) with permission).

The precise function of MEPPs has not been established yet, but might involve regulation of local postsynaptic protein synthesis (Sutton et al., 2004). Otherwise, it may be an intrinsic property of the molecular machinery that mediates synaptic vesicle function (Lou et al., 2005). However, since spontaneous and evoked release seem to originate from distinct vesicle pools a functional relevance for spontaneous release cannot be excluded.

The EPP activates voltage-gated Na^+channels, which initiate a muscle action potential that leads to contraction of the muscle fiber. (Fatt and Katz, 1951). In

general, the EPP amplitude is several times higher than minimally required to excite the muscle fiber. This safety factor ensures that during prolonged, high-frequency activation of muscles, when the amount of transmitter released per nerve impulse declines substantially, transmission does not fail. (Wood and Slater, 2001).

In vitro electrophysiological analysis of ACh release at the NMJ

Several mouse nerve-muscle preparations can be used for studying NMJ electrophysiology. In this thesis, the diaphragm-phrenic nerve preparation was mainly used, as well as the soleus-tibialis nerve preparation. The diaphragm preparation has the advantage that it is a flat, thin muscle (typically 10-15 fibers thick) and that its fibers can be easily visualized and are well accessible by microelectrodes. In addition, NMJs are localized in a central band along both hemi-diaphragms that can be easily visually identified. A further advantage is the length of the phrenic nerve which can be dissected, so that it can be placed over a bipolar electrode for stimulation (Figure 2A). The diaphragm is a mixture of both slow- and fast-switch fibers. The soleus muscle is a technically somewhat more demanding preparation, as the NMJ region is not very well identifiable and nerve stimulation requires a suction electrode configuration. Soleus muscles consist of slow-twitch fibers. After dissection, the muscles are pinned on a silicone rubber-coated dish containing a physiological Ringer's solution.

A glass micro electrode (1 μm tip diameter), coupled to an amplifier, is impaled in the muscle cell near the endplate-region using a micromanipulator. The membrane potential is then measured, which is in rest around -75 mV. MEPPs can be recorded; typical values for diaphragm are 1 mV, occurring at a frequency of 1 s^{-1}. Using a stimulus generator, the nerve can be electrically stimulated and the ensuing EPPs can be recorded. Because the measured resting membrane potential varies between the multiple muscle fibers sampled, amplitudes at each NMJ are normalized to -75 mV.

Measures have to be taken to prevent muscle action potentials, since these obscure the EPP and cause contraction which in general will disrupt the recording. Several methods exist to prevent muscle action potentials; the most straight-forward of these is selectively blocking the muscle Na^+ current by μ-conotoxin-GIIIB, a marine snail venom component. Other methods involve reducing the EPP amplitude to sub-threshold values for Na^+ channel activation by blocking part of the AChRs using the reversible antagonist d-tubocurarine. The drawback of this method is that MEPPs will become too small to be measured.

From the EPP and MEPP values recorded, the quantal content at an endplate can be calculated by dividing the EPP amplitude by the MEPP amplitude. Beforehand,

the EPP amplitude needs to be corrected for non-linear summation (McLachlan and Martin, 1981).

Some of the experiments described in this thesis have been carried out on embryonic or one day old mice. In addition to a slightly more complicated dissection, it appeared that muscle action potentials could not be blocked by μ-conotoxin-GIIIB. In these experiments, a depolarization-induced inactivation of the Na^+ channels was used to prevent muscle action potentials. To this end, diaphragm muscle fibers were shortened by cutting away some length from the central tendon side until depolarization of the muscle fibers to about -40 mV was reached, preventing the triggering of action potentials by EPPs.

Myasthenia gravis

Clinical symptoms

MG is a prototype for both synaptic and autoimmune disorders, with a prevalence of around 20-500 per million (reviewed by Lindstrom, 2000; Vincent et al., 2001). The disorder is characterized by a painless, fatigable weakness. At onset, patients often have ptosis (eyelid drooping) and diplopia (double-vision) arising from levator palpebrae and extraocular muscle weakness. Typically within one year, 75% of the patients will develop bulbar weakness (for example, facial weakness, difficult chewing and defective articulation) and/or extremity weakness. Weakness can remain localized to one group of muscles for many years (commonly in the eye-muscles, termed 'ocular myasthenia') or spread to affect other skeletal muscles (generalized MG). Myasthenic crises (life threatening episodes of respiratory or bulbar paralysis) may occur.

MG is often accompanied by thymic abnormalities, and around 10% of patients suffer from a lymphoepithelial thymoma (Oosterhuis, 1989).

Histological analysis of intercostal biopsies from myasthenic patients show a reduction or disappearance of functional folds, with widened secondary folds and synaptic cleft (Vincent, 1987).

Mechanism

The majority (85%) of patients with MG is seropositive for antibodies against the nicotinic AChR. The titers of antibodies are highly variable amongst patients, and do not correlate well with severity of the clinical symptoms between individuals. However, individual patient titers correlate well with clinical scores after plasma exchange, thymectomy and/or immunosuppressive treatment. The remaining 15% of the patients is classified as seronegative MG. In a subset of this group antibodies against muscle specific kinase (MuSK) have been found. The proportion of seronegative MG patients with antibodies against MuSK seems to vary (60-70% in sera

from Oxford (Hoch et al., 2001) and Italy, 30-40% in sera from the USA and Japan, and none has yet been identified in Norway (reviewed in: Vincent and Leite, 2005).

The autoantibodies decrease the ACh sensitivity of the NMJ, thereby reducing the safety-factor of neuromuscular transmission. In healthy NMJs, the EPP amplitudes decrease during repetitive stimulation (i.e. during voluntary muscle contraction) which is probably the result from depletion of the vesicle pool in the presynaptic terminal in combination with the behaviour of $Ca_v2.1$ channels during high frequency stimulation. However, due to the safety-factor of the NMJ, the EPPs will remain supra-threshold and will all elicit muscle action potentials. However, the reduced safety factor of MG NMJs results in sub-threshold EPPs during repetitive stimulation which results in the observed (fatigable) weakness of patients.

There are three mechanisms by which the autoantibodies to the AChR lead to decreased ACh sensitivity at the NMJ: 1) complement-mediated damage of the postsynaptic membrane by antibodies, 2) increased internalization due to cross-linking by antibodies and 3) AChR block by direct binding of antibodies (reviewed by: Boonyapisit et al., 1999). Complement-mediated lysis is by far the most important effect.

Depending on the type of MG and the severity of the symptoms several treatments are given. These include the administration of acetylcholinesterase inhibitors (in order to prolong the life-time of ACh in the synaptic cleft), thymectomy, plasma-exchange and immune-suppressive therapy.

Clinical and in vitro electrophysiology

Electromyographical methods are used in the diagnosis of MG (reviewed in Meriggioli and Sanders, 2004). The two tests that are used are repetitive nerve stimulation (RNS) and single-fiber electromyography (SFEMG). In RNS the peripheral nerve is stimulated supramaximally and the compound muscle action potential (CMAP) is recorded with surface electrodes. In healthy muscles, the amplitudes of the CMAPs will remain constant during the repetitive stimulation. In MG muscles however, the CMAP amplitude decreases during the train of stimuli because an increasing number of fibers no longer contracts due to EPPs that become sub-threshold for action potential generation. In SFEMG, a needle is used to record from an individual muscle fiber during contraction of a muscle (voluntary or stimulated). There is a small variation in the delay between the stimulation and the recorded muscle action potential between the successive stimuli. This 'jitter' phenomenon is caused by the variation in the time it takes for the EPP to reach the threshold and the initiation of the muscle action potential. Increased jitter is reflecting a defect in neuromuscular transmission, EPPs being peri-threshold. Sometimes an EPP will not be able to generate a muscle action potential at all, which is termed a 'blocking'.

In vitro electrophysiological recording from muscle biopsies from MG patients showed a decreased MEPP amplitude (Elmqvist et al., 1964), indicating a decreased postsynaptic sensitivity for ACh. EPPs, measured at low frequency stimulation, showed a decreased amplitude, which is however higher than would be expected based on the MEPP amplitude reduction. This is caused by an increase in the quantal content (Cull-Candy et al., 1980; Plomp et al., 1995), resulting from a homeostatic presynaptic response of the NMJ in attempt to maintain successful transmission (see below). During high frequency stimulation of the nerve, EPPs show increased rundown of amplitude, compared to normal.

Experimental models of myasthenia gravis

Several animal models of MG have been developed in order to study the pathophysiological mechanisms and possible treatments of this disease.

The first model of MG comprised injections of rabbits with AChR purified from the Torpedo electrical organ, which caused paralytic symptoms. This experimental auto-immune myasthenia gravis (EAMG) model provided much information about the pathophysiological mechanisms of MG but the condition of the animals proved to be difficult to control. After an initial phase with mild muscle weakness a more generalized MG follows, including breathing problems which ultimately lead to death of the animals.

A more controllable model is toxin-induced MG (TIMG), in which the decreased ACh-sensitivity is achieved by repeated intraperitoneal injections with low doses of α-BTx (Figure 3). Initially developed for rats (Molenaar et al., 1991), it has been changed and re-evaluated for the use in mice.

Homeostatic upregulation of neurotransmitter release at (neuromuscular) synapses

As outlined in the previous section, myasthenic synapses aim to compensate for the decreased sensitivity of the postsynaptic cell to ACh by releasing more ACh upon nerve stimulation. This compensatory increase of quantal content has been found in NMJs from MG patient muscle biopsies (Molenaar et al., 1979; Cull-Candy et al., 1980), and has been confirmed by recordings in NMJs from animal models for MG (Molenaar et al., 1979; Cull-Candy et al., 1980; Takamori et al., 1984; Molenaar et al., 1991; Plomp et al., 1992; Plomp et al., 1995). The increase in quantal content is correlated with the reduction of the MEPP amplitude, indicating that regulation takes place at individual endplate level (Plomp et al., 1992; Plomp et al., 1995).

The increase of neurotransmitter release in the myasthenic NMJ suggests that the neural activity in the NMJ is under homeostatic control (Davis and Bezprozvanny, 2001; Burrone and Murthy, 2003). Homeostatic regulation of transmitter release in response to decreased postsynaptic sensitivity in the NMJ has been described in

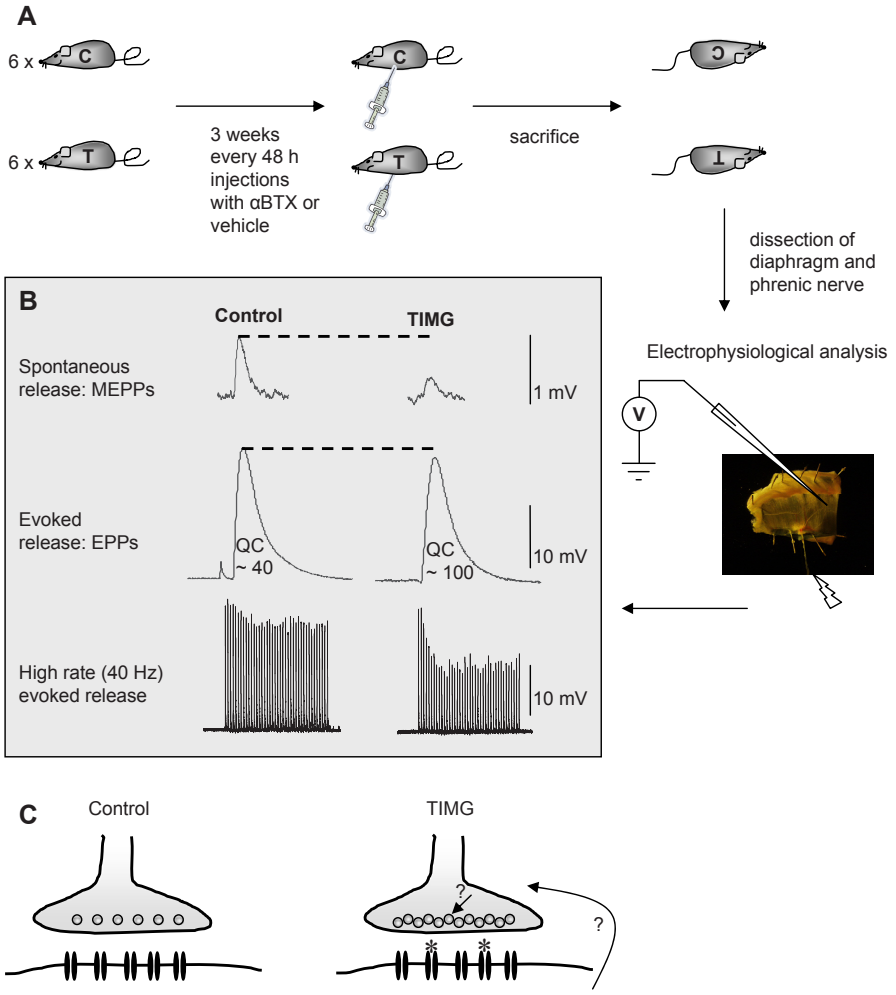

Figure 3. Toxin-induced myasthenia gravis
Toxin-induced myasthenia gravis (TIMG) is a non-immunogenic model of MG, where reduced ACh sensitivity of the NMJ is induced by injection of the nAChR-blocker α-BTx into mice.
(A) For 3 weeks, mice receive every 48 h an injection with either a 0.8 μg dose α-BTx ('T') or control vehicle ('C'). (B) Reduced MEPP amplitudes in TIMG reflect the reduced ACh sensitivity due to block of part of the AChRs by α-BTx at the NMJ. Typically, the EPP amplitudes in TIMG NMJs are only slightly reduced, hence the quantal content of these NMJs has been increased to compensate for the reduced ACh sensitivity. High rate (40 Hz) evoked release in TIMG NMJs typically shows increased rundown. (C) Schematic representations of control and TIMG NMJs (star indicates α-BTx.). Arrows indicate unknown pathways that are being employed to increase vesicle fusion in response to AChR blockade.

additional models. For example, in mice heterozygous knock-out for the Ig-containing isoform of neuregulin the AChR density was reduced. This was compensated for by increased quantal content (Sandrock, Jr. et al., 1997). A similar phenomenon was seen in studies at the glutamatergic *Drosophila* NMJ. In one of these studies mutations were induced in the glutamate receptor subunit GluRIIA (Petersen et al., 1997). Expression of a dominant negative form of GluRIIA resulted in the decrease

of the response to single quantum. However, the response to nerve stimulation was the same due to an increase in quantal content. In another study a constitutively active catalytic subunit of protein kinase A (PKA) was expressed (Davis et al., 1998) to achieve decreased postsynaptic sensitivity. In a third *Drosophila* study the excitability of the postsynaptic muscle was decreased by postsynaptic expression of the $K_{ir}2.1$ K^+ channel (Paradis et al., 2001). In all these cases the reduced postsynaptic sensitivity for the transmitter was (partly) counteracted by a compensatory increase in presynaptic transmitter release.

Homeostatic control of presynaptic release requires retrograde signaling to provide the presynapse with feedback on the current state of neurotransmission. Many candidate retrograde messengers have been proposed, including soluble factors like brain-derived neurotrophic factor (BDNF), neurotrophins, nitric oxide, and endocannabinoids (Fitzsimonds and Poo, 1998; Tao and Poo, 2001). Especially BDNF has been given much attention (Lohof et al., 1993; Lessmann et al., 1994; Berninger and Poo, 1996; Lessmann, 1998; Schinder et al., 2000; Tyler et al., 2002). Magby and colleagues described the action of BDNF as a retrograde messenger in cultured hippocampal neurons (Magby et al., 2006). It was proven by pharmacological means that BDNF was released from postsynaptic neurons upon depolarization, and that this had a direct enhancing effect on the spontaneous transmitter release of the presynaptic cell. This process was dependent on activation of presynaptic tyrosine kinase B (trk-B) and the postsynaptic intracellular Ca^{2+} concentration.

Direct cell-cell contact by transsynaptic protein complexes may be employed as well in retrograde signaling (Davis and Bezprozvanny, 2001; Dean and Dresbach, 2006; Futai et al., 2007). An example of these trans-synaptic protein complexes that mediate presynaptic release in the CNS is a neuroligin-neurexin complex, formed by presynaptic Neurexin-β and the postsynaptic complex PSD-95-Neuroligin. Futai and colleagues described an experiment performed in cultured hippocampal neurons where the levels of postsynaptic PSD-95 and neuroligin were found to affect presynaptic release. This mechanism was dependent on the presence of presynaptic β-neurexin (Dean and Dresbach, 2006; Futai et al., 2007).

Studies in *Drosophila* have revealed the bone morphogenic protein (BMP) glass bottom boat (Gbb) as a retrograde signal in homeostatic synaptic plasticity. As mentioned above, expression of a dominant negative of GluRIIA induced a compensational increase of transmitter release, but this was not the case in mutants lacking the BMP receptor wishful thinking (Wit) (Haghighi et al., 2003). Gbb is a good candidate for the retrograde signal because it is expressed by developing muscle fibers, and Gbb deletion mutants have a similar phenotype as Wit deletion mutants (Keshishian and Kim, 2004). However, more recent evidence seems to contradicts this because both post- and presynaptic expression of Gbb restores synaptic ho-

meostatis in Gbb deletion mutants (Goold and Davis, 2007). Thus, the identity of the retrograde signal remains unknown.

Another *Drosophila* study on a specific motoneuron-interneuron synapse describes a Gbb-Wit indendent example of synaptic homeostatis. Deleting Dp186, one of the *Drosophila* isoforms of Dystrophin increases evoked presynaptic release. Mutants can be restored to wild-type levels by postsynaptic (but not presynaptic) expression of Dp186 (Fradkin et al., 2008), indicating that the protein is involved in the retrograde signaling pathway. Interestingly, another Dystrophin isoform (DLP2) has shown to be involved in a similar manner in synaptic homeostasis in the NMJ (van der Plas et al., 2006). Recently, yet another protein, Dysbindin, was found to play a role in homeostatic modulation of neurotransmission (Dickman and Davis, 2009). Dysbindin is necessary on the presynaptic side in synaptic homeostasis. It colocalizes with synaptic vesicle proteins, indicating that it functions at or near the synaptic vesicle pool. Dysbindin has been linked to schizophrenia in humans, suggesting that a defect in synaptic homeostasis is possibly contributing to this disease. However, this remains to be investigated.

Synaptic exocytosis

Exocytosis is defined as the process by which molecules are secreted from eukaryotic cells through fusion of membrane-bound vesicles with the plasma membrane. The most extensively studied example of exocytosis is chemical synaptic transmission, used intensively by cells in the nervous system to transduce electrical signals. Upon arrival of an electrical signal in the presynaptic terminal, fusion of vesicles takes place. The released transmitter substance binds to receptor molecules on the postsynaptic cell, which in turn generates an electrical signal that travels onwards.

Vesicle pools and life cycle

Synaptic vesicles in the nerve terminal are organized in different pools, depending on their level of fusion-readiness (Rizzoli and Betz, 2004). Vesicles in the readily releasable pool (RRP) are primed for fusion and await the Ca^{2+} trigger, in contrast to vesicles in the reserve pool (RP). Vesicles in this pool have to undergo several maturation steps in order to 'prime' them to make them readily releasable. These pools together are called 'recycling pool'. There is a third pool, the 'resting pool' of vesicles. The latter pool most likely provides the vesicles that undergo spontaneous release, while the RRP is responsible for regulated release (Fredj and Burrone, 2009)

Vesicles that take part in regulated exocytosis have a life cycle, starting with the synthesis of the lipids and membrane proteins in the endoplasmatic reticulum and modification in the Golgi apparatus. The vesicle then is translocated from the soma to the nerve terminal, where neurotransmitter molecules are transported in the lu-

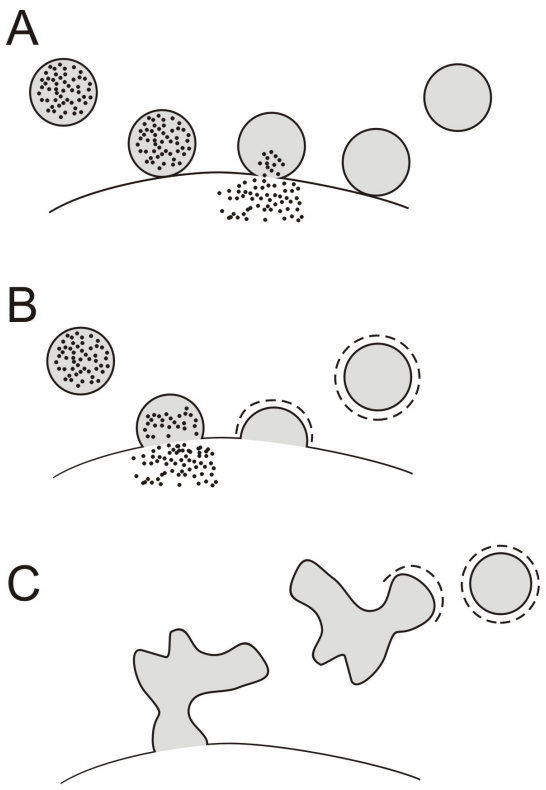

Figure 4. Endocytotic pathways
Three different pathways have been proposed for endocytosis as depicted in this figure. (A) "Kiss and run", where the vesicle fuses, is emptied and closes again, and refilling takes place after it has been relocated from the site of fusion. (B) The vesicle fuses completely with the membrane, loosing its identity. The membrane is retrieved by clathrin coated pits (Clathrin is depicted by black bars) (C) A larger amount of membrane can be retrieved in bulk endocytosis. An endosomal structure is formed, from which vesicles can bud.

reserve pool of vesicles, or it will be directed to the active zone. At the active zone the vesicle docks at the plasma membrane and undergoes priming steps, making it ready ('competent') for Ca^{2+}-triggered fusion-pore opening.

Three endocytotic modes have been proposed (Figure 4) (reviewed by Smith et al., 2008). One mode is the 'kiss-and-run' pathway, where vesicles are retrieved before full collapse has occurred, maintaining the vesicle identity. Another mode is full-collapse fusion, where complete fusion of the vesicle with the membrane takes place, the vesicle membrane has become part of the cell membrane. Retrieval of the membrane occurs via clathrin coated pits. Alternatively, retrieval can take place via 'bulk endocytosis' where an endosomal structure is formed. In this case new vesicles are formed by budding from the endosomal structure. Most likely, these three modes coexist in synapses.

Neuro-exocytotic proteins

A large number of different proteins is implicated in the regulation of the different stages of the synaptic vesicle life cycle. Whereas some of them are essential, others may have auxiliary or regulatory functions. The basic mechanism of exocytosis is conserved from yeast to man and in different cell-types. Although homologous proteins acting in specific steps in exocytosis have been identified across many species,

it has become clear that there is a wide variety of differences in the specific steps of exocytosis, and homologous proteins may have distinct roles in different cell types or organisms. Therefore, many conflicting reports on the precise roles of some of the exocytotic proteins exist. To discuss the detailed roles of all existing neuro-exocytotic proteins is beyond the scope of this thesis Introduction. I will limit myself to a description of the soluble N-ethylmaleimide-sensitive factor attachment protein receptors proteins (SNAREs) (Figure 5), which are believed to be the key-role players of fusion and, in addition, the proteins studied in the experimental chapters of this thesis (Figure 6).

SNAREs

At present, it is widely accepted that SNAREs are the key players in the final stages of docking and subsequent fusion of synaptic vesicles (Jahn and Sudhof, 1999; Chen and Scheller, 2001; Rizo and Sudhof, 2002; Jahn et al., 2003). They are small proteins (10-35 kDa), characterized by the SNARE motif, which comprises of a stretch of 60 to 70 amino acids, often localized next to a C-terminal transmembrane anchor. Most SNARE proteins contain one SNARE motif. However, the soluble NSF attachment proteins (SNAPs) SNAP-25, SNAP-29 and SNAP-23 contain two of them. SNAREs can be functionally divided into vesicle-associated (v-), and target-associated (t-) SNAREs (Sollner et al., 1993). However, as these functional categories do not apply to all types of fusion reactions (e.g. fusion of yeast vacuoles), a categorization based on a single key residue in the SNARE motif, being either arginine (R) or glutamine (Q) was developed (see below).

Unstructured in solution, SNAREs can assemble into 'SNARE-complexes', which are formed by four SNARE motifs adopting an α-helical configuration in the center of which there are four conserved, interacting amino acids (three glutamines, one argine). Based on this, a new classification has been made, Qa-SNAREs (or syntaxins), Qb-, and Qc- SNAREs (homologs of the N- and C-terminal SNARE motif, respectively, of SNAP-25), and R-SNAREs (vesicle-associated membrane proteins, VAMPs, also called synaptobrevins) (Fasshauer et al., 1998). The four α-helices zip together from the N-terminal end of the SNARE motifs toward the C-terminal membrane anchors, thereby pulling the membranes close together (Hanson et al., 1997; Lin and Scheller, 1997).

It is generally accepted that SNAREs provide the energy necessary to overcome the energy barrier for membrane fusion through their assembly into SNARE complexes. These are extraordinarily stable, indicating that a lot of energy was released upon assembly (Fasshauer et al., 2002).

In neuronal exocytosis, the t-SNARES syntaxin 1a (Qa) and SNAP-25 (Qb and Qc) are predominantly located on the plasma membrane, whereas the v-SNARE VAMP/synaptobrevin (R) is located on the synaptic vesicle (Figure 5). If the com-

plex is located on both the vesicle and plasma-membrane, it is called a trans-SNARE complex. After fusion however, the complex is located only on the plasma membrane, in 'cis-configuration', and needs to be disassembled. Disassembly is achieved by action of the ATP-ase N-ethylmaleimide-sensitive fusion protein (NSF). In order to recruit NSF, binding of the co-factors SNAPs is required. ATP hydrolysis by NSF leads to disassembly of the complex (Sollner et al., 1993). After this, v-SNAREs are recycled to synaptic vesicles, while the t-SNAREs are re-organized for new rounds of docking and fusion events (Figure 5)

Using in vitro assays of liposome fusions, it has been shown that SNARE proteins alone are sufficient for the actual fusion of membranes, although the kinetics of this reaction are very slow (Weber et al., 1998). However, several observations argue against their exclusive role in membrane fusion. First, deletion of the R-SNARE synaptobrevin in mice does not completely abolish synaptic exocytosis (10% remains) in mice (Schoch et al., 2001). Similar results were obtained from mice lacking the t-SNARE SNAP-25 (Washbourne et al., 2002). Second, deletion of the non-SNARE protein Munc18-1 abolished exocytosis completely (Verhage et al., 2000). This shows that SNARE proteins alone are not sufficient for fusion. Thus, although being the core proteins of membrane fusion, other factors in addition to SNAREs are required for exocytosis in vivo.

Synaptic communication of neuronal cells is a very delicate and precise process, which is highly tuned in time and space. Precise control of synaptic exocytosis has evolved, in which many proteins play a role in the several aspects of exocytosis. Below, a subset of these is discussed, with relevance to the experimental studies of this thesis. For more information see the following reviews: (Jahn and Sudhof, 1999; Chen and Scheller, 2001; Rizo and Sudhof, 2002; Jahn et al., 2003; Sudhof, 2004; Sudhof and Rothman, 2009).

Munc18

Munc18-1 is a member of the Sec1/Munc18 protein family, referred to as SM proteins (Toonen and Verhage, 2003), consisting of highly conserved cytosolic proteins of ~60 to 80 kD. Deletion of SM proteins generally leads to an impairment of vesicle trafficking and fusion, and is lethal in most organisms (reviewed in Toonen and Verhage, 2003). Although all SM proteins have shown to be important in vesicle trafficking and fusion, it appeared difficult to pinpoint their exact roles (Weimer and Jorgensen, 2003; Toonen and Verhage, 2003; Weimer and Richmond, 2005).

Munc18-1 was first discovered as a binding-partner of syntaxin-1 (Hata et al., 1993) and was found to be the mammalian homologue of the *C. elegans* protein Unc18, deletion of which gives an uncoordinated movement phenotype (Hosono et al., 1992). Deletion of Munc18-1 in mice resulted in a lethal phenotype at birth and a complete blockade of synaptic vesicle fusion (Verhage et al., 2000). Munc18-1 is

one of the seven SM proteins discovered in mammals and is exclusively expressed in neurons (Toonen and Verhage, 2003).

SM proteins are arch-shaped molecules consisting of three domains that form a central V-shaped cleft (Bracher et al., 2000; Misura et al., 2000). The interaction with syntaxin-1 is a common feature of SM proteins (reviewed in Toonen and Verhage, 2003).

Munc18-1 binds to syntaxin in two different modes, namely to the 'open' and the 'closed' form of syntaxin. In the 'closed' form of syntaxin, the N-terminal Habc domain of syntaxin folds back on the C-terminal SNARE motif and blocks SNARE complex assembly (Dulubova et al., 1999). Munc18-1's arch shaped form clasps this 'closed' conformation of syntaxin (Misura et al., 2000). Munc18-1 can also bind via its N-terminal to an N-terminal sequence of syntaxin, leaving its arch shaped cavity

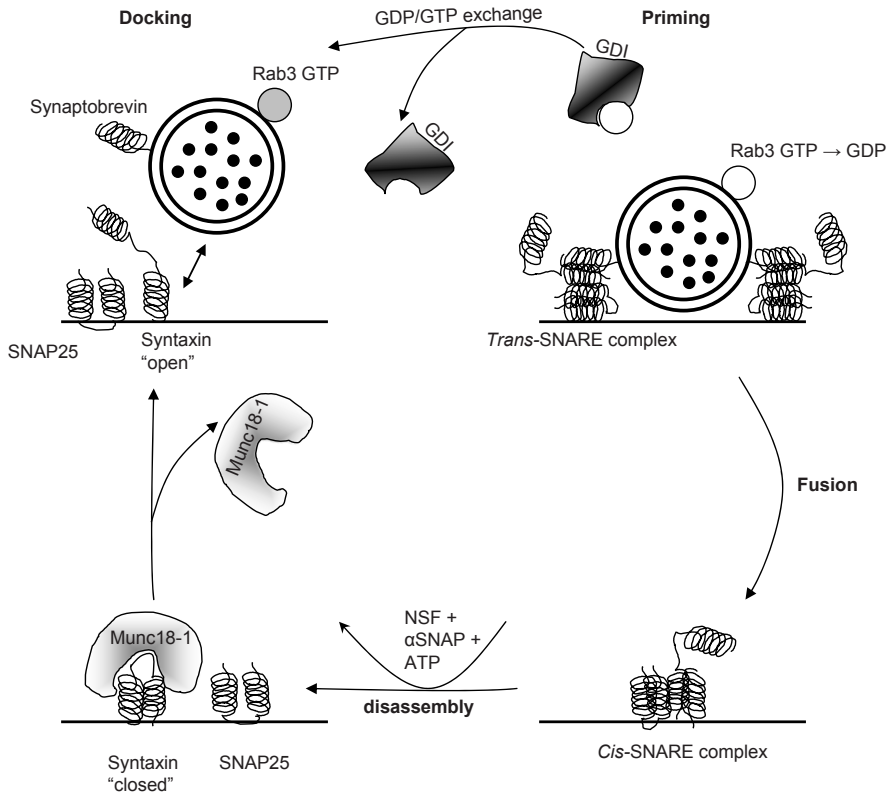

Figure 5. Vesicle fusion protein machinery
Conformational cycle of SNARE proteins. Syntaxin in 'open' state is able to form a trans SNARE complex with SNAP25 and synaptobrevin, releasing enough energy to induce membrane fusion. After fusion, αSNAP and NSF bind, and after ATP hydrolysis induce disassembly of the cis SNARE complex. Munc18-1 binds to the 'closed' state of syntaxin and needs to unbind to induce the open state. Not depicted here is the relocation of synaptobrevin, most likely upon retrieval of the vesicle membrane. The top panels include a schematic representation of the 'Rab3A' cycle, from the vesicle-bound GTP form, which is after ATP hydrolysis relocated by GTP-dissociation inhibiting protein (GDI)

open. This cavity then can be used to bind the assembling four-helical structure of the SNARE complex (see Sudhof and Rothman, 2009).

There has been a lot of debate about SM proteins being either positive or negative regulators of release. Genetic deletion of SM proteins results in a strong impairment or abolishment of release, suggesting a positive role of SM proteins. However, data on increasing SM protein levels (overexpression, injection) has led to conflicting results, suggesting either a positive or a negative role for the SM protein in exocytosis (Schulze et al., 1994; Dresbach et al., 1998; Wu et al., 1998; Voets et al., 2001). The most likely explanation is that the dual mode of interaction of the SM proteins and their cognate SNARE proteins represents two roles of the SM proteins. In membrane fusion, SM proteins have positive role (Shen et al., 2007) via the binding to the 'open' form of syntaxin and providing selectivity as well since binding only occurs to the cognate syntaxin. In addition, SM proteins can have a chaperone role to protect syntaxin during intercellular transport via binding to the 'closed' form of syntaxin (Medine et al., 2007).

Munc13

Unc13 was discovered in a classical genetic screen for *C. elegans* aiming at identifying mutant genes responsible for 'uncoordinated movements' (Brenner, 1974). It has one *Drosophila* homologue, Dunc13 (Aravamudan et al., 1999). Three Munc13 isoforms function in synaptic exocytosis (Munc13-1, bMunc13-2/ubMunc13-2 (splice variants of the Munc13-2 gene), and Munc13-3). Two other, ubiquitously expressed isoforms, presumably act in non-synaptic forms of exocytosis (Munc13-4 (Feldmann et al., 2003) and BAP-3 (Shiratsuchi et al., 1998)).

Munc13 proteins are large multidomain proteins with variable N-terminal sequences, but conserved central and C-terminal domains: a C2B (Ca^{2+} binding) domain, a large Munc13-homology region (the MUN domain) and a Ca^{2+}-independent C2C domain.

Deletion of Munc13 proteins in *C. elegans*, *Drosophila*, and mice showed severely reduced evoked and spontaneous release, but a normal number of docked vesicles (Aravamudan et al., 1999; Augustin et al., 1999; Richmond et al., 1999). The readily releasable pool of vesicles is strongly reduced, indicating that Munc13 acts after docking but prior to acquisition of 'fusion competence', called priming.

Munc13 interacts with syntaxin via its MUN domain, overexpression of which rescues synaptic transmission in Munc13 deletion (Stevens et al., 2005). Unc13 binds syntaxin at the same binding site as Unc18, and is even able to replace Unc18 (Sassa et al., 1999).

Munc13 and Munc18 have overlapping binding sites in the regulatory Habc domain of syntaxin. Munc13 could potentially displace Munc18 when it is clamping syntaxin in the 'closed' conformation to enable transition to the 'open' conforma-

tion, thereby enabling SNARE complex formation. Correspondingly, expression of a constitutively 'open' mutant of syntaxin (but not wild-type) rescued the release properties of a *C. elegans* Unc13 mutant (Richmond et al., 2001).

Munc13 participates in a tripartite complex with Rab3 and RIM, presumably to bring vesicles to the fusion machinery (Dulubova et al., 2005). Recent data suggests that this complex might be much more complex, also involving big presynaptic active zone proteins like Bassoon, Acyonin/Piccolo and CAST. The N-terminus of Munc13 seems to be site where all binding converges (Wang et al., 2009).

Next to being involved in basic release of neurotransmission, Munc13 has been shown to play a role in plasticity as well. The N terminal C1 domain is involved, which binds phorbol ester [4ß-phorbol-12, 13-dibutyrate (PDBu)] and diacyglycerol (DAG). This interaction is crucial for short term plasticity in the mouse hippocampus (Rhee et al., 2002). In addition, recently it was shown that the C2B domain of Munc13 functions as a Ca^{2+} regulator of short-term synaptic plasticity as well (Shin et al., 2010).

a-Neurexin

Neurexin1α was originally discovered as a neuronal cell-surface protein that binds the neurotoxin α-latrotoxin (Ushkaryov et al., 1992; Petrenko et al., 1993). The latter stimulates synaptic vesicle exocytosis and induces massive neurotransmitter release (reviewed in: Sudhof, 2001). Neurexin1α is a member of the neurexin protein family, which in mammals is encoded by three large genes (neurexin1, -2, and -3) (Tabuchi and Sudhof, 2002). Each of these genes contains a separate promoter for α- and β-neurexins. Neurexin genes are subject to intensive alternative splicing, potentially giving rise to thousands of isoforms (Missler and Sudhof, 1998).

α-Neurexins are transmembrane proteins, containing an N-terminal signal peptide followed by a three times repeated domain. Intracellularly, α-neurexins bind structural proteins with PDZ domains, Ca^{2+}/calmodulin-dependent serine protein kinase (CASK), Munc interacting protein (Mint) and the SNARE synaptotagmin. Extracellularly, α-neurexins bind to the postsynaptic cell-adhesion proteins dystroglycan (Missler and Sudhof, 1998; Sugita et al., 2001), neurexophilin (Missler et al., 1998) and neuroligin (Boucard et al., 2005).

Based on their structure and binding partners, neurexins have been suggested to function as cell-adhesion molecules that play an active role in the functional organization of the presynaptic machinery (Missler et al., 1998; Missler and Sudhof, 1998; Sudhof, 2001; Tabuchi and Sudhof, 2002; Missler et al., 2003). Deletion of α-neurexins in mice, however, showed morphologically normal synapses in brain. Interestingly, mutants lacking all three isoforms of α-neurexin display reduced synaptic N-type Ca^{2+} channel function, but unchanged numbers of cell-surface Ca^{2+}

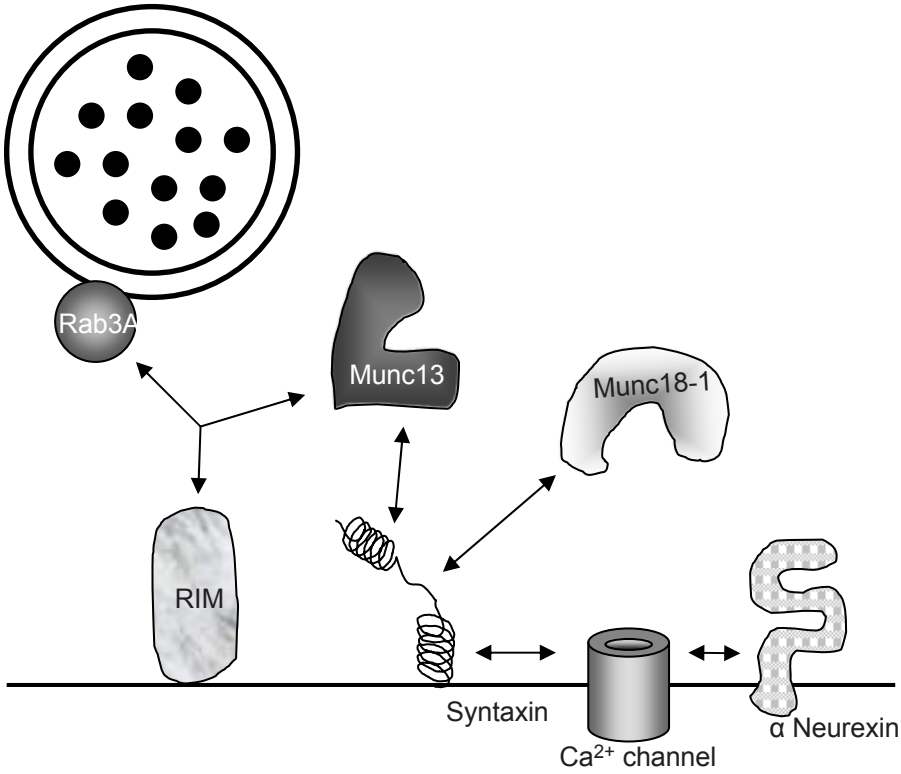

Figure 6. Exocytotic proteins studied in this thesis
Depicted here are the proteins that have been studied in this thesis (indicated with an asterisk), along with some key-role players in the process of exocytosis. Arrows indicate interactions, see main text for further details.

channels, suggesting that α-neurexins play a role in functionally coupling Ca^{2+} channels to the exocytotic machinery.

As mentioned above, β-neurexin has been implicated in a transsynaptic retrograde signaling pathway with neuroligin (Futai et al., 2007). α-Neurexins potentially could act in a similar pathway with a specific splice variant of neuroligin (Boucard et al., 2005).

Rab3A

Rab3A, B, C and D are small GTP-binding proteins that are involved in regulating membrane traffic (reviewed by Darchen and Goud, 2000). Rab3A, the most abundant brain isoform (Geppert et al., 1994), is associated with synaptic vesicles, but dissociates upon GTP-to-GDP hydrolysis during, or shortly after the fusion event (Fischer von Mollard et al., 1991; Star et al., 2005). Rab3A is therefore alternating between a GTP- and a GDP-bound form, which may function as a molecular switch regulating interaction with binding partners.

Rab3A binds to rabphilin (Shirataki et al., 1993), Rab-interacting molecule (RIM) (Wang et al., 1997), and synapsin-I (Giovedi et al., 2004). Deleting Rab3A in mice

only leads to a mild synaptic phenotype that includes altered short-term synaptic plasticity, and the absence of PKA-dependent long-term potentiation (Castillo et al., 1997; Geppert et al., 1997), suggesting a modulatory role for Rab3A. Mice that lack Rab3A, B, C, and D (quadruple knock-outs) are not viable, while the individual knock-outs display no or only a mild phenotype, indicating that Rab3 proteins are indispensable but individually are functionally redundant (Schluter et al., 2004). Analysis of cultured hippocampal neurons from these quadruple knock-out mice showed impaired evoked neurotransmitter release, whilst leaving spontaneous release unchanged (Schluter et al., 2004). The *C. elegans* Rab3 homologue interacts with the RIM homologue and this interaction is likely to play a role in placing the vesicle in the proximity of the presynaptic calcium channels (Gracheva et al., 2008).

RIM1a

Rab interacting molecule-1α (RIM1α) is located presynaptically at the active zone and plays an important role in neurotransmitter release (Wang et al., 1997; Schoch et al., 2002; Schoch et al., 2006). It is a large multi-domain scaffolding protein that was originally discovered as a binding partner of GTP-Rab3A, hence its name (Wang et al., 1997). So far, four genes (Rim1-4) encoding RIMs have been discovered in the mammalian genome. They encode six isoforms (RIM1α, 2α, 2β, 2γ, 3γ, and 4γ) (Wang et al., 2000; Wang and Sudhof, 2003).

RIM1α interacts with Rab3 and Munc13 (Wang et al., 1997; Betz et al., 2001; Wang et al., 2001). Originally it was thought that this binding was mutually exclusive (Betz et al., 2001). However, simultaneous binding can occur (Dulubova et al., 2005). In addition to Rab3 and Munc13, RIM1α interacts with ELKS proteins (also known as Rab6-interacting protein or CAST, also abbreviated as ERC), α-liprins, synaptotagmin and RIM-binding protein (reviewed by Kaeser and Sudhof, 2005). Via the latter, RIM may in turn bind to voltage-gated Ca_v1 and $Ca_v2.2$ Ca^{2+} channels (Hibino et al., 2002), although immunoprecipitation experiments with $Ca_v2.2$ antibodies failed to show co-immunoprecipitation (Khanna et al., 2006; Wong and Stanley, 2010).

RIM1α and Rab3A seem to jointly participate in several forms of presynaptic, PKA dependent LTP (Castillo et al., 2002; Lonart et al., 2003; Huang et al., 2005; Simsek-Duran and Lonart, 2008). RIM1α is likely to be the PKA substrate in the signaling pathway and therefore might function as a phosphoswitch.

Aims and outline of this thesis

This thesis characterizes the function of several neuro-exocytotic proteins in ACh release at the mouse NMJ. For a selection of these proteins it has been investigated whether they play a role in the mechanism underlying homeostatic upregulation of presynaptic ACh release resulting from reduction of the density of functional

postsynaptic AChRs, such as present under myasthenic condition. To this end, NMJ electrophysiology and morphology of several strains of mice genetically deficient for one or more members of neuro-exocytotic protein families has been investigated under normal conditions as well as after inducing experimental myasthenia gravis using α-BTx to block part of the AChRs.

Combined elimination of Munc13-1 and Munc13-2 genes leads to a lethal phenotype around birth. This prevents analysis of Munc13 function in the adult NMJ. In Chapter 2, a study of NMJ function and morphology is therefore performed on Munc13-1/2 double knock-out mouse embryos. In Chapter 3 the effect of genetic deletion of single or multiple isoforms of α-neurexin is reported. Morphological and electrophysiological studies have been performed on soleus muscle NMJ from adult mice and diaphragm NMJs from adult and one day-old mice. This chapter also describes the effect on ACh release homeostasis following application of the toxin model of myasthenia gravis on mice lacking both α-neurexin1 and -2. Chapter 4 reports on the effect of deleting Rab3A on neuromuscular transmission in soleus and diaphragm NMJs. Chapter 5 describes the effect of reducing or increasing Munc18-1 protein levels on exocytotic parameters at the NMJ, in comparison with the effects on cultured glutamatergic and GABAergic central synapses. In view of its modulatory roles, Munc18-1 might be a presynaptic target of the retrograde signals involved in transsynaptic homeostatic upregulation of transmitter release following reduction of postsynaptic AChRs at the NMJ. In chapter 6, the effect of reducing or increasing Munc18-1 protein levels on ACh release homeostasis was investigated in a mouse model for myasthenia gravis. Chapter 7 investigates basic transmitter release properties at NMJs of mice lacking RIM1α as well as the homeostatic response of ACh release to toxin-induced myasthenia gravis. Chapter 8 provides the reader with a general discussion on the findings presented in this thesis and raises some ideas for future research.

References

Aravamudan B, Fergestad T, Davis WS, Rodesch CK, Broadie K (1999) *Drosophila* UNC-13 is essential for synaptic transmission. Nat Neurosci 2:965-971.

Augustin I, Rosenmund C, Sudhof TC, Brose N (1999) Munc13-1 is essential for fusion competence of glutamatergic synaptic vesicles. Nature 400:457-461.

Berninger B, Poo M (1996) Fast actions of neurotrophic factors. Curr Opin Neurobiol 6:324-330.

Betz A, Thakur P, Junge HJ, Ashery U, Rhee JS, Scheuss V, Rosenmund C, Rettig J, Brose N (2001) Functional interaction of the active zone proteins Munc13-1 and RIM1 in synaptic vesicle priming. Neuron 30:183-196.

Boonyapisit K, Kaminski HJ, Ruff RL (1999) Disorders of neuromuscular junction ion channels. Am J Med 106:97-113.

Boucard AA, Chubykin AA, Comoletti D, Taylor P, Sudhof TC (2005) A splice code for trans-synaptic cell adhesion mediated by binding of neuroligin 1 to alpha- and beta-neurexins. Neuron 48:229-236.

Bracher A, Perrakis A, Dresbach T, Betz H, Weissenhorn W (2000) The X-ray crystal structure of neuronal Sec1 from squid sheds new light on the role of this protein in exocytosis. Structure Fold Des 8:685-694.

Brenner S (1974) The genetics of *Caenorhabditis elegans*. Genetics 77:71-94.

Burrone J, Murthy VN (2003) Synaptic gain control and homeostasis. Curr Opin Neurobiol 13:560-567.

Castillo PE, Janz R, Sudhof TC, Tzounopoulos T, Malenka RC, Nicoll RA (1997) Rab3A is essential for mossy fibre long-term potentiation in the hippocampus. Nature 388:590-593.

Castillo PE, Schoch S, Schmitz F, Sudhof TC, Malenka RC (2002) RIM1alpha is required for presynaptic long-term potentiation. Nature 415:327-330.

Chen YA, Scheller RH (2001) SNARE-mediated membrane fusion. Nat Rev Mol Cell Biol 2:98-106.

Couteaux R (1973) Motor endplate structure. In: Structure and Function of. Muscle (Bourne G, ed), pp 483-530. New York: Academic.

Cull-Candy SG, Miledi R, Trautmann A, Uchitel OD (1980) On the release of transmitter at normal, myasthenia gravis and myasthenic syndrome affected human end-plates. J Physiol 299:621-638.

Dale HH, Feldberg W, Vogt M (1936) Release of acetylcholine at voluntary motor nerve endings. J Physiol353-380.

Darchen F, Goud B (2000) Multiple aspects of Rab protein action in the secretory pathway: focus on Rab3 and Rab6. Biochimie 82:375-384.

Davis GW, Bezprozvanny I (2001) Maintaining the stability of neural function: a homeostatic hypothesis. Annu Rev Physiol 63:847-869.

Davis GW, DiAntonio A, Petersen SA, Goodman CS (1998) Postsynaptic PKA controls quantal size and reveals a retrograde signal that regulates presynaptic transmitter release in *Drosophila*. Neuron 20:305-315.

Dean C, Dresbach T (2006) Neuroligins and neurexins: linking cell adhesion, synapse formation and cognitive function. Trends Neurosci 29:21-29.

Dickman DK, Davis GW (2009) The schizophrenia susceptibility gene dysbindin controls synaptic homeostasis. Science 326:1127-1130.

Dresbach T, Burns ME, O'Connor V, DeBello WM, Betz H, Augustine GJ (1998) A neuronal Sec1 homolog regulates neurotransmitter release at the squid giant synapse. J Neurosci 18:2923-2932.

Dulubova I, Lou X, Lu J, Huryeva I, Alam A, Schneggenburger R, Sudhof TC, Rizo J (2005) A Munc13/RIM/Rab3 tripartite complex: from priming to plasticity? EMBO J 24:2839-2850.

Dulubova I, Sugita S, Hill S, Hosaka M, Fernandez I, Sudhof TC, Rizo J (1999) A conformational switch in syntaxin during exocytosis: role of munc18. EMBO J 18:4372-4382.

Elmqvist D, Hofmann WW, Kugelberg J, Quastel DM (1964) An electrophysiological investigation of neuromuscular transmission in myasthenia gravis.J Physiol 174:417-434.

Engel AG (1994) The neuromuscular junction. In: Myology: Basic and Clinical (Engel AG, Franzini-Armstrong C, eds), pp 261-302. New York: McGraw-Hill.

Fasshauer D, Antonin W, Subramaniam V, Jahn R (2002) SNARE assembly and disassembly exhibit a pronounced hysteresis. Nat Struct Biol 9:144-151.

Fasshauer D, Sutton RB, Brunger AT, Jahn R (1998) Conserved structural features of the synaptic fusion complex: SNARE proteins reclassified as Q- and R-SNAREs. Proc Natl Acad Sci U S A 95:15781-15786.

Fatt P, Katz B (1950) Membrane potentials at the motor end-plate. J Physiol 111:46p-47p.

Fatt P, Katz B (1951) An analysis of the end-plate potential recorded with an intracellular electrode. J Physiol 115:320-370.

Fatt P, Katz B (1952) Spontaneous subthreshold activity at motor nerve endings. J Physiol 117:109-128.

Feldmann J, Callebaut I, Raposo G, Certain S, Bacq D, Dumont C, Lambert N, Ouachee-Chardin M, Chedeville G, Tamary H, Minard-Colin V, Vilmer E, Blanche S, Le DF, Fischer A, de Saint BG (2003) Munc13-4 is essential for cytolytic granules fusion and is mutated in a form of familial hemophagocytic lymphohistiocytosis (FHL3). Cell 115:461-473.

Feng Z, Ko CP (2007) Neuronal glia interactions at the vertebrate neuromuscular junction. Current Opinion in Pharmacology 7:316-324.

Fertuck HC, Salpeter MM (1976) Quantitation of junctional and extrajunctional acetylcholine receptors by electron microscope autoradiography after 125I-alpha-bungarotoxin binding at mouse neuromuscular junctions. J Cell Biol 69:144-158.

Fischer von Mollard G, Sudhof TC, Jahn R (1991) A small GTP-binding protein dissociates from synaptic vesicles during exocytosis. Nature 349:79-81.

Fitzsimonds RM, Poo MM (1998) Retrograde signaling in the development and modification of synapses. Physiol Rev 78:143-170.

Fradkin LG, Baines RA, van der Plas MC, Noordermeer JN (2008) The dystrophin Dp186 isoform regulates neurotransmitter release at a central synapse in *Drosophila*. J Neurosci 28:5105-5114.

Fredj NB, Burrone J (2009) A resting pool of vesicles is responsible for spontaneous vesicle fusion at the synapse. Nat Neurosci 12:751-758.

Futai K, Kim MJ, Hashikawa T, Scheiffele P, Sheng M, Hayashi Y (2007) Retrograde modulation of presynaptic release probability through signaling mediated by PSD-95-neuroligin. Nat Neurosci 10:186-195.

Geppert M, Bolshakov VY, Siegelbaum SA, Takei K, De Camilli P, Hammer RE, Sudhof TC (1994) The role of Rab3A in neurotransmitter release. Nature 369:493-497.

Geppert M, Goda Y, Stevens CF, Sudhof TC (1997) The small GTP-binding protein Rab3A regulates a late step in synaptic vesicle fusion. Nature 387:810-814.

Giovedi S, Vaccaro P, Valtorta F, Darchen F, Greengard P, Cesareni G, Benfenati F (2004) Synapsin is a novel Rab3 effector protein on small synaptic vesicles. I. Identification and characterization of the synapsin I-Rab3 interactions in vitro and in intact nerve terminals. J Biol Chem 279:43760-43768.

Goold CP, Davis GW (2007) The BMP ligand Gbb gates the expression of synaptic homeostasis independent of synaptic growth control. Neuron 56:109-123.

Gracheva EO, Hadwiger G, Nonet ML, Richmond JE (2008) Direct interactions between *C. elegans* RAB-3 and Rim provide a mechanism to target vesicles to the presynaptic density. Neurosci Lett 444:137-142.

Gu Y, Hall ZW (1988) Immunological evidence for a change in subunits of the acetylcholine receptor in developing and denervated rat muscle. Neuron 1:117-125.

Haghighi AP, McCabe BD, Fetter RD, Palmer JE, Hom S, Goodman CS (2003) Retrograde control of synaptic transmission by postsynaptic CaMKII at the *Drosophila* neuromuscular junction. Neuron 39:255-267.

Hanson PI, Roth R, Morisaki H, Jahn R, Heuser JE (1997) Structure and conformational changes in NSF and its membrane receptor complexes visualized by quick-freeze/deep-etch electron microscopy. Cell 90:523-535.

Hata Y, Slaughter CA, Sudhof TC (1993) Synaptic vesicle fusion complex contains unc-18 homologue bound to syntaxin. Nature 366:347-351.

Hibino H, Pironkova R, Onwumere O, Vologodskaia M, Hudspeth AJ, Lesage F (2002) RIM Binding Proteins (RBPs) Couple Rab3-Interacting Molecules (RIMs) to Voltage-Gated $Ca^{(2+)}$ Channels. Neuron 34:411-423.

Hoch W, McConville J, Helms S, Newsom-Davis J, Melms A, Vincent A (2001) Auto-antibodies to the receptor tyrosine kinase MuSK in patients with myasthenia gravis without acetylcholine receptor antibodies. Nat Med 7:365-368.

Hosono R, Hekimi S, Kamiya Y, Sassa T, Murakami S, Nishiwaki K, Miwa J, Taketo A, Kodaira KI (1992) The unc-18 gene encodes a novel protein affecting the kinetics of acetylcholine metabolism in the nematode *Caenorhabditis elegans*. J Neurochem 58:1517-1525.

Huang YY, Zakharenko SS, Schoch S, Kaeser PS, Janz R, Sudhof TC, Siegelbaum SA, Kandel ER (2005) Genetic evidence for a protein-kinase-A-mediated

presynaptic component in NMDA-receptor-dependent forms of long-term synaptic potentiation. Proc Natl Acad Sci U S A 102:9365-9370.

Jahn R, Lang T, Sudhof TC (2003) Membrane fusion. Cell 112:519-533.

Jahn R, Sudhof TC (1999) Membrane fusion and exocytosis. Annu Rev Biochem 68:863-911.

Kaeser PS, Sudhof TC (2005) RIM function in short- and long-term synaptic plasticity. Biochem Soc Trans 33:1345-1349.

Kaja S (2007) Synaptic effects of mutations in neuronal $Ca_v2.1$ calcium channels.

Karlin A (2002) Emerging structure of the nicotinic acetylcholine receptors. Nat Rev Neurosci 3:102-114.

Katz B (1966) Nerve, Muscle, and Synapse. New York: McGraw-Hill.

Keshishian H, Kim YS (2004) Orchestrating development and function: retrograde BMP signaling in the *Drosophila* nervous system. Trends Neurosci 27:143-147.

Khanna R, Li Q, Sun L, Collins TJ, Stanley EF (2006) N type Ca^{2+} channels and RIM scaffold protein covary at the presynaptic transmitter release face but are components of independent protein complexes. Neuroscience 140:1201-1208.

Krejci E, Thomine S, Boschetti N, Legay C, Sketelj J, Massoulie J (1997) The mammalian gene of acetylcholinesterase-associated collagen. J Biol Chem 272:22840-22847.

Lessmann V (1998) Neurotrophin-dependent modulation of glutamatergic synaptic transmission in the mammalian CNS. Gen Pharmacol 31:667-674.

Lessmann V, Gottmann K, Heumann R (1994) BDNF and NT-4/5 enhance glutamatergic synaptic transmission in cultured hippocampal neurones. Neuroreport 6:21-25.

Lin RC, Scheller RH (1997) Structural organization of the synaptic exocytosis core complex. Neuron 19:1087-1094.

Lindstrom JM (2000) Acetylcholine receptors and myasthenia. Muscle Nerve 23:453-477.

Lohof AM, Ip NY, Poo MM (1993) Potentiation of developing neuromuscular synapses by the neurotrophins NT-3 and BDNF. Nature 363:350-353.

Lonart G, Schoch S, Kaeser PS, Larkin CJ, Sudhof TC, Linden DJ (2003) Phosphorylation of RIM1alpha by PKA triggers presynaptic long-term potentiation at cerebellar parallel fiber synapses. Cell 115:49-60.

Lou X, Scheuss V, Schneggenburger R (2005) Allosteric modulation of the presynaptic Ca^{2+} sensor for vesicle fusion. Nature 435:497-501.

Magby JP, Bi C, Chen ZY, Lee FS, Plummer MR (2006) Single-cell characterization of retrograde signaling by brain-derived neurotrophic factor. J Neurosci 26:13531-13536.

McLachlan EM, Martin AR (1981) Non-linear summation of end-plate potentials in the frog and mouse. J Physiol 311:307-324.

Medine CN, Rickman C, Chamberlain LH, Duncan RR (2007) Munc18-1 prevents the formation of ectopic SNARE complexes in living cells. J Cell Sci 120:4407-4415.

Meir A, Ginsburg S, Butkevich A, Kachalsky SG, Kaiserman I, Ahdut R, Demirgoren S, Rahamimoff R (1999) Ion channels in presynaptic nerve terminals and control of transmitter release. Physiol Rev 79:1019-1088.

Meriggioli MN, Sanders DB (2004) Myasthenia gravis: diagnosis. Semin Neurol 24:31-39.

Mishina M, Takai T, Imoto K, Noda M, Takahashi T, Numa S, Methfessel C, Sakmann B (1986) Molecular distinction between fetal and adult forms of muscle acetylcholine receptor. Nature 321:406-411.

Missias AC, Chu GC, Klocke BJ, Sanes JR, Merlie JP (1996) Maturation of the acetylcholine receptor in skeletal muscle: regulation of the AChR gamma-to-epsilon switch. Dev Biol 179:223-238.

Missler M, Hammer RE, Sudhof TC (1998) Neurexophilin binding to alpha-neurexins. A single LNS domain functions as an independently folding ligand-binding unit. J Biol Chem 273:34716-34723.

Missler M, Sudhof TC (1998) Neurexins: three genes and 1001 products. Trends Genet 14:20-26.

Missler M, Zhang W, Rohlmann A, Kattenstroth G, Hammer RE, Gottmann K, Sudhof TC (2003) Alpha-neurexins couple Ca^{2+} channels to synaptic vesicle exocytosis. Nature 424:939-948.

Misura KM, Scheller RH, Weis WI (2000) Three-dimensional structure of the neuronal-Sec1-syntaxin 1a complex. Nature 404:355-362.

Molenaar PC, Oen BS, Plomp JJ, van Kempen GT, Jennekens FG, Hesselmans LF (1991) A non-immunogenic myasthenia gravis model and its application in a study of transsynaptic regulation at the neuromuscular junction. Eur J Pharmacol 196:93-101.

Molenaar PC, Polak RL, Miledi R, Alema S, Vincent A, Newsom-Davis J (1979) Acetylcholine in intercostal muscle from myasthenia gravis patients and in rat diaphragm after blockade of acetylcholine receptors. Prog Brain Res 49:449-458.

Ogata T (1988) Structure of motor endplates in the different fiber types of vertebrate skeletal muscles. Arch Histol Cytol 51:385-424.

Oosterhuis HJ (1989) The natural course of myasthenia gravis: a long term follow up study. J Neurol Neurosurg Psychiatry 52:1121-1127.

Paradis S, Sweeney ST, Davis GW (2001) Homeostatic control of presynaptic release is triggered by postsynaptic membrane depolarization. Neuron 30:737-749.

Petersen SA, Fetter RD, Noordermeer JN, Goodman CS, DiAntonio A (1997) Genetic analysis of glutamate receptors in *Drosophila* reveals a retrograde signal regulating presynaptic transmitter release. Neuron 19:1237-1248.

Petrenko AG, Lazaryeva VD, Geppert M, Tarasyuk TA, Moomaw C, Khokhlatchev AV, Ushkaryov YA, Slaughter C, Nasimov IV, Sudhof TC (1993) Polypeptide composition of the alpha-latrotoxin receptor. High affinity binding protein consists of a family of related high molecular weight polypeptides complexed to a low molecular weight protein. J Biol Chem 268:1860-1867.

Plomp JJ, van Kempen GT, De Baets MB, Graus YM, Kuks JB, Molenaar PC (1995) Acetylcholine release in myasthenia gravis: regulation at single end-plate level. Ann Neurol 37:627-636.

Plomp JJ, van Kempen GT, Molenaar PC (1992) Adaptation of quantal content to decreased postsynaptic sensitivity at single endplates in alpha-bungarotoxin-treated rats. J Physiol 458:487-499.

Rhee JS, Betz A, Pyott S, Reim K, Varoqueaux F, Augustin I, Hesse D, Sudhof TC, Takahashi M, Rosenmund C, Brose N (2002) Beta phorbol ester- and diacylglycerol-induced augmentation of transmitter release is mediated by Munc13s and not by PKCs. Cell 108:121-133.

Richmond JE, Davis WS, Jorgensen EM (1999) UNC-13 is required for synaptic vesicle fusion in *C. elegans*. Nat Neurosci 2:959-964.

Richmond JE, Weimer RM, Jorgensen EM (2001) An open form of syntaxin bypasses the requirement for UNC-13 in vesicle priming. Nature 412:338-341.

Rizo J, Sudhof TC (2002) Snares and munc18 in synaptic vesicle fusion. Nat Rev Neurosci 3:641-653.

Rizzoli SO, Betz WJ (2004) The structural organization of the readily releasable pool of synaptic vesicles. Science 303:2037-2039.

Sandrock AW, Jr., Dryer SE, Rosen KM, Gozani SN, Kramer R, Theill LE, Fischbach GD (1997) Maintenance of acetylcholine receptor number by neuregulins at the neuromuscular junction in vivo. Science 276:599-603.

Sanes JR, Lichtman JW (1999) Development of the vertebrate neuromuscular junction. Annu Rev Neurosci 22:389-442.

Sassa T, Harada S, Ogawa H, Rand JB, Maruyama IN, Hosono R (1999) Regulation of the UNC-18-*Caenorhabditis elegans* syntaxin complex by UNC-13. J Neurosci 19:4772-4777.

Schinder AF, Berninger B, Poo M (2000) Postsynaptic target specificity of neurotrophin-induced presynaptic potentiation. Neuron 25:151-163.

Schluter OM, Schmitz F, Jahn R, Rosenmund C, Sudhof TC (2004) A complete genetic analysis of neuronal Rab3 function. J Neurosci 24:6629-6637.

Schoch S, Castillo PE, Jo T, Mukherjee K, Geppert M, Wang Y, Schmitz F, Malenka RC, Sudhof TC (2002) RIM1alpha forms a protein scaffold for regulating neurotransmitter release at the active zone. Nature 415:321-326.

Schoch S, Deak F, Konigstorfer A, Mozhayeva M, Sara Y, Sudhof TC, Kavalali ET (2001) SNARE function analyzed in synaptobrevin/VAMP knockout mice. Science 294:1117-1122.

Schoch S, Mittelstaedt T, Kaeser PS, Padgett D, Feldmann N, Chevaleyre V, Castillo PE, Hammer RE, Han W, Schmitz F, Lin W, Sudhof TC (2006) Redundant functions of RIM1alpha and RIM2alpha in $Ca^{(2+)}$-triggered neurotransmitter release. EMBO J 25:5852-5863.

Schulze KL, Littleton JT, Salzberg A, Halachmi N, Stern M, Lev Z, Bellen HJ (1994) rop, a *Drosophila* homolog of yeast Sec1 and vertebrate n-Sec1/Munc-18 proteins, is a negative regulator of neurotransmitter release in vivo. Neuron 13:1099-1108.

Shen J, Tareste DC, Paumet F, Rothman JE, Melia TJ (2007) Selective activation of cognate SNAREpins by Sec1/Munc18 proteins. Cell 128:183-195.

Shin OH, Lu J, Rhee JS, Tomchick DR, Pang ZP, Wojcik SM, Camacho-Perez M, Brose N, Machius M, Rizo J, Rosenmund C, Sudhof TC (2010) Munc13 C(2) B domain is an activity-dependent $Ca^{(2+)}$ regulator of synaptic exocytosis. Nat Struct Mol Biol.

Shirataki H, Kaibuchi K, Sakoda T, Kishida S, Yamaguchi T, Wada K, Miyazaki M, Takai Y (1993) Rabphilin-3A, a putative target protein for smg p25A/rab3A p25 small GTP-binding protein related to synaptotagmin. Mol Cell Biol 13:2061-2068.

Shiratsuchi T, Oda K, Nishimori H, Suzuki M, Takahashi E, Tokino T, Nakamura Y (1998) Cloning and characterization of BAP3 (BAI-associated protein 3), a C2 domain-containing protein that interacts with BAI1. Biochem Biophys Res Commun 251:158-165.

Simsek-Duran F, Lonart G (2008) The role of RIM1alpha in BDNF-enhanced glutamate release. Neuropharmacology 55:27-34.

Smith SM, Renden R, von GH (2008) Synaptic vesicle endocytosis: fast and slow modes of membrane retrieval. Trends Neurosci 31:559-568.

Sollner T, Whiteheart SW, Brunner M, Erdjument-Bromage H, Geromanos S, Tempst P, Rothman JE (1993) SNAP receptors implicated in vesicle targeting and fusion. Nature 362:318-324.

Star EN, Newton AJ, Murthy VN (2005) Real-time imaging of Rab3a and Rab5a reveals differential roles in presynaptic function. J Physiol 569:103-117.

Stevens DR, Wu ZX, Matti U, Junge HJ, Schirra C, Becherer U, Wojcik SM, Brose N, Rettig J (2005) Identification of the minimal protein domain required for priming activity of Munc13-1. Curr Biol 15:2243-2248.

Sudhof TC (2001) alpha-Latrotoxin and its receptors: neurexins and CIRL/latrophilins. Annu Rev Neurosci 24:933-962.

Sudhof TC (2004) The synaptic vesicle cycle. Annu Rev Neurosci 27:509-547.

Sudhof TC, Rothman JE (2009) Membrane fusion: grappling with SNARE and SM proteins. Science 323:474-477.

Sugita S, Saito F, Tang J, Satz J, Campbell K, Sudhof TC (2001) A stoichiometric complex of neurexins and dystroglycan in brain. J Cell Biol 154:435-445.

Sutton MA, Wall NR, Aakalu GN, Schuman EM (2004) Regulation of dendritic protein synthesis by miniature synaptic events. Science 304:1979-1983.

Tabuchi K, Sudhof TC (2002) Structure and evolution of neurexin genes: insight into the mechanism of alternative splicing. Genomics 79:849-859.

Takamori M, Sakato S, Okumura S (1984) Presynaptic function modified by acetylcholine-receptor interaction in experimental autoimmune myasthenia gravis. J Neurol Sci 66:245-253.

Tao HW, Poo M (2001) Retrograde signaling at central synapses. Proc Natl Acad Sci U S A 98:11009-11015.

Toonen RF, Verhage M (2003) Vesicle trafficking: pleasure and pain from SM genes. Trends Cell Biol 13:177-186.

Tyler WJ, Perrett SP, Pozzo-Miller LD (2002) The role of neurotrophins in neurotransmitter release. Neuroscientist 8:524-531.

Uchitel OD, Protti DA, Sanchez V, Cherksey BD, Sugimori M, Llinas R (1992) P-type voltage-dependent calcium channel mediates presynaptic calcium influx and transmitter release in mammalian synapses. Proc Natl Acad Sci U S A 89:3330-3333.

Ushkaryov YA, Petrenko AG, Geppert M, Sudhof TC (1992) Neurexins: synaptic cell surface proteins related to the alpha-latrotoxin receptor and laminin. Science 257:50-56.

van der Plas MC, Pilgram GS, Plomp JJ, de Jong A, Fradkin LG, Noordermeer JN (2006) Dystrophin is required for appropriate retrograde control of neurotransmitter release at the *Drosophila* neuromuscular junction. J Neurosci 26:333-344.

Verhage M, Maia AS, Plomp JJ, Brussaard AB, Heeroma JH, Vermeer H, Toonen RF, Hammer RE, van den Berg TK, Missler M, Geuze HJ, Sudhof TC (2000) Synaptic assembly of the brain in the absence of neurotransmitter secretion. Science 287:864-869.

Vincent A (1987) The molecular biology of end-plate diseases. In: The Vertebrate Neuromuscular Junction (Salpeter MM, ed), New York: Alan R. Liss.

Vincent A, Leite MI (2005) Neuromuscular junction autoimmune disease: muscle specific kinase antibodies and treatments for myasthenia gravis. Curr Opin Neurol 18:519-525.

Vincent A, Palace J, Hilton-Jones D (2001) Myasthenia gravis. Lancet 357:2122-2128.

Voets T, Toonen RF, Brian EC, de Wit H, Moser T, Rettig J, Sudhof TC, Neher E, Verhage M (2001) Munc18-1 promotes large dense-core vesicle docking. Neuron 31:581-591.

Wang X, Hu B, Zieba A, Neumann NG, Kasper-Sonnenberg M, Honsbein A, Hultqvist G, Conze T, Witt W, Limbach C, Geitmann M, Danielson H, Kolarow R, Niemann G, Lessmann V, Kilimann MW (2009) A protein interaction node at the neurotransmitter release site: domains of Aczonin/Piccolo, Bassoon, CAST, and rim converge on the N-terminal domain of Munc13-1. J Neurosci 29:12584-12596.

Wang X, Hu B, Zimmermann B, Kilimann MW (2001) Rim1 and rabphilin-3 bind Rab3-GTP by composite determinants partially related through N-terminal alpha -helix motifs. J Biol Chem 276:32480-32488.

Wang Y, Okamoto M, Schmitz F, Hofmann K, Sudhof TC (1997) Rim is a putative Rab3 effector in regulating synaptic-vesicle fusion. Nature 388:593-598.

Wang Y, Sudhof TC (2003) Genomic definition of RIM proteins: evolutionary amplification of a family of synaptic regulatory proteins(small star, filled). Genomics 81:126-137.

Wang Y, Sugita S, Sudhof TC (2000) The RIM/NIM family of neuronal C2 domain proteins. Interactions with Rab3 and a new class of Src homology 3 domain proteins. J Biol Chem 275:20033-20044.

Washbourne P, Thompson PM, Carta M, Costa ET, Mathews JR, Lopez-Bendito G, Molnar Z, Becher MW, Valenzuela CF, Partridge LD, Wilson MC (2002) Genetic ablation of the t-SNARE SNAP-25 distinguishes mechanisms of neuroexocytosis. Nat Neurosci 5:19-26.

Weber T, Zemelman BV, McNew JA, Westermann B, Gmachl M, Parlati F, Sollner TH, Rothman JE (1998) SNAREpins: minimal machinery for membrane fusion. Cell 92:759-772.

Weimer RM, Jorgensen EM (2003) Controversies in synaptic vesicle exocytosis. J Cell Sci 116:3661-3666.

Weimer RM, Richmond JE (2005) Synaptic vesicle docking: a putative role for the Munc18/Sec1 protein family. Curr Top Dev Biol 65:83-113.

Wheeler DB, Randall A, Sather WA, Tsien RW (1995) Neuronal calcium channels encoded by the alpha 1A subunit and their contribution to excitatory synaptic transmission in the CNS. Prog Brain Res 105:65-78.

Wong FK, Stanley EF (2010) Rab3a interacting molecule (RIM) and the tethering of pre-synaptic transmitter release site-associated $Ca_v2.2$ calcium channels. J Neurochem 112:463-473.

Wood SJ, Slater CR (2001) Safety factor at the neuromuscular junction. Prog Neurobiol 64:393-429.

Wu MN, Littleton JT, Bhat MA, Prokop A, Bellen HJ (1998) ROP, the *Drosophila* Sec1 homolog, interacts with syntaxin and regulates neurotransmitter release in a dosage-dependent manner. EMBO J 17:127-139.

2

Aberrant morphology and residual transmitter release at the Munc13-deficient mouse neuromuscular synapse

Michèle S. Sons,[2*] Frédérique Varoqueaux,[1*]
Jaap J. Plomp,[2] and Nils Brose[1]

1 Department of Molecular Neurobiology, Max-Planck-Institute for Experimental Medicine, Göttingen, Germany
2 Departments of Neurology and Neurophysiology, Leiden University Medical Center, Leiden, The Netherlands
** M.S. and F.V. contributed equally to this study.*

Published in Molecular and Cellular Biology (2005) 25(14):
5973 -5984

Abstract

In cultured hippocampal neurons, synaptogenesis is largely independent of synaptic transmission, while several accounts in the literature indicate that synaptogenesis at cholinergic neuromuscular junctions in mammals appears to partially depend on synaptic activity. To systematically examine the role of synaptic activity in synaptogenesis at the neuromuscular junction, we investigated neuromuscular synaptogenesis and neurotransmitter release of mice lacking all synaptic vesicle priming proteins of the Munc13 family. Munc13 deficient mice are completely paralyzed at birth and die immediately, but form specialized neuromuscular end-plates that display typical synaptic features. However, the distribution, number, size, and shape of these synapses, as well as the number of motor neurons they originate from and the maturation state of muscle cells are profoundly altered. Surprisingly, Munc13 deficient synapses exhibit significantly increased spontaneous quantal acetylcholine release, although fewer fusion-competent synaptic vesicles are present and nerve stimulation-evoked secretion is hardly elicitable and strongly reduced in magnitude. We conclude that the residual transmitter release in Munc13 deficient mice is not sufficient to sustain normal synaptogenesis at the neuromuscular junction, essentially causing morphological aberrations that are also seen upon total blockade of neuromuscular transmission in other genetic models. Our data confirm the importance of Munc13 proteins in synaptic vesicle priming at the neuromuscular junction but indicate also that priming at this synapse may differ from priming at glutamatergic and GABAergic synapses and is partly Munc13-independent. Thus, non-Munc13 priming proteins exist at this synapse or vesicle priming occurs in part spontaneously, i.e. without dedicated priming proteins in the release machinery.

Acknowledgements
This work was supported by a grant from the German Research Foundation (SFB406/A1) to N.B., and the Netherlands Organisation for Scientific Research, NWO, (903-42-073) to J.J.P.. We thank M. Dutschmann, D. Fasshauer, J. Heeroma, A. Mansouri, and G. Meyer for helpful scientific discussion, K. Hellmann, S. Wenger, and J. Mairesse for excellent technical assistance, A. Arand and the staff of the Transgenic Animal Facility at the Max-Planck-Institute for Experimental Medicine, Göttingen for help with mouse colonies, and J. Ficner for help with graphics.

Introduction

Transmitter release from presynaptic terminals is mediated by the exocytotic fusion of transmitter filled synaptic vesicles. Fusion of these vesicles is triggered by membrane depolarization and concomitant influx of Ca^{2+} ions, and is dependent on the SNARE proteins synaptobrevin/VAMP 2, syntaxin 1, and SNAP-25, whose assembly into a highly stable SNARE complex (Sutton et al., 1998) is thought to drive the fusion reaction (Reviewed in: Rettig and Neher, 2002; Jahn et al., 2003; Fasshauer, 2003).

Before fusion can be initiated, synaptic vesicles must be primed into a fusion-competent state (for review, see: Brose et al., 2000; Rettig and Neher, 2002; Rosenmund et al., 2003). Members of the Munc13 family, mammalian homologues of *C. elegans* Unc-13 (Brose et al., 1995), play an essential role during this priming reaction (Aravamudan et al., 1999; Richmond et al., 1999; Ashery et al., 2000; Rhee et al., 2002; Rosenmund et al., 2002). At the molecular level, synaptic vesicle priming is thought to depend on a conformational switch of the SNARE protein syntaxin 1 from a closed conformation, which prevents SNARE complex assembly, to an open conformation, which permits it (Dulubova et al., 1999). It is believed that Munc13 plays an important role during this conformational switch, since the overexpression of an open syntaxin mutant in *C. elegans* bypassed the strict requirement for Unc-13 (Richmond et al., 1999). In *C. elegans*, Unc-13 is essential for vesicle priming at both cholinergic and GABAergic synapses (Brenner, 1974; Richmond et al., 1999; Lackner et al., 1999).

In mammals, the Munc13 protein family comprises three highly homologous members, Munc13-1, bMunc13-2/ubMunc13-2 (splice variants of the Munc13-2 gene), and Munc13-3 (Brose et al., 2000), which are differentially distributed in the brain (Augustin et al., 1999a) and confer differential short-term plasticity characteristics to the synapses they equip (Rosenmund et al., 2002; Junge et al., 2004). Transmitter release from both glutamatergic and GABAergic neurons in the hippocampus is strictly dependent on Munc13 function. In the absence of Munc13-1 and Munc13-2, these neurons show neither spontaneous nor evoked synaptic release events, yet develop normal numbers of synapses which contain an electrophysiologically normal postsynaptic AMPA and GABA receptor complement, but exhibit a broader active zone (Varoqueaux et al., 2002). These findings led to the conclusion that genesis and assembly of synapses between hippocampal nerve cells are largely independent of synaptic activity. Rather, synaptogenesis in the central nervous system may follow a default developmental program that is only modulated, stabilized, and refined by synaptic activity (Varoqueaux et al., 2002).

In many aspects, the neuromuscular synapse, which uses acetylcholine as a neurotransmitter, is similar to central synapses and therefore a widely used model for the study of synaptogenesis. The formation and maturation of the neuromuscular

junction (NMJ) is known to rely in part on activity-dependent signals. Initially, evidence in support of this view was obtained in studies where the developmental role of synaptic transmission at the NMJ had been examined using anti-cholinergic or activity-blocking drugs (reviewed in: Misgeld et al., 2002; Brandon et al., 2003). More recently, genetic studies on mutant mice lacking choline acetyltransferase (ChAT), the enzyme responsible for producing acetylcholine, provided compelling evidence for the requirement of neurotransmitter release in NMJ formation (Misgeld et al., 2002; Brandon et al., 2003).

Based on our observations in the central nervous system (Varoqueaux et al., 2002), and the fact that Munc13 deficient mice are completely paralysed, we expected to find a total blockade of transmitter release at the NMJ in the absence of Munc13s. We report here the unexpected finding that neuromuscular synaptic transmission is not entirely abolished in the absence of Munc13s. Nevertheless, the morphology of the NMJ shows abnormalities comparable to those seen in ChAT deletion mutant mice. We characterize the features of the neuromuscular apparatus in Munc13 deficient NMJs and discuss the role of different types of synaptic activity in regulating synaptogenesis at NMJs, and the function of Munc13s at peripheral and central synapses.

Materials and Methods

Mouse lines

Single deletion mutant mice lacking Munc13-1, Munc13-2, or Munc13-3 were published previously (Augustin et al., 1999b; Augustin et al., 2001; Varoqueaux et al., 2002). Double and triple mutant mice were obtained by interbreeding of the single mutant lines. Prior to experiments, mice heteroyzygous for the lethal Munc13-1 deletion and heterozygous or homozygous for the Munc13-2 deletion, and in some cases also for the Munc13-3 deletion were mated for 24 h (embryonic day E0). At embryonic day E18.5, the pregnant mothers were sacrificed by cervical dislocation. Embryos were recovered by hysterectomy and further processed on ice. Homozygous Munc13-1/2 double mutant and Munc13-1/2/3 triple mutant embryos were easily recognizable in the litter due to their complete paralysis and exhibited identical phenotypes in all subsequent experiments. Embryos heterozygous for the Munc13-1 and Munc13-2 deletion, or heterozygous for the Munc13-1 deletion and homozygous for the Munc13-2 deletion were indistinguishable from wild type animals (not shown) and served as littermate controls in all subsequent analyses.

Animal preparation

For spinal cord preparations, E18.5 embryos were fixed by perfusion with 4% paraformaldehyde in phosphate buffer. The spinal cord (cervical levels 3-5) was then dissected out under a binocular. For diaphragm preparations, E18.5 embryos were

decapitated, and the ribcage was quickly isolated and fixed by immersion (2-12 h). Subsequently, the diaphragm muscle was taken out and further processed for staining.

Histology

In toto staining of E18.5 embryos for bone and cartilage was performed by immersion fixation of the eviscerated embryo in absolute ethanol (4 days) and then acetone (3 days). After several washes in water, embryos were stained for 10 days in a solution containing 0.015% alcian blue, 0.005% alizarin red, 5% acetic acid, and 93% ethanol. After washes in water, samples were kept in 20% glycerol/1% KOH for 16 h at 37°C, and then at room temperature until cleared. Samples were stored in 20% glycerol.

Western blotting

The presence of Munc13 isoforms at the NMJ was assessed by Western blotting of muscle membranes that were prepared as follows. The diaphragm muscles from 20 newborn mice were dissected out under a binocular and flash-frozen in liquid nitrogen. Diaphragms were then thawed, homogenized in buffer containing 20 mM HEPES pH 7.4, 150 mM NaCl, 2 mM EDTA, 2 mM EGTA, 300 mM sucrose, 0.2 mM PMSF, and 1 μg/ml Aprotinin, and centrifuged at 1,000 x g, 4°C for 10 min. The supernatant was further centrifuged at 15,000 x g, 4°C for 20 min, and the resulting pellet was resuspended in Laemmli sample buffer and analyzed in parallel with newborn mouse brain or lung homogenates (positive control) by SDS-PAGE (10 to 20 μg per lane). Blots were probed with Munc13 isoform-specific rabbit polyclonal antibodies that were raised against recombinant protein fragments (Munc13-1, residues 3-317; bMunc13-2, residues 1-305; ubMunc13-2, residues 182-407; Munc13-3, residues 294-574; BAP3, residues 9-181; Munc13-4, residues 889-1088).

Immunocytochemistry

50 μm-thick free-floating vibratome sections of the spinal cord were made at the cervical level and either stained for the vesicular acetylcholine transporter (vAChT) using a rabbit polyclonal antibody (1:500, Chemicon) or Nissl-stained. Free-floating diaphragms from mutant and control mice were incubated with α-Bungarotoxin-Alexa 568 (1:2000, Molecular Probes) or with antibodies against synapsin (rabbit polyclonal, 1:500, Synaptic Systems), or S-100 (Mouse monoclonal, 1:500, DAKO), to visualize acetylcholine receptors, presynaptic terminals, and Schwann cells, respectively. Acetylcholinesterase activity was visualized histochemically by incubation of the fixed diaphragms for 30 min at 37°C in 0.5 mM 5-bromoindoxyl acetate (23). All preparations were used as whole-mounts.

Imaging.

Fluorescent images were acquired on a Zeiss Axiovert 200-LSM 510 confocal laser scanning microscope, and bright-field images were obtained with a Camedia (Olympus) digital camera fixed on a Leica Binocular (for embryos) or a Zeiss Axiophot upright microscope (for Nissl staining). Alternatively, fluorescent and bright-field images were acquired on an Olympus BX61 microscope with an F-View (EsiVision) digital camera coupled to an image acquisition and analysis software (EsiVision).

Ultrastructural analysis

Ultrastructural investigation of the right phrenic nerve and whole diaphragm muscle synapses was carried out on samples that had been fixed by immersion with 4% paraformaldehyde and 0.5% glutaraldehyde and classically processed for epoxy-embedding with Durcupan (ACM, Fluka). 50-nm thick sections were contrasted and observed in a LEO912AB transmission electron microscope, and digital pictures taken with a Proscan CCD camera coupled to the EsiVision Software which was also used for quantitative analysis.

Electrophysiology

Ex vivo electrophysiological measurement of acetylcholine release was performed at 26-28°C on NMJs of diaphragm nerve-muscle preparations from Munc13-1/2-DKO, Munc13-1/2/3-TKO and control E18 embryos. Muscles were dissected and mounted in Ringer's medium (containing in mM: NaCl 116, KCl 4.5, $CaCl_2$ 2, $MgSO_4$ 1, NaH_2PO_4 1, $NaHCO_3$ 23, glucose 11, pH 7.4, pre-bubbled with 95% O_2 / 5% CO_2). Muscle fibres were impaled at the endplate region with a 20-40 MΩ glass capillary micro-electrode, connected to standard recording equipment (Plomp et al., 1992). Intracellular recordings of miniature endplate potentials (MEPPs), the spontaneous depolarizing events due to uniquantal acetylcholine release, were made at different NMJs within the muscle. The phrenic nerve was stimulated supramaximally via a suction electrode. The resulting muscle contraction was visually monitored and muscle action potentials, if present, were recorded. To be able to record evoked synaptic responses (endplate potentials, EPPs) in control preparations, muscle fibres were cut alongside the endplate region to induce depolarization to -20 - -40 mV (Barstad and Lilleheil, 1968). This inactivates Na^+ channels, so that muscle action potentials and the ensuing contractions no longer occur and the underlying EPP can be recorded. In Munc13-DKO/TKO muscles this procedure was not necessary because depolarization to -20 to -40 mV often occurred spontaneously after impalement with the micro-electrode. Munc13-DKO/TKO fibres were more fragile and thinner than controls and probably became damaged by the impalement. Also, synaptic recordings were much less disturbed by contraction of neighbouring fibres, because these were much less vigorous than in control muscles. From each NMJ 11-

144 responses to nerve stimulation at 0.3 Hz were recorded. The mean amplitudes of EPP and MEPP recorded at each NMJ were linearly normalized to -75 mV resting membrane potential. From the grand-mean values of each muscle, the number of acetylcholine vesicles released per nerve impulse, i.e. the quantal content, was calculated by dividing the mean EPP amplitude by the mean MEPP amplitude.

In intact control and Munc13-DKO/TKO muscles, MEPPs were recorded before and after application of 2.5 nM α-latrotoxin (Alomone Laboratories, Jerusalem, Israel) or 0.5 M sucrose, to probe the acetylcholine vesicle pool available for immediate release. In these experiments tetrodotoxin (1 μM, Sigma-Aldrich, Zwijn-

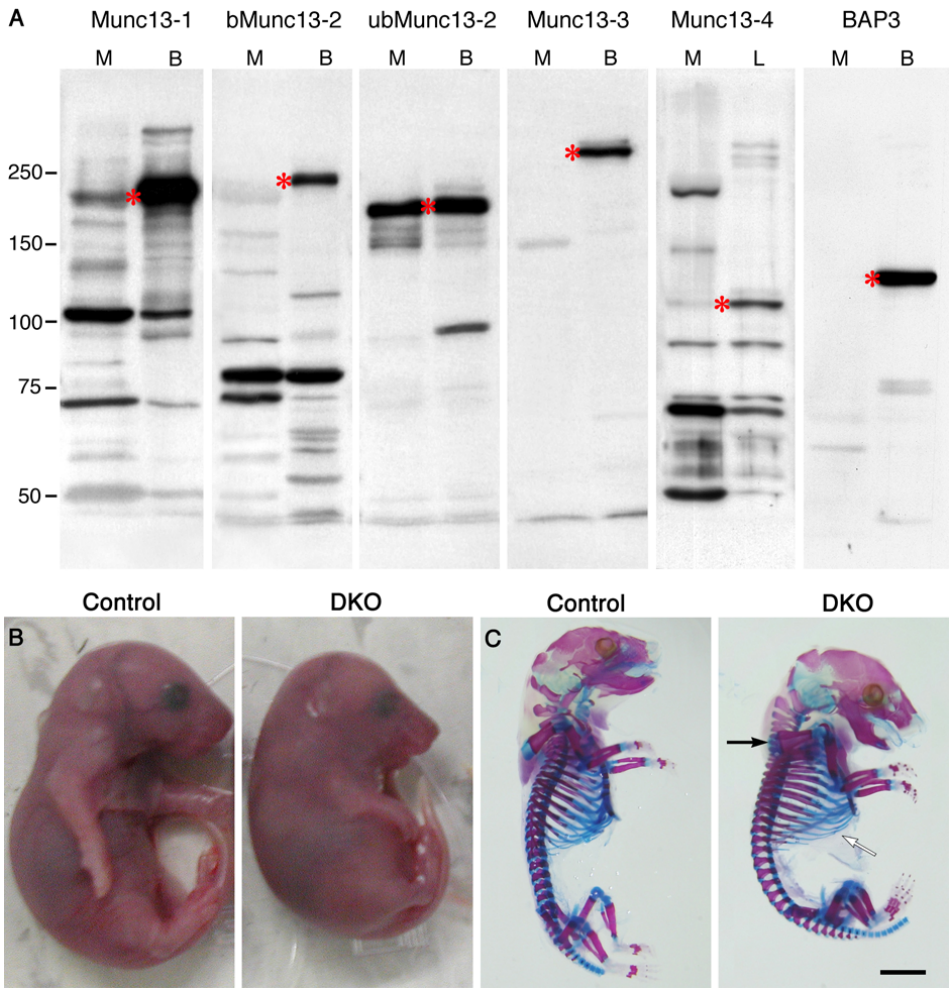

Figure 1. Munc13 isoforms at the neuromuscular junction and phenotypic alterations in the Munc13-1/2-DKO mouse mutant.
(A), Immunoblot analysis of muscle membrane extract ("M") with anti-Munc13-1, -b/ubMunc13-2, -Munc13-3, -Munc13-4 and -BAP3 isoform-specific antibodies. Brain ("B") or lung ("L") homogenates were used as positive control. (B,C), E18.5 Munc13-1/2-DKO mutant and control littermate mice gross morphology (B) and skeleton (C; bones are stained in blue and cartilage in pink). White arrow points to a broadened rib cage, black arrow to a stiffened neck and a compacted spinal cord. Scale bar: 3 mm.

drecht, The Netherlands) was added to reduce the spontaneous contractions of fibers which can occur in embryonic muscle. All electrophysiological data are given as group mean values ± S.E.M. with n as number of muscles per group and 1-20 NMJs sampled per muscle.

Results

Macroscopic phenotype of Munc13-1/2 double deficient mutants

Munc13-2 and Munc13-3 single mutant mice are viable, fertile, and show no abnormalities (Augustin et al., 2001; Varoqueaux et al., 2002), while Munc13-1 deficient mice die within a few hours after birth (Augustin et al., 1999b).

The Munc13-1/2 double deletion mutant mice (Munc13-1/2-DKO) and Munc13-1/2/3 triple deletion mutant mice (Munc13-1/2/3-TKO) studied here showed even stronger phenotypic alterations, whereas Munc13-2/3 double mutant mice (Munc13-2/3-DKO) were viable and fertile, indicating a dominant role of Munc13-1 in mice. Munc13-1/2-DKOs and Munc13-1/2/3-TKOs were morphologically indistinguishable from each other, and had identical phenotypes with respect to neuromuscular synaptic structure and function (see below). This could be due to the fact that NMJ axon terminals contain Munc13-1 and ubMunc13-2, but neither bMunc13-2 nor Munc13-3, as determined by Western blot analysis of muscle membrane preparations (Figure 1A). Therefore, results obtained from Munc13-1/2-DKOs and Munc13-1/2/3-TKOs were pooled and subsequently referred to as 'Munc13-1/2-DKO' for clarity. More distantly related Munc13 homologues are either faintly (Munc13-4; MW 112 kDa) or not detectable (BAP3; MW 125 kDa) in muscle membrane preparations (Figure 1A). Because Munc13-1/2-DKOs were often born dead, all experiments were carried out on E18.5 embryos, whose central and peripheral nervous systems are developed extensively and which can be recovered alive upon hysterectomy. Munc13-2-KO and Munc13-2/3-DKO littermates were used as controls as they were indistinguishable from wild type animals with respect to neuromuscular synaptic transmission.

Munc13-1/2-DKO embryos were completely paralyzed, did not breathe or respond to tactile stimulation, and had a very fragile appearance. They had a hunched posture (Figure 1B), and often showed hematomes along the spinal cord and on the skull. In the Munc13-1/2-DKO (Figure 1C), no developmental defect of the skeleton was detectable after in toto staining for bone and cartilage. However, the ribcage appeared larger and the vertebra more compact at the cervical level, probably reflecting a permanent paralysis of the embryo throughout development.

The total paralysis we observed in Munc13-1/2-DKO embryos indicated a profound defect at the NMJ in addition to the central nervous system dysfunction seen in these mice (Augustin et al., 1999b; Varoqueaux et al., 2002). To examine this in

more detail, we investigated the structure and function of the NMJ using the well characterized phrenic nerve/diaphragm muscle preparation as a model system.

Muscle morphology in Munc13-1/2 double deficient mutants

The fragile appearance of the Munc13-1/2-DKOs was paralleled by an abnormally thin musculature. In E18.5 embryos, the diaphragm muscle appeared fully developed along its rostro-caudal axis, but its outermost edges indicated an impaired lateral extension of myotubes (Figure 2A). Moreover, muscle fibers were not strictly aligned and formed intermingled bundles (Figure 2A). Muscle cells were more loosely attached to each other, on average smaller than in diaphragms of control littermates (muscle cell area: 389 ± 25 μm^2, n=104, control, vs. 136 ± 5 μm^2, n=227, Munc13-1/2-DKO), and exhibited centrally localized nuclei that had apparently not migrated to the cell periphery (Figure 2B), indicating a maturation delay or defect of some of the myotubes. In addition, many mostly oversized blood vessels ran throughout the diaphragm (Figure 2B), possibly due to a lack of muscle tone.

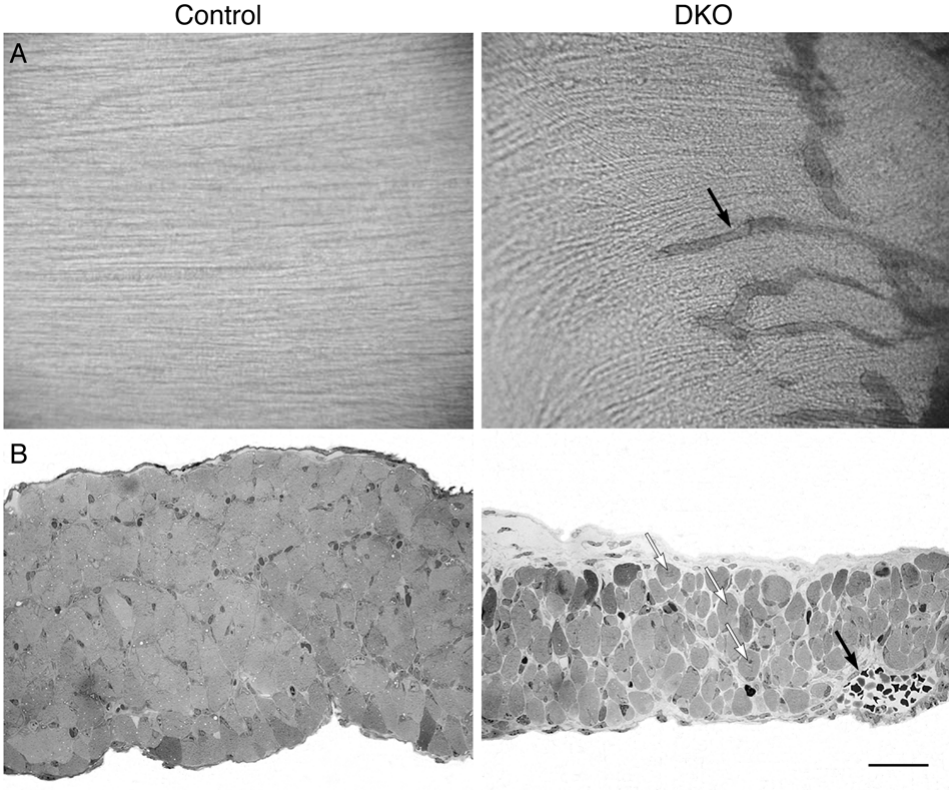

Figure 2. Impaired morphology of the Munc13-1/2-DKO diaphragm muscle.
(A,B), Detail of wholemount (A) and Nissl-stained semithin cross-section (B) of Munc13-1/2-DKO mutant and control littermate. Black arrows indicate oversized blood vessels, white arrows poorly differentiated myotubes. Scale bar: 100 μm in A, 30 μm in B.

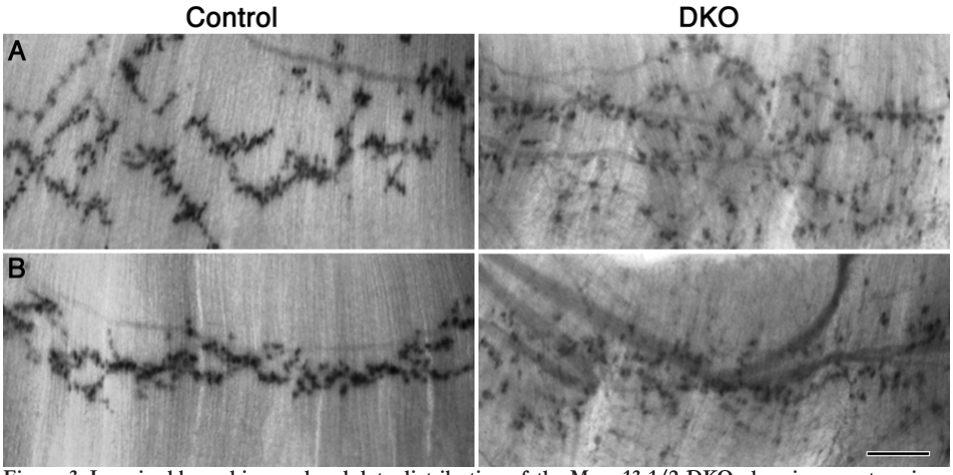

Figure 3. Impaired branching and endplate distribution of the Munc13-1/2-DKO phrenic nerve terminating onto the diaphragm surface.
(A,B), Detail of the left (A) and right (B) hemidiaphragms of Munc13-1/2-DKO mutant and control littermate, stained for acetylcholinesterase. Scale bar: 180 μm.

Diaphragm innervation in Munc13-1/2 double deficient mutants

The diaphragm is innervated by the left and right phrenic nerves, each of which branches and forms synapses that are typically organized in a discrete end-plate band within the central region of the respective hemidiaphragm. Using a whole-mount enzymatic staining for acetylcholinesterase, which is particularly abundant at the synaptic cleft, we observed regularly distributed synapses in both hemidiaphragms of control mice (Figure 3). In Munc13-1/2-DKOs however, the phrenic nerves exhibited an abnormally extensive branching throughout the muscle, and its terminal arborizations covered a much broader surface of the muscle (Figure 3). The acetylcholinesterase staining intensity in Munc13-1/2-DKO diaphragms, which correlates with the amount of acetylcholineesterase present at a given synapse, was slightly reduced as compared to control levels.

To further analyze the neuromuscular connectivity in Munc13-1/2-DKOs, combined immunostainings for synapsin-containing presynaptic terminals, α-bungarotoxin-binding acetylcholine receptors, and S-100-expressing Schwann cells were carried out. In control as well as in Munc13-1/2-DKO diaphragms, all axon terminals were juxtaposed to acetylcholine receptor clusters, and vice versa, and all terminals were ensheated by Schwann cells (Figure 4). However, acetylcholine receptor and synapsin stainings showed that motor endplate units in the Munc13-1/2-DKO diaphragm were only poorly aligned along the midline of the diaphragm and no longer confined to it, but rather distributed as a large array of clusters (Figure 4). Quantitative analyses showed that the area occupied by endplates (as defined by α-bungarotoxin labeled acetylcholine receptor clusters) at the midline of the diaphragm was larger in the Munc13-1/2-DKO than in the control mice (4984 ± 1150

μm^2 per 0.2 mm^2, n=5, in Munc13-1/2-DKOs vs. 2144 ± 436 μm^2 per 0.2 mm^2, n=5, in control mice, $p<0.05$). In addition, the number of synapses was clearly increased in the Munc13-1/2-DKO diaphragms mouse (not shown).

Cytoarchitecture of the spinal cord and morphology of the phrenic nerve in Munc13-1/2 double deficient mutants

The phrenic motor neuron cell bodies that innervate the diaphragm are located at cervical levels C3-C5 of the spinal cord, and typically undergo massive apoptosis around E15-17 in the rat and mouse embryo (Harris and McCaig, 1984; Allan and Greer, 1997). We analyzed the number of the large cell body phrenic motor neurons in control and Munc13-1/2-DKO mice in Nissl-stained vibratome sections. We found that at all cervical levels these motor neuron groups in the ventral horn were larger in Munc13-1/2-DKOs and contained more cells than the corresponding areas in control sections (Figure 5A). No sign of degeneration was detectable in dorsal root ganglia (not shown). Motor neuron somata receive a specific recurrent cholinergic innervation which we visualized by immunostaining for the vesicular acetylcholine transporter vAChT. Cholinergic terminals in the ventral horn of cervical levels C3-C5 in the Munc13-1/2-DKO showed a density that was comparable to that in control sections, but were covering a larger area of the ventral horn, again indicating an abnormally large population of motor neurons in the mutant (Figure 5B). Low magnification ultrastructural analysis of phrenic nerves showed that as a result of the increased motor neuron number in Munc13-1/2-DKOs, the nerves were larger and contained more axons (367 ± 27, n=6, in Munc13-1/2-DKO vs. 213 ± 16, n=8, in controls, $p<0.001$) (Figure 5C,D). This mutant phenotype was accompanied by an increased number of Schwann cell bodies (44 ± 5.8, n=3, in Munc13-1/2-DKO vs. 27 ± 1.5, n=3, in controls, $p<0.05$), but the extent of axon myelinization was similar in control and Munc13-1/2-DKO nerves (not shown).

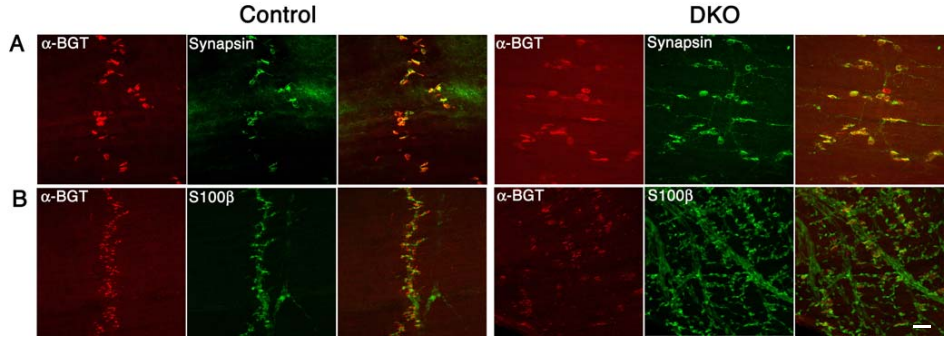

Figure 4. Normal apposition of presynaptic, postsynaptic, and glial elements at the Munc13-1/2-DKO motor endplate.
(A, B), Confocal micrographs of Munc13-1/2-DKO mutant and control littermate, double-immunostained for α-bungarotoxin (to visualize acetylcholine receptors) and synapsin (as a marker for presynapses) (A) or S-100 (as a marker for Schwann cells) (B). Scale bar: 90 μm in A, 190 μm in B.

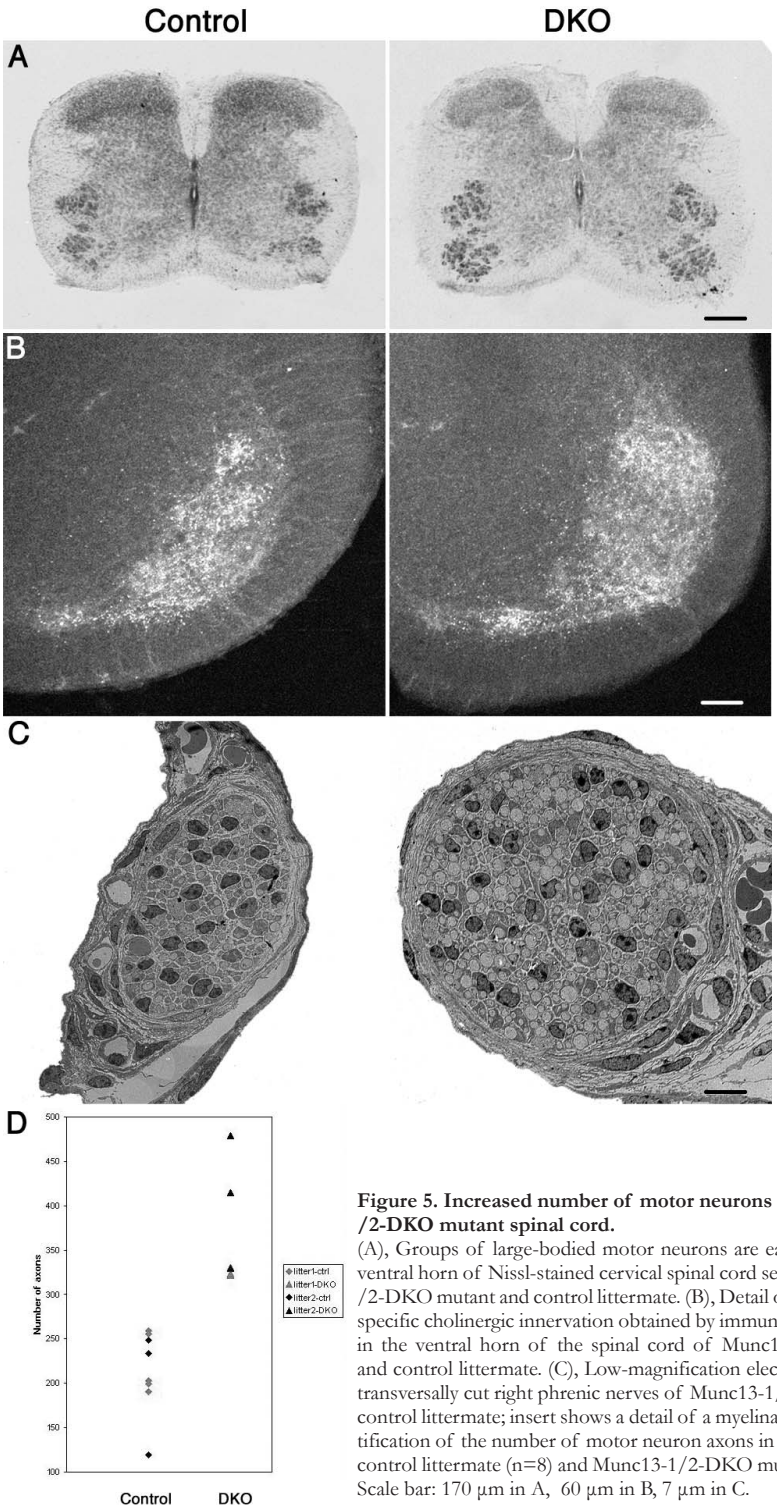

Figure 5. Increased number of motor neurons in the Munc13-1-/2-DKO mutant spinal cord.
(A), Groups of large-bodied motor neurons are easily identified in the ventral horn of Nissl-stained cervical spinal cord sections of Munc13-1-/2-DKO mutant and control littermate. (B), Detail of the motor neuron-specific cholinergic innervation obtained by immunostaining for vAChT in the ventral horn of the spinal cord of Munc13-1/2-DKO mutant and control littermate. (C), Low-magnification electron micrographs of transversally cut right phrenic nerves of Munc13-1/2-DKO mutant and control littermate; insert shows a detail of a myelinated axon; (D), Quantification of the number of motor neuron axons in the phrenic nerve of control littermate (n=8) and Munc13-1/2-DKO mutant embryos (n=6). Scale bar: 170 μm in A, 60 μm in B, 7 μm in C.

Electrophysiological properties of neuromuscular synaptic transmission in Munc13-1/2-DKO mice

We investigated the characteristics of synaptic transmission at the NMJ of Munc13-1/2-DKOs and Munc13-1/2/3-TKOs. As predicted by the lack of Munc13-3 immunoreactivity in NMJ terminals, our analyses showed no difference between Munc13-1/2-DKOs (n=13) and Munc13-1/2/3-TKOs (n=3). Therefore, as for morphological observations, data from Munc13-1/2-DKOs and Munc13-1/2/3-TKOs were subsequently pooled.

Surprisingly, and in contrast to glutamatergic and GABAergic synapses in hippocampal neurons, intracellular recordings of MEPPs revealed that neurotransmitter release is not completely abolished at the NMJs of Munc13-1/2-DKOs. MEPP amplitude (2.89 ± 0.28 mV, n=15 muscles) was not statistically significantly different from control embryos (2.96 ± 0.28 mV, n=15, p=0.86), and MEPP frequency was more than doubled in Munc13-1/2-DKOs (4.42 ± 0.60 per min, n=15), as compared to controls (1.80 ± 0.34 per min, n=15, $p<0.001$, Figure 6A). α-Latrotoxin elicits massive asynchronous uniquantal acetylcholine release through exocytosis from all synaptic vesicles that are fusion-competent and therefore are probably in a primed state. Application of this toxin revealed that this type of neurotransmitter release is strongly impaired at NMJs of Munc13-1/2-DKO embryos. MEPP frequency was 591 ± 137 per min (n=8) in Munc13-1/2-DKO and 1996 ± 500 per min (n=7, $p<0.05$) in control NMJs (Figure 6B). MEPP amplitudes were similar in Munc13-1/2-DKO (4.00 ± 0.6 mV, n=6) and controls (2.81± 0.30 mV, n=7, p=0.09). Like α-latrotoxin, application of hypertonic sucrose solution, which triggers the release of fusion-competent synaptic vesicles, induced much lower MEPP frequencies in Munc13-1/2-DKO (144 ± 66 per min, n=5) as compared to controls (619 ± 100 per min, n=7, $p<0.01$) (Figure 6C). Unexpectedly, sucrose treatment reduced MEPP amplitude to 1.33 ± 0.24 mV, n=5, compared to 3.35 ± 0.23 mV, n=7, in the controls. Thus, the asynchronous uniquantal acetylcholine release induced by α-latrotoxin or hypertonic shock is severely reduced at Munc13-1/2-DKO NMJs.

We stimulated the phrenic nerve at 0.3 and 20 Hz through a suction electrode to evoke acetylcholine release by nerve impulses. The resulting muscle contractions were monitored visually through the microscope. We observed a robust contraction of the whole control muscle preparation, involving all muscle fibres, which was well sustained at 20 Hz. However, contraction of Munc13-1/2-DKO preparations was much weaker because not all fibres contracted and was not very well sustained at 20 Hz. This indicated that presynaptic transmitter release can at least to some extent induce postsynaptic action potentials in these mutants (Figure 6D). EPPs were recorded in depolarized fibres. In 77.1 ± 4.0% of the cases (n=12), evoked stimulation failed to induce an EPP in the muscle fibers of Munc13-1/2-DKOs, while in con-

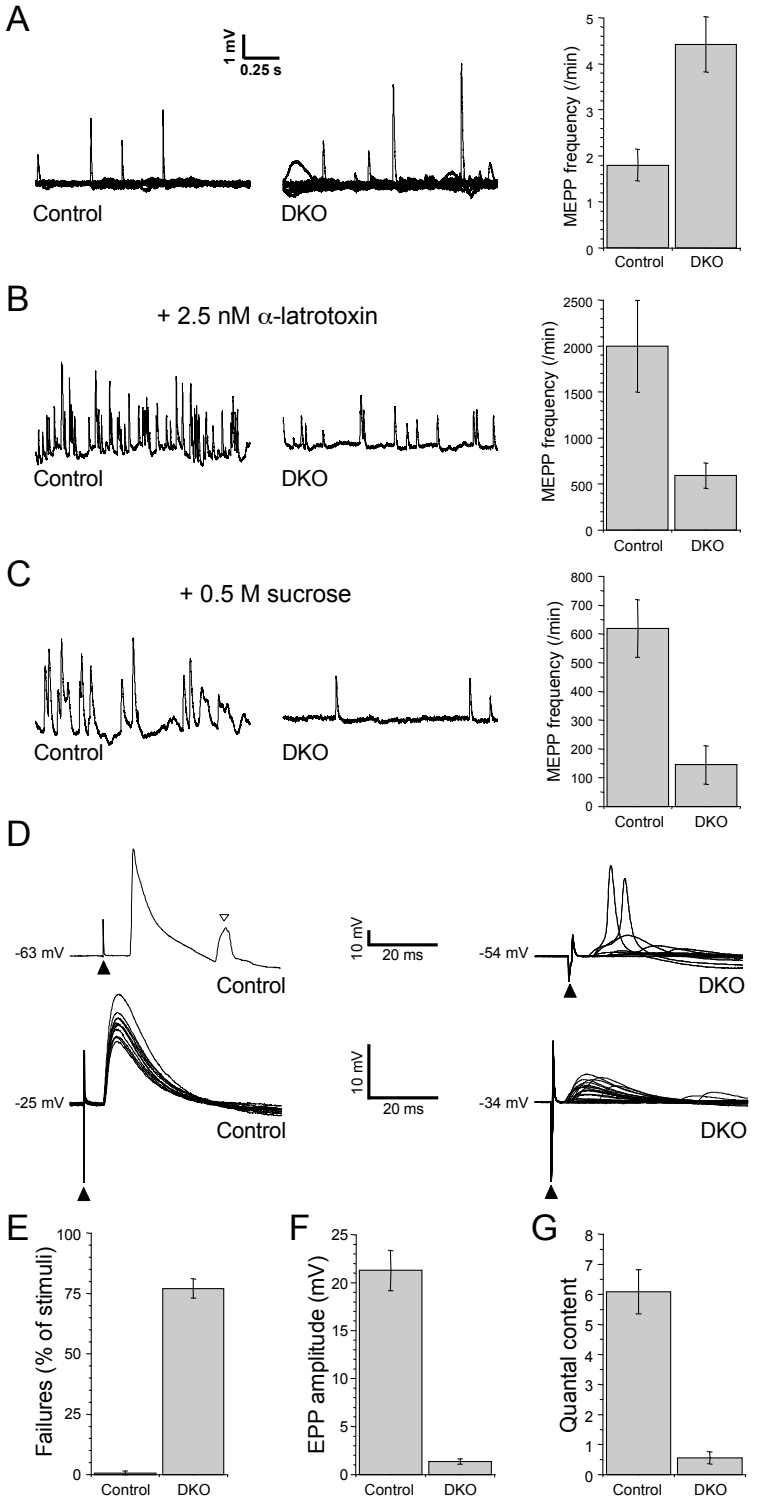
A
1 mV
0.25 s
Control
DKO
MEPP frequency (/min)
Control
DKO
B
+ 2.5 nM α-latrotoxin
Control
DKO
MEPP frequency (/min)
Control
DKO
C
+ 0.5 M sucrose
Control
DKO
MEPP frequency (/min)
Control
DKO
D
-63 mV
Control
10 mV
20 ms
-54 mV
DKO
-25 mV
Control
10 mV
20 ms
-34 mV
DKO
E
Failures (% of stimuli)
Control
DKO
F
EPP amplitude (mV)
Control
DKO
G
Quantal content
Control
DKO

Figure 6. Strongly reduced acetylcholine release evoked by nerve impulses, α-latrotoxin, or hypertonic medium at Munc13-1/2-DKO NMJs.
Bar graphs display the group mean values ± S.E.M (n=5-15 embryos, 1-21 NMJs sampled per muscle). (A), Spontaneous uniquantal acetylcholine release, MEPPs, recorded in normal Ringer's medium. Superimposed example traces show the MEPPs observed during a 135 s measuring period. (B), MEPPs recorded in the presence of 2.5 nM α-latrotoxin. (C), MEPPs recorded in the presence of 0.5 M sucrose-Ringer. (D), Examples of nerve stimulation evoked responses. The moment of phrenic nerve stimulation is indicated with a black triangle. At relative hyperpolarized membrane potentials, a full-size muscle action potential is elicited in control muscle (upper left), leading to contraction that is visible as an artifact on the signal (indicated by open triangle). At Munc13-1/2-DKO NMJs, subthreshold and delayed EPPs and failures were observed (upper right), sometimes leading to delayed muscle action potentials. Subsequent traces (0.3 Hz stimulation) have been superimposed. At depolarized muscle fibres, EPPs become unmasked. At control NMJs, no failures were observed at 0.3 Hz stimulation (bottom left), while at Munc13-1/2-DKO NMJs there were many failures and very small, delayed EPPs. (E), Percentage of stimuli leading to failures. F, EPP amplitude, normalized to 75 mV membrane potential, failures taken into account. (G), Quantal content, i.e. the number of acetylcholine quanta release upon a single nerve impulse.

trols, only 0.7 ± 0.7% (n=6) failures were observed (Figure 6D, E). In the Munc13-1/2-DKO, stronger variability in the delay between the time of nerve stimulation and EPP-ocurrence was observed (Figure 6D). The amplitude of the evoked EPP was significantly smaller in Munc13-1/2-DKO (5.52 ± 0.46 mV, without failures taken into account; 1.34 ± 0.26 mV, with failures taken into account; n=12) than in control NMJs (21.40 ± 2.10 mV, n=6, $p<0.001$) (Figure 6F). The calculated quantal content was decreased by 81%, from 6.09 ± 0.74 (n=6) in control NMJs to 0.56 ± 0.20 (n=6) in the Munc13-1/2-DKO NMJ (Figure 6G). Thus, nerve impulse-evoked acetylcholine release is dramatically reduced at Munc13-1/2-DKO NMJs.

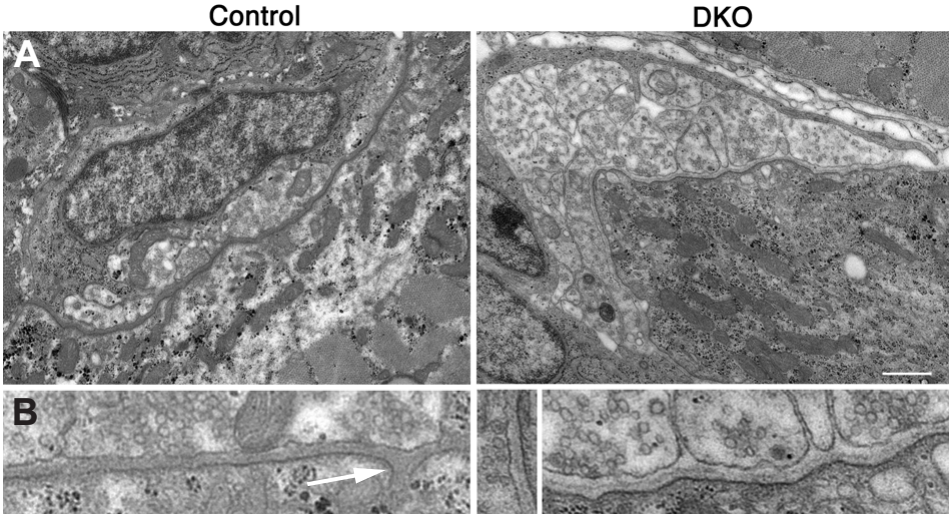

Figure 7. Immature but well-formed neuromuscular synapses in the Munc13-1/2-DKO mutant.
Electron micrographs of representative motor endplates in Munc13-1/2-DKO mutant and control littermate. At low magnification (A), Munc13-1/2-DKO motor endplates are always composed of more presynaptic elements, containing numerous small synaptic vesicles, than the littermate ones. In either case, magnified areas of the synaptic active zone (B) allow to recognize small synaptic vesicles docked at the active zone membrane, large dense-core vesicles, clathrin-coated vesicles, and an intact basal lamina. However, the postsynaptic membrane of the Munc13-1/2-DKO muscle cell fails to develop secondary folds that normally accompany the maturation process of neuromuscular synapses (arrow in control). Scale bar: 700 nm in upper panels, 220 nm in lower panels.

Ultrastructural characteristics of NMJs in Munc13-1/2 double deficient mutants

At the ultrastructural level, well-formed synapses were observed in both control animals and Munc13-1/2-DKOs. Synapses in the mutants tended to contain more boutons than control synapses, which may be a correlate of the increased complexity of innervation and the larger endplate size observed in the mutants at the light microscopic level (Figure 4). Synaptic boutons at NMJs of Munc13-1/2-DKOs contained normal sized small synaptic vesicles, but also dense core and clathrin-coated vesicles (Figure 7). Boutons in mutant synapses were aligned with postsynaptic densities in muscle cells and exhibited clusters of small synaptic vesicles that were occasionally observed along the plasma membrane or docked at the active zone (Figure 7, insert). Pre- and postsynaptic membranes were continuously juxtaposed to each other and separated by a well-developed basal lamina. In the control samples, many synapses showed junctional folds reflecting a normal maturation process. In contrast, small invaginations, but no deep folds were observed at the postsynaptic membranes of NMJs in Munc13-1/2-DKOs (Figure 7, insert).

Discussion

The functional relevance of differential Munc13 protein expression at the NMJ

Munc13-1, -2, and -3 are essential for synaptic vesicle priming in central synapses. Data on the priming activity of N-terminally truncated Munc13-1 fragments (Ashery et al., 2000) indicate that the evolutionarily conserved domain structure in Munc13-1, -2, and -3 and the related Munc13-4 (Koch et al., 2000) and BAP3 (Shiratsuchi et al., 1998) proteins, which consists of two Munc13-homology domains (MHDs) flanked by two C2 domains, acts as the minimal priming module. This module covers most of the C-terminal two thirds of Munc13-1/2/3 (Brose et al., 2000), and is thought to mediate Munc13 priming activity by binding to (Betz et al., 1997) and regulating the function of syntaxins (Richmond et al., 2001). Differences between members of the Munc13 protein family with respect to their priming activity or the fusion reaction they regulate could be due to the type of syntaxin-like SNARE protein their minimal priming module interacts with.

We found the murine NMJ to contain Munc13-1 and ubMunc13-2, but not bMunc13-2, Munc13-3, or the more distantly related BAP3, and only trace amounts of Munc13-4. The two Munc13 isoforms expressed at the NMJ are the most closely related Munc13 variants. In contrast to other family members, they do not only share the highly conserved C-terminal region but also have highly homologous N-terminal regions which contain a C2 domain that binds the active zone components RIM1 and RIM2 (Betz et al., 2001) and a calmodulin binding site (Junge et al., 2004). Thus, Munc13-1 and ubMunc13-2 may interact with the same protein partners and have similar basic functions, and mutual compensation upon loss of one of the two isoforms is highly likely at the NMJ, as was also reported for hippocampal GABAer-

gic synapses (Varoqueaux et al., 2002). Nevertheless, Munc13-1 and ubMunc13-2 differentially modulate short-term plasticity at hippocampal synapses (Rosenmund et al., 2002; Junge et al., 2004), and their coexpression at the NMJ may allow for the tuning of presynaptic molecular mechanisms over a wide range of synaptic activity rates in order to guarantee high fidelity of synaptic transmission.

Using the diaphragm NMJ as a model system, we found that upon genetic deletion of Munc13s (Munc13-1, -2, and -3) and in the absence of significant levels of the related Munc13-4 and BAP3 proteins, evoked synaptic transmission is strongly reduced while spontaneous release persists, and the NMJ system exhibits all classical developmental aberrations that are typically observed upon complete block of spontaneous and evoked synaptic transmission (Misgeld et al., 2002; Brandon et al., 2003). In the light of previous studies on the function of Munc13s at central synapses, two of our findings at the NMJ are very unexpected: (i) Synaptic vesicle priming in the NMJ appears to be partially independent of bona fide Munc13s (Munc13-1, -2, and -3), and (ii) despite the quite large spontaneous transmitter release activity at Munc13-1/2-DKO NMJs, the innervation of the diaphragm exhibits the same developmental aberrations that are also observed in the complete absence of NMJ synaptic transmission (Misgeld et al., 2002; Brandon et al., 2003).

Munc13 independent synaptic vesicle priming at the NMJ

Synaptic transmission at glutamatergic and GABAergic synapses of murine hippocampal neurons is strictly dependent on the presence of Munc13-1 and -2. Munc13-3, Munc13-4 or BAP3 do not functionally replace Munc13-1 and -2 in these synapses (Varoqueaux et al., 2002). Likewise, spontaneous and evoked transmitter release at the cholinergic NMJ in *C. elegans* is entirely blocked in worms carrying the complete loss-of-function allele of unc-13, unc-13(s69) (Richmond et al., 1999), although an Unc-13 homologue similar to BAP3 and Munc13-4 (Koch et al., 2000) is most likely present. In contrast, at murine NMJs lacking Munc13s, spontaneous transmitter release persists and some evoked transmitter release is elicitable. It is unlikely that trace amounts of Munc13-4 or BAP3 mediate the residual synaptic vesicle priming at these mutant NMJs because even robust levels of BAP3 are not sufficient to ameliorate the Munc13 deficient mutant phenotype in hippocampal synapses (Varoqueaux et al., 2002), and Munc13-4 does not bind to RIM (Koch et al., 2000). Apart from Munc13-4 and BAP3, CAPS proteins (i.e. CAPS1 and CAPS2 in mammals) have been proposed to be priming proteins (Berwin et al., 1998; Tandon et al., 1998; Koch et al., 2000; Renden et al., 2001). However, CAPS proteins do not compensate the loss of Munc13s from hippocampal neurons in spite of strong expression at their synaptic terminals (Varoqueaux et al., 2002; Speidel et al., 2003), and are therefore also unlikely to support synaptic vesicle priming in NMJs.

As the murine and human genomes do not contain any additional genes with homology to Munc13s, our findings indicate that some vesicle priming at the NMJ occurs in the absence of Munc13s and that therefore either non-Munc13 priming proteins must exist or vesicle priming at the NMJ can occur in part spontaneously without priming proteins. Vesicle priming independent of Munc13-1, -2, and -3 has previously been suggested to occur in chromaffin cells (Ashery et al., 2000). According to the current molecular model, Munc13s mediate synaptic vesicle priming by stabilizing the open conformation of the SNARE syntaxin 1, thereby allowing the formation of SNARE dimers containing syntaxin 1 and SNAP25 or of trans SNARE complexes (Brose et al., 2000; Richmond et al., 2001; Fasshauer, 2003). Constitutive SNARE-mediated intracellular and secretory membrane fusion reactions do not require a Munc13-like priming step, *Saccharomyces cerevisiae* does not express homologues of Munc13-1, -2, -3, -4 or BAP3 (Koch et al., 2000), and bona fide Munc13s first appear during evolution in organisms with a central nervous system (Koch et al., 2000), indicating that Munc13 independent spontaneous SNARE priming does occur. It is likely that synaptic vesicle exocytosis at the mouse NMJ involves in part a syntaxin variant or other SNARE complex components such as SNAP23 that are less dependent on Munc13s stabilizing the open conformation of syntaxin, with the consequence that some vesicle priming indeed occurs spontaneously.

The SNARE protein complement of murine NMJs is only partially known. NMJs lacking SNAP25 exhibit increased spontaneous transmitter release but lack evoked release (Washbourne et al., 2002). It is possible that spontaneous release in SNAP25 KO mutants is due to the presence of SNAP23, which can partly replace SNAP25 but has strikingly different functional features (Sorensen et al., 2003). Essentially, our data and the published account in the literature are best compatible with a scenario according to which Munc13-mediated vesicle priming is essential for a majority of synaptic vesicles at NMJs, while a small subpopulation of vesicles can undergo spontaneous priming. This would explain why in the absence of Munc13-1, -2, and -3 evoked transmitter release is strongly reduced while spontaneous release persists. The increase in the frequency of spontaneous release events seen in SNAP25 KO (Washbourne et al., 2002) and Munc13-1/2-DKO NMJs may then simply be due to the increased number of synapses formed in these mutant NMJs.

The importance of synaptic activity for NMJ formation

The phenotypic alterations seen at the Munc13-1/2-DKO NMJ are similar to those reported for the ChAT-deficient mouse NMJ, in which synaptic vesicles are no longer loaded with acetylcholine (Misgeld et al., 2002; Brandon et al., 2003). The same type of abnormal nerve arborizations and disorganized termination areas with more/

larger synaptic endplates is also seen in SNAP25-deficient NMJs (Washbourne et al., 2002).

Functionally, the Munc13-1/2/3 and SNAP25 KO mice differ from ChAT KO mutants in various aspects. In the ChAT KO, transmission is blocked at the NMJ, while motor neuron cell bodies receive functionally normal synaptic inputs. In the Munc13-1/2-DKO and SNAP25 KO, synaptic transmission at spinal cord synapses is either abolished (not shown) or strongly reduced. This situation is similar to that described for Munc18-1 deletion mutant mice which are characterized by a complete lack of spontaneous and evoked transmitter release at the NMJ as well as at central snyapses (Verhage et al., 2000; Heeroma et al., 2003; Bouwman et al., 2004). In these mutants, motor neurons form synaptic contacts very transiently in early embryonal life and soon thereafter degenerate and retract axonal processes (Jahn et al., 2003). This phenomenon, which is not seen in ChAT KOs (Misgeld et al., 2002; Brandon et al., 2003) or Munc13-1/2-DKOs, was explained by the lack of synaptic signaling onto motor neurons in Munc18-1 mutants (Heeroma et al., 2003). However, given the fact that in Munc13-1/2-DKOs no motor neuron degeneration is seen despite a complete shut-down of synaptic transmission onto these neurons, this explanation may be wrong. Rather, the role of Munc18-1 may extend to the regulation of intracellular membrane trafficking events necessary for neuronal survival or of developmentally earlier and more general secretory events whose impairment dramatically compromises neuronal survival (e.g. neurotrophin signaling). As a consequence, Munc18-1 may exert a more stringent control of exocytosis at the NMJ, abolishing not only fast synaptic transmission but also the secretion of neuroactive peptides, neurotrophic factors, or hormones. In contrast, Munc13-1/2/3 deletion still allows for the fusion of a small population of synaptic and peptidergic vesicles, and ChAT deletion still permits the release of transmitter-deficient vesicles that contain neuroactive or neurotrophic peptides. These may influence synapse formation, synapse maintenance, and neuronal survival (Misgeld et al., 2002; Brandon et al., 2003).

The increased number of motor neurons in the spinal cord of Munc13-DKOs is presumably due to a cessation of their apoptosis, which occurs normally around E15-E17 (Harris and McCaig, 1984; Allan and Greer, 1997). As mentioned above, this blockade of apoptosis is unlikely to result from a block of synaptic signaling in the spinal cord. Instead, it might be due to the local malfunction of the NMJ, thus influencing the well-described process of embryonic synapse elimination that usually leads to the consolidation of only one axon/endplate per muscle fiber (Lichtman and Colman, 2000; Buffelli et al., 2002; Buffelli et al., 2003; Kasthuri and Lichtman, 2003).

Spontaneous action potentials, which typically occur in motor neurons during development (Hanson and Landmesser, 2003), are likely to be important for shaping nerve-muscle connectivity. They originate from either the spiking of premotor

interneurons or the coordinated quantal neurotransmitter release from motor neurons, which is unlikely to occur in Munc13-1/2-DKO embryos. Thus, muscle action potentials and contractions driven by action potentials in motor neurons are unlikely to take place in vivo in the Munc13-DKO embryo, despite the fact that stimulation of the cut phrenic nerve can elicit action potentials and evoke some contractile response. Similarly, ChAT and SNAP25 deficiencies presumably lead to the elimination of muscle activation driven by motor neuron action potentials. Given that all three mutants exhibit the same phenotype with respect to motor neuron survival and refinement of NMJ connectivity, we conclude that the proper development of motor neurons and NMJs does not depend on a trophic action of spontaneous quantal acetylcholine release. Rather, successful and reliable action potential driven postsynaptic depolarizations, which can even occur spontaneously during development, appear to be necessary to regulate motor neuron survival and shape mature NMJs.

It is likely that retrograde signaling from the muscle to the innervating motor neuron is involved in the effects of these action potential driven synaptic events on motor neuron number and NMJ morphology. Interestingly, a pattern of connectivity similar to the one found in Munc13-1/2-DKO NMJs is seen in MyoD deficient mice. Here, the abnormal branching must be due to an impaired retrograde signaling because MyoD is a muscle-specific transcription factor (Wang et al., 2003). In addition, the phenotypes of Rapsyn- and MuSK-deficient mice, which show the same aberrant motor neuron survival seen in Munc13-1/2-DKOs and ChAT KOs (Terrado et al., 2001; Banks et al., 2001), indicate a role of retrograde signaling from muscle in motor neuron survival. By analogy, it is possible that impaired transmission at the Munc13-, ChAT-, or SNAP25-deficient NMJ affects muscle electrical activity, thereby influencing the levels of myogenic regulatory factors or other signaling molecules and, in turn, retrograde signalling.

Reference List

Allan DW, Greer JJ (1997) Development of phrenic motoneuron morphology in the fetal rat. J Comp Neurol 382: 469-479.

Aravamudan B, Fergestad T, Davis WS, Rodesch CK, Broadie K (1999) *Drosophila* UNC-13 is essential for synaptic transmission. Nat Neurosci 2: 965-971.

Ashery U, Varoqueaux F, Voets T, Betz A, Thakur P, Koch H, Neher E, Brose N, Rettig J (2000) Munc13-1 acts as a priming factor for large dense-core vesicles in bovine chromaffin cells. EMBO J 19: 3586-3596.

Augustin I, Betz A, Herrmann C, Jo T, Brose N (1999a) Differential expression of two novel Munc13 proteins in rat brain. Biochem J 337 (Pt 3): 363-371.

Augustin I, Korte S, Rickmann M, Kretzschmar HA, Sudhof TC, Herms JW, Brose N (2001) The cerebellum-specific Munc13 isoform Munc13-3 regulates

cerebellar synaptic transmission and motor learning in mice. J Neurosci 21: 10-17.

Augustin I, Rosenmund C, Sudhof TC, Brose N (1999b) Munc13-1 is essential for fusion competence of glutamatergic synaptic vesicles. Nature 400: 457-461.

Banks GB, Chau TN, Bartlett SE, Noakes PG (2001) Promotion of motoneuron survival and branching in rapsyn-deficient mice. J Comp Neurol 429: 156-165.

Barstad JA, Lilleheil G (1968) Transversaly cut diaphragm preparation from rat. An adjuvant tool in the study of the physiology and pbarmacology of the myoneural junction. Arch Int Pharmacodyn Ther 175: 373-390.

Berwin B, Floor E, Martin TF (1998) CAPS (mammalian UNC-31) protein localizes to membranes involved in dense-core vesicle exocytosis. Neuron 21: 137-145.

Betz A, Okamoto M, Benseler F, Brose N (1997) Direct interaction of the rat unc-13 homologue Munc13-1 with the N terminus of syntaxin. J Biol Chem 272: 2520-2526.

Betz A, Thakur P, Junge HJ, Ashery U, Rhee JS, Scheuss V, Rosenmund C, Rettig J, Brose N (2001) Functional interaction of the active zone proteins Munc13-1 and RIM1 in synaptic vesicle priming. Neuron 30: 183-196.

Bouwman J, Maia AS, Camoletto PG, Posthuma G, Roubos EW, Oorschot VM, Klumperman J, Verhage M (2004) Quantification of synapse formation and maintenance in vivo in the absence of synaptic release. Neuroscience 126: 115-126.

Brandon EP, Lin W, D'Amour KA, Pizzo DP, Dominguez B, Sugiura Y, Thode S, Ko CP, Thal LJ, Gage FH, Lee KF (2003) Aberrant patterning of neuromuscular synapses in choline acetyltransferase-deficient mice. J Neurosci 23: 539-549.

Brenner S (1974) The genetics of *Caenorhabditis elegans*. Genetics 77: 71-94.

Brose N, Hofmann K, Hata Y, Sudhof TC (1995) Mammalian homologues of *Caenorhabditis elegans* unc-13 gene define novel family of C2-domain proteins. J Biol Chem 270: 25273-25280.

Brose N, Rosenmund C, Rettig J (2000) Regulation of transmitter release by Unc-13 and its homologues. Curr Opin Neurobiol 10: 303-311.

Buffelli M, Burgess RW, Feng G, Lobe CG, Lichtman JW, Sanes JR (2003) Genetic evidence that relative synaptic efficacy biases the outcome of synaptic competition. Nature 424: 430-434.

Buffelli M, Busetto G, Cangiano L, Cangiano A (2002) Perinatal switch from synchronous to asynchronous activity of motoneurons: link with synapse elimination. Proc Natl Acad Sci U S A 99: 13200-13205.

Dulubova I, Sugita S, Hill S, Hosaka M, Fernandez I, Sudhof TC, Rizo J (1999) A conformational switch in syntaxin during exocytosis: role of munc18. EMBO J 18: 4372-4382.

Fasshauer D (2003) Structural insights into the SNARE mechanism. Biochim Biophys Acta 1641: 87-97.

Hanson MG, Landmesser LT (2003) Characterization of the circuits that generate spontaneous episodes of activity in the early embryonic mouse spinal cord. J Neurosci 23: 587-600.

Harris AJ, McCaig CD (1984) Motoneuron death and motor unit size during embryonic development of the rat. J Neurosci 4: 13-24.

Heeroma JH, Plomp JJ, Roubos EW, Verhage M (2003) Development of the mouse neuromuscular junction in the absence of regulated secretion. Neuroscience 120: 733-744.

Jahn R, Lang T, Sudhof TC (2003) Membrane fusion. Cell 112: 519-533.

Junge HJ, Rhee JS, Jahn O, Varoqueaux F, Spiess J, Waxham MN, Rosenmund C, Brose N (2004) Calmodulin and Munc13 form a Ca2+ sensor/effector complex that controls short-term synaptic plasticity. Cell 118: 389-401.

Kasthuri N, Lichtman JW (2003) The role of neuronal identity in synaptic competition. Nature 424: 426-430.

Koch H, Hofmann K, Brose N (2000) Definition of Munc13-homology-domains and characterization of a novel ubiquitously expressed Munc13 isoform. Biochem J 349: 247-253.

Lackner MR, Nurrish SJ, Kaplan JM (1999) Facilitation of synaptic transmission by EGL-30 Gqalpha and EGL-8 PLCbeta: DAG binding to UNC-13 is required to stimulate acetylcholine release. Neuron 24: 335-346.

Lichtman JW, Colman H (2000) Synapse elimination and indelible memory. Neuron 25: 269-278.

Misgeld T, Burgess RW, Lewis RM, Cunningham JM, Lichtman JW, Sanes JR (2002) Roles of neurotransmitter in synapse formation: development of neuromuscular junctions lacking choline acetyltransferase. Neuron 36: 635-648.

Plomp JJ, van Kempen GT, Molenaar PC (1992) Adaptation of quantal content to decreased postsynaptic sensitivity at single endplates in alpha-bungarotoxin-treated rats. J Physiol 458: 487-499.

Renden R, Berwin B, Davis W, Ann K, Chin CT, Kreber R, Ganetzky B, Martin TF, Broadie K (2001) *Drosophila* CAPS is an essential gene that regulates dense-core vesicle release and synaptic vesicle fusion. Neuron 31: 421-437.

Rettig J, Neher E (2002) Emerging roles of presynaptic proteins in Ca++-triggered exocytosis. Science 298: 781-785.

Rhee JS, Betz A, Pyott S, Reim K, Varoqueaux F, Augustin I, Hesse D, Sudhof TC, Takahashi M, Rosenmund C, Brose N (2002) Beta phorbol ester- and diacylglycerol-induced augmentation of transmitter release is mediated by Munc13s and not by PKCs. Cell 108: 121-133.

Richmond JE, Davis WS, Jorgensen EM (1999) UNC-13 is required for synaptic vesicle fusion in *C. elegans*. Nat Neurosci 2: 959-964.

Richmond JE, Weimer RM, Jorgensen EM (2001) An open form of syntaxin bypasses the requirement for UNC-13 in vesicle priming. Nature 412: 338-341.

Rosenmund C, Rettig J, Brose N (2003) Molecular mechanisms of active zone function. Curr Opin Neurobiol 13: 509-519.

Rosenmund C, Sigler A, Augustin I, Reim K, Brose N, Rhee JS (2002) Differential control of vesicle priming and short-term plasticity by Munc13 isoforms. Neuron 33: 411-424.

Shiratsuchi T, Oda K, Nishimori H, Suzuki M, Takahashi E, Tokino T, Nakamura Y (1998) Cloning and characterization of BAP3 (BAI-associated protein 3), a C2 domain-containing protein that interacts with BAI1. Biochem Biophys Res Commun 251: 158-165.

Sorensen JB, Nagy G, Varoqueaux F, Nehring RB, Brose N, Wilson MC, Neher E (2003) Differential control of the releasable vesicle pools by SNAP-25 splice variants and SNAP-23. Cell 114: 75-86.

Speidel D, Varoqueaux F, Enk C, Nojiri M, Grishanin RN, Martin TF, Hofmann K, Brose N, Reim K (2003) A family of Ca2+-dependent activator proteins for secretion: comparative analysis of structure, expression, localization, and function. J Biol Chem 278: 52802-52809.

Sutton RB, Fasshauer D, Jahn R, Brunger AT (1998) Crystal structure of a SNARE complex involved in synaptic exocytosis at 2.4 A resolution. Nature 395: 347-353.

Tandon A, Bannykh S, Kowalchyk JA, Banerjee A, Martin TF, Balch WE (1998) Differential regulation of exocytosis by calcium and CAPS in semi-intact synaptosomes. Neuron 21: 147-154.

Terrado J, Burgess RW, DeChiara T, Yancopoulos G, Sanes JR, Kato AC (2001) Motoneuron survival is enhanced in the absence of neuromuscular junction formation in embryos. J Neurosci 21: 3144-3150.

Varoqueaux F, Sigler A, Rhee JS, Brose N, Enk C, Reim K, Rosenmund C (2002) Total arrest of spontaneous and evoked synaptic transmission but normal synaptogenesis in the absence of Munc13-mediated vesicle priming. Proc Natl Acad Sci U S A 99: 9037-9042.

Verhage M, Maia AS, Plomp JJ, Brussaard AB, Heeroma JH, Vermeer H, Toonen RF, Hammer RE, van den Berg TK, Missler M, Geuze HJ, Sudhof TC (2000) Synaptic assembly of the brain in the absence of neurotransmitter secretion. Science 287: 864-869.

Wang ZZ, Washabaugh CH, Yao Y, Wang JM, Zhang L, Ontell MP, Watkins SC, Rudnicki MA, Ontell M (2003) Aberrant development of motor axons and neuromuscular synapses in MyoD-null mice. J Neurosci 23: 5161-5169.

Washbourne P, Thompson PM, Carta M, Costa ET, Mathews JR, Lopez-Bendito G, Molnar Z, Becher MW, Valenzuela CF, Partridge LD, Wilson MC (2002) Genetic ablation of the t-SNARE SNAP-25 distinguishes mechanisms of neuroexocytosis. Nat Neurosci 5: 19-26.

3

α-Neurexins are required for efficient transmitter release and synaptic homeostasis at the mouse neuromuscular junction

Michèle S. Sons,[1,2*] Niels Busche,[1*] Nikola Strenske,[3] Tobias Moser,[3] Uwe Ernsberger,[4] Frank C. Mooren,[5] Weiqi Zhang,[1] Mohiuddin Ahmad,[1] Heinz Steffens,[1] Eike D. Schomburg,[1] Jaap J. Plomp,[2] and Markus Missler[1,6]

1 Center for Physiology and Pathophysiology, Georg-August University, Humboldtallee 23, 37073 Göttingen, Germany
2 Departments of Neurology and Neurophysiology, Leiden University Medical Center, Leiden, The Netherlands
3 InnerEar Laboratory, Department of Oto-laryngology, Georg-August University, Göttingen, Germany
4 Institute of Anatomy and Cell Biology, University of Heidelberg, Germany
5 Institute for Sports Medicine, University of Münster, Germany
6 Department of Genetics and Molecular Neurobiology, Otto-von-Guericke-University, Magdeburg, Germany
**M.S. and N.B. contributed equally to this study.*

Published in Neuroscience (2006) 138: 433 - 446

Abstract

Neurotransmission at chemical synapses of the brain involves α-neurexins, neuron-specific cell-surface molecules that are encoded by three genes in mammals. Deletion of α-neurexins in mice previously demonstrated an essential function, leading to early postnatal death of many double-knockout mice and all triple mutants. Neurotransmitter release at central synapses of newborn knockouts was severely reduced, a function of α-neurexins that requires their extracellular sequences. Here, we investigated the role of α-neurexins at neuromuscular junctions, presynaptic terminals that lack a neuronal postsynaptic partner, addressing an important question because the function of neurexins was hypothesized to involve cell-adhesion complexes between neurons. Using systems physiology, morphological analyses and electrophysiological recordings, we show that quantal content, i.e. the number of acetylcholine quanta released per nerve impulse from motor nerve terminals, and frequency of spontaneous miniature endplate potentials at the slow-twitch soleus muscle are reduced in adult α-neurexins double-knockouts, consistent with earlier data on central synapses. However, the same parameters at diaphragm muscle neuromuscular junctions showed no difference in basal neurotransmission. To reconcile these observations, we tested the capability of control and α-neurexins-deficient diaphragm neuromuscular junctions to compensate for an experimental reduction of postsynaptic acetylcholine receptors by a compensatory increase of presynaptic release: Knockout neuromuscular junctions produced significantly less upregulation of quantal content than synapses from control mice. Our data suggest that α-neurexins are required for efficient neurotransmitter release at neuromuscular junctions, and that they may perform a role in the molecular mechanism of synaptic homeostasis at these peripheral synapses.

Acknowledgements:
We thank Thomas C. Südhof for discussion and support, and S. Gerke for excellent technical assistance. This study was supported by the Deutsche Forschungsgemeinschaft, DFG (SFB 406-C9 grant to MM), and the Netherlands Organization for Scientific Research, NWO (#903-42-073 to JJP).

Introduction

Neurexins constitute a family of highly variable neuronal transmembrane proteins (for review, Missler and Südhof, 1998), that were discovered as a receptor for α-latrotoxin (Ushkaryov et al., 1992; Ushkaryov and Südhof, 1993, Ushkaryov et al., 1994, Geppert et al., 1998; Sugita et al., 1999), a neurotoxin from black-widow spiders that causes massive transmitter release from central and peripheral synapses, including neuromuscular junctions (NMJs) (Valtorta et al., 1984). In mammals, neurexins are encoded by three genes, each of which includes independent promoters for the long α-neurexins and the shorter β-neurexins (Rowen et al., 2002; Tabuchi and Sudhof, 2002). α-Neurexins contain substantially more extracellular sequences than β-neurexins, but share with α-neurexins the same C-terminal extracellular domain, transmembrane region, and short intracellular tail (Missler et al., 1998a). Consequently, earlier biochemical studies have revealed shared intracellular binding partners (Hata et al., 1996; Butz et al., 1998; Biederer and Südhof, 2000; Biederer and Sudhof, 2001), but distinct extracellular interactions for α- and β-neurexins (Itchenko et al., 1995; Missler et al., 1989b; Sugita et al., 2001, but see Boucard et al., 2005).

To determine the function of neurexins, we previously generated knockout mice that lack one, two or all three α-neurexins (Missler et al., 2003). Double-knockout mutants (DKO) with different combinations of knockout alleles as well as triple-knockout mice (TKO) mostly died prematurely due to respiratory problems. Analyses of newborn mice deficient for multiple α-neurexins revealed almost no changes in brain architecture or synapse structure but uncovered a severe reduction in neurotransmitter release. As the presumptive cause for the inefficient exocytosis in mutant mice, we suggested that voltage-dependent Ca^{2+}-channels (VDCCs) were impaired because the response pattern of synaptic transmission to specific Ca^{2+}-channels blockers was altered, and whole-cell Ca^{2+}-currents were reduced (Missler et al., 2003). The regulation of VDCCs by α-neurexins predominantly affects N- ($Ca_V2.2$) and P/Q-type ($Ca_V2.1$) Ca^{2+}-channels but leaves L-type ($Ca_V1.3$) channels unscathed (Zhang et al., 2005). In addition, another Ca^{2+}-permeable channel, the N-methyl-D-aspartate receptor (NMDAR) at neocortical synapses also appears to be affected because NMDAR-mediated currents were reduced in α-neurexin triple-knockouts (Kattenstroth et al., 2004). Transgenic rescue experiments furthermore showed that the effect on neurotransmission and Ca^{2+}-currents is specific for α-neurexins and requires their extracellular domains (Zhang et al., 2005). These studies established a role for α-neurexins as organizer molecules of the synaptic release machinery. However, an additional aspect of their function exists: As originally proposed when neurexins were discovered as highly variable cell-surface receptors (Ushkaryov et al., 1992), they may be involved in cell-adhesion and/or cell-recognition function via their highly variable extracellular sequences (Missler and Südhof, 1998). This hypothesis was subsequently supported when neuroligins were discovered as post-

synaptic binding partners of α-neurexins (Ichtchenko et al., 1995; Ichtchenko et al., 1996; Nguyen and Südhof, 1997; Song et al., 1999), and has recently attracted considerable attention by numerous laboratories, proposing that the neurexin/neuroligin cell-adhesion complex can promote the formation of de novo synapses and differentiation of postsynaptic receptors at least in vitro (Scheiffele et al., 2000; Dean et al., 2003, Graf et al., 2004; Chih et al., 2005; Chubykin et al., 2005; Sara et al., 2005). Since analyses of α-neurexin and neuroligin knockout mice have not been published yet, it is presently impossible to decide if the proposed aspects of neurexin function, i.e. regulator of neurotransmitter release/VDCCs or promoter of synapse formation/differentiation, represent (i) mutually exclusive roles, (ii) equally important roles, or (iii) functional specializations of different neurexin isoforms, e.g. of α- versus β-neurexins.

Here, we explored the α-neurexin function at neuromuscular junctions (NMJs) to better distinguish between the alternative roles. The NMJ appears as an excellent model for many structural and functional aspects of chemical synapses but important differences to central synapses exist, for example, presence of a basal lamina in the synaptic cleft, absence of a postsynaptic neuronal partner, capacity to regenerate after lesions, coverage by Schwann cells and the importance of agrin signaling (Sanes and Lichtman, 1999). Neurotransmission and synaptogenesis have been studied intensely at NMJs of invertebrate and vertebrate species, making it a widely used system for investigating the molecular mechanisms of the presynaptic release machinery (e.g., Wu et al., 1998; Verhage et al., 2000; Misgeld et al., 2002; Urbano et al., 2003; Varoqueaux et al., 2005), and cell-adhesion molecules (Rafuse et al., 2000; Knight et al., 2003; Nishimune et al., 2004; Polo-Parada et al., 2004). Taking advantage of the NMJs as a presynaptic terminal that lacks a neuronal postsynaptic partner, we applied systems physiology, morphological analyses and electrophysiological recordings to adult α-neurexin double-knockout mice. Our current data demonstrate that α-neurexins perform a role as regulators of neurotransmitter release at synapses of the peripheral nervous system, and contribute significantly to their synaptic homeostasis. These findings suggest that α-neurexins exert their function as presynaptic organizer molecules even in the absence of a neuronal postsynaptic partner.

Materials and Methods

Mice and Reagents

α-Neurexin knockout mice were generated previously, and genotyped by short genomic PCR as described (Missler et al., 2003). Mice were housed under a 12-h light/dark regime with access to food and water ad libitum. Animal procedures were carried out according to German and Dutch laws and ethical guidelines set by the Universities of Göttingen and Leiden. All experiments were performed with adult

DKOs deficient for either neurexins 1α and 2α (DKO1/2), or neurexins 2α and 3α (DKO2/3), respectively. Littermate single-knockout mice deficient only for neurexin 2α (SKO2) and a wild-type (WT) background line served as controls as described before (Missler et al., 2003, Zhang et al., 2005). Initial experiments were done on strictly separated genetic groups. As no significant differences were observed in the NMJ experiments between WT and SKO2, and DKO2/3 and DKO1/2 animals, respectively, mice were pooled into two groups for statistical analysis (control and DKO). Reagents were obtained from Sigma-Aldrich (Taufkirchen, Germany) or VWR (Darmstadt, Germany), except where stated otherwise.

Systems physiology

Auditory brainstem recordings.

Animals were deeply anaesthetized at 8 weeks of age using ketamine/xylazine. Tone bursts (4, 6, 8, 12, 16, 24, 32 kHz; 10 ms plateau phase with 1 ms $\cos^2$ onset and offset) or clicks of 0.03 ms were generated with a System 2 (Tucker Davis Tech, Alachua, FL, USA) driving a high-frequency speaker (Monacor, Bremen, Germany). Intensities are presented as sound pressure level (dB root mean square for tone bursts, dB peak equivalent for clicks). The difference potential between vertex and mastoid was amplified, filtered and sampled at a rate of 50 kHz. Stimuli were presented 2000 times at a rate of 20 Hz. The EEG was recorded for 20 ms and averaged to obtain mean ABR traces. Latencies of ABR were analyzed following stimulation with 80 dB clicks, and the thresholds were estimated with a 10 dB precision, essentially as described (Lacas-Gervais et al., 2004).

Treadmill running in a metabolic chamber.

Oxygen uptake (VO_2) in mice was tested during running exercise on a custom-made single-lane treadmill placed in a metabolic chamber, essentially as published (Kemi et al., 2002). Briefly, ambient air was led through the chamber at a rate of 0.5 l/min, and 200 ml/min samples were diverted to the paramagnetic oxygen analyzer (type 1155, Servomex) and the carbon dioxide analyzer (LAIR 12, M & C Instruments). The gas analyzers were calibrated with standardized gas mixtures before every test session (accuracy of measurements is appr. ±2%). To keep mice from stepping off the treadmill lanes, stainless steel grids at the end of the lines provided an electrical stimulus of 0.25 mA, 1 Hz, and 200-ms length. The exercise protocol for determination of VO_2max consisted of a regular warm-up period followed by a stepwise increase of treadmill velocity from 0.2 m/s by 0.05 m/s every third minute at 25° inclination. VO_2max was reached when oxygen uptake remained constant despite further increasing running velocity. Tests were terminated when the mice were unable to continue, or refused to run further.

Whole-body plethysmography.

Ventilation activity was assessed in awake animals using a custom-made closed chamber connected to a transducer as described elsewhere (Missler et al., 2003).

Isometric contraction force of hindlimb muscles.

The measuring set-up was modified from published procedures (Ellrich and Wesselak, 2003). Briefly, anaesthesized animals (70 mg kg^{-1} pentobarbital i.p.) were fixed to a warmed aluminium plate, and their body temperature maintained between 37.5 and 38.5 °C. The right jugular vein was cannulated to infuse 0.5 % methohexital solution (Brevimytal, Lilly, 40-60 mg kg^{-1} h^{-1}) for continuation of anaesthesia for up to 8 hr. The common carotids were ligated to stabilize blood circulation in the rest of the body, and a tracheal tube was inserted for artificial ventilation if necessary. Two recording needles (platinum wire, 0.3 mm) inserted into the lower fore legs monitored the ECG, and the heart rate was used to adjust anaesthesia. The left hind leg muscles and nerves were prepared as follows: skin on the dorsal surface was cut from the thigh down to the heel to expose the triceps surae and the posterior biceps muscle. The posterior biceps was removed and the sural nerve and the common peroneal were cut and removed from the sciatic nerve. The common tibial nerve was left intact and mounted on a stimulation electrode. The Achilles tendon was dissected from the calcaneus and connected with a strain gauge that allowed measuring the combined contraction force of the gastrocnemius and soleus muscles upon nerve stimulation. Electromyogram (EMG) recording electrodes were fixed on the surface of the GS muscle. For recordings, the tibial nerve was stimulated repetitively with rectangular pulses (duration 0.1 ms, stimulation strength 5 times above threshold strength as estimated from EMG responses). Repetitive stimulation was done using decreasing stimulation intervals at 1 s (stimulation frequency: 1 Hz), 500 ms (2 Hz), 250 ms (4 Hz), 125 ms (8 Hz), 62.5 ms (16 Hz), 31.2 ms (32 Hz), 16 ms (62.5 Hz), 8 ms (125 Hz), and 4 ms (250 Hz). Stimulation trials lasted for 30 s, and interrupted by a 2.5 min pause before the start of the next trial.

Electrophysiological recordings of neuromuscular junctions

Measurements were performed on nerve/muscle preparations of soleus and hemidiaphragm muscles of control and DKO mice killed by carbon dioxide inhalation. We intracellularly recorded endplate potentials (EPPs) and spontaneous release of single quanta (miniature EPPs, MEPPs), essentially as described before (Plomp et al., 1994, Verhage et al., 2000, van den Maagdenberg et al., 2004). At least 10 NMJs were sampled per muscle, and at least 30 EPPs and MEPPs were measured per NMJ. Briefly, muscles with the nerve supply left intact were dissected, placed in oxygenated Ringer's solution, and pinned flat in a Sylgard (Dow Corning, Midlang, MI)-coated recording chamber. Muscle fibers were impaled near the NMJ with a 10-

20 MΩ glass capillary microelectrode filled with 3 M KCl. Recordings of synaptic transmission at the NMJ ex vivo was performed at 26-28°C in Ringer's medium containing (in mM): NaCl, 116; KCl, 4.5; $MgCl_2$, 1; $CaCl_2$, 2; NaH_2PO_4, 1; $NaHCO_3$, 23; glucose 11; pH 7.4, gassed with 95 % O_2/5 % CO_2. Muscle preparations were incubated with 3.1 μM μ-conotoxin GIIIB (Scientific Marketing Associates, Herts, UK) which specifically blocks voltage-gated sodium channels in muscle, preventing contraction. This allowed for the undisturbed recording of EPPs during 0.3 and 40 Hz electrical nerve stimulation delivered by a Master8 Stimulus Generator (AMPI, Jerusalem, Israel; supramaximal squared pulse, 0.1 ms) using either a bipolar stimulation electrode (in case of the phrenic nerve) or a Ringer's medium-filled suction electrode (for the tibial nerve). The quantal content (i.e., the number ACh quanta released upon a single nerve impulse) at each NMJ was calculated from EPP and MEPP amplitudes after normalization to -75 mV membrane potential. The EPP amplitude was corrected for non-linear summation as described before (Plomp et al., 1994). During high-frequency stimulation, EPP amplitudes have the tendency to decrease to a plateau level. Therefore, the run-down level of EPP amplitude during 40 Hz stimulation for 1 s was determined by averaging the amplitudes of the last 10 EPPs in the train and has been expressed as percentage of the amplitude of the first EPP in the train. A GeneClamp 500B amplifier (Axon Instruments, Union City, CA, USA) was used for amplifying and filtering (10 kHz low-pass) of the signals. The recordings were digitized and analyzed using a Digidata 1200 interface, Clampex 8.0 and Clampfit 8.0 programs (Axon Instruments) and routines programmed in Matlab software (The MathWorks Inc., Natick, MA, USA).

Toxin-induced myasthenia gravis model

The toxin-induced myasthenia gravis model (TIMG) is based on repeated injections of α-bungarotoxin (α-BTx), a treatment causing chronic reduction of the number of functional acetylcholine (ACh) receptors, resulting in a presynaptic homeostatic response, i.e. an upregulation of quantal content. It was initially developed for rats (Molenaar et al., 1991, Plomp et al., 1994), and subsequently adjusted for mice (Sons et al., 2003). For a period of four weeks, adult control and DKO mice were injected intraperitoneally with a low dose of α-BTx (Biotoxins Inc., FA, USA) on Mondays, Wednesdays and Fridays. As a first dose, 1.2 μg α-BTx was injected. Thereafter, doses of 0.8 μg of the toxin were administered three times a week. Three hours after an injection the mice showed slightly invaginated flanks, indicating mild muscle weakness which ususally disappeared during the intermittent (toxin-free) day. Treatment control groups for both genotypes received injections of saline solution (0.9% NaCl). After the treatment, isolated phrenic nerve-diaphragm preparations from these mice were subjected to intracellular recordings of synaptic signals at the NMJ as described above.

Morphological analysis

To stain NMJs with labeled α-BTx and/or primary antibodies, teased fiber preparations of soleus and diaphragm muscles were made (Wood and Slater, 1998), allowing en face pictures of NMJs for quantification of their area and perimeter. Muscles were pinned on Sylgard-coated petri dishes, fixed with 0.5% paraformaldehyde in 0.1 M phosphate-buffered saline for 30 min, teased into bundles of 3-10 fibers in PBS, and incubated with 1% Triton-X100 in PBS for 30 min. After blocking in 5% normal goat serum/ PBS, muscle fibers were incubated with Alexa488-conjugated α-BTx alone or together with antisera, washed and mounted using Prolong Antifade reagent (Molecular Probes, Eugene, OR, USA). Primary antibodies to synapsins (E028) and synaptotagmin 1 (W855) were characterized previously (Rosahl et al., 1995, Butz et al., 1998), or obtained commercially: VAChT, anti-vesicular acetylcholine transporter (Chemicon, Temecula, CA, USA), and SMI32, anti-phosphorylated neurofilament (Sternberger Monoclonals Inc., Lutherville, ML, USA). All fluorescently-labeled secondary antibodies and neurotoxins, α-BTx and phalloidin (Phall-Alexa633), were puchased from Molecular Probes. In order to analyze the distribution of immunostained proteins, images were digitally photographed via a AxioCam HRc camera system mounted on a Axioskop 2 microscope, and quantitated using AxioVision 3.0 software (all from Fa. Zeiss, Oberkochen, Germany). In situ hybridization was performed with DIG-labeled cRNAs as described (Ernsberger et al., 2005), using probes to detect α-neurexins (a 515 bp KpnI/XbaI fragment from pCMVL2) and the VAChT (Burau et al., 2004). Color reaction was allowed for 5 d for neurexin riboprobes, and specificity of reactions was monitored with appropriate antisense riboprobes. Any modifications to digitally acquired images were limited to changes in color brightness and contrast using Adobe Photoshop 8.0 (Adobe Systems, San Jose, CA), and applied similarly when genotypes were compared.

Statistical analysis

In the electrophysiological experiments, between 10 – 15 individual NMJs were measured per muscle, and for morphology between 40 – 70 NMJs were analyzed per mouse. Genotype mean values were calculated with *n* as the number of mice in the respective group. Statistical significance was tested with a two-tailed Student's *t*-test in Excel spreadsheets or with Prism 4.0 software (GraphPad, USA), and in case of TIMG treatment differences between genotypes were analyzed with the multivariate general linear model and the post-hoc Tukey test using SPSS 10.0 software (SPSS Inc., Chicago, IL, USA).

Results

α-Neurexins play a role at peripheral synapses containing P/Q-type ($Ca_V2.1$) calcium channels

Knockout mice that lack all three α-neurexin genes (TKOs) die a few hours after birth (Missler et al., 2003), limiting the choice of synaptic systems that can be analyzed at postnatal stages. Here, we took advantage of the fact that a proportion of double-knockout mice deficient for either neurexin 1α and 2α (DKO1/2) or neurexin 2α & 3α (DKO2/3) survive into adulthood (about 5-10% of DKO1/2, and 40% of DKO2/3; (Missler et al., 2003)). To explore if surviving α-neurexin DKOs display a phenotype of impaired neurotransmission and Ca^{2+}-channel function in the peripheral nervous system similar to our previous observations in the central nervous system, we screened two different types of peripheral synapses, one dominated by L-type ($Ca_V1.3$) the other by P/Q-type ($Ca_V2.1$) VDCCs (Figure 1). In the auditory system, the inner hair cell ribbon synapse in the cochlea is entirely $Ca_V1.3$ dependent, and any impairment of neurotransmitter release at this synapse results in hearing loss (Platzer et al., 2000, Brandt et al., 2003). Auditory thresholds of young-adult α-neurexin DKO and littermate control mice were measured by recording auditory brainstem responses (ABR) following click and tone burst stimulation (Figure 1A-B). Figure 1A shows a large overlap of ABR data for wave I, which reflects the synchronized activation of spiral ganglion neurons by the hair cell ribbon synapses. Quantification of the wave I latencies revealed no significant delays in the mutants (WT 1.33 ± 0.03 ms, n = 7 mice; DKOs 1.47 ± 0.06, n = 8, n.s.), and a normal auditory threshold was observed in mutant animals (Figure 1B). These data suggest that $Ca_V1.3$ channel-dependent synaptic release does not require α-neurexins which is consistent with our earlier observations in central synapses of newborn mutants (Missler et al., 2003, Zhang et al., 2005).

In contrast, when we tested α-neurexin DKO and control mice during a running exercise that involves mostly $Ca_V2.1$ channel-dependent neuromuscular junctions of limb and respiratory muscles (Day et al., 1997, Plomp et al., 2000), mutants performed significantly worse than controls (Figure 1C). To avoid confounding effects of the about 30% lower body weight of α-neurexin DKOs on physical exercise, we used oxygen uptake (VO_2) as the measure to monitor their performance. Although the maximum oxygen uptake (VO_2max) during treadmill running was compatible between genotypes (control 69.5 ± 4.3 ml kg, 0.75 min^{-1}, n = 6 mice; DKO 70.7 ± 7.7, n = 11, n.s.), mutant mice reached VO_2max values after shorter mean running times (control 28.8 ± 2.4 min, n = 6 mice; DKO 16.1 ± 1.7, n = 11, $p<0.01$; Figure 1C), indicating that neurotransmission at NMJs of DKOs is less efficient. To exclude that the early exhaustion is entirely due to an impaired respiratory rhythm generator in the central nervous system, we measured the ventilation frequency in both genotypes using whole-body plethysmography but found no significant difference (con-

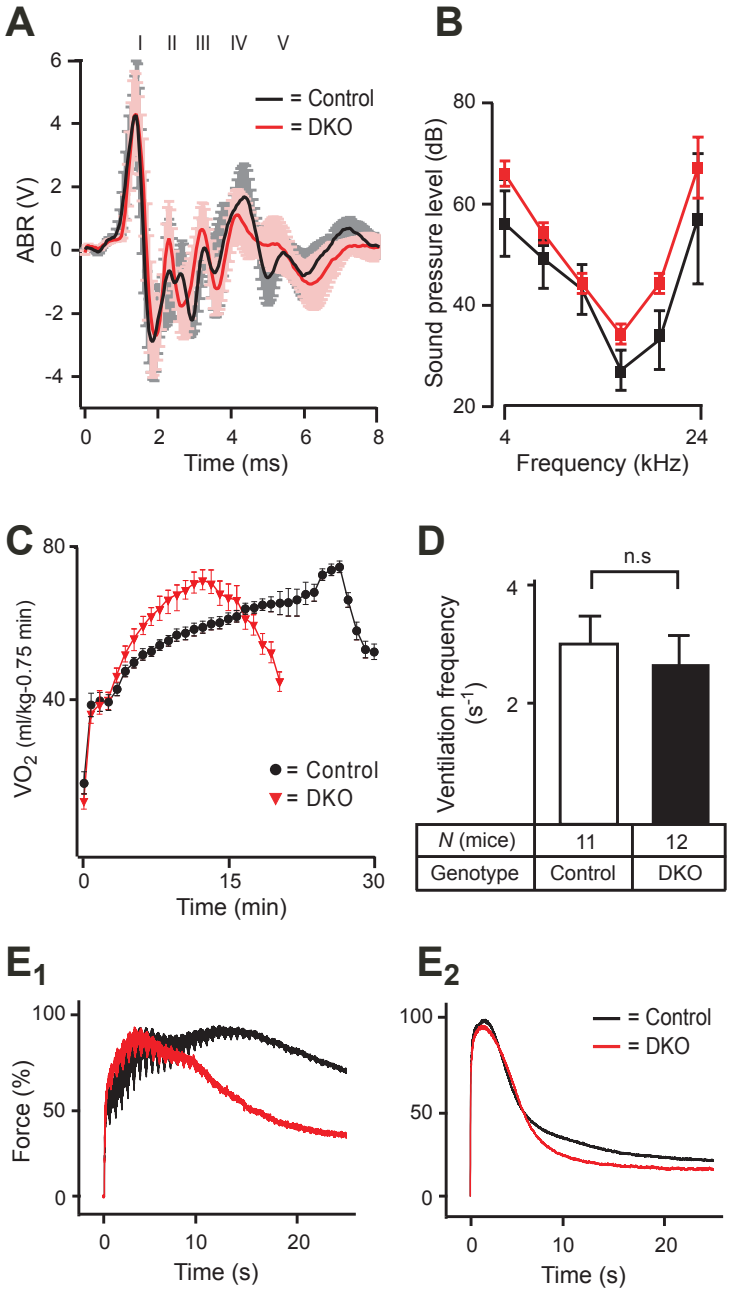

Figure 1. α-Neurexins perform a significant role at synapses of the peripheral nervous system that depend on P/Q-type ($Ca_v2.1$) Ca^{2+} channels.

(A) Graphic representation of auditory brainstem responses (ABR) recorded from adult control (black line, control, n = 7) and α-neurexin double KO mice (red, DKO, n = 8) KO mice, and (black, n = 7). The waves were sampled following stimulation with 80 dB clicks. Roman numbers above the graph indicate the ABR voltage peaks according to Jewett (Jewett et al., 1970). The first peak (I) represents mainly the activation of spiral ganglion neurons by the inner hair cell ribbon synapse. (B) Averaged hearing thresholds (in dB SPL) of the same mice. Auditory thresholds were determined at various frequencies following tone bursts and at click stimulation, but show no significant

trol 3.3 ± 0.3 s^{-1}, n = 11 mice, DKO 2.6 ± 0.3, n = 12; Figure 1D). To demonstrate the impaired function of mutant nerve-muscle transmission in the intact animal, we next developed an in vivo preparation of one of the muscle groups involved in the running exercise (triceps surae, consisting of gastrocnemius and soleus muscles). Repetitive stimulation of the tibial nerve with increasing stimulation frequencies from 1 – 250 Hz caused single twitches at lower stimulation frequencies that fuse to tetanic contractions at frequencies faster 30 Hz both in control and α-neurexin knockout mice (data not shown). We used the higher stimulation frequencies (corresponding to 16 and 8 ms interstimulus interval) to compare the maximal forces elicited by the nerve-muscle transmission under condition of tetanus (Figure 1E). We observed that α-neurexin DKO mice reach similar peak forces when normalized for body weight, however, mutant NMJs are not able to sustain the contraction as long as control preparations (Figure 1E). Together, these experiments suggest that neurotransmission at $Ca_V2.1$ channel-dependent NMJs is less effective and may exhaust earlier in the absence of α-neurexins.

Neurotransmitter release at neuromuscular junctions is impaired in adult α-neurexin KO mice

To test directly if neurotransmitter release from individual NMJs of adult α-neurexin DKO mice is reduced, we studied release parameters with ex vivo electrophysiology, using micro-electrode recordings of MEPPs and nerve stimulus-evoked EPPs in μ-conotoxin-paralyzed tibial nerve/soleus muscle preparations. Compared to littermate control animals, spontaneous release of single ACh quanta appeared less frequent in α-neurexin DKO muscles as shown by representative traces of MEPPs (Figure 2A). MEPP frequency at this slow-twitch muscle was reduced by almost 30% in adult α-neurexin DKOs (control 2.1 ± 0.2 s^{-1}, n = 21 mice; DKO 1.4 ± 0.1, n = 20; $P<0.05$; Figure 2B). Application of the selective $Ca_V2.1$ blocker ω-agatoxin IVA (200 nM) reduced the MEPP frequency in both genotypes to similar levels (fMEPP ± ω-Aga, Table 1), indicating that only the Ca^{2+}-sensitive fraction of spontaneous release was diminuished in the mutant NMJs, which is consistent with the hypothesis of impaired calcium channel function in absence of α-neurexins (Missler et al., 2003, Zhang et al., 2005). To assess the evoked release of ACh in response to a single action potential at soleus NMJs, we next recorded EPPs by supramaximal stimulation of the tibial nerve at low rate (0.3 Hz). We observed that quantal

differences between genotypes at this L-type VDCC-dependent synapse. Data shown are means ± SEM. (C) Oxygen uptake (VO_2) was measured on a treadmill set-up in control (black line; n = 8 mice) and α-neurexin DKO animals (red; n = 11) with increasing running speed from 0.2 m/s with 0.05 m/s every 3 min until exhaustion. Note that similar VO_2max values are reached but knockout mice fatigue much earlier at lower running velocities. Data shown are means ± SEM. (D) Whole-body plethysmography was used to determine the respiratory activity of adult DKO and control mice. Data shown are means ± SEM. n.s. = not significant. (E) Time course of tetanic contractions of triceps surae muscle group from control (black line, average for n = 3 mice) and DKO mutants (red, n = 4) were normalized to their maximal force at 16 ms (E1, still incomplete tetanic contraction) and 8 ms (E2, complete tetanus) stimulation intervals. DKO muscles do not sustain contractions as long as controls.

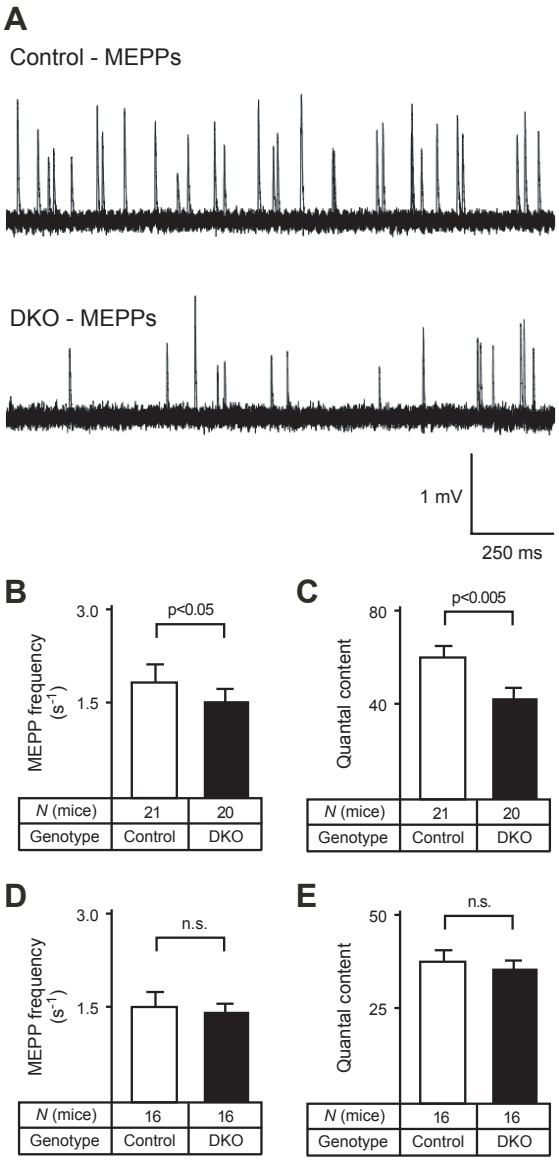

Figure 2. Basal spontaneous and evoked ACh release is reduced at soleus NMJs of α-neurexin DKO mice but not at their diaphragm NMJs. (A) Representative traces show typical examples of MEPP recordings from soleus muscle of control (upper panel) and α-neurexin DKO mice (lower panel). Traces show 7x 1.5 s long recordings superimposed for each genotype. (B, C) Intracellular recordings from a tibial nerve/soleus muscle ex vivo preparation show a reduced spontaneous (MEPP frequency, panel B) and evoked (Quantal content, panel C) ACh transmitter release in α-neurexin mutants. (D, E) The frequency of spontaneous release events (D) and evoked ACh release (E) does not differ between diaphragm NMJs of control and α-neurexin DKO mice. In all graphs, statistical significance is indicated above the bars. Data shown are means ± SEM.

content, i.e. the number of quanta released per nerve impulse), was also diminished at mutant NMJs to about 70% of control values (control 60 ± 4, n = 21 mice; DKO 43 ± 3, n = 20; P<0.01, Figure 2C). The findings of impaired spontaneous and evoked release at soleus NMJs are consistent with the earlier observation of reduced mini frequency and evoked postsynaptic currents at central synapses of newborn α-neurexin knockout mice (Missler et al., 2003). In contrast, the unchanged ventilation activity in adult α-neurexin DKOs as reported above (Figure 1D) is surprising because newborn α-neurexin knockouts breathed more slowly than control mice (Missler et al., 2003), raising the question if the reduced transmission as

demonstrated in the soleus (Figure 2B, C) was a general phenomenon of all mutant NMJs. Since the central respiratory rhythm generator was largely intact in the few surviving adult knockouts as judged from the hypoglossal nerve output (data not shown), a reduced ACh release from NMJs at the diaphragm, a predominantly fast-twitch muscle responsible for inspiration, should cause massive respiratory problems. Therefore, we explored neurotransmitter release from diaphragm NMJs, using the same methods and parameters as for the soleus NMJ recordings. However, the frequency of MEPPs (control 1.5 ± 0.1 s^{-1}, n = 16 mice; DKO 1.4 ± 0.1, n = 16; n.s.; Figure 2D) and quantal content (control 38 ± 2, n = 16 mice; DKO 35 ± 1, n = 16; n.s.; Figure 2E) appeared unchanged between control and α-neurexin DKO diaphragms. Since DKOs used in this study still contain the remaining third neurexin gene (Nrxn 2α), we reasoned that the unchanged release at the diaphragm may be due to the continued presence of this single isoform, contributing to a presumably higher safety factor at this particular NMJ (Wood and Slater, 2001). To explore this possibility experimentally, we obtained some NMJ recordings from diaphragm preparations of newborn TKOs lacking all α-neurexins, applying the so-called cut-fiber method (depolarization block) to record EPPs. Quantal content was calculated but no difference in evoked ACh release could be observed between control and

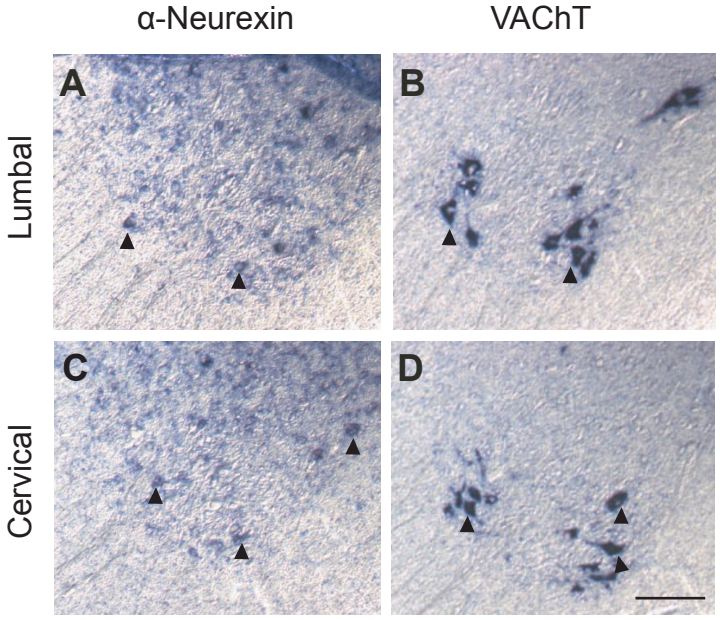

Figure 3.α-Neurexins are expressed in motorneurons innervating soleus and diaphragm muscles.
In situ hybridizations of spinal cord sections derived from wild-type mice at the lower lumbar level (about L5, panels A-B) and at cervical segments (about C6, panels C-D) using probes against α-neurexin (A, C) and VAChT (B, D). Motoneurons (arrow heads) as well as most other neurons in the ventral horn express α-neurexin. Scale bar in D (for A-D), 150 μm.

	Muscle preparation			
	Soleus		Diaphragm	
Genotype	Control (n)	DKO (n)	Control (n)	DKO (n)
fMEPP/± ω-Aga[a] (s-1)	0.57 ± 0.1 (6)	0.55 ± 0.1 (8)	---	---
fMEPP/sucrose (s-1)	60.7 ± 3.6 (13)	53.9 ± 3.4 (12)	41.0 ± 6.9 (10)	48.9 ± 5.5 (11)
QC (ratio ± ω-Aga)[a]	0.003 ± 0.001 (6)	0.004 ± 0.001 (6)	0.08 ± 0.01 (14)	0.02 ± 0.01 (15) ***
EPP rundown (%)[b]	75.5 ± 0.7 (16)	73.9 ± 0.9 (19)	82.9 ± 0.8 (16)	83.5 ± 0.5 (16)
EPP amplitude (mV)	26.8 ± 0.9 (20)	26.1 ± 0.8 (21)	25.4 ± 0.8 (16)	28.7 ± 1.1 (16) *
EPP halfwidth (ms)	3.1 ± 0.1 (15)	2.9 ± 0.1 (12)	3.1 ± 0.1 (16)	3.1 ± 0.1 (16)
MEPPamplitude (mV)	0.7 ± 0.1 (21)	0.9 ± 0.1 (20) **	1.0 ± 0.1 (16)	1.3 ± 0.1 (16) **
MEPP halfwidth (ms)	2.9 ± 0.1 (15)	2.9 ± 0.1 (12)	2.8 ± 0.1 (16)	2.9 ± 0.1 (16)

TABLE 1. Characterization of neurotransmission at the NMJ of α-neurexin double-knockout mice
Intracellular recording techniques were used to compare biophysical properties of nerve-muscle transmission in soleus (slow-twitch) and diaphragm (mixed slow and fast-twitch) muscles prepared from 5-6 week old α-neurexin double-knockouts (DKO), and their respective controls. Data are means ± SEM; n = number of animals used; 10-15 NMJs tested per muscle/mouse. fMEPP, frequency of miniature endplate potential (MEPP); QC, quantal content; EPP, endplate potential; ω-Aga, $Ca_V2.1$ specific calcium channel inhibitor ω-agatoxin IVA; ---, not done.
* P<0.05;
** P<0.01;
*** P<0.001 (Student's *t*-test).
[a]Recordings were performed before and after addition of 200 nM ω-agatoxin IVA, and results expressed as the ratio of agatoxin/control.
[b]Expressed as percent of first EPP amplitude, recorded under high-rate (40 Hz) nerve stimulation.

TKO diaphragm muscles (control 2.9 ± 0.5, n = 7 mice; TKO 2.4 ± 0.2, n = 3; n.s.). Similarly, MEPP frequences were unchanged (around 3-4 min^{-1}; data not shown). As the phenotype was not more pronounced in the diaphragm and evoked release recordings from the soleus preparation in newborns proved technically impossible, all further analyses were restricted to the adult α-neurexin DKOs. To exclude the possibility that α-neurexins are absent in motorneurons innervating the diaphragm, we performed in-situ hybridization of histological sections from different levels of the spinal cord, showing that α-neurexin mRNAs are present in the respective segments (Figure 3). These results prompted the question if the difference between soleus and diaphragm physiology in α-neurexin DKOs reflects a different regulation of the presynaptic release machinery.

To analyze if the deletion of α-neurexins affected Ca^{2+}-independent steps of neurotransmission at the NMJ, we applied hypertonic solution (500 mM sucrose) to both soleus and diaphragm muscle preparations, and recorded MEPP frequencies. Consistent with previous results in central synapses (Missler et al., 2003), secretion of the readily-releasible pool triggered by high sucrose solution did not differ between control and α-neurexin DKO NMJs of both muscle preparations (Table 1). The lack of reduced ACh release in diaphragm NMJs of α-neurexin DKOs might be due to a compensation by other types of voltage-gated calcium channels as found in calcium channels mutants (Muth et al., 2001; Urbano et al., 2003). In order to test

for possible compensation, we measured quantal content before and after application of the $Ca_V2.1$ blocker ω-agatoxin IVA (200 nM), but no apparent compensatory upregulation was observed. The amount of ACh released after removal of the $Ca_V2.1$ component was even slightly lower in DKOs than in control mice (Table 1), possibly reflecting the likewise impaired function of $Ca_V2.2$ channels in α-neurexin KOs (Zhang et al., 2005).

Since NMJs on different types of muscle fibers such as slow-twitch and fast-twitch fibers differ in structure and function (Bewick, 2003), we further compared the biophysical parameters of evoked and spontaneous ACh release at both preparations of control and α-neurexin DKO mice. To test if the difference between soleus and diaphragm NMJs in α-neurexin knockouts could be attributed to a change in the safety factor, we measured the EPP amplitude rundown at high-rate nerve stimulation (40 Hz). However, no differences in rundown profiles (data not shown) and relative reduction of rundown amplitudes could be observed (Table 1) between the genotypes under high intensity use. The halfwidth of EPP and MEPP recordings revealed also no changes in the activation kinetics of ACh release and of the postsynaptic ACh receptors (Table 1). Although the quantal content was reduced at mutant soleus NMJs (Figure 2C), their overall EPP amplitude was unchanged, and the EPP amplitude measured at mutant diaphragm NMJs was even slightly elevated (Table 1). This effect can be explained by the about 20% reduced fibre diameter in DKO muscles (Table 2), leading to an increased electrical input resistance that causes the

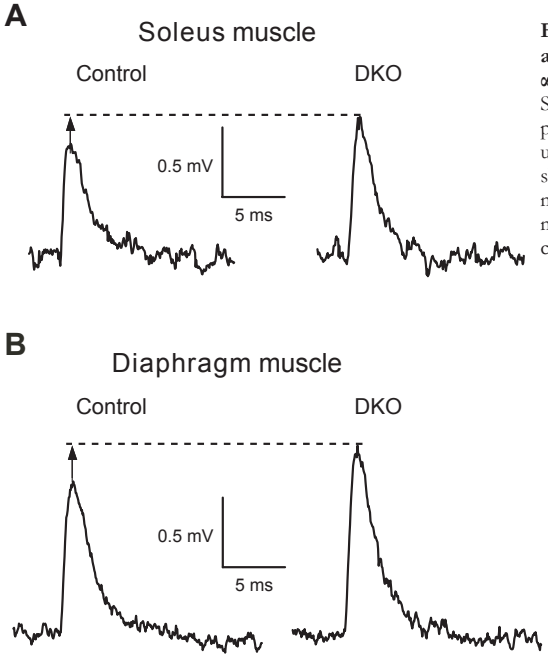

Figure 4. MEPP amplitudes are increased at soleus and diaphragm NMJs of α-neurexin DKO mice.
Single representative traces of miniature endplate potentials (MEPPs) recorded from soleus (A) and diaphragm (B) ex vivo preparations show slightly higher amplitudes in mutant mice (DKO) as compared to control animals, most likely reflecting the overall reduced muscle fiber diameter (see Table 2).

Figure 5. Morphological analysis of α-neurexin-deficient NMJs.
Teased fiber preparations (A1, differential interference contrast picture) were stained with fluorescently-labeled α-BTx to identify NMJs (A2) by visualizing postsynaptic ACh receptors. (B) Images of randomly sampled NMJs were outlined interactively by an investigator unaware of the genotype, and their area and perimeter quantitated by image analysis (results see table 2). (C, D) Double-labelings of soleus muscle NMJs from control (C1) and mutant mice (D1) with antibodies against the synaptic vesicle protein synapsin, and α-BTx (C2, D2), showing precise overlap of pre- and postsynaptic sites in merged images (C3, D3). (E, F) Similar experiment using antibodies againt the vesicular ACh transporter, VAChT, on NMJs of control (E1) and mutant mice (F1), counter-stained with fluorescently-labeled α-BTx (E2, F2). (G) The number of axons per synaptic site in control (G1) and DKO mice (G2) was estimated by co-labeling ACh receptor clusters (α-BTx, green) with antibodies against neurofilament (SMI32, red), and in some experiments with Alexa633-phalloidin to stain target cells (G3).
Scale bar in (A2) for A-G, 50 μm; scale bar in (B), 10 μm.

about 25% increase in MEPP amplitude which can be observed on representative MEPP traces from both muscle preparations (Figure 4) and their quantifications (Table 1).

Effect of the deletion of a-neurexins on the morphology of neuromuscular junctions

The reduced neurotransmitter release in the soleus muscle and the smaller muscle fibers in both soleus and diaphragm of α-neurexin DKOs raised the question if the localization or morphology of NMJs were affected as well. Formation and maturation of NMJs are known to rely at least partly on activity-dependent signals, as evidenced, for example, by deletion of choline acetytransferase, the enzyme responsible for the synthesis of ACh (Misgeld et al., 2002). To address this issue, we performed histological experiments on NMJs of both soleus and diaphragm muscles. Teased fibers were incubated with fluorescently-labeled α-BTx to visualize NMJs by their postsynaptic ACh receptors (Figure 5A1-A2). NMJs were normally distributed in their target field of innervation in both muscles of control and DKO mice (Figure

	Muscle preparation			
	Soleus		**Diaphragm**	
Genotype	**Control (n)**	**DKO (n)**	**Control (n)**	**DKO (n)**
Muscle Fibre Diameter (μm)	31.6 ± 1.1 (6)	25.4 ± 1.7 (6) *	29.8 ± 0.9 (6)	25.4 ± 1.6 (6) *
NMJ Area (μm^2)	375 ± 17 (7)	293 ± 11 (6) **	261 ± 14 (7)	224 ± 12 (7)
NMJ Perimeter (μm)	241 ± 15 (7)	199 ± 6 (6) **	195 ± 9 (7)	171 ± 8 (7)
Complexity (μm^{-1})[a]	0.7 ± 0.04 (7)	0.7 ± 0.03 (6)	0.8 ± 0.04 (7)	0.8 ± 0.02 (7)
NMJs/fiber (No.)[b]	0.99 ± 0.01 (7)	0.98 ± 0.02 (6)	1.01 ± 0.01 (7)	0.99 ± 0.01 (6)

TABLE 2. Neuromuscular junction morphology in α-neurexin double-knockout mice
Teased muscle fibers of soleus and diaphragm were prepared from 5-6 week old mice (α-neurexin double-knockouts and littermate controls), and the outlines of their fluorescently–labeled NMJs (see Figure 5) quantitated using an image analysis software (see Experimental Procedures). Data are means ± SEM; n = number of animals used; 40-70 NMJs analyzed per muscle/mouse.
* $P<0.05$;
** $P<0.01$; (Student's *t*-test)
[a] Complexity is a derived measure that represents the shape of the pretzel-like NMJ, and was calculated by dividing Perimeter/Area. A lower value of complexity would reflect more disc-like, immature NMJs.
[b] The number of synaptic sites per muscle fiber was counted in double-labelings as described in Results.

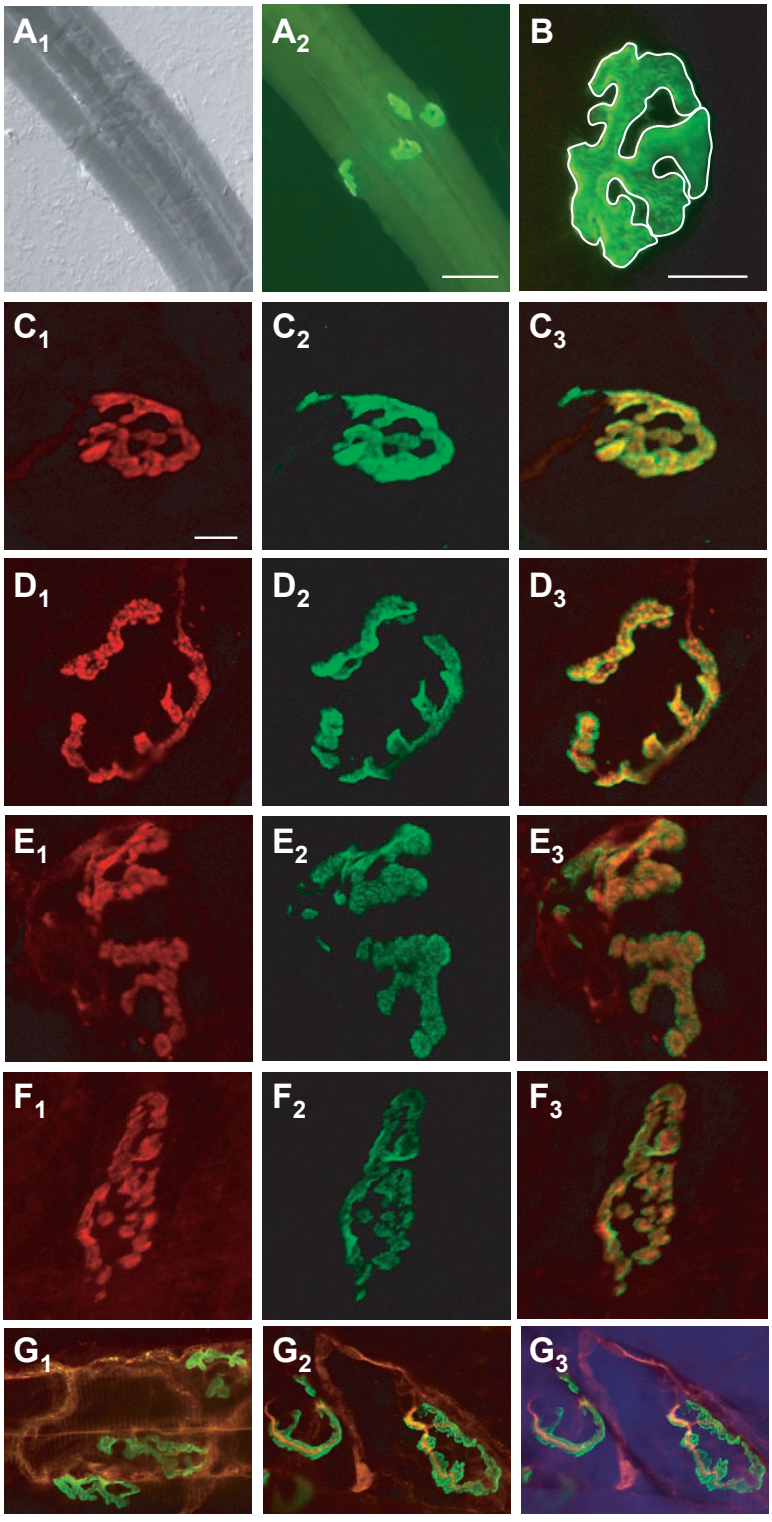
A1
A2
B
C1
C2
C3
D1
D2
D3
E1
E2
E3
F1
F2
F3
G1
G2
G3

A2, and data not shown). Their en face images were outlined interactively (example in Figure 5B), and the area, perimeter and complexity quantitated by automated image analysis (Table 2). To ensure that the postsynaptic ACh receptor distribution visualized by fluorescent α-BTx is a true representative also of the presynaptic terminal of NMJs especially in mutant mice, we performed double-labelings with antibodies against the presynaptic proteins synapsins (Figure 5C-D) and VAChT

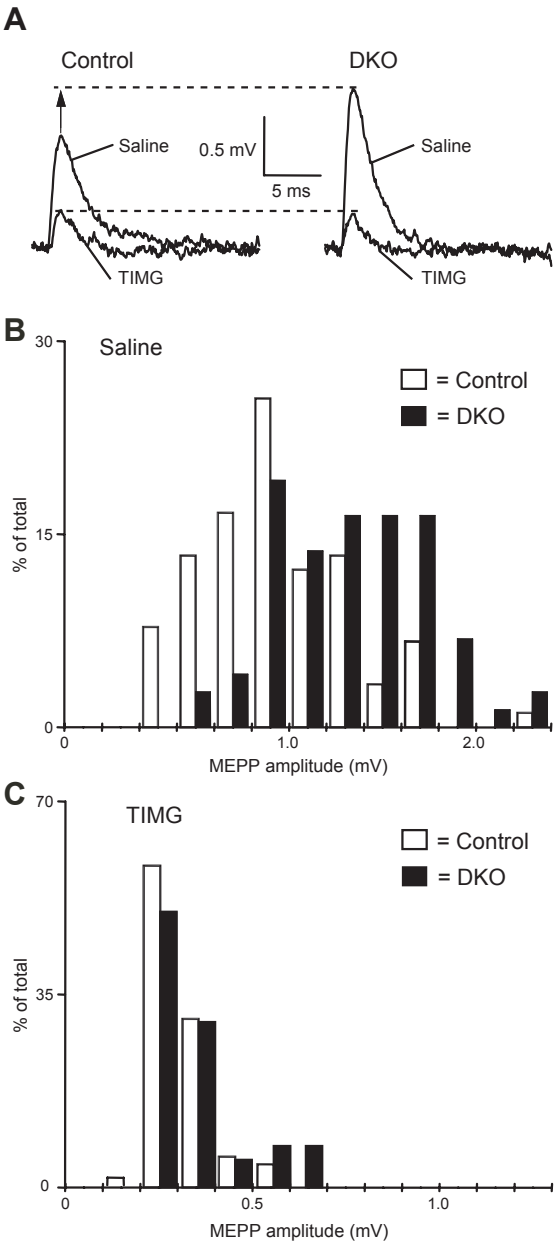

Figure 6. Effect of chronic α-BTx treatment on postsynaptic ACh receptor density in control and α-neurexin DKO mice.
(A) Representative traces of single MEPP recordings from control and DKO diaphragm NMJs that received saline or α-BTx injections for four weeks, leading to a strong reduction of amplitudes in both genotypes under toxin-induced myastenia gravis-like (TIMG) conditions. The slightly elevated amplitude in DKOs before injections is most likely due to a smaller muscle fiber diameter (see also Figure 4, and Table 2) (B, C) Histograms of MEPP amplitude distributions following saline (B) or α-BTx (C) treatment.

(Figure 5E-F). Overlap of pre- and postsynaptic markers was found in both control and mutant muscle preparations, allowing the use of α-BTx stained ACh receptors to draw conclusions on the structure of the entire NMJs. In line with the reduced ACh release from soleus NMJs, we found an about 22% smaller area and 19% reduced perimeter of these synapses in (Table 2). In contrast, the structure of NMJs in the diaphragm muscle of mutant mice was not significantly altered (Table 2). The smaller size of mutant soleus NMJs did not reflect a more immature type of junction because the complexity of all NMJs as a measure of their degree of differentiation was indistinguishable between genotypes (Table 2). To finally test if the deletion of α-neurexins possibly affected the elimination of the surplus of axonal branches innervating individual muscle fibers during development, we performed double-labelings of NMJs (α-BTx) and axons (phosphorylated neurofilaments) (Figure 5G). Analysing the number of NMJs per terminal nerve branch revealed no differences between control animals and DKOs, both displaying the expected ratio of one NMJ/ terminal axon and muscle fiber (Table 2).

a-Neurexins contribute to synaptic homeostasis at neuromuscular junctions

The finding that the deletion of two α-neurexin genes had no significant effect on ACh release from diaphragm NMJs is surprising because reduced neurotransmission was observed at soleus NMJs (Figure 2, Table 1), and at various excitatory and inhibitory synapses of the central nervous system (Missler et al., 2003; Kattenstroth et al., 2004; Zhang et al., 2005). Since the α-neurexin function at some but not all NMJs may be partially overlapping with other molecules such as laminins (Knight et al., 2003; Nishimune et al., 2004), we wanted to illuminate their contribution to release under conditions of synaptic plasticity. Two groups of each genotype (n = 6 + 6 control mice, and n = 5 + 5 DKO mice) were subjected to the TIMG protocol, a chronic treatment of intraperitoneal injections with either saline or α-BTx. The toxin paradigm has been previously shown to lead to a compensatory upregulation of ACh release that is induced by a decreased sensitivity of postsynaptic ACh receptors (Plomp et al., 1994). Mice were sacrified at about 10 weeks of age after 4 weeks of treatment, and phrenic nerve/ diaphragm preparations used for intracellular recordings as decribed above. Consistent with our basic characterization of neurotransmission at the diaphragm NMJ described above, the amplitude of MEPPs was slightly increased in the saline-injected DKOs compared to saline-injected control mice (control 0.93 ± 0.08 mV; DKO 1.33 ± 0.06, $P<0.01$; Figure 6). Four-weeks TIMG treatment caused a robust decrease of the MEPP amplitudes to almost identical levels in both genotypes (control 0.3 ± 0.01 mV; DKO 0.32 ± 0.03, n.s.; Figure 6), indicating that the toxin treatment was similarly effective, and postsynaptic ACh receptor sensitivity about equal in both control and α-neurexin DKO mice. However, the expected compensatory increase in quantal content was

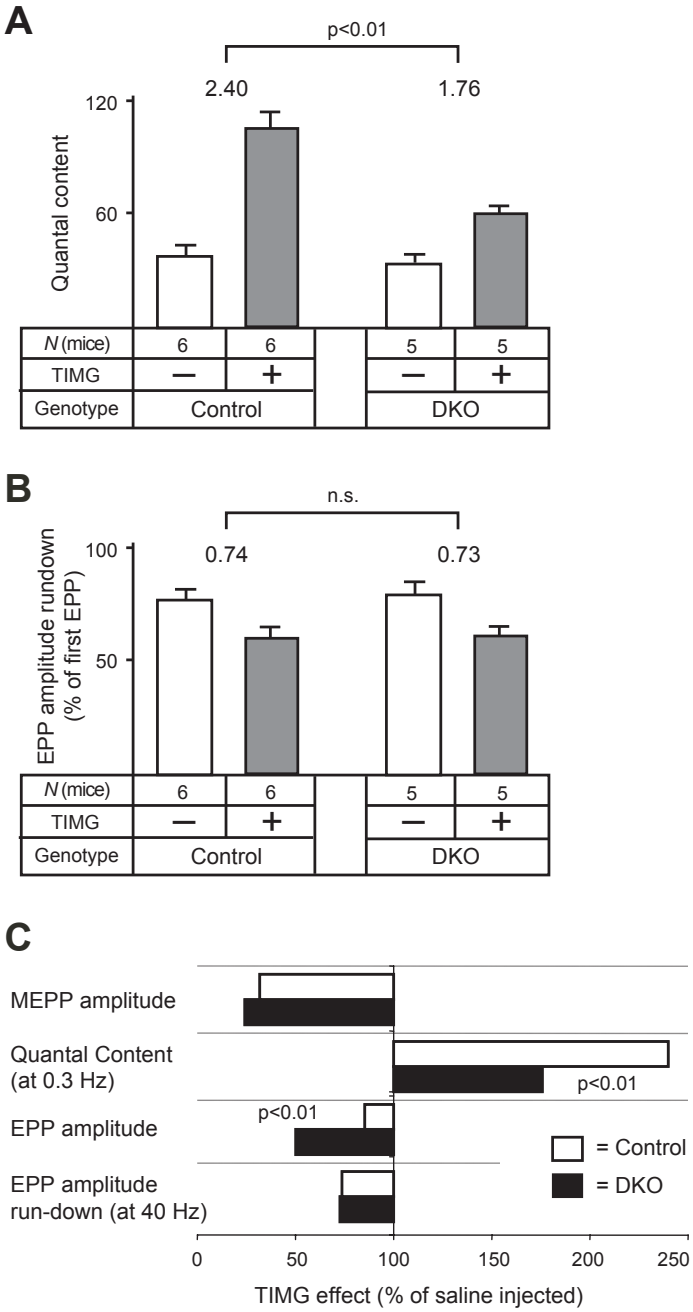

Figure 7. Impaired upregulation of evoked ACh release in α-neurexin-deficient NMJs.
(A) Following TIMG treatment, quantal content as a measure of evoked ACh release from diaphragm NMJs is increased to 240% (control) but only to 176% (DKOs) of saline-treated animals of the same genotype. (B) Following TIMG treatment, high frequency (40 Hz) stimulation of diaphragm NMJs leads to a similar reduction of EPP run-down in both control and DKO mice. (C) Diagram summarizing the electrophysiological effects of TIMG treatment on control and α-neurexin DKO mice, expressed as percentage of changes from injections with saline alone. In all graphs and panels, statistical significance is indicated above the bars. Data shown are means ± SEM.

much less pronounced in α-neurexin DKO NMJs (about 176%; quantal content in DKO mice/saline-injected 34.9 ± 2.3, DKO mice/α-BTx-injected 61.3 ± 5.4, Figure 7A) as compared to control mice (about 240%; quantal content in control mice/saline 40.6 ± 4.5, control mice/α-BTx 97.4 ± 6.9; Figure 7A). The impaired upregulation of presynaptic release following postsynaptic reduction of functional ACh receptors was also reflected by a more pronounced reduction of EPP amplitudes in mutant mice (about 50%; EPP amplitude in DKO mice/saline-injected 29.7 ± 1.4 mV, DKO mice/α-BTx-injected 14.9 ± 2.7) as compared to controls (about 15%; EPP amplitude in control mice/saline 24.6 ± 0.9 mV, control mice/α-BTx 21 ± 1.0). The change in high-rate (40 Hz) stimulated EPP amplitude rundown following α-BTx treatment, however, was indistinguishable between the genotypes (control 61 ± 2.7%, DKO 61 ± 2.5%, Fig 7B). The TIMG experiment suggests that α-neurexins perform an important role in the regulation of presynaptic release under conditions of synaptic plasticity (for summary of the effects see Figure 7C), and are possibly involved in translating the retrograde signals from muscle fibers with reduced postsynaptic ACh receptors to the presynaptic release machinery.

Discussion

Neurexins are neuron-specific cell-surface molecules that were proposed to have a function at synapses (Missler et al., 1998a; Missler, 2003; Scheiffele, 2003) because (i) their structure resembles that of a receptor (Ushkaryov et al., 1992; Ushkaryov and Südhof, 1993; Ushkaryov et al., 1994), (ii) they bind to postsynaptic cell-surface proteins, e.g. neuroligins (Ichtchenko et al., 1995) and dystroglycan (Sugita et al., 2001), (iii) they are receptors for α-latrotoxin which induces massive neurotransmitter release (Geppert et al., 1998; Sugita et al., 1999), and (iv) they are highly polymorphic in their extracellular sequences due to extensive alternative splicing which appears to be functionally relevant (Ullrich et al., 1995; Tabuchi and Sudhof, 2002). Most importantly, deletion of α-neurexins strongly points towards a specifically synaptic function because their absence severely impairs both excitatory and inhibitory neurotransmitter release at synapses of the central nervous system, presumably due to impaired Ca^{2+}-channel function, whilst unaffecting brain architecture and synaptic ultrastructure (Missler et al., 2003).

Here, we have investigated the contribution of α-neurexins to neurotransmission at NMJs by analysing the phenotype of surviving adult DKO mice. Our findings on reduced spontaneous and evoked ACh release in the soleus muscle (Figure 2, Table 1) are in line with the data on impaired physical exercise and tetanic contraction (Figure 1C-E), and are consistent with previous results on reduced spontaneous and evoked release from central synapses (Missler et al., 2003). In fact, the degree of consistency between our current analysis of peripheral synapses (i.e., NMJs) and the earlier data on central synapses underscores the ubiquitous importance of the

molecules, and the validity of our conclusions. However, there are also important differences between the analyses of central and peripheral synapses in α-neurexin-deficient mice as shown in this study, leading to novel insights into the function of α-neurexin as regulators of neurotransmitter release.

The reduction of transmitter release at the soleus DKO NMJ (about 25% compared to controls) was much less than that found at central synapses (between 50-95% at different synapses of newborn TKOs). Several reasons may contribute to this discrepancy. (i) The NMJs investigated here are derived from DKO mice that represent "survivors" of a population with high mortality, since only 40% of DKO2/3 and 10% of DKO1/2 live beyond 3 weeks of age (Missler et al., 2003). Therefore, the NMJ data obtained here from mice aged 4-6 weeks may be biased towards a milder synaptic phenotype. (ii) The possiblity exists that the developmental switch from Ca_V1 and $Ca_V2.2$ to almost exclusively $Ca_V2.1$ channels at NMJs during the early postnatal period (Rosato Siri and Uchitel, 1999) prevents development of the full extent of the phenotype. Although $Ca_V2.1$ channels can be regulated by α-neurexins (Zhang et al., 2005), both populations of central synapses characterized in the newborn TKOs contain a significant proportion of $Ca_V2.2$ channels (Missler et al., 2003) which may be affected more severely by the mutations. (iii) The more subdued role of α-neurexins in basal transmitter release at the NMJ, compared to central synapses, may be due to a partially overlapping function with other cell-adhesion molecules that are not at all present or less active at central synapses. For example, neural cell adhesion molecule (NCAM) is present at NMJs and affects morphology and function, as evidenced by smaller NMJ size and reduced high-rate ACh release in NCAM knockout mice (Rafuse et al., 2000). Another candidate for functional overlap with α-neurexin at the NMJ is laminin-β2 that binds to an extracellular loop of the $Ca_V2.1$ pore-forming subunit, thereby influencing aggregation of components at ACh release sites, and consequently, the level of neurotransmission (Noakes et al., 1995; Knight et al., 2003; Nishimune et al., 2004).

Evidence for an additional role of α-neurexins in synaptic homeostasis followed from the experiments in which we forced a homeostatic response at NMJs by lowering the functional ACh receptor number by chronic treament with α-BTx. (Figure 6-7). The normal response to this TIMG treatment is a compensatory increase of the quantal content, most likely via retrograde transsynaptic signaling (Plomp et al., 1992). Diaphragm NMJs of DKO mice were much less able to respond to the treatment compared to control animals, suggesting that α-neurexins are involved in the mechanism of synaptic homeostasis. Such an hypothesis is supported by the proposed function of α-neurexins in coupling calcium channels to transmitter release (Missler et al., 2003) because the homeostatic increase in quantal content depends on calcium influx (Plomp et al., 1994). In line with such an interpretation, it has recently been hypothesized that ACh release sites at mouse NMJs have "slots" that

are preferentially filled with $Ca_V2.1$ channels (Urbano et al., 2003). The scaffolding molecules forming these proposed "slots" may include CASK and Mint1, both of which can bind to the C-terminus of $Ca_V2.1$ channels (Maximov et al., 1999) as well as to the cytoplasmic portion of neurexins (Hata et al., 1996; Biederer and Südhof, 2000), suggesting a possible way to regulate the amount of $Ca_V2.1$ channels at ACh release sites. Further experiments are needed, however, to elucidate the nature of the interaction between α-neurexins and the various calcium channel subtypes. Unfortunately, we were not able to determine the TIMG response at NMJs of the soleus muscle as the α-BTx treatment lowered the already small MEPP amplitudes at this NMJ to values below the detection limit (about 0.15 mV, data not shown), precluding reliable calculation of quantal content. However, the link between α-neurexins and presynaptic Ca^{2+} influx may provide an explanation why both reduced basal transmission and/or impaired synaptic homeostasis are observed as NMJ phenotypes, albeit at different ratios in the two populations studied here.

The difference between soleus and diaphragm NMJs with respect to the influence of α-neurexins on their basal release is interesting (Figure 2, Table 1) because their release properties may be related to the difference in muscle fiber types, the soleus being a slow-twitch and the diaphragm a muscle with mixed slow- and fast-twitch fiber composition (Prakash et al., 1996; Bewick, 2003). NMJs on those fiber types differ in structure and function in a way that NMJs on slow-twitch fibers display a lower initial release level (Bewick, 2003), presumably making them more vulnerable to the deletion of α-neurexins as demonstrated here. The difference was not due, in turn, to a differential expression in the respective motor neurons innervating both muscle types as shown in the in situ hybridization experiments (Figure 3). The finding that soleus-but not diaphragm-NMJs of α-neurexin DKO mice were smaller than those from control animals (Table 2) presumably reflects the difference in neurotransmission, since NMJ size and levels of evoked and spontaneous ACh release are positively correlated (Harris and Ribchester, 1979; Plomp et al., 1992). Other knockout studies leading to decreased neurotransmitter release have reported similar changes of NMJ structure (for recent examples, e.g. Knight et al., 2003; Polo-Parada et al., 2004; Varoqueaux et al., 2005), while the morphology of central synapses in the same mutant mice was remarkably unaffected as was the case in α-neurexin KO animals (Missler et al., 2003). Although our hypothesis that the changes in adult NMJ structure at soleus NMJs are secondary to the functional defects in release caused by the deletion of α-neurexins is further supported by the lack of a structural phenotype in newborns, a different interpretation cannot be completely excluded at present: If neurexins in some indirect way caused the mild growth retardation observed (DKO body weight was ~30% lower than controls) and this was the sole reason that muscle fibers remained smaller, one could consider the reduced evoked release at the α-neurexin DKO soleus NMJ as the result of a proper functioning

homeostatic mechanism where the smaller muscle fiber diameter dictates a lower evoked and spontaneous ACh release. Muscle fiber diameter is known to be inversely related to electrical input resistance (which in turn dictates MEPP amplitude), and positively correlated with NMJ size and level of evoked and spontaneous ACh release. However, if the reduced ACh release at soleus α-neurexin DKO NMJs is regarded as the proper level for such small diameter muscle fibers, the level of spontaneous and evoked ACh release at α-neurexin DKO diaphragm NMJs, which was similar to controls (Figure 2D–E), must be considered as too high for its small fiber diameter. If this idea was true, it could be concluded that lack of α-neurexins causes incorrect transmitter release homeostasis at diaphragm NMJs, rather than a direct reduction of ACh release at soleus NMJs. Finally, it may also be possible that both effects, reduced basal neurotransmission and impaired synaptic homeostasis, coexist but in varying ratios at the NMJs of the different muscles. Irrespective of the actual interpretation, however, our current data on NMJ function and morphology clearly demonstrate that α-neurexins can perform their role as presynaptic regulators even in the absence of a postsynaptic neuronal partner.

References

Bewick GS (2003) Maintenance of transmitter release from neuromuscular junctions with different patterns of usage "in vivo". J Neurocytol 32:473-487.

Biederer T, Sudhof TC (2000) Mints as adaptors. Direct binding to neurexins and recruitment of munc18. J Biol Chem 275:39803-39806.

Biederer T, Sudhof TC (2001) CASK and protein 4.1 support F-actin nucleation on neurexins. J Biol Chem 276:47869-47876.

Boucard AA, Chubykin AA, Comoletti D, Taylor P, Sudhof TC (2005) A splice code for trans-synaptic cell adhesion mediated by binding of neuroligin 1 to alpha- and beta-neurexins. Neuron 48:229-236.

Brandt A, Striessnig J, Moser T (2003) CaV1.3 channels are essential for development and presynaptic activity of cochlear inner hair cells. J Neurosci 23:10832-10840.

Burau K, Stenull I, Huber K, Misawa H, Berse B, Unsicker K, Ernsberger U (2004) c-ret regulates cholinergic properties in mouse sympathetic neurons: evidence from mutant mice. Eur J Neurosci 20:353-362.

Butz S, Okamoto M, Sudhof TC (1998) A tripartite protein complex with the potential to couple synaptic vesicle exocytosis to cell adhesion in brain. Cell 94:773-782.

Chih B, Engelman H, Scheiffele P (2005) Control of excitatory and inhibitory synapse formation by neuroligins. Science 307:1324-1328.

Chubykin AA, Liu X, Comoletti D, Tsigelny I, Taylor P, Sudhof TC (2005) Dissection of synapse induction by neuroligins: effect of a neuroligin mutation associated with autism. J Biol Chem 280:22365-22374.

Day NC, Wood SJ, Ince PG, Volsen SG, Smith W, Slater CR, Shaw PJ (1997) Differential localization of voltage-dependent calcium channel alpha1 subunits at the human and rat neuromuscular junction. J Neurosci 17:6226-6235.

Dean C, Scholl FG, Choih J, DeMaria S, Berger J, Isacoff E, Scheiffele P (2003) Neurexin mediates the assembly of presynaptic terminals. Nat Neurosci.

Ellrich J, Wesselak M (2003) Electrophysiology of sensory and sensorimotor processing in mice under general anesthesia. Brain Res Brain Res Protoc 11:178-188.

Ernsberger U, Esposito L, Partimo S, Huber K, Franke A, Bixby JL, Kalcheim C, Unsicker K (2005) Expression of neuronal markers suggests heterogeneity of chick sympathoadrenal cells prior to invasion of the adrenal anlagen. Cell Tissue Res 319:1-13.

Geppert M, Khvotchev M, Krasnoperov V, Goda Y, Missler M, Hammer RE, Ichtchenko K, Petrenko AG, Sudhof TC (1998) Neurexin I alpha is a major alpha-latrotoxin receptor that cooperates in alpha-latrotoxin action. J Biol Chem 273:1705-1710.

Graf ER, Zhang X, Jin SX, Linhoff MW, Craig AM (2004) Neurexins induce differentiation of GABA and glutamate postsynaptic specializations via neuroligins. Cell 119:1013-1026.

Harris JB, Ribchester RR (1979) The relationship between end-plate size and transmitter release in normal and dystrophic muscles of the mouse. J Physiol 296:245-265.

Hata Y, Butz S, Sudhof TC (1996) CASK: a novel dlg/PSD95 homolog with an N-terminal calmodulin-dependent protein kinase domain identified by interaction with neurexins. J Neurosci 16:2488-2494.

Ichtchenko K, Hata Y, Nguyen T, Ullrich B, Missler M, Moomaw C, Sudhof TC (1995) Neuroligin 1: a splice site-specific ligand for beta-neurexins. Cell 81:435-443.

Ichtchenko K, Nguyen T, Sudhof TC (1996) Structures, alternative splicing, and neurexin binding of multiple neuroligins. J Biol Chem 271:2676-2682.

Jewett DL, Romano MN, Williston JS (1970) Human auditory evoked potentials: possible brain stem components detected on the scalp. Science 167:1517-1518.

Kattenstroth G, Tantalaki E, Sudhof TC, Gottmann K, Missler M (2004) Postsynaptic N-methyl-D-aspartate receptor function requires alpha-neurexins. Proc Natl Acad Sci U S A 101:2607-2612.

Kemi OJ, Loennechen JP, Wisloff U, Ellingsen O (2002) Intensity-controlled treadmill running in mice: cardiac and skeletal muscle hypertrophy. J Appl Physiol 93:1301-1309.

Knight D, Tolley LK, Kim DK, Lavidis NA, Noakes PG (2003) Functional analysis of neurotransmission at beta2-laminin deficient terminals. J Physiol 546:789-800.

Lacas-Gervais S, Guo J, Strenzke N, Scarfone E, Kolpe M, Jahkel M, De CP, Moser T, Rasband MN, Solimena M (2004) BetaIVSigma1 spectrin stabilizes the nodes of Ranvier and axon initial segments. J Cell Biol 166:983-990.

Maximov A, Sudhof TC, Bezprozvanny I (1999) Association of neuronal calcium channels with modular adaptor proteins. J Biol Chem 274:24453-24456.

Misgeld T, Burgess RW, Lewis RM, Cunningham JM, Lichtman JW, Sanes JR (2002) Roles of neurotransmitter in synapse formation: development of neuromuscular junctions lacking choline acetyltransferase. Neuron 36:635-648.

Missler M (2003) Synaptic cell adhesion goes functional. Trends Neurosci 26:176-178.

Missler M, Fernandez-Chacon R, Sudhof TC (1998a) The making of neurexins. J Neurochem 71:1339-1347.

Missler M, Hammer RE, Sudhof TC (1998b) Neurexophilin binding to alpha-neurexins. A single LNS domain functions as an independently folding ligand-binding unit. J Biol Chem 273:34716-34723.

Missler M, Sudhof TC (1998) Neurexins: three genes and 1001 products. Trends Genet 14:20-26.

Missler M, Zhang W, Rohlmann A, Kattenstroth G, Hammer RE, Gottmann K, Sudhof TC (2003) Alpha-neurexins couple Ca2+ channels to synaptic vesicle exocytosis. Nature 424:939-948.

Molenaar PC, Oen BS, Plomp JJ, van Kempen GT, Jennekens FG, Hesselmans LF (1991) A non-immunogenic myasthenia gravis model and its application in a study of transsynaptic regulation at the neuromuscular junction. Eur J Pharmacol 196:93-101.

Muth JN, Varadi G, Schwartz A (2001) Use of transgenic mice to study voltage-dependent Ca2+ channels. Trends Pharmacol Sci 22:526-532.

Nguyen T, Sudhof TC (1997) Binding properties of neuroligin 1 and neurexin 1beta reveal function as heterophilic cell adhesion molecules. J Biol Chem 272:26032-26039.

Nishimune H, Sanes JR, Carlson SS (2004) A synaptic laminin-calcium channel interaction organizes active zones in motor nerve terminals. Nature 432:580-587.

Noakes PG, Gautam M, Mudd J, Sanes JR, Merlie JP (1995) Aberrant differentiation of neuromuscular junctions in mice lacking s-laminin/laminin beta 2. Nature 374:258-262.

Platzer J, Engel J, Schrott-Fischer A, Stephan K, Bova S, Chen H, Zheng H, Striessnig J (2000) Congenital deafness and sinoatrial node dysfunction in mice lacking class D L-type Ca2+ channels. Cell 102:89-97.

Plomp JJ, van Kempen GT, Molenaar PC (1992) Adaptation of quantal content to decreased postsynaptic sensitivity at single endplates in alpha-bungarotoxin-treated rats. J Physiol 458:487-499.

Plomp JJ, van Kempen GT, Molenaar PC (1994) The upregulation of acetylcholine release at endplates of alpha-bungarotoxin-treated rats: its dependency on calcium. J Physiol 478 (Pt 1):125-136.

Plomp JJ, Vergouwe MN, Van den Maagdenberg AM, Ferrari MD, Frants RR, Molenaar PC (2000) Abnormal transmitter release at neuromuscular junctions of mice carrying the tottering alpha(1A) Ca(2+) channel mutation. Brain 123 Pt 3:463-471.

Polo-Parada L, Bose CM, Plattner F, Landmesser LT (2004) Distinct roles of different neural cell adhesion molecule (NCAM) isoforms in synaptic maturation revealed by analysis of NCAM 180 kDa isoform-deficient mice. J Neurosci 24:1852-1864.

Prakash YS, Miller SM, Huang M, Sieck GC (1996) Morphology of diaphragm neuromuscular junctions on different fibre types. J Neurocytol 25:88-100.

Rafuse VF, Polo-Parada L, Landmesser LT (2000) Structural and functional alterations of neuromuscular junctions in NCAM-deficient mice. J Neurosci 20:6529-6539.

Rosahl TW, Spillane D, Missler M, Herz J, Selig DK, Wolff JR, Hammer RE, Malenka RC, Sudhof TC (1995) Essential functions of synapsins I and II in synaptic vesicle regulation. Nature 375:488-493.

Rosato S, Uchitel OD (1999) Calcium channels coupled to neurotransmitter release at neonatal rat neuromuscular junctions. J Physiol 514 (Pt 2):533-540.

Rowen L, Young J, Birditt B, Kaur A, Madan A, Philipps DL, Qin S, Minx P, Wilson RK, Hood L, Graveley BR (2002) Analysis of the human neurexin genes: alternative splicing and the generation of protein diversity. Genomics 79:587-597.

Sanes JR, Lichtman JW (1999) Development of the vertebrate neuromuscular junction. Annu Rev Neurosci 22:389-442.

Sara Y, Biederer T, Atasoy D, Chubykin A, Mozhayeva MG, Sudhof TC, Kavalali ET (2005) Selective capability of SynCAM and neuroligin for functional synapse assembly. J Neurosci 25:260-270.

Scheiffele P (2003) Cell-cell signaling during synapse formation in the CNS. Annu Rev Neurosci 26:485-508.

Scheiffele P, Fan J, Choih J, Fetter R, Serafini T (2000) Neuroligin expressed in nonneuronal cells triggers presynaptic development in contacting axons. Cell 101:657-669.

Song JY, Ichtchenko K, Sudhof TC, Brose N (1999) Neuroligin 1 is a postsynaptic cell-adhesion molecule of excitatory synapses. Proc Natl Acad Sci U S A 96:1100-1105.

Sons MS, Verhage M, Plomp JJ (2003) Role of Munc18-1 in synaptic plasticity at the myasthenic neuromuscular junction. Ann N Y Acad Sci 998:404-406.

Sugita S, Khvochtev M, Sudhof TC (1999) Neurexins are functional alpha-latrotoxin receptors. Neuron 22:489-496.

Sugita S, Saito F, Tang J, Satz J, Campbell K, Sudhof TC (2001) A stoichiometric complex of neurexins and dystroglycan in brain. J Cell Biol 154:435-445.

Tabuchi K, Sudhof TC (2002) Structure and evolution of neurexin genes: insight into the mechanism of alternative splicing. Genomics 79:849-859.

Ullrich B, Ushkaryov YA, Sudhof TC (1995) Cartography of neurexins: more than 1000 isoforms generated by alternative splicing and expressed in distinct subsets of neurons. Neuron 14:497-507.

Urbano FJ, Piedras-Renteria ES, Jun K, Shin HS, Uchitel OD, Tsien RW (2003) Altered properties of quantal neurotransmitter release at endplates of mice lacking P/Q-type Ca2+ channels. Proc Natl Acad Sci U S A 100:3491-3496.

Ushkaryov YA, Hata Y, Ichtchenko K, Moomaw C, Afendis S, Slaughter CA, Sudhof TC (1994) Conserved domain structure of beta-neurexins. Unusual cleaved signal sequences in receptor-like neuronal cell-surface proteins. J Biol Chem 269:11987-11992.

Ushkaryov YA, Petrenko AG, Geppert M, Sudhof TC (1992) Neurexins: synaptic cell surface proteins related to the alpha-latrotoxin receptor and laminin. Science 257:50-56.

Ushkaryov YA, Sudhof TC (1993) Neurexin III alpha: extensive alternative splicing generates membrane-bound and soluble forms. Proc Natl Acad Sci U S A 90:6410-6414.

Valtorta F, Madeddu L, Meldolesi J, Ceccarelli B (1984) Specific localization of the alpha-latrotoxin receptor in the nerve terminal plasma membrane. J Cell Biol 99:124-132.

Van den Maagdenberg AM, Pietrobon D, Pizzorusso T, Kaja S, Broos LA, Cesetti T, van de Ven RC, Tottene A, van der KJ, Plomp JJ, Frants RR, Ferrari MD (2004) A Cacna1a knockin migraine mouse model with increased susceptibility to cortical spreading depression. Neuron 41:701-710.

Varoqueaux F, Sons MS, Plomp JJ, Brose N (2005) Aberrant morphology and residual transmitter release at the Munc13-deficient mouse neuromuscular synapse. Mol Cell Biol 25:5973-5984.

Verhage M, Maia AS, Plomp JJ, Brussaard AB, Heeroma JH, Vermeer H, Toonen RF, Hammer RE, van den Berg TK, Missler M, Geuze HJ, Sudhof TC (2000) Synaptic assembly of the brain in the absence of neurotransmitter secretion. Science 287:864-869.

Wood SJ, Slater CR (1998) beta-Spectrin is colocalized with both voltage-gated sodium channels and ankyrinG at the adult rat neuromuscular junction. J Cell Biol 140:675-684.

Wood SJ, Slater CR (2001) Safety factor at the neuromuscular junction. Prog Neurobiol 64:393-429.

Wu MN, Littleton JT, Bhat MA, Prokop A, Bellen HJ (1998) ROP, the Drosophila Sec1 homolog, interacts with syntaxin and regulates neurotransmitter release in a dosage-dependent manner. EMBO J 17:127-139.

Zhang W, Rohlmann A, Sargsyan V, Aramuni G, Hammer RE, Sudhof TC, Missler M (2005) Extracellular domains of alpha-neurexins participate in regulating synaptic transmission by selectively affecting N- and P/Q-type Ca2+ channels. J Neurosci 25:4330-4342.

4

Rab3A deletion selectively reduces spontaneous neurotransmitter release at the mouse neuromuscular synapse

Michèle S. Sons and Jaap J. Plomp

Departments of Neurology and Molecular Cell Biology - Group Neurophysiology, Leiden University Medical Centre, Leiden, The Netherlands

Brain Research (2006) 1089: 126 - 134

Abstract

Rab3A is a synaptic vesicle-associated GTP-binding protein thought to be involved in modulation of presynaptic transmitter release through regulation of vesicle trafficking and membrane fusion. Electrophysiological studies at central nervous system synapses of Rab3A null-mutant mice have indicated that nerve stimulation-evoked transmitter release, and its short- and long-term modulation, is partly dependent on Rab3A, while spontaneous uniquantal release is completely independent of it. Here, we studied with intracellular microelectrode methods the acetylcholine (ACh) release at the neuromuscular junction (NMJ) of diaphragm and soleus muscles from Rab3A deficient mice. Surprisingly, we found 20-40% reduction of spontaneous ACh release, measured as miniature endplate potential frequency, but completely intact nerve action potential-evoked release at either high- or low-rate stimulation or during recovery from intense release. ACh release induced by hypertonic medium or α-latrotoxin was also unchanged, indicating that the pool of vesicles that is immediately available for release is unaltered at the Rab3A deficient NMJ. These results indicate a selective role of Rab3A in spontaneous transmitter release at the NMJ for which the closely related Rab3B, -C, or -D isoforms apparently do not, or incompletely, compensate when Rab3A is deleted. It has been hypothesized that Rab3A mutation underlies human presynaptic myasthenic syndromes, in which severely reduced nerve action potential-evoked ACh release at the NMJ causes paralysis. Our observation that Rab3A deletion does not reduce evoked ACh release at the mouse NMJ, argues against this hypothesis.

Acknowledgements
This study was supported by the Netherlands Organization for Scientific Research (NWO) (#903-42-073 to J.J.P.). We thank Prof. Matthijs Verhage (Center for Neurogenomics and Cognitive Research, Vrije Universiteit, Amsterdam, The Netherlands) for supplying us with the Rab3A KO mice used in this study

Introduction

Exocytosis of neurotransmitter from synaptic vesicles involves a complex interplay of many presynaptic proteins that regulate vesicle transport, docking, priming, fusion, and recycling (for review, see Lin and Scheller, 2000; Sudhof, 2004). Many of these processes are subjected to modulation, tuning synaptic signaling to ensure proper neuronal network function. Rab3A seems one important modulating factor and is a member of the Rab family of GTP-binding proteins with a general function in intracellular traffic (for review, see Darchen and Goud, 2000). It is thought that the Rab3A, B, C and D subfamily, of which Rab3A is the most abundant in the brain (Geppert et al., 1994), plays a role in mammalian exocytosis. Rab3A is a GTP/GDP-binding protein which, in the GTP-state, is associated with the synaptic vesicle membrane but becomes detached upon GTP to GDP hydrolysis during or shortly after the exocytotic event (Fischer von Mollard et al., 1991; Fischer von Mollard et al., 1994; Star et al., 2005). So far, two putative GTP-Rab3 binding partners have been demonstrated, rabphilin (Shirataki et al., 1993) and Rab Interacting Molecule (RIM) 1α/2α (Wang et al., 2000).

Transgenic deletion in mice showed that Rab3A is not of crucial importance for nervous system function, since these knock-out (KO) mice are viable and do not show overt behavioural abnormalities (Geppert et al., 1994). Detailed analyses of mutant and KO Rab3A mice, however, revealed mild anomalies in exploration behaviour and sleep (Kapfhamer et al., 2002; D'Adamo et al., 2004). Electrophysiological analyses of cultured and brain-slice hippocampal synapses from Rab3A-deficient mice suggested a modulatory role for Rab3A, selective for evoked but not spontaneous release, by showing unchanged or increased initial release, increased paired-pulse facilitation, and a more pronounced rundown at high-rate stimulation, compared to wild-type (Geppert et al., 1994; Geppert et al., 1997). Rab3A-D proteins appear to act mutually compensatory since each single KO mouse is viable and fertile, but the Rab3A-D quadruple KO mouse shows postnatal lethality (Schluter et al., 2004). Analysis of transmitter release at embryonic autaptic cultures from Rab3A-D quadruple deficient hippocampal neurons showed unchanged spontaneous release properties (Schluter et al., 2004), confirming the finding of unchanged spontaneous release at Rab3A single KO synapses (Geppert et al., 1997). However, an about 30% decrease in evoked transmitter release was revealed, resulting from a decrease in release probability (Schluter et al., 2004). From K^+-evoked transmitter release studies at Rab3A KO synaptosomes it appeared that recruitment of synaptic vesicles to active zones after vigorous stimulation is impaired (Leenders et al., 2001).

The modulatory role of Rab3A on evoked transmitter release seems to differ amongst synapse types, as illustrated by different effects of Rab3A deletion on long-term potentiation of synaptic strength in different types of hippocampal excitatory

synapses (Geppert et al., 1994; Castillo et al., 2002). Possibly, differential expression of compensatory Rab3B-D proteins is of importance here.

Here, we investigate a possible role of Rab3A on the release of ACh from motor nerve terminals at the neuromuscular junction (NMJ). It is of importance to understand the roles of neuro-exocytotic proteins at the neuromuscular junction (NMJ). At this peripheral synapse, transmitter release is tightly regulated, in order to maintain successful contraction of muscle fibres, which is crucial for the organism. Defective function of Rab3A and other presynaptic proteins may underlie human congenital presynaptic myasthenic syndromes, where reduced ACh release leads to paralysis (Maselli et al., 2001; Maselli et al., 2003a), alike the auto-immune Lambert-Eaton myasthenic syndrome where presynaptic $Ca_v2.1$ channels are targeted by auto-antibodies (Kim and Neher, 1988).

Rab3A is localized at transmitter release sites of the mammalian presynaptic NMJ (Mizoguchi et al., 1992), as are many other proteins that have been shown to be involved in exocytosis at central synapses. Previously, we demonstrated an identical silencing effect of Munc18-1 deletion on central synapses and the NMJ (Verhage et al., 2000). However, absence of specific presynaptic proteins does not always yields identical effects at central synapses and the NMJ. For instance, recent analysis of NMJ function in double KO Munc13-1/2 embryos contrasted the finding of completely silenced central synapses (Varoqueaux et al., 2002). A severely reduced but not completely blocked evoked transmitter release was found at the NMJ, together with intact spontaneous release (Varoqueaux et al., 2005).

With intracellular microelectrode methods we measured ACh release at NMJs of nerve-muscle preparations from diaphragm and soleus muscles from Rab3A KO mice. We found 20-40% reduction of the spontaneous ACh release, but unchanged nerve action potential-evoked release at low- as well as high-rate stimulation frequencies, and normal release induced by hypertonic medium or α-latrotoxin. These results suggest a selective role of Rab3A in spontaneous transmitter release at the NMJ for which Rab3B, -C, or -D do not, or incompletely, compensate when Rab3A is deleted. Our study shows that Rab3A deficiency does not endanger successful neuromuscular transmission, leaving the Rab3A gene as an unlikely mutation candidate for causing human congenital presynaptic myasthenic syndromes.

Materials and methods

Mice

The generation and genotyping of the Rab3A KO mice has been described previously (Geppert et al., 1994). Mice were housed under a 12 h light / 12 h dark regime and ad libitum food and water. About 3 months-old animals were killed by CO_2 inhalation, and hemi-diaphragms and soleus muscles with their nerves were rapidly dissected and mounted in Ringer's solution (see below) at room temperature. All

animal experiments were carried out in agreement with the Dutch law and Leiden University guidelines.

NMJ electrophysiology

Intracellular voltage measurements were performed on diaphragm and soleus nerve/muscle preparations from Rab3A KO mice and littermate wild-type controls, pinned out on the bottom of a silicone rubber-lined dish in Ringer's medium containing (mM): NaCl, 116; KCl, 4.5; $MgCl_2$, 1; $CaCl_2$, 2; NaH_2PO_4, 1; $NaHCO_3$, 23; glucose 11; pH 7.4, gassed with 95 % O_2/5 % CO_2 at 26-28°C. The nerve was electrically stimulated through either a bipolar electrode (diaphragm) or a suction electrode (soleus) with supramaximal pulses (100 μs duration) from a Master-8 programmable stimulus generator (AMPI, Jerusalem, Israel). Upon stimulation, the nerve terminal synchronously releases a number of ACh quanta that stimulate postsynaptic ACh receptors and thus cause an endplate potential (EPP). Spontaneous release of single quanta results in miniature EPPs (MEPPs). We recorded EPPs and MEPPs by impaling muscle fibres near the NMJ with a 10-20 MΩ glass capillary microelectrode filled with 3 M KCl and connected to a GeneClamp 500B amplifier (Axon Instruments/Molecular Devices, Union City, CA, USA) for amplifying and filtering (10 kHz low-pass) of the signal. Signals were digitized, stored and analyzed (off-line) using a Digidata 1200 interface, Clampex 8.0 and Clampfit 8.0 programs (all from Axon Instruments/Molecular Devices) and routines programmed in Matlab (The MathWorks Inc., Natick, MA, USA). Muscles were incubated with 3.1 μM μ-Conotoxin GIIIB (Scientific Marketing Associates, Herts, UK), a selective blocker of muscle sodium channels, to prevent muscle action potentials. This allowed for the undisturbed recording of EPPs during electrical nerve stimulation (0.3, 20, 30, 40 and 50 Hz). The amplitudes of EPPs and MEPPs were normalized to –75 mV, assuming 0 mV as the reversal potential for ACh-induced current (Magleby and Stevens, 1972), using the formula: $EPP_{normalized} = EPP \times (-75/V_m)$, where V_m is the measured resting membrane potential. The quantal content (i.e. the number ACh quanta released upon a single nerve impulse) at each NMJ at 0.3 Hz stimulation was calculated by dividing the normalized EPP by the normalized MEPP amplitude. The EPP amplitude was first corrected for non-linear summation, as described before (Plomp et al., 1994). During high-frequent stimulation, EPP amplitudes decrease to a plateau level. This rundown level was determined by calculating the average amplitude of the last 10 EPPs in a 40 Hz train of 1s duration and expressing it as percentage of the amplitude of the first EPP of the train.

MEPPs were also recorded shortly after exposure of preparations to hypertonic medium (0.5 M sucrose Ringer), assessing the pool of ACh vesicles ready for immediate release (Stevens and Tsujimoto, 1995). Furthermore, MEPPs were recorded after application of 2.5 nM α-latrotoxin (Alomone Laboratories, Jerusalem, Israel).

Statistical analyses

The data is given as mean ± S.E.M, with n representing the number of muscles tested. At least 30 MEPPs and EPPs were recorded at each NMJ. From the mean NMJ values, a muscle mean value was calculated (at least 10 NMJs were sampled per muscle per experimental condition), which was used to calculated a genotype group mean value. Four to six mice were used per genotype, from each mouse one diaphragm and one soleus muscle was analyzed. Possible differences between the mean values of genotype groups were tested with Student's *t*-test and were considered statistically significant if the p-value was <0.05.

Results

Spontaneous ACh release is reduced at Rab3A deficient NMJs

Spontaneous ACh release at diaphragm NMJs from Rab3A KO mice and wild-type littermates was electrophysiologically determined by recording MEPPs, the spontaneous uniquantal release events. At diaphragm NMJs, a decrease of 19% in MEPP frequency was observed in Rab3A KO NMJs, compared to wild-type (1.24 ± 0.06 s^{-1} and 1.54 ± 0.08 s^{-1}, respectively, n=6 mice, $p<0.05$, Figure 1A). The amplitude of the MEPPs was similar for both genotypes (0.94 ± 0.09 mV at wild-type, and 1.00 ± 0.06 mV at Rab3A KO NMJs, n=6, p=0.5, Figure 1C, D). Similarly, the MEPP kinetics (rise times, decay times and half-widths) were unchanged (data not shown, Figure 1D), indicating that there were no changes in postsynaptic ACh receptor function due to the Rab3A deficiency. The diaphragm muscle consists of a mixed population of fast- and slow-twitch fibres, which are known to have different NMJ characteristics (Bewick, 2003). To investigate whether Rab3A deletion has differential effects on slow-twitch fibres we also investigated spontaneous ACh release at NMJs of the soleus muscle, which exclusively consists of slow-twitch fibres. Again, we found a decreased MEPP frequency (~40%) in Rab3A KO NMJs compared to wild-type (1.63 ± 0.11 s^{-1} and 2.77 ± 0.28 s^{-1}, respectively; n=6, $p<0.001$, Figure 1A). This decrease was more pronounced than that observed at diaphragm NMJs ($p<0.01$, Figure 1B). MEPP kinetics as well as amplitudes (~0.65 mV, n=6, p=0.6, Figure 1C, D) were again not different from wild-type. Thus, in contrast to central synapses (Hughes et al., 1999), Rab3A deletion reduces spontaneous transmitter release at NMJs, in particular those of slow-twitch muscles.

Unaltered size of readily releasable vesicle pool

The observed reduction in spontaneous ACh release may be caused by a reduction of the number of transmitter vesicles that are ready for release. In order to probe for this vesicle pool (Stevens and Tsujimoto, 1995) we added hypertonic medium (0.5 M sucrose-Ringer) and measured the resulting elevated MEPP frequency. No

difference between genotypes was observed (diaphragm: 53.6 ± 6.5 s^{-1} at wild-type and 58.3 ± 9.3 s^{-1} at Rab3A KO NMJs, n=5-6 mice, p=0.68; soleus: 53.9 ± 6.9 s^{-1} at wild-type and 52.8 ± 9.6 s^{-1} at Rab3A KO NMJs, n=5 mice, p=0.61, Figure 1E, F).

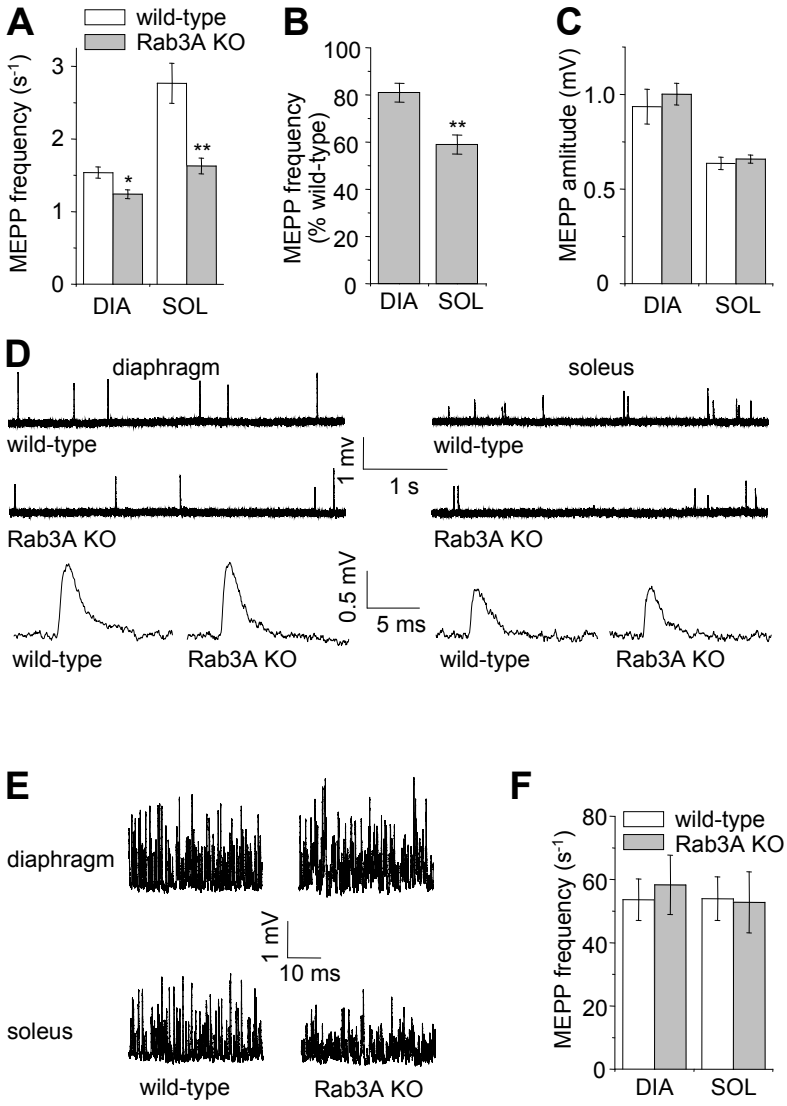

Figure 1. Deletion of Rab3A reduces spontaneous transmitter release at mouse diaphragm and soleus NMJs.

(A) Mean MEPP frequency at NMJs from diaphragm (DIA) and soleus (SOL) from wild-type and Rab3A KO mice. (B) The reduction of MEPP frequency is more pronounced at soleus than at diaphragm Rab3A KO NMJs. (C) No difference in MEPP amplitude between Rab3A KO and wild-type NMJs of either diaphragm or soleus muscles. (D) Typical examples of 4 s recording traces of MEPPs, at diaphragm (left) and soleus (right) NMJs. Lower traces are typical examples of individual MEPPs.(E) Typical examples of 1 s recording traces of MEPPs measured in the presence of hypertonic medium (0.5 M sucrose-Ringer). (F) No difference in mean values of MEPP frequency measured in the presence of 0.5 M sucrose-Ringer.

Data obtained from n=5-6 mice, 10-15 NMJs per muscle. Error bars represent SEM. *p<0.05, and **p<0.01.

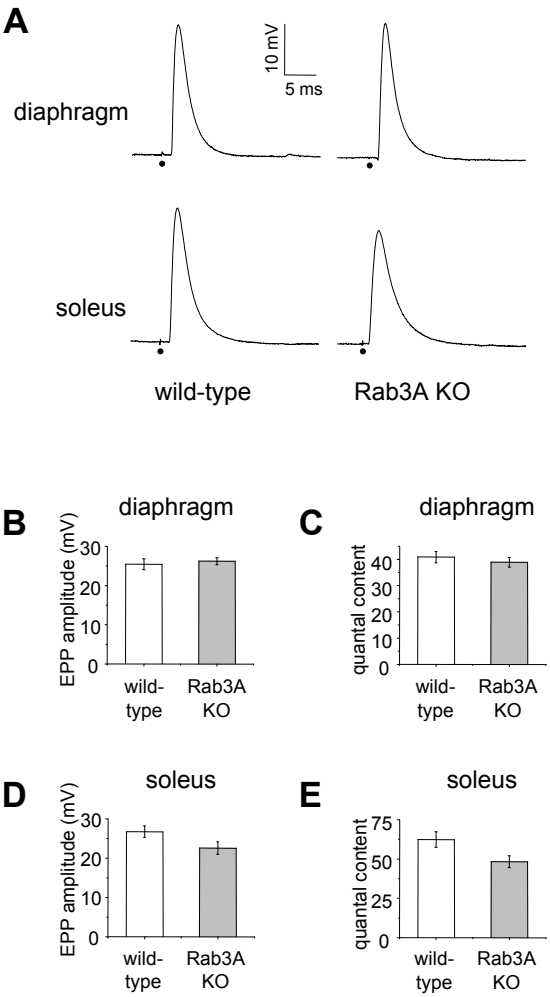

Figure 2. No differences in low-rate (0.3 Hz) nerve stimulation-evoked evoked ACh release between Rab3A KO and wild-type NMJs.
(A) Typical examples of EPPs recorded at diaphragm and soleus NMJs of wild-type and Rab3A KO mice. Black dots indicate moment of nerve stimulation. (B) Mean values of EPP amplitudes recorded at diaphragm NMJs. (C) Mean values of the calculated quantal contents at diaphragm NMJs. (D) Mean values of EPP amplitudes recorded at soleus NMJs. (E) Mean values of the calculated quantal contents at soleus NMJs. Data obtained from n=5-6 mice, 10-15 NMJs per muscle. Error bars represent SEM.

This result suggests unaltered size of the readily releasable vesicle pool at Rab3A KO NMJs.

Unchanged nerve action potential-evoked ACh release

We measured ACh release at diaphragm NMJs evoked by low-frequent (0.3 Hz) electrical stimulation of the phrenic nerve (Figure 2A). EPP amplitudes of wild-type and Rab3A KO NMJs were similar (25.4 ± 1.4 and 26.2 ± 0.9 mV, respectively, n=6 mice, p=0.6). The calculated quantal content, the number of ACh quanta re-

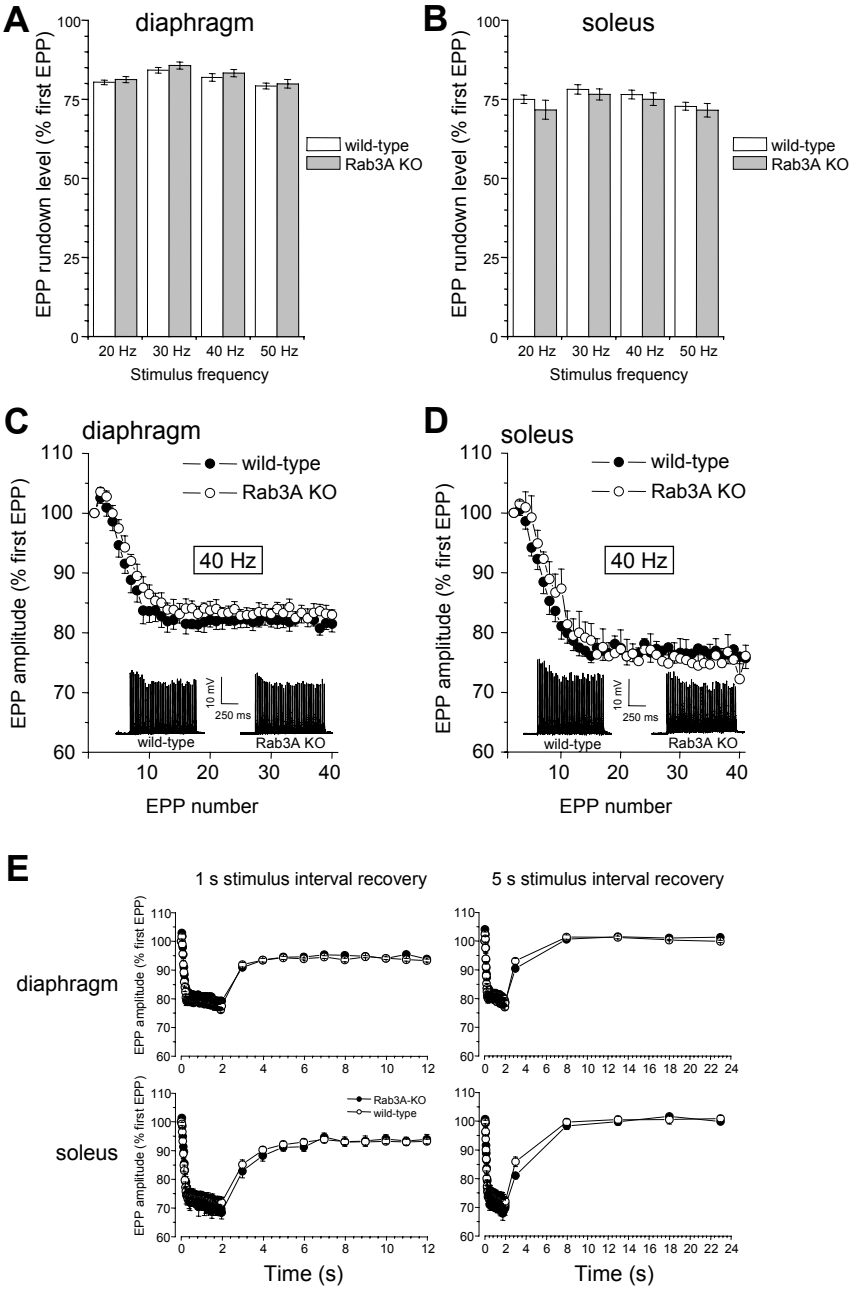

Figure 3. No differences in high-rate nerve stimulation-evoked ACh release between Rab3A KO and wild-type NMJs.

Equal EPP rundown level (mean value of the 21-35th EPP in the train, expressed as percentage of the amplitude of the first EPP), upon 20, 30, 40 or 50 Hz nerve stimulation at Rab3A KO and wild-type NMJs from diaphragm (A) or soleus (B) muscles. Data obtained from n=5-6 mice, 10-15 NMJs per muscle. Averaged 40 Hz EPP rundown profiles from diaphragm (C) or soleus (D) muscles, with examples of individual EPP trains as insets. Kinetics and level of recovery form EPP rundown was equal for Rab3A and wild-type NMJs of diaphragm (E) and soleus (F) NMJs, as assessed with a protocol applying single nerve stimuli at 1 or 5 s intervals.

leased upon nerve stimulation was similar (40.9 ± 2.1 at wild-type, and 38.9 ± 1.8 at Rab3A KO NMJs, n=6 mice, p=0.5). At soleus muscle NMJs, we found a somewhat decreased (23%) quantal content at Rab3A KO NMJs, but this reduction was not statistically significant (p=0.06, Figure2B). The EPP amplitudes were slightly smaller in Rab3A KO NMJs, but again this difference was not statistically significant (26.7 ± 1.5 mV in wild-type, and 22.6 ± 1.6 mV in Rab3A KO NMJs, n=5-6 mice, p=0.09, Figure 2B). These results indicate that low-rate evoked release is not dependent on Rab3A presence.

In view of the more pronounced rundown of evoked transmitter release at high-rate stimulation at central synapses (Geppert et al., 1994), we studied the ACh release at NMJs upon 1 s trains of 20, 30, 40 and 50 Hz stimulation. At all stimulation frequencies, EPP amplitudes ran down to a similar level in both Rab3A KO and wild-type diaphragm NMJs, with EPP amplitudes at the plateau phase of the stimulus train being about 80-85% of the first EPP in the trains (p=0.48-0.70, n=6 mice, Figure 2C, E). Similarly, at soleus NMJs, high-rate stimulation resulted in equal EPP run-down level in both genotypes for all tested frequencies (to about 72-78%, of the first EPP in the trains, p=0.30-0.61, n=5-6 mice, Figure 3A-D). Thus, Rab3A deletion does not affect high-rate evoked ACh release at NMJs.

Normal recovery from high-rate ACh release

Rab3A may be important for replenishment of the readily releasable vesicle pool after intense transmitter release. Therefore, we monitored the recovery of the EPP amplitude after a 2 s train of 40 Hz stimuli, by giving single stimuli with intervals of either 1 or 5 s, starting 1 s after the end of the 40 Hz train. No differences in recovery rates were observed between Rab3A and wild-type NMJs, of either diaphragm or soleus NMJs (Figure 3E) .

a-Latrotoxin-induced transmitter release

As an alternative means to evoke transmitter release, we applied 2.5 nM α-latrotoxin to diaphragm NMJs. This toxin binds to presynaptic receptors and evokes Ca^{2+}-dependent and -independent transmitter release by insertion of ion-pores and stimulation of secondary messengers (Ushkaryov et al., 2004), resulting in high frequency MEPPs at the NMJ. However, the MEPP frequency was not statistically significantly different between genotypes, 120.8 ± 23.4 s^{-1} in wild-type NMJs, compared to 88.3 ± 13.9 s^{-1} in Rab3A NMJs (n=4-5 mice, p=0.25).

Discussion

We have examined the effect of Rab3A deficiency on ACh release at the NMJ and found that spontaneous uniquantal release, but not the release evoked by either low- or high-rate electrical stimulation, hypertonic medium or α-latrotoxin, is reduced.

These results indicate that Rab3A has a specific role in the mechanism underlying spontaneous transmitter release at the NMJ, which is not compensated for by other Rab3 family members. The absence of effects on evoked ACh release indicates that Rab3A is either not involved in the underlying mechanism, or that other Rab3 family members fully compensate for its loss. Together these results show that Rab3A deletion does not endanger successful neuromuscular transmission.

The present finding of reduced spontaneous ACh release at NMJs due to Rab3A deletion is surprising in view of the central synapse studies (on primary cultured Rab3A-deficient hippocampal neurons) that showed unaltered frequency of spontaneous synaptic events (Geppert et al., 1997; Schluter et al., 2004). Although developmental reasons can not be ruled out (the central studies used embryonic material, while we studied NMJs from adult mice), the discrepancy most likely follows from more fundamental differences between hippocampal synapses and NMJs. It may be that expression of Rab3B, C, and D isoforms is lower at the NMJ, so that their compensatory action upon Rab3A deletion is less pronounced. Alternatively, the specific composition of the neuro-exocytotic release machinery at the NMJ may differ from hippocampal synapses, in that it is more dependent on Rab3A for spontaneous release. For instance, the Rab3A binding partners rabphilin and/or RIM1α may be relative highly expressed at NMJs. About half of the spontaneous uniquantal ACh release at the mammalian NMJ is caused by Ca^{2+} influx via $Ca_v2.1$ channels, which apparently undergo some opening at resting membrane potential (Plomp et al., 2000; Kaja et al., 2005). Rab3A might have some (indirect) stimulatory effect on the opening of such channels. In this respect it is of interest that NMJs of some $Ca_v2.1$-mutant mice show altered spontaneous ACh release without having altered low-rate evoked ACh release (Plomp et al., 2000; Kaja et al., 2004; Kaja et al., 2005).

The similar response of Rab3A KO and wild-type NMJs to α-latrotoxin and hypertonic medium application indicate that it is not likely that the reduced MEPP-frequency in Rab3A KO NMJs results from a decrease in the number of vesicles in the readily releasable vesicle pool. Unchanged vesicle pool-size was also found at Rab3A KO hippocampal synapses (Geppert et al., 1997).

Postsynaptic MEPPs caused by spontaneous uniquantal ACh release at NMJs do neither influence the postsynaptic response to nerve stimulation-evoked release (EPPs), nor do they trigger muscle contraction by themselves (Wood and Slater, 2001). Thus, the selective reduction of spontaneous uniquantal ACh release at Rab3A deficient NMJs does not acutely endanger the successful transmission of impulses at the NMJ. However, it may have indirect effects in the longer term. At central synapses, miniature events have recently been shown to inhibit postsynaptic protein synthesis (Sutton et al., 2004). If a similar mechanism exists at the NMJ, reduced spontaneous release at Rab3A KO NMJs would lead to upregulated postsynaptic protein synthesis, possibly affecting ACh receptor expression or homeostatic

mechanisms regulating presynaptic transmitter release via retrograde messengers (Plomp et al., 1992). For hippocampal synapses it has been hypothesized that transmitter quanta for spontaneous and nerve stimulation-evoked release originate from functionally distinct vesicle pools (Sara et al., 2005), although findings at another synapse seem not in agreement (Lou et al., 2005). If, however, such separate pools would also exist at NMJs, it might be speculated on the basis of the present results that Rab3A is selectively involved in trafficking of the vesicle pool that fuels spontaneous ACh release at the NMJ.

The reduction of spontaneous ACh release in Rab3A KO mice was more pronounced at soleus than at diaphragm NMJs. This may be related to the difference in muscle fibre types: the soleus is a slow-twitch muscle, while the diaphragm is a muscle with mixed slow- and fast-twitch fibre composition (Prakash et al., 1996; Bewick, 2003). NMJs on slow- and fast-twitch fibres differ in structure and function, those on slow fibers being less elongated, more fatigue-resistant, and having a lower initial ACh release level (Bewick, 2003). These differences are probably related to differences in stimulation frequency and history of use, possibly affecting local expression of neuro-exocytotic proteins. It may be that Rab3A (as well as Rab3B, C, and D) expression level is differentially regulated at motor nerve terminals on different muscle fibre types, leading to the observed difference in magnitude of the reduction of spontaneous ACh release. In a recent study we showed that neuro-exocytotic proteins other than Rab3A also have differential roles at NMJs of different fibre types: in mice deficient for α-neurexins we found differential reducing effects on ACh release at soleus and diaphragm NMJs (Sons et al., 2006).

Low-rate nerve stimulation-evoked ACh release was unaltered at Rab3A deficient NMJs. Again, as for spontaneous release, this finding seems at variance with data obtained from central synapses from Rab3A KO mice. In hippocampal synapses, basal electrical stimulation-evoked release was found unchanged (brain slices, Geppert et al., 1994) or increased (cultured neurons, Geppert et al., 1997). Furthermore, at the Rab3A KO NMJ we did not observe increased rundown of transmitter release upon repetitive stimulation as observed at hippocampal synapses (Geppert et al., 1994). We excluded a role for Rab3A in recovery from high-rate evoked release by showing that EPP amplitudes of wild-type and Rab3A NMJs returned with similar time-course to similar levels after a 2 s 40 Hz stimulus train. Similarly, recovery from hypertonic stimulation-induced transmitter release was shown unchanged at hippocampal synapses (Geppert et al., 1997), indicating that Rab3A is not generally involved in recovery of the readily releasable vesicle pool and evoked transmitter release. However, a role of Rab3A in vesicle trafficking upon recovery of K^+ depolarization-evoked transmitter release has been proposed in a study of Rab3A deficient forebrain synaptosomes (Leenders et al., 2001).

ACh release at diaphragm NMJs from Rab3A KO mice has been studied to some extent by Hirsh and colleagues (Hirsh et al., 2002). In that study, spontaneous ACh release was found reduced by ~30%, although this change was not statistically significant. Furthermore, it was reported that low-rate evoked ACh release was unchanged, which we confirmed in the present study. However, a less pronounced rundown of EPPs was shown at 50 Hz nerve stimulation at Rab3A deficient NMJs, which we could not reproduce at any of the high-rate stimulation frequencies used in the current study. One reason for this apparent discrepancy may be that Hirsh et al. in their experiments used d-tubocurarine to reduce the EPPs to subthreshold levels in order to prevent the triggering of muscle action potentials. Besides blocking postsynaptic ACh receptors, d-tubocurarine is known to have a presynaptic effect, possibly mediated by nicotinergic autoreceptors, resulting in increased EPP rundown (Glavinovic, 1979). The reduced EPP rundown at Rab3A deficient NMJs, compared to wild-type, in the presence of d-tubocurarine in the experiments of Hirsh et al. may indicate that Rab3A is in some way involved in the mechanism underlying this presynaptic effect of d-tubocurarine. However, in our experiments using μ-conotoxin as a tool to eliminate muscle action potentials (which has no presynaptic effects and does not interfere with ACh receptors) we failed to observe any effect of Rab3A deletion on EPP rundown. This indicates that increased EPP rundown is not a physiological feature of the Rab3A deficient NMJ.

The present study argues against the hypothesis that Rab3A mutation could underlie paralysis in human congenital presynaptic myasthenic syndromes. Rab3A mice do not show symptoms of muscle weakness, which is in agreement with the lack of effects we observed on nerve stimulation-evoked ACh release at their NMJs. Furthermore, mutational analyses have not yielded any mutation or polymorphism in the Rab3A gene in patients with congenital presynaptic myasthenic syndromes (Maselli et al., 2001; Maselli et al., 2003a). Thus far, only some episodic ataxia type-2 associated mutations in *CACNA1A*, the gene encoding presynaptic $Ca_v2.1$ channels, have been shown to cause presynaptic dysfunction at human NMJs (Maselli et al., 2003b).

Taken together, the present study shows that the synaptic phenotype resulting from Rab3A deletion at the NMJ clearly differs from that observed at central synapses, especially with respect to spontaneous transmitter release, adding further evidence to the view that Rab3A has distinct roles at different synapse types (Castillo et al., 2002; Sudhof, 2004).

References

Bewick GS (2003) Maintenance of transmitter release from neuromuscular junctions with different patterns of usage "in vivo". J Neurocytol 32:473-487.

Castillo PE, Schoch S, Schmitz F, Sudhof TC, Malenka RC (2002) RIM1alpha is required for presynaptic long-term potentiation. Nature 415:327-330.

D'Adamo P, Wolfer DP, Kopp C, Tobler I, Toniolo D, Lipp HP (2004) Mice deficient for the synaptic vesicle protein Rab3a show impaired spatial reversal learning and increased explorative activity but none of the behavioral changes shown by mice deficient for the Rab3a regulator Gdi1. Eur J Neurosci 19:1895-1905.

Darchen F, Goud B (2000) Multiple aspects of Rab protein action in the secretory pathway: focus on Rab3 and Rab6. Biochimie 82:375-384.

Fischer von Mollard G, Stahl B, Khokhlatchev A, Sudhof TC, Jahn R (1994) Rab3C is a synaptic vesicle protein that dissociates from synaptic vesicles after stimulation of exocytosis. J Biol Chem 269:10971-10974.

Fischer von Mollard G, Sudhof TC, Jahn R (1991) A small GTP-binding protein dissociates from synaptic vesicles during exocytosis. Nature 349:79-81.

Geppert M, Bolshakov VY, Siegelbaum SA, Takei K, De Camilli P, Hammer RE, Sudhof TC (1994) The role of Rab3A in neurotransmitter release. Nature 369:493-497.

Geppert M, Goda Y, Stevens CF, Sudhof TC (1997) The small GTP-binding protein Rab3A regulates a late step in synaptic vesicle fusion. Nature 387:810-814.

Glavinovic MI (1979) Presynaptic action of curare. J Physiol 290:499-506.

Hirsh JK, Searl TJ, Silinsky EM (2002) Regulation by Rab3A of an endogenous modulator of neurotransmitter release at mouse motor nerve endings. J Physiol 545:337-343.

Hughes RA, Hadden RD, Gregson NA, Smith KJ (1999) Pathogenesis of Guillain-Barre syndrome. J Neuroimmunol 100:74-97.

Kaja S, van de Ven RC, Broos LA, Frants RR, Ferrari MD, Van Den Maagdenberg AM, Plomp JJ (2004) Increased transmitter release at neuromuscular synapses of a novel Cacna1a S218L knock-in mouse model for familial hemiplegic migraine. Soc Neurosci Abstr:593.4.

Kaja S, van de Ven RC, Broos LA, Veldman H, Van Dijk JG, Verschuuren JJ, Frants RR, Ferrari MD, Van Den Maagdenberg AM, Plomp JJ (2005) Gene dosage-dependent transmitter release changes at neuromuscular synapses of CACNA1A R192Q knockin mice are non-progressive and do not lead to morphological changes or muscle weakness. Neuroscience 135:81-95.

Kapfhamer D, Valladares O, Sun Y, Nolan PM, Rux JJ, Arnold SE, Veasey SC, Bucan M (2002) Mutations in Rab3a alter circadian period and homeostatic response to sleep loss in the mouse. Nat Genet 32:290-295.

Kim YI, Neher E (1988) IgG from patients with Lambert-Eaton syndrome blocks voltage-dependent calcium channels. Science 239:405-408.

Leenders AG, Lopes da Silva FH, Ghijsen WE, Verhage M (2001) Rab3a is involved in transport of synaptic vesicles to the active zone in mouse brain nerve terminals. Mol Biol Cell 12:3095-3102.

Lin RC, Scheller RH (2000) Mechanisms of synaptic vesicle exocytosis. Annu Rev Cell Dev Biol 16:19-49.

Lou X, Scheuss V, Schneggenburger R (2005) Allosteric modulation of the presynaptic Ca^{2+} sensor for vesicle fusion. Nature 435:497-501.

Magleby KL, Stevens CF (1972) A quantitative description of end-plate currents. J Physiol 223:173-197.

Maselli RA, Books W, Dunne V (2003a) Effect of inherited abnormalities of calcium regulation on human neuromuscular transmission. Ann N Y Acad Sci 998:18-28.

Maselli RA, Kong DZ, Bowe CM, McDonald CM, Ellis WG, Agius MA, Gomez CM, Richman DP, Wollmann RL (2001) Presynaptic congenital myasthenic syndrome due to quantal release deficiency. Neurology 57:279-289.

Maselli RA, Wan J, Dunne V, Graves M, Baloh RW, Wollmann RL, Jen J (2003b) Presynaptic failure of neuromuscular transmission and synaptic remodeling in EA2. Neurology 61:1743-1748.

Mizoguchi A, Arakawa M, Masutani M, Tamekane A, Yamaguchi H, Minami N, Takai Y, Ide C (1992) Localization of smg p25A/rab3A p25, a small GTP-binding protein, at the active zone of the rat neuromuscular junction. Biochem Biophys Res Commun 186:1345-1352.

Plomp JJ, van Kempen GT, Molenaar PC (1992) Adaptation of quantal content to decreased postsynaptic sensitivity at single endplates in alpha-bungarotoxin-treated rats. J Physiol 458:487-499.

Plomp JJ, van Kempen GT, Molenaar PC (1994) The upregulation of acetylcholine release at endplates of alpha-bungarotoxin-treated rats: its dependency on calcium. J Physiol 478 (Pt 1):125-136.

Plomp JJ, Vergouwe MN, Van Den Maagdenberg AM, Ferrari MD, Frants RR, Molenaar PC (2000) Abnormal transmitter release at neuromuscular junctions of mice carrying the tottering alpha(1A) Ca(2+) channel mutation. Brain 123:463-471.

Prakash YS, Miller SM, Huang M, Sieck GC (1996) Morphology of diaphragm neuromuscular junctions on different fibre types. J Neurocytol 25:88-100.

Sara Y, Virmani T, Deak F, Liu X, Kavalali ET (2005) An isolated pool of vesicles recycles at rest and drives spontaneous neurotransmission. Neuron 45:563-573.

Schluter OM, Schmitz F, Jahn R, Rosenmund C, Sudhof TC (2004) A complete genetic analysis of neuronal Rab3 function. J Neurosci 24:6629-6637.

Shirataki H, Kaibuchi K, Sakoda T, Kishida S, Yamaguchi T, Wada K, Miyazaki M, Takai Y (1993) Rabphilin-3A, a putative target protein for smg p25A/rab3A p25

small GTP-binding protein related to synaptotagmin. Mol Cell Biol 13:2061-2068.

Sons MS, Busche NS, Strenske N, Moser T, Ernsberger U, Mooren FC, Zhang W, Ahmad M, Steffens H, Schomburg ED, Plomp JJ, Missler M (2006) Alpha-neurexins are required for efficient transmitter release and synaptic homeostasis at the mouse neuromuscular junction. Neuroscience:in press.

Star EN, Newton AJ, Murthy VN (2005) Real-time imaging of Rab3a and Rab5a reveals differential roles in presynaptic function. J Physiol 569:103-117.

Stevens CF, Tsujimoto T (1995) Estimates for the pool size of releasable quanta at a single central synapse and for the time required to refill the pool. Proc Natl Acad Sci U S A 92:846-849.

Sudhof TC (2004) The synaptic vesicle cycle. Annu Rev Neurosci 27:509-547.

Sutton MA, Wall NR, Aakalu GN, Schuman EM (2004) Regulation of dendritic protein synthesis by miniature synaptic events. Science 304:1979-1983.

Ushkaryov YA, Volynski KE, Ashton AC (2004) The multiple actions of black widow spider toxins and their selective use in neurosecretion studies. Toxicon 43:527-542.

Varoqueaux F, Sigler A, Rhee JS, Brose N, Enk C, Reim K, Rosenmund C (2002) Total arrest of spontaneous and evoked synaptic transmission but normal synaptogenesis in the absence of Munc13-mediated vesicle priming. Proc Natl Acad Sci U S A 99:9037-9042.

Varoqueaux F, Sons MS, Plomp JJ, Brose N (2005) Aberrant morphology and residual transmitter release at the Munc13-deficient mouse neuromuscular synapse. Mol Cell Biol 25:5973-5984.

Verhage M, Maia AS, Plomp JJ, Brussaard AB, Heeroma JH, Vermeer H, Toonen RF, Hammer RE, van den Berg TK, Missler M, Geuze HJ, Sudhof TC (2000) Synaptic assembly of the brain in the absence of neurotransmitter secretion. Science 287:864-869.

Wang Y, Sugita S, Sudhof TC (2000) The RIM/NIM family of neuronal C2 domain proteins. Interactions with Rab3 and a new class of Src homology 3 domain proteins. J Biol Chem 275:20033-20044.

Wood SJ, Slater CR (2001) Safety factor at the neuromuscular junction. Prog Neurobiol 64:393-429.

5

Munc18-1 expression levels control synapse recovery by regulating readily releasable pool size

Michèle S. Sons,[1*] Ruud F. G. Toonen,[2*] Keimpe Wierda,[2*] Heidi de Wit,[2] L. Niels Cornelisse,[2] Arjen Brussaard,[3] Jaap J. Plomp,[1] and Matthijs Verhage[2,4]

1 Departments of Neurology and Neurophysiology, Leiden University Medical Center, Research Building, P.O. Box 9600, 2300 RC, Leiden, The Netherlands
2 Department of Functional Genomics Center for Neurogenomics and Cognitive Research, Vrije Universiteit, De Boelelaan 1087,1081 HV, Amsterdam, The Netherlands
3 Department of Experimental Neurophysiology Center for Neurogenomics and Cognitive Research, Vrije Universiteit, De Boelelaan 1087,1081 HV, Amsterdam, The Netherlands
4 Department of Pharmacology and Anatomy, Rudolf Magnus Institute of Neuroscience, University Medical Center, Universiteitsweg 100, 3584 CG, Utrecht, The Netherlands

**M.S., R.T, and K.W. contributed equally to this study.*

Published in PNAS (2006) 103: 18332 - 18337.

Abstract

Prompt recovery after intense activity is an essential feature of most mammalian synapses. Here we show that synapses with reduced expression of the presynaptic gene munc18-1 suffer from increased depression during intense stimulation at glutamatergic, GABAergic, and neuromuscular synapses. Conversely, Munc18-1 overexpression makes these synapses recover faster. Concomitant changes in the readily releasable vesicle pool and its refill kinetics were found. The number of vesicles docked at the active zone and the total number of vesicles per terminal correlated with both Munc18-1 expression levels and the size of the releasable vesicle pool. These data show that varying expression of a single gene controls synaptic recovery by modulating the number of docked, release-ready vesicles and thereby replenishment of the secretion capacity.

Acknowledgements

We thank Robbert Zalm, Desiree Schut, Hans Lodder, and Ineke Lavrijsen for invaluable technical assistance. This work was supported by Dutch Organization for Scientific Research Grants NWO-GBMW 903-42-073 (to J.J.P.) and NWO-GBMW 903-42-023; ZonMW Veni Grants 016-066-101 (to R.F.G.T.), GpD 970-10-036 (to M.V. and H.d.W.), and 916-36-043 (to H.d.W.); Zon-MW Pionier Grant MW-PI0900-01-001 (to M.V.); and NeuroBsik Mouse Phenomics Consortium (Grant BSIK03053).

Introduction

Reliable and sustainable neurotransmitter release is essential for effective neuronal communication. However, neurons only have a limited number of fusion-ready vesicles that reside in a vesicle pool at the membrane of the presynaptic terminal (Rizzoli and Betz, 2005). During periods of increased activity, this vesicle pool is depleted, resulting in a decreased reliability of neurotransmission. To ensure efficient neurotransmission, neurons need to be able to increase the initial number of fusion-ready vesicles [the so-called readily releasable pool (RRP)] and/or the rate at which this pool is replenished during activity. However, surprisingly little is known about the molecular mechanisms that control the size of the RRP and the way vesicles are recruited to this pool.

The Sec1/Munc18-like (SM) protein Munc18-1 has emerged as a key component for calcium-dependent neurotransmitter release (Rizo and Sudhof, 2002). SM proteins function in all intracellular membrane trafficking pathways across species. Genetic deletion of munc18-1 and most other SM genes involved in synaptic-vesicle release across species results in a complete block of neurotransmitter release (Harrison et al., 1994; Verhage et al., 2000; Weimer et al., 2003), which shows that Munc18-1 and probably all SM proteins are indispensable factors that promote vesicle secretion (Rizo and Sudhof, 2002; Toonen and Verhage, 2003; Sudhof, 2004). However, identifying where SM proteins act in the cascade of events leading to the release of neurotransmitter has proven to be difficult and has generated apparently conflicting data (Schulze et al., 1994; Dresbach et al., 1998; Scott et al., 2004).

Here, we analyzed the effect of different Munc18-1 expression levels on synaptic function in autaptic synapses of GABAergic and glutamatergic central neurons, as well as in the peripheral neuromuscular junction (NMJ). We combined electrophysiological and optical measurements to show that Munc18-1 controls synapse efficacy in a bidirectional way via the control of the size and replenishment rate of the RRP.

Materials and Methods

Transgenic null-mutant mice.

Two independent null-mutant mouse lines were produced for the munc18-1 gene as described (Verhage et al., 2000). Mice were bred as heterozygotes by using standard mouse husbandry and back-crossed for at least six generations to a C57BL/6 background.

Transgenic Munc18-overexpressing mice.

The genotypes of all offspring were analyzed by Southern blot or PCR. The promoter of the neuron specific enolase (NSE) gene from rat (Forss-Petter et al., 1990)

was used to create Munc18-1 overexpressing transgenic mice. The Munc18-1 cDNA containing its endogenous Kozak sequence was inserted into the HindIII site of the pNSE-Ex4 minigene consisting of 2.8 kb 5' flanking DNA, exon I (50 bp), intron I (1.2 kb), and 6 bp of exon II of the rat NSE gene followed by a 1.0-kb SV40 polyadenylation signal (Figure 10 A and B). Transgenic mice were generated by pronuclear injection of the linearized minigene into zygotes of a C57BL/6 x CBA background. Five independent lines were analyzed, and two lines showed expression in spinal cord motoneurons. Motoneurons at the C1-C3 level of the spinal cord, the level innervating the diaphragm, showed transgene expression that colocalized with staining for the motoneuron marker choline acetyltransferase (Figure 10C). All animal experiments were performed according to the Dutch law and ethical guidelines of the Vrije Universiteit Amsterdam and the Leiden University.

Neuromuscular synapse electrophysiology.

Measurements were performed on nerve/muscle preparations from the diaphragm of 2- to 5-month-old WT, munc18-1$^{+/-}$, and munc18^{OE} mice. We recorded EPPs and MEPPs at the NMJ using 10-20 MΩ glass capillary microelectrodes and standard recording equipment at 26-28°C (1) in Ringer's medium (116 mM NaCl; 4.5 mM KCl; 1 mM $MgCl_2$; 2 mM $CaCl_2$; 1mM NaH_2PO_4; 23 mM $NaHCO_3$; 11 mM glucose, pH7.4, gassed with 95% O_2/5% CO_2). Hemidiaphragms were treated with 3.1 μM μ-conotoxin (Scientific Marketing Associates, Herts, U.K.), a selective blocker of muscle sodium channels, to prevent action potentials. This allowed the undisturbed recording of EPPs during electrical nerve stimulation (0.3 and 40 Hz) of the phrenic nerve. Spontaneous MEPPs were recorded during a period without nerve stimulation. The quantal content at each endplate was calculated from EPP and MEPP amplitudes as described before (Plomp et al., 1994). Binomial parameters n and p were calculated from EPP and MEPP data according to the method of Miyamoto (Miyamoto, 1975). MEPPs also were recorded in preparations shortly after addition of hypertonic medium (0.5 M sucrose added to the standard Ringer's solution)

Cell culture and viral transduction.

Microisland cultures were prepared from munc18-1$^{+/-}$and WT littermate embryos at embryonic day 18 (see Rosenmund and Stevens, 1996). Lenti viral particles containing Munc18-1 cDNA coupled to enhanced GFP (EGFP) via an internal ribosomal entry site (IRES), and particles containing IRES-EGFP as control were prepared according to (Naldini et al., 1996) and Semliki Forest particles were prepared as described in (Voets et al., 2001). Neurons were infected at DIV 1 with Lenti virus or 6-8 h before electrophysiological recordings with Semliki Forest virus.

Autaptic electrophysiology.

Neurons were plated at 6,000 per cm2 on microislands of glia cells and cultured in Neurobasal medium (Invitrogen, Carlsbad, CA) supplemented with 2% B-27 (Invitrogen), 0.5 mM glutamax (Invitrogen), 0.1% penicillin/streptomycin, and 25 μM 2-mercaptoethanol. Receptor blockers bicuculline (GABA, 20 μM) and CNQX (glutamate, 10 μM) were used to characterize autaptic neurons. Whole-cell voltage-clamp recordings (holding potential, -70 mV) were performed on individual GABAergic (cultured from neocortex) or glutamatergic (cultured from hippocampus) autaptic neurons. The patch pipette contained the following solution: 125 mM K^+-gluconic acid, 10 mM NaCl, 4.6 mM $MgCl_2$, 4 mM K2-ATP, 15 mM creatine phosphate, 1 mM EGTA, and 20 units/ml phospocreatine kinase (pH 7.30). External medium contained 140 mM NaCl, 2.4 mM KCl, 4 mM $CaCl_2$, 4 mM $MgCl_2$, 10 mM Hepes, and 10 mM glucose (pH 7.30). Spontaneous release was mostly recorded in the presence of TTX (200 nM). Compared to recordings without TTX, this did not change amplitude or frequency, indicating that we recorded only miniature (nonevoked) input. Because TTX did not have an effect on basic electrophysiology, we pooled data sets recorded with and without TTX. For hyperosmotic sucrose applications, 500 or 200 mM sucrose was applied to the external medium for 3-4 seconds via a double-barrel application pipette that ensured instant application and rapid clearance of the sucrose medium. Axopatch 200A (Axon Instruments, Union City, USA) was used for whole-cell recordings and signals were acquired using Digidata 1322A and Clampex 8.1 (Axon Instruments). Clampfit 8.0 was used for offline analysis.

Fluorscence imaging.

To selectively label the RRP in WT and SFVM18 overexpressing neurons, cells were loaded with FM4-64 in calcium free Tyrode's containing 500 mM sucrose for 3-4 seconds (16 μM FM4-64, 500 mM sucrose, 0 mM $CaCl_2$, 2.5 mM KCl, 119 mM NaCl, 3 mM $MgCl_2$, 30 mM glucose, 25 mM HEPES, pH 7.4). The 500 mM sucrose containing solution was replaced by calcium free Tyrode's containing 16 μM FM4-64 for an additional 60 seconds to ensure labeling of all exocytosed vesicles. Cells were washed for 10 minutes with calcium free Tyrode's. All solution changes were made using a fast microperfusion system (SF77B, Warner Instruments). Images were acquired with a Coolsnap CCD camera (Roper Scientific) with constant and identical camera settings between coverslips. To ensure that identified puncta were synapses, calcium containing Tyrode's with a high concentration of potassium (2 mM $CaCl_2$, 60 mM KCl, 61.5 mM NaCl, 2 mM $MgCl_2$, 30 mM glucose, 25 mM HEPES, pH 7.4) was applied to the neurons for 60 seconds and loss of fluorescence was observed by comparing puncta before and after the high potassium application. Images were analyzed using fixed region sizes of 1 μm^2. Fluorescent intensity was obtained by averaging these regions. Background fluorescence was measured after four times

of 60 s application of high potassium and subtracted from all frames to give total releasable fluorescence.

Microscopy

Microisland cultures at DIV 14 were fixed in 4% PFA, permeabilized with 0.2% Triton X-100, and blocked with 2% goat serum. Cells were stained with monoclonal anti-MAP2 (Chemicon) and polyclonal anti-synapsin (E028) antibodies using goat anti-mouse Alexa 546 and goat anti-rabbit Cy5 secondary antibodies. Images were acquired on a Zeiss LSM510, and total synapse number (synapsin positive) and dendrite length (MAP2) were calculated with custom written routines in Matlab (written by Dr. W. Veldkamp, Leiden University Medical Centre).

Diaphragm muscles of Munc18-1 heterozygote (munc18-1$^{+/-}$), wild-type (WT), and Munc18-1 overexpressing (munc18^{OE}) littermates at postnatal day 16 (PN16) were dissected and fixed in 2% PFA for 1-2 h. Muscles were rinsed thoroughly with PBS and incubated with Texas red-conjugated α-bungarotoxin (Molecular Probes, Eugene, OR) for 2-3 h at room temperature. After extensive washes in PBS, tissues were mounted and examined with a Zeiss confocal fluorescent microscope (LSM510) with filter sets and optics selective for rhodamine, and images were processed with Adobe Photoshop. For analysis of endplate diameter, images of α-bungarotoxin-positive neuromuscular junctions were taken at three confocal depths resulting in an average diameter per endplate.

Electron microscopy.

Hippocampal islands cultures of munc18-1$^{+/-}$ or littermate WT mice (embryonic day 18) obtained from four different litters were grown on BELLCO photo-etched grid coverslips (BELLCO Glass Inc., Vineland, NJ). WT hippocampal neurons were infected (DIV 14) with SFV munc18-1-IRES-EGFP or SFV IRES-EGFP as control and observed under a fluorescence microscope 6 h after infection to map the location of infected cells.

As for electrophysiology, only glia islands containing a single neuron were used for analysis. Cells were fixed for 45 min at room temperature with 2.5% glutaraldehyde in 0.1 M cacodylate buffer (pH 7.4). After fixation cells were washed three times for 5 min with 0.1 M cacodylate buffer (pH 7.4), postfixed for 2 h at room temperature with 1% OsO4 in bidest, washed, and stained with 1% uranyl acetate for 40 min in the dark. After dehydration through a series of increasing ethanol concentrations, cells were embedded in Epon and polymerized for 24 h at 60°C After polymerization of the Epon, the coverslip was removed by alternately dipping it in liquid nitrogen and hot water. Cells of interest were selected by observing the flat Epon embedded cell monolayer (containing the BELLCO grid) under the light microscope and mounted on prepolymerized Epon blocks for thin sectioning.

Ultrathin sections (~90 nm) were cut parallel to the cell monolayer and collected on single-slot, formvar-coated copper grids, and stained in uranyl acetate and lead citrate. Autaptic synapses were selected in serial ultrathin sections at low magnification by using a JEOL (Tokyo, Japan) 1010 electron microscope, and high-resolution images were acquired at x100,000 magnification.

The distribution of synaptic vesicles, total vesicle number, size of the vesicle cluster, post synaptic density, and active zone length were measured on digital images taken at x100.000 magnification using analySIS software (Soft Imaging System, Germany). The observer was blinded for the genotype. No difference was observed in any of the parameters measured between WT synapses expressing SFV IRES-EGFP and noninfected WT synapses, these synapse were therefore pooled.

Statistical analysis.

Data shown are mean values ± SEM. Statistical significance was determined by using Student's *t*-test, and overall group differences were analyzed by using ANOVA.

Northern blot, in situ hybridization, and protein analysis.

Total RNA was prepared from mouse brain at different postnatal days using TRIzol (Invitrogen). Ten micrograms was loaded on denaturing formaldehyde gels and transferred to Hybond N+ (Amersham Pharmacia). A 1.0-kb fragment of the SV40 polyadenylation signal labeled with 32P was used as a transgene specific probe. For in situ hybridization, brains and cervical spinal cord sections were quickly removed and frozen on dry ice. Sagittal sections (16 μm) were prepared on a cryostat and mounted on poly(L)lysine coated glass slides. Sections were dried and kept at -80°C until used. Antisense digoxygenin-labeled RNA probe was transcribed from the vector pGEM4SV40 containing the 1.0-kb SV40 polyadenylation signal of the pNSE-Ex4

Protein	Level
Munc18-1	49 ± 12%
Hexokinase	100%
GDP dissociation inhibitor (GDI)	97 ± 13%
Calmodulin	103 ± 12%
Syntaxin 1A	97 ± 5%
Syntaxin 1B	90 ± 8%
SNAP25 (A+B)	105 ± 15%
Synaptobrevin/VAMP-2	104 ± 6%
Synaptophysin	114 ± 20%
Doc2A	97 ± 5%
Doc2B	99 ± 8%
Rab3A	100 ± 3%
Rabphilin3A	89 ± 11%

Table 1. Quantification of synaptic protein levels in munc18-1 heterozygous null mutant mice. Table shows the quantification of a number of synaptic proteins in brain homogenates from E18 mouse embryos. Immunoblots were loaded with three different amounts of brain protein from heterozygote and WT littermates and signals were normalized for the WT hexokinase level as a general marker. Data are averages ± SEM, n = 4 to 8. Only the Munc18-1 level differed significantly between heterozygote and WT mice ($P < 0.001$).

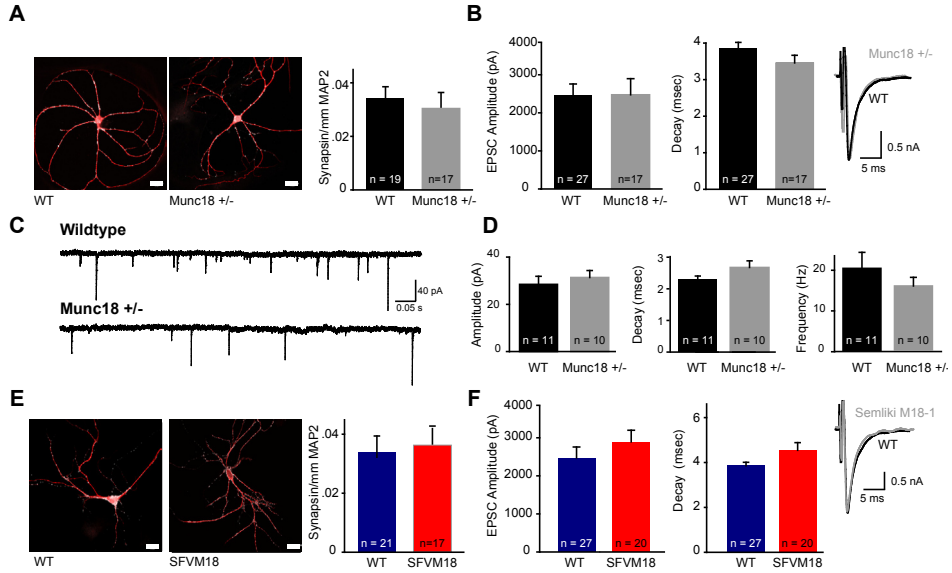

Figure 1 Basal synaptic transmission in munc18-1 heterozygous, wildtype and Semliki Forest virus Munc18 overexpressing glutamatergic autaptic neurons.

(A) Examples of MAP2 (red) and Synapsin (white) immunostaining of glutamatergic autaptic neurons and quantification of the amount of Synapsin positive synapses/µm MAP2 positive dendrite length. No difference was observed between WT and munc18-1$^{+/-}$ neurons. (WT total dendritic length 3288 ± 86.3 µm, total synapse number 118 ± 4.8 and 0.036 ± 0.003 synapses/µm dendrite, n = 19; munc18-1$^{+/-}$ total dendritc length 3588 ± 97.67 µm, total synapse number 122 ± 8.9 and 0.034 ± 0.004 synapses/µm dendrite, n = 17, p > 0.05 for all parameters). Bars are 20 µm. (B) EPSC amplitude and decay time are similar in WT and munc18-1$^{+/-}$ neurons (WT 2471 ± 286 pA, 3.9 ± 0.2 msec, n = 27; munc18-1$^{+/-}$ 2473 ± 432 pA, 3.4 ± 0.2 msec, n = 17, p > 0.05 for both parameters). Inset shows representative traces of WT and munc18-1$^{+/-}$ EPSCs. (C) Example traces of spontaneous glutamatergic release (mEPSCs) in WT and munc18-1$^{+/-}$ neurons. (D) Average mEPSC amplitude, decay time and frequency do not differ between WT and munc18-1$^{+/-}$ neurons (WT 28.5 ± 3.4 pA, 2.28 ± 0.12 msec, 20.3 ± 4.0 Hz, n = 11 cells, 2200 events; munc18-1$^{+/-}$ 31.4 ± 2.9 pA, 2.67 ± 0.21 msec, 16 ± 2.1 Hz, n = 10 cells, 2000 events, p > 0.05 for all parameters tested). (E) Example MAP2 and Synapsin immunostaining. Quantification in WT and Semliki forest virus overexpressing Munc18-1 (SFVM18) glutamatergic autaptic neurons shows no significant difference between the two genotypes (WT total dendritic length 3285 ± 101.2 µm, total synapse number 115 ± 6.3 and 0.035 ± 0.005 synapses/µm dendrite, n = 21; SFVM18 total dendritic length 3184 ± 104.2 µm, total number of synapses 121.5 ± 5.7 and 0.038 ± 0.004 synapses/µm dendrite, n = 17, p > 0.05 for all parameters). Bars are 20 µm. Semi-quantitative immuno fluorescence analysis showed that SFVM18 infection led to a 2.8 ± 0.3 times higher Munc18-1 protein level after 7 hours (WT n = 11 and SFVM18 n = 10).(F) No difference in EPSC amplitude and decay time between WT and Semliki Forest mediated overexpression of Munc18-1 (WT amplitude 2471 ± 286 pA, decay 3.86 ± 0.15 msec, n = 27; SFVM18 amplitude 2894 ± 303 pA, decay 4.37 ± 0.33 msec, n = 20, p > 0.05 for both parameters). Inset shows example EPSC of WT and SFVM18 neuron.

construct. Hybridization, color reaction, and double labeling with choline acetyltransferase antibodies were performed according to standard procedures. Mouse brains were solubilized, and equal amounts of protein were subjected to 8-15% SDS/PAGE. Depending on the size of the investigated protein, the following internal standards were used: calmodulin (17 kDa), GDI (54 kDa), and hexokinase (96 kDa). Monoclonal antibodies (Synaptic Systems, Göttingen, Germany; except Munc18-1 from Transduction Labs, Lexington) against the following proteins were used (code names given in brackets when applicable): Munc18-1, synaptobrevin II (Cl69.1); Rab3A/C (Cl42.1). Polyclonal antibodies against the following proteins were used: SNAP-25 (I733); syntaxin 1 (I378); synaptophysin 1 (P611); rabphilin-3A

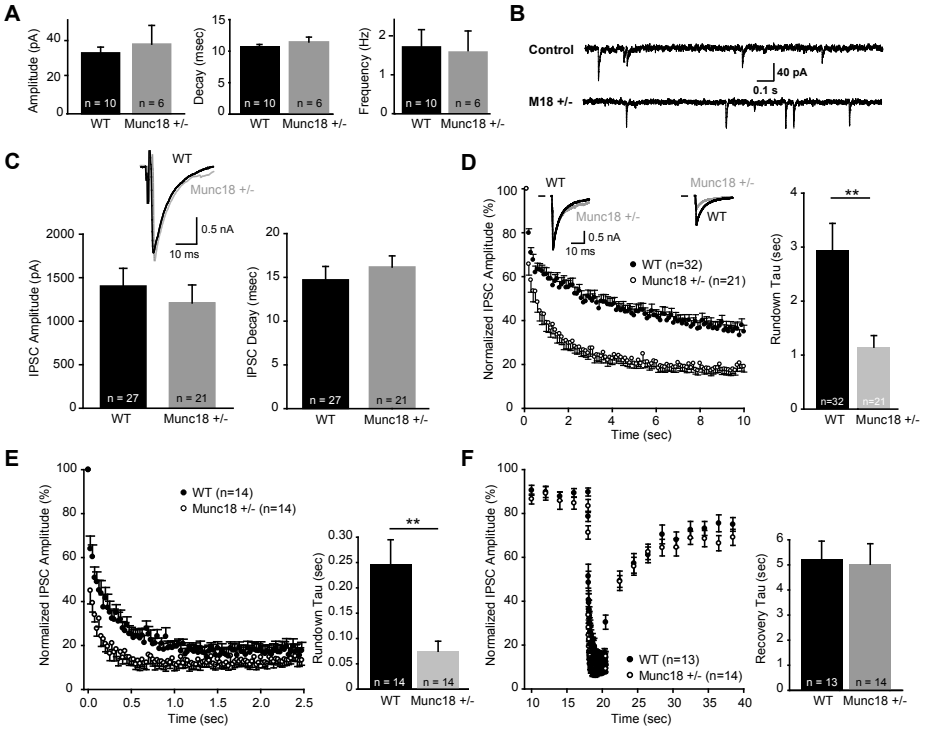

Figure 2. GABAergic transmission in Munc18-1 heterozygote autaptic neurons.
(A) Spontaneous GABAergic release is unaffected in munc18-$1^{+/-}$ autaptic neurons. Average mIPSC amplitude, decay time, and frequency are identical in WT and munc18-$1^{+/-}$ neurons (WT 32.5± 3.1 pA, 14.4 ± 0.4 ms, 1.7 ± 0.5 Hz, n = 10 cells, 2,100 events; munc18-$1^{+/-}$ 37.2 ± 10.0 pA, 14.8 ± 0.9 ms, 1.6 ± 0.5 Hz, n = 6 cells, 1,200 events, $P > 0.05$ for all parameters). (B) Example traces of mIPSCs in WT and munc18-$1^{+/-}$ neurons. (C) IPSC amplitude and decay time are similar in WT and munc18-$1^{+/-}$ neurons (WT 1,403 ± 203 pA, 14.7 ± 1.5 ms, n = 27; munc18-$1^{+/-}$ 1,209 ± 206 pA, 16.1 ± 1.3 ms, n = 21, $P > 0.05$ for both parameters). (Inset) Representative traces of WT and munc18-$1^{+/-}$ IPSCs. (D) Synaptic rundown of GABAergic IPSCs during 10-Hz stimulation is faster in munc18-$1^{+/-}$ compared to WT and reaches a lower steady-state plateau. Shown are averaged τs of mono-exponential fits (** $P < 0.01$). Biexponential fitting of the same data shows a significantly reduced τ slow for munc18-$1^{+/-}$ neurons, in line with glutamatergic neurons (Fig. 1A). (Inset) Example traces of the first and last IPSC from WT and munc18-$1^{+/-}$ neurons. For clarity, the stimulus artifact (see C Inset) was removed from the traces. (E) Synaptic rundown of GABAergic IPSCs during high-frequency stimulation (40 Hz, 2.5 s) is faster in munc18-$1^{+/-}$ compared to WT. Monoexponential fits revealed a significant increase in synaptic rundown in munc18-$1^{+/-}$ neurons (WT τ = 0.25 ± 0.05 s, n = 14; munc18-$1^{+/-}$ τ = 0.07 ± 0.02 s, n = 14, $P < 0.01$). (F) Activity- and calcium-dependent refill kinetics of the RRP after depletion of the pool by 2.5-s stimulation at 40 Hz are similar between WT and munc18-$1^{+/-}$ neurons (WT recovery τ = 5.2 ± 0.7 s, n = 13; munc18-$1^{+/-}$ recovery τ = 5.0 ± 0.9 s, n = 14, $P > 0.05$).

(I374); Doc2A/B (I734 and N321), and choline acetyltransferase (AB114P, Chemicon).

Results

In homozygous munc18-1-null mutant mice, synapses are silent (Verhage et al., 2000), identifying munc18-1 as an essential gene but providing little information on its molecular function. Heterozygous mice (munc18-$1^{+/-}$) had a 50% reduction of Munc18-1 protein expression but no reduction in the levels of any of its known

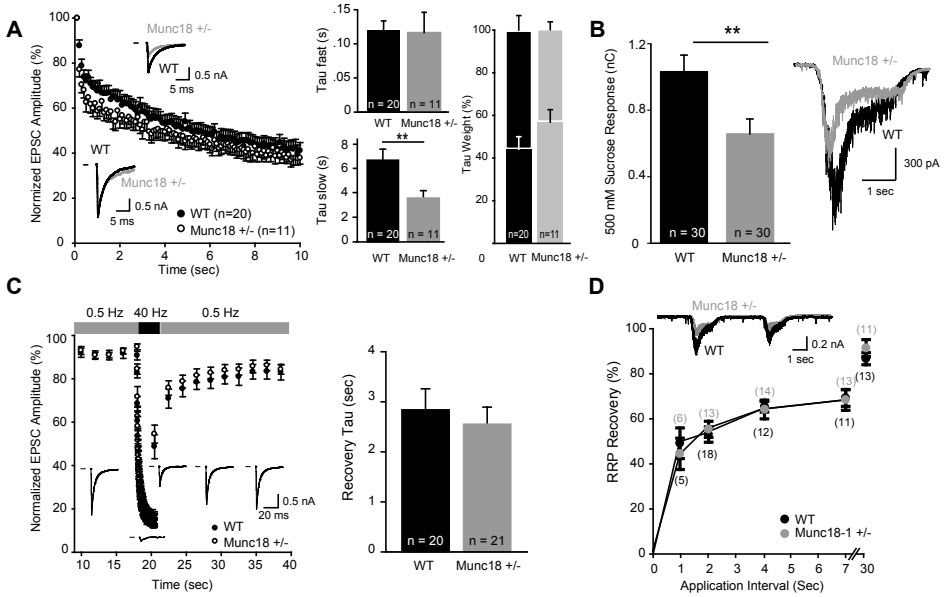

Figure 3. Synaptic transmission in munc18-1 heterozygous autaptic neurons.
(A) Synaptic rundown of glutamatergic EPSCs during 10-Hz stimulation is faster in munc18-1$^{+/-}$ compared with WT. Rundown kinetics were best characterized with biexponential fits and revealed that the slow component of the rundown was decreased in munc18-1$^{+/-}$ neurons. EPSC τfast = 0.12 ± 0.03, τslow = 3.93 ± 0.87 for munc18-1$^{+/-}$ neurons, and τfast = 0.12 ± 0.01, τslow = 6.86 ± 1.11 for WT (n =11 and n = 20, P< 0.05 for τslow). Averaged weights of τfast and τslow were not different between WT and munc18-1$^{+/-}$. (Insets) The first and last EPSC of the 10-Hz stimulation. For clarity, the stimulus artifact (see B Inset) was blanked from the traces. (B) Hypertonic sucrose (500 mM) application shows a 36% decrease in RRP size in munc18-1$^{+/-}$ neurons compared with WT neurons (WT: 1.06 ± 0.1 nC, n = 30; munc18-1$^{+/-}$: 0.67 ± 0.09 nC, n = 30, P < 0.01). (Inset) Example traces duration 500 mM sucrose application. (C) Activity-and calcium-dependent refill kinetics of the RRP after depletion of the pool by 2.5-s stimulation at 40 Hz are similar between WT and munc18-1$^{+/-}$ neurons (WT recovery: τ = 2.9 ± 0.4 s, n = 20; munc18-1$^{+/-}$ recovery: τ = 2.6 ± 0.3 s, n = 21, P> 0.05). (Insets) Individual WT traces during the paradigm. (D) Activity- and calcium-independent refill kinetics of the RRP tested by paired sucrose application with different interstimulus intervals are not different between WT and munc18-1$^{+/-}$ neurons (number of cells is in brackets, no significant difference at each of the different time points tested). The response of the second stimulus is plotted as a percentage of the first stimulus. (Inset) Typical responses to two sucrose applications with 4-s interval for WT and munc18-1$^{+/-}$ neurons.

binding partners or 22 other synaptic proteins (Table 1) (Toonen et al., 2005). Autaptic cultures from these mice had similar dendrite length and number of synapses as cultures from WT littermates (Figure 1).

Munc18-1 heterozygous autapses contain a smaller pool of readily releasable vesicles.

Whole-cell recordings of autaptic glutamatergic or GABAergic munc18-1$^{+/-}$ and WT littermate neurons showed similar excitatory and inhibitory postsynaptic currents (EPSCs and IPSCs) upon single depolarizations (Figures. 1B and 2C). The characteristics of spontaneous miniature (m) excitatory and inhibitory postsynaptic events (amplitude, frequency, and decay time) also did not differ between munc18-1$^{+/-}$ and WT neurons (Figures 1 C and D and 2 A and B). Thus, a reduction of Munc18-1 protein level does not affect synaptic physiology under basal conditions nor does it appear to influence postsynaptic receptor number or sensitivity.

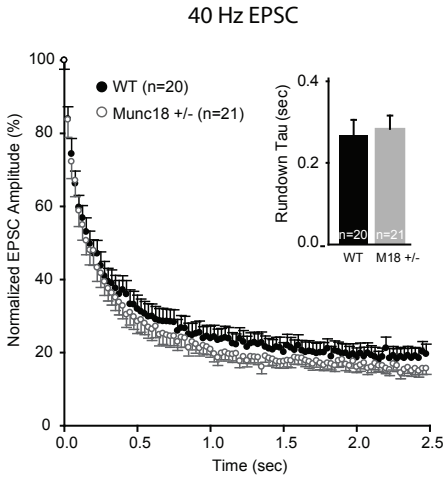

Figure 4. Synaptic rundown during high-frequency stimulation in glutamatergic WT and munc18-1$^{+/-}$ autaptic neurons.
Synaptic rundown during high frequency stimulation (40 Hz, 2.5 s) is similar for WT and munc18-1$^{+/-}$.

However, repeated stimulation produced a more pronounced rundown of evoked responses (synaptic depression) in munc18-1$^{+/-}$ neurons compared with WT neurons. This increased synaptic depression was observed both in glutamatergic and in GABAergic synapses and was most pronounced at 10-Hz stimulation (Figure 3 A and Figure 2 D). The rundown kinetics of glutamatergic synapses at 10 Hz were best characterized by biexponential curve fits (Pyott and Rosenmund, 2002), which revealed an increased rundown especially of the slow phase (τ_{slow}) in munc18-1$^{+/-}$ neurons. At 40-Hz stimulation, 80% depression was reached within 1 s in all groups, and a significant increase in depression in munc18-1$^{+/-}$ neurons was observed in GABAergic (Figure 2E) but not in glutamatergic neurons (Figure 4). Differences in synaptic release probability, RRP size, and replenishment rate all may contribute to the observed increase in synaptic depression. To test RRP size, we applied hypertonic sucrose solution to empty the RRP via a Ca^{2+}-independent mechanism (Stevens and Tsujimoto, 1995; Rosenmund and Stevens, 1996). The sucrose response in munc18-1$^{+/-}$ neurons was significantly smaller (0.67 ± 0.1 nC, n = 30) compared with WT neurons (1.06 ± 0.1 nC, n = 30, P < 0.01; Figure 3B). To test whether a reduction of Munc18-1 also affected the RRP refilling, we used two approaches. First, we depleted the RRP with 40-Hz stimulation and measured the recovery by using 0.5-Hz stimulations (Rhee et al., 2002). The 40-Hz stimulation resulted in similar depletion of the RRP in both genotypes (see also Figure 4), and recovery from RRP depletion was not significantly slower in munc18-1$^{+/-}$ neurons (Figure 3C). Second, we applied paired pulses of hypertonic sucrose with different time intervals between pulses (Rosenmund et al., 2002). Again, no difference in RRP recovery was observed between WT and munc18-1$^{+/-}$ neurons (Figure 3D).

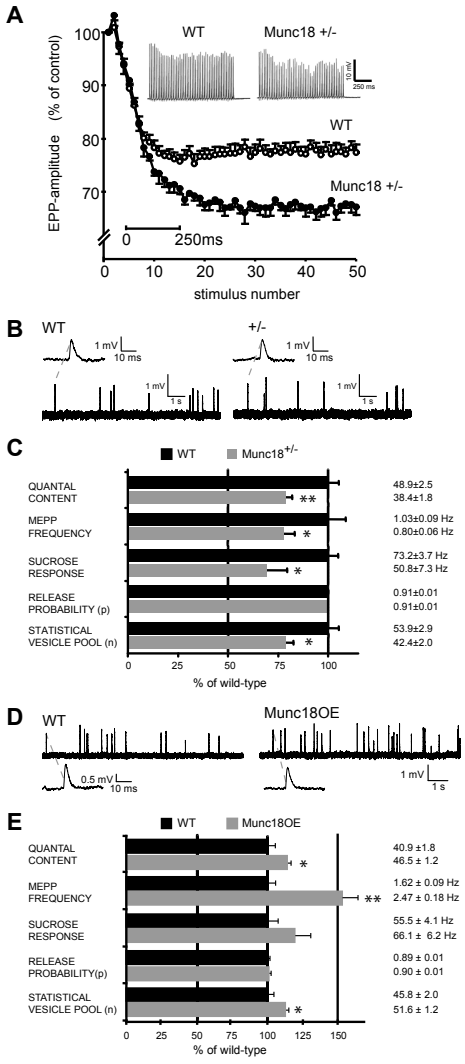

Figure 5. Synaptic transmission at NMJs of munc18-1 heterozygote, WT, and Munc18-1-overexpressing littermates.
(A) munc18-$1^{+/-}$ mice are less able to sustain high-frequency evoked transmitter release at neuromuscular synapses. Indicated are the amplitudes of synaptic responses (EPPs) to each individual stimulus for 40 stimuli delivered to the phrenic nerve at 40 Hz, expressed as percentage of the first response. Data represent means ± SEM of five animals per group and 15 NMJs sampled per animal. (Inset) A typical example of the 40-Hz EPP rundown. No gross morphological differences were observed between NMJs of the two genotypes (Figure 7 E and D). (B) Typical examples of MEPP frequency recordings in WT and munc18-$1^{+/-}$ NMJs. (C) Several physiological parameters in munc18-$1^{+/-}$ and WT NMJs. WT value was set at 100%. Where applicable, absolute values are indicated. Data represent means ± SEM of eight to nine animals per group and 10-15 NMJs sampled per animal. Differences between the groups were statistically significant for quantal content ($P < 0.01$), MEPP frequency ($P < 0.05$), sucrose response ($P < 0.05$), and statistical releasable pool n ($P < 0.01$). (D) Spontaneous MEPPs in munc18^{OE} and WT mice (Upper, 10 s). The amplitude and kinetics of MEPPs were similar at WT and munc18^{OE} NMJs (Lower). (E) Physiological parameters at NMJs of munc18^{OE} and WT mice. WT value was set at 100%. Where applicable, absolute values are indicated. Data represent means ± SEM of 10-11 animals per group and 10-15 NMJs sampled per animal. Differences between groups were significant for quantal content ($P < 0.05$), MEPP frequency ($P < 0.001$), and statistical releasable pool n ($P < 0.05$).

Thus, Munc18-1 levels are rate-limiting during high-frequency neurotransmission. A 50% reduction in protein levels results in a reduction of the RRP size without affecting the rate by which this (smaller) pool is replenished.

Munc18-1 heterozygous mice have impaired neuromuscular synaptic function.

Studies on SM proteins in *Drosophila* and *Caenorhabditis elegans* have been conducted on neuromuscular synapses (Wu et al., 1998; Weimer et al., 2003). To be able to directly compare our results, we performed electrophysiological recordings on diaphragm NMJs of munc18-$1^{+/-}$ mice and WT littermates. To test whether munc18-$1^{+/-}$ NMJs, like the autaptic cultures, were impaired in sustaining vesicle release during periods of high activity, we applied a high-rate (40-Hz) nerve-stimulation proto-

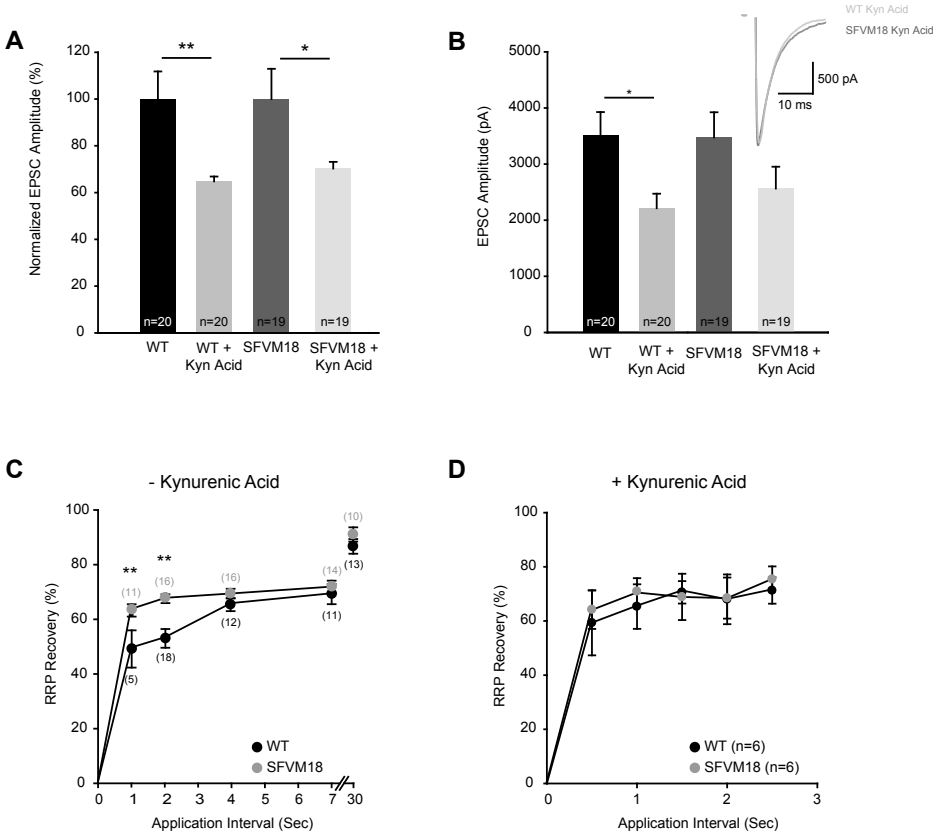

Figure 6. Munc18-1 overexpression does not increase quantal content during evoked release nor activity-independent RRP recovery.

(A) We used the competitive AMPA/NMDA channel blocker kynurenic acid to unmask possible receptor saturation during single evoked release. Application of 200 μM kynurenic acid reduced EPSC amplitude to the same extent in WT neurons as compared to neurons overexpressing Munc18-1. (Relative reduction of EPSC amplitudes in 200 μM kynurenic acid, WT 64.81 ± 2.03%, n = 20; SFVM18 70.31 ± 2.83%, n = 19, P = 0.12). (B) Absolute effect of 200 μM kynurenic acid on EPSC amplitude (WT 3,511.47 ± 414.71 pA, n = 20; WT + kynurenic acid 2,213.48 ± 257.50 pA, n = 20; SFVM18 3,474.60 ± 449.30 pA, n = 19; SFVM18 + kynurenic acid 2,563.59 ± 389.36 pA, n = 19). Reduction in EPSC amplitude due to kynurenic acid application was indistinguishable between WT and Munc18-1-overexpressing neurons. Thus, Munc18-1 overexpression does not increase the amount of glutamate released during single evoked release. Note that these experiments were conducted paired with the sucrose applications in Fig. 8E showing that 500 mM sucrose application does result in receptor saturation in SFVM18-overexpressing neurons. (C) In the absence of the 200 μM kynurenic acid, SFVM18-overexpressing neurons show an apparent increase in activity independent recovery of the RRP as probed with dual 500 mM sucrose applications with 1-, 2-, 4-, 7-, and 30-s intervals. The response of the second stimulus is plotted as a percentage of the first stimulus (number of cells in brackets, ** $P < 0.01$). (D) In the presence of 200 μM kynurenic acid, which prevents postsynaptic receptor saturation, no effect of SFVM18 overexpression on activity independent recovery is observed. Thus, 500 mM sucrose application in SFVM18-overexpressing neurons leads to receptor saturation (see Fig. 6C), this clips the initial sucrose response when kynurenic acid is not present in the bathing solution, thereby introducing an apparent increase in RRP refilling during the consecutive sucrose application.

col. Munc18-1$^{+/-}$ NMJs displayed a significantly larger rundown of evoked endplate potential (EPP) amplitudes (to 67% of the first EPP compared with 78% for WT, $P < 0.01$; Figure 5A).

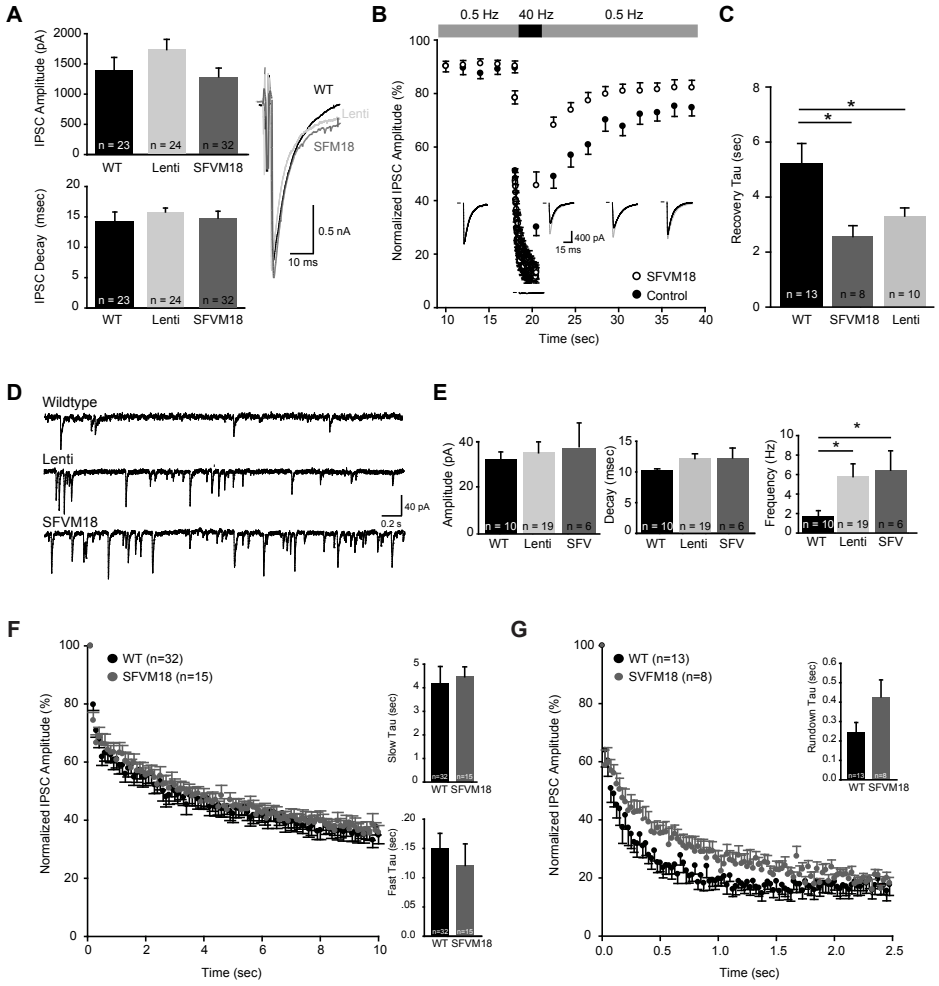

Figure 7. GABAergic transmission in Munc18-1-overexpressing autaptic neurons.
(A) No difference in IPSC amplitude and decay time between WT, Semliki Forest (SFVM18) and Lenti virus (Lenti)-mediated overexpression of Munc18-1. (WT amplitude 1,403 ±203 pA, decay 14.7 ± 1.5 ms, n = 23; LentiM18 amplitude 1,724 ± 168 pA, decay 15.8 ± 1.2 ms, n = 24; SFVM18 amplitude 1,287 ± 143 pA, decay 14.1 ± 0.8 ms, n = 32, P > 0.05 for both parameters). (Inset) Typical example of IPSC of WT, Semliki, and Lenti-mediated overexpression of Munc18-1. Semiquantitative immunofluorescence analysis showed that SFVM18 infection led to a 2.8 ± 0.3 times higher Munc18-1 protein level after 7 h (WT n = 11 and SFVM18 n = 10). Infection with Lenti virus resulted in a milder overexpression (1.86 ± 0.4, n = 11). Neurons were stained with a polyclonal antibody specific for Munc18-1, and fluorescence intensity was compared between transfected and nontransfected cells using identical settings (regions of interest placed on three different positions in the cell soma). (B) Munc18-1 overexpression results in faster activity dependent refilling of the RRP in GABAergic neurons. IPSC amplitude was sampled at a frequency of 0.5 Hz after depletion of the RRP with a 40-Hz stimulation train for 2.5 s. (Insets) Individual WT (black) and SFVM18 (gray) traces during the paradigm. (C) Quantification of the RRP recovery kinetics in GABAergic autaptic neurons overexpressing Munc18-1 either via Semliki Forest or Lenti virus-mediated infection. (SFV M18 τ= 2.56 ± 0.40 s, n = 8; Lenti τ = 3.29 ± 0.3s, n = 10; WT τ = 5.24 ± 0.71 s, n = 13, P < 0.05 for WT versus SFV or Lenti). (D) Example traces of spontaneous release (mIPSCs) in WT, Lenti virus, Munc18-1, and SFVM18-overexpressing neurons. (E) Spontaneous release (mIPSCs) frequency is increased upon SFVM18 and Lenti virus-mediated Munc18-1 (Lenti) overexpression (WT 1.7± 0.6 Hz, n = 10 cells, 2,100 events; SFVM18 6.5 ± 2.0 Hz, n = 6 cells, 800 events; Lenti 5.8 ± 1.3 Hz, n = 19, 3,700 events P < 0.001 for SFVM18 and Lenti versus WT). mIPSC amplitude and decay time are not affected by Munc18-1 overexpression (WT 32.5± 3.1 pA, 14.4 ± 0.4 ms; SFVM18 37.2 ± 5.6 pA, 13.0 ± 2.3 ms; Lenti 35.2 ± 4.7 pA, 13.0 ± 1.8 ms, P > 0.05 for SFVM18 and Lenti

As in autapses, we tested whether the EPP rundown could be explained by a reduction in RRP size by applying 500 mM sucrose. The response, measured as miniature endplate potential (MEPP) frequency, was 31% lower at munc18-1$^{+/-}$ endplates ($P < 0.05$; Figure 5C). As an alternative approach, we used the calculation method of Miyamoto (Miyamoto, 1975) to estimate RRP size and release probability from our EPP data. This method showed that the release probability was unchanged at munc18-1$^{+/-}$ NMJs, whereas the RRP size was reduced by 21% ($P < 0.01$; Figure 5C and Table 2). In addition, in munc18-1$^{+/-}$ NMJs, the frequency of spontaneous uniquantal acetylcholine release events (measured as MEPP frequency) and the 0.3-Hz evoked release (quantal content) were reduced by 20-25% ($P < 0.05$ and < 0.01, respectively; Figure 5C). These single synapse recordings reveal a reduction in the RRP size as well as a concomitant decrease in evoked release (quantal content). Given that the quantal content is the product of the size of the RRP and the probability that a vesicle is released upon stimulation (Del Castillo and Katz, 1954), these data suggest that Munc18-1 does not substantially influence vesicular release probability.

Genotype	Vesicle pool (n)	sem	n	P value
WT	53.87	2.85	8	0.0047
Munc18-1$^{+/-}$	42.43	2.04	9	
WT	45.78	1.96	13	0.024
Munc18^{OE}	51.60	1.20	11	
	Release probability (p)			
WT	0.91	0.004	8	0.6
Munc18-1$^{+/-}$	0.91	0.004	9	
WT	0.89	0.006	13	0.3
Munc18^{OE}	0.90	0.005	11	

Table 2. Calculated release probability and vesicle pool in WT, munc18-1$^{+/-}$, and Munc18^{OE} NMJs
Table shows the data obtained from calculating release probability (p) and statistical vesicle pool (n) in NMJs according to the method of Miyamoto (Miyamoto, 1975)

Munc18-1 overexpression results in a larger RRP and enhances activity-dependent RRP replenishment.

To investigate the effect of Munc18-1 overexpression on synaptic-vesicle release, we applied two viral-expression systems in autaptic cultures. We tested the effect of acute, high overexpression of Munc18-1 with the Semliki Forest virus system, 6 to 8 h postinfection (Ashery et al., 1999). In addition, we used a Lenti viral system to investigate the effect of long-term, moderate overexpression of Munc18-1, 10 to 14 days postinfection (Naldini et al., 1996). Munc18-1 overexpression with either Semliki (SFVM18) or Lenti virus did not affect neuronal morphology or total synapse number in glutamatergic autaptic neurons (Figure 1E). Also, evoked postsynaptic

versus WT). (F) Similar to glutamatergic neurons (Fig. 7), synaptic rundown during 10-Hz stimulation is not different between WT and SFVM18-overexpressing GABAergic neurons. Rundown kinetics were best characterized with biexponential fits. IPSC τ fast = 0.15 ± 0.3, τ slow = 4.1 ± 0.6 for WT neurons and τ fast = 0.12 ± 0.4, τ slow = 4.3 ± 0.4 for SFVM18 (n = 32 and n = 15). (G) Synaptic rundown during high-frequency stimulation (40 Hz, 2.5 s) in SFVM18 and WT GABAergic neurons. SFVM18-overexpressing neurons appear to depress more slowly although averaged rundown τs are not significantly different.

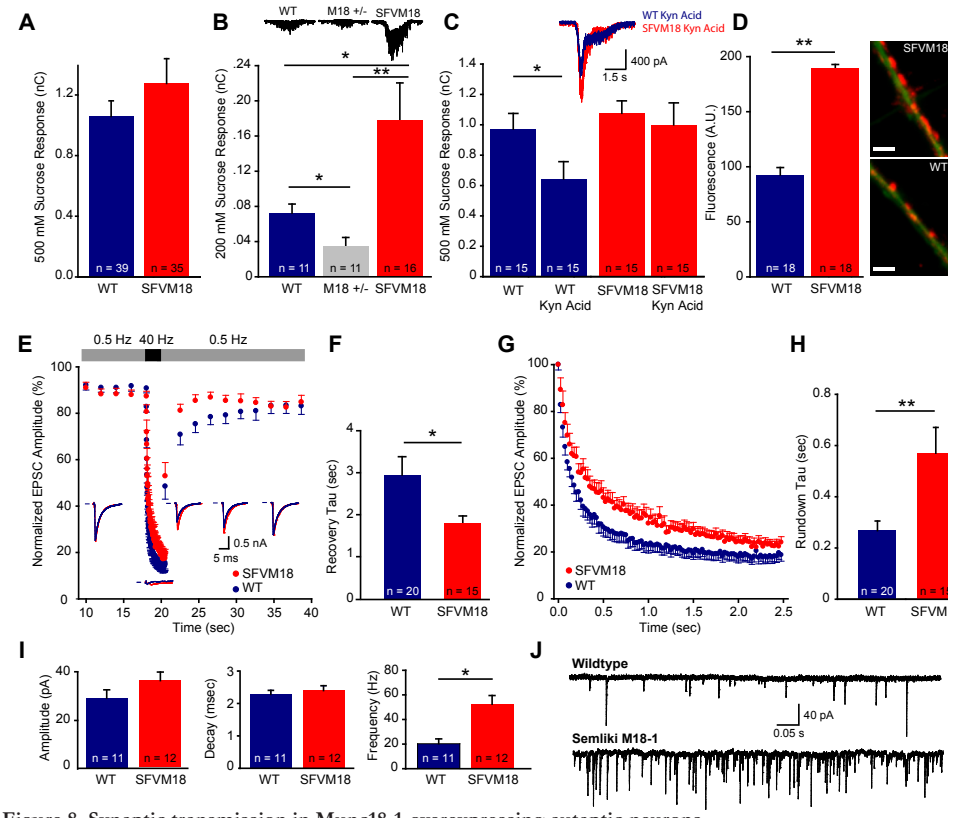

Figure 8. Synaptic transmission in Munc18-1-overexpressing autaptic neurons.
(A) Single 500 mM sucrose response is not significantly different between WT and SFVM18 overexpression (WT: 1.1 ± 0.1 nC, n = 39; SFVM18: 1.3 ± 0.2 nC, n = 35, P = 0.4). (B) Single 200 mM sucrose application reveals an increased RRP size in SFVM18-overexpressing neurons (V T: 0.074 ± 0.011 nC, n =11; munc18-$1^{+/-}$: 0.035 ± 0.011 nC, n =11; SFVM18: 0.17 ± 0.041 nC, n =16, P< 0.05 between V T and SFVM18 and P < 0.01 between SFVM18 and munc18-$1^{+/-}$ neurons). (Inset) Typical responses to 200 mM sucrose application for the three genotypes tested. (C) Single 500 mM sucrose application in the presence of 200 µM of the NMDA/α-amino-3-hydroxy-5-methy1-4-isoxazolepropionic acid (AMPA) receptor blocker kynurenic acid results in an expected decreased response in WT neurons, whereas the response of SFVM18-overexpressing neurons is unaffected (WT minus kynurenic acid: 0.95 ± 0.14 nC, n = 15 and WT plus kynurenic acid: 0.63 ± 0.1 nC, n =15, P < 0.05; SFVM18 minus kynurenic acid:1.04 ± 0.1 nC, n =15 and SFVM18 plus kynurenic acid: 0.96 ± 0.08, n = 15, P = 0.5). This finding shows that the increased release of glutamate in SFVM18-overexpressing neurons leads to receptor saturation and indicates that the RRP is increased on Munc18-1 overexpression. (D) Direct labeling of the RRP by using 500 mM sucrose solution containing 16 µM FM4-64 reveals a 2-fold larger RRP in SFVM18-overexpressing neurons compared with WT. Shown are average arbitrary fluorescent units (a.u.) from 769 synapses on 18 neurons for WT and 960 synapses on 18 neurons for SFVM18 from four independent experiments (WT: 91 ± 7.6 a.u., SFVM18: 191 ± 10.8 a.u., P < 0.01 with n = 4). (Insets) Examples of VUT and SFVM18-overexpressing presynaptic terminals labeled with FM4-64 (red) by using 500 mM sucrose on EGFP (green)-filled dendrites. (Bar: 5 µm.) (E) Munc18-1 overexpression increases the recovery rate after activity-dependent RRP depletion. EPSC amplitude was sampled at a frequency of 0.5 Hz after depletion of the RRP with a 40-Hz stimulation train for 2.5 s. (Insets) Individual WT and SFVM18 traces during the paradigm. (F) Single exponential fits of RRP recovery show a significant faster replenishment in neurons overexpressing Munc18-1 (SFV Munc18-1: τ =1.8 ± 0.2 s, n =15; WT: τ = 2.9 ± 0.4 s, n = 20, P < 0.05). (G) Munc18-1 overexpression decreases synaptic rundown during high-frequency stimulation (40-Hz, 2.5 s). (H) Single exponential fits of the synaptic rundown show significant decrease in synaptic rundown in neurons overexpressing Munc18-1 (SFV Munc18-1: τ = 0.57 ± 0.1 s, n =15, WT: τ = 0.27 ± 0.04 s, n = 20, P = 0.003). (I) mEPSC frequency is significantly increased on Munc18-1 overexpression (WT: 20.3 ± 3.9 Hz, n =11 cells, .2,300 events; SFVM18: 51.6 ± 7.0 Hz, n =12 cells, 2,000 events, P < 0.001). Miniature amplitude and decay time are not affected by Munc18-1 overexpression (WT: 28.5 ± 3.4 pA, 2.28 ± 0.12 ms; SFVM18: 35.7 ± 3.5 pA, 2.40 ± 0.15 ms, P> 0.05 for both parameters). (J) Example traces of spontaneous glutamatergic release in WT and SFVM18-overexpressing neurons.

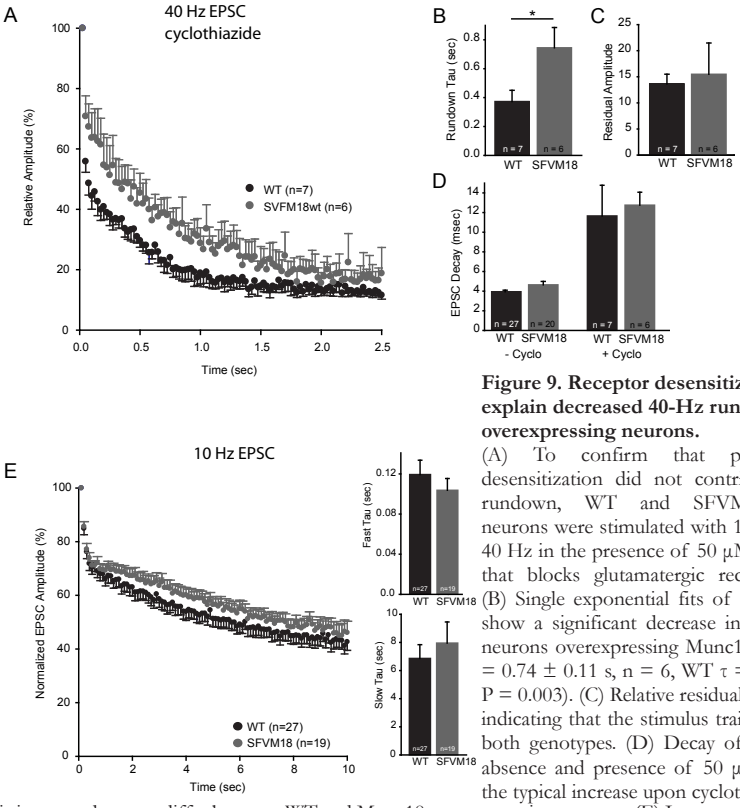

Figure 9. Receptor desensitization does not explain decreased 40-Hz rundown in Munc18-overexpressing neurons.

(A) To confirm that postsynaptic receptor desensitization did not contribute to the synaptic rundown, WT and SFVMunc18-overexpressing neurons were stimulated with 100 action potentials at 40 Hz in the presence of 50 μM cyclothiazide, a drug that blocks glutamatergic receptor desensitization. (B) Single exponential fits of the synaptic rundown show a significant decrease in synaptic rundown in neurons overexpressing Munc18-1 (SFV Munc18-1 $\tau = 0.74 \pm 0.11$ s, n = 6, WT $\tau = 0.38 \pm 0.07$ s, n = 7, P = 0.003). (C) Relative residual amplitudes are similar indicating that the stimulus train emptied the RRP in both genotypes. (D) Decay of single EPSCs in the absence and presence of 50 μM cyclothiazide show the typical increase upon cyclothiazide application but this increase does not differ between WT and Munc18-overexpressing neurons. (E) In contrast to 40 Hz stimulation (A and B and Fig. 8I), Synaptic rundown during 10-Hz stimulation is not significantly different between WT and SFVM18-overexpressing neurons.

responses in SFVM18-overexpressing glutamatergic neurons did not differ from WT responses (Figure 1F, EPSC). Effects of Munc18-1 overexpression on evoked responses may be masked by postsynaptic receptor saturation. Therefore, evoked responses were measured in the presence of the competitive NMDA/α-amino-3-hydroxy-5-methy1-4-isoxazolepropionic acid (AMPA) receptor blocker kynurenic acid (Meyer et al., 2001). In the presence of 200 μM kynurenic acid, the EPSC amplitude in WT and SFVM18 neurons was reduced to the same extent, indicating that saturation of postsynaptic receptors did not mask an effect in SFVM18 neurons (Figure 6 A and B). Evoked responses after SFVM18- or Lenti virus-mediated Munc18-1 overexpression in GABAergic neurons also were similar to WT (IPSC, Figure 7A). Thus, acute as well as chronic overexpression of Munc18-1 does not affect basal synaptic strength or synapse formation in autaptic cultures.

To test whether overexpression of Munc18-1 increases RRP size, we applied hypertonic sucrose (500 mM). The response from SFVM18-overexpressing neurons was not significantly different from WT neurons (SFVM18: 1.3 ± 0.2 nC, n = 26; WT: 1.1 ± 0.1 nC, n = 30, P = 0.4; Figure 8A). Again, postsynaptic receptor

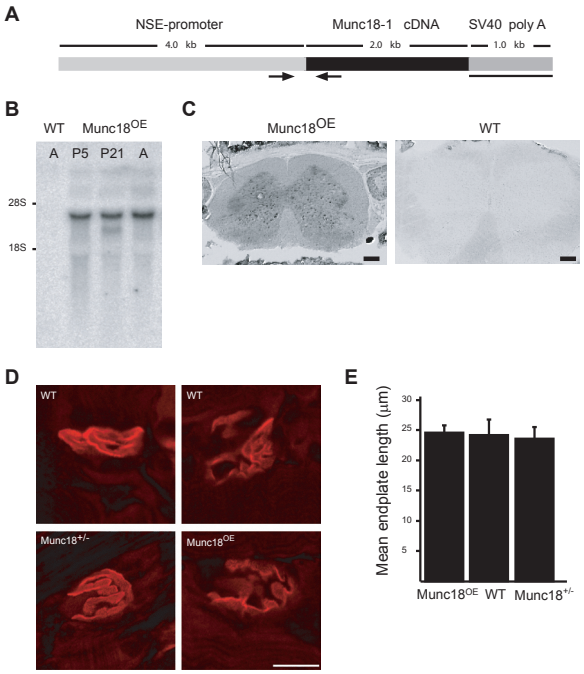

Figure 10. Generation of Munc18-1-overexpressing mice and NMJ morphology of munc18-1 heterozygote, overexpressing, and WT littermates.

(A) Schematic diagram of the NSE-Munc18-1 minigene. Four kilobases of rat NSE promoter sequence precedes the Munc18-1 cDNA, which is followed by the SV40 polyadenylation signal. PCR primers for genotyping are depicted as arrows, and Northern blot and in situ probe are depicted as solid black bar. (B) The PN04 line expresses Munc18-1 mRNA in whole-brain lysate at postnatal day 5 (P5) and expression increases with age (A, 3-month-old adults). A 32P-labeled probe specific for the transgenic Munc18-1 was used, which does not recognize endogenous Munc18-1 (see Materials and Methods). (C) Colocalization with an antibody staining for the motoneuron marker choline acetyltransferase at the C1-C3 level of the spinal cord shows that a high percentage of motoneurons do express the transgene. (Bar: 250 µm.) (D) NMJs in whole-mount diaphragms were stained with Texas red-labeled α-bungarotoxin to label acetylcholine receptors on the postsynaptic muscle membrane. No morphological changes were observed between the different genotypes (representative NMJs for the different genotypes are shown). Fluorescence intensity was identical for all genotypes indicating that the amount of acetylcholine receptors at the endplate was not altered as a result of different Munc18-1 protein levels. (Bars: 10 µm.) (E) Endplate diameter measured at three confocal depths at random intervals throughout the entire diaphragms off all genotypes. No significant change in mean endplate diameter was observed: WT (24.01 ± 1.1 µm, n = 48), munc18^{OE} (24.6 ± 0.8 µm, n = 79), and munc18-1$^{+/-}$ (23.50 ± 0.6 µm, n = 67). Data are mean ± SEM.

saturation could mask potential effects of Munc18-1 overexpression. Therefore, we conducted three additional experiments. First, we applied a milder osmotic stimulus (200 mM sucrose) known to result in submaximal RRP depletion (Rosenmund and Stevens, 1996) to WT, munc18-1$^{+/-}$, and SFVM18-overexpressing neurons. This stimulus resulted in a >2-fold higher response in Munc18-overexpressing neurons compared with WT, and, consistent with the data in Figure 3, munc18-1$^{+/-}$neurons showed a significantly smaller response (SFVM18: 0.17 ± 0.041 nC, n =16; munc18-1$^{+/-}$: 0.035 ± 0.011 nC, n =11; and WT: 0.074 ± 0.011 nC, n =11, $P < 0.05$ between WT and SFVM18; Figure 8B). This result suggests that application of 500 mM sucrose indeed saturated postsynaptic receptors, masking an increase in RRP size. Second, we applied 500 mM sucrose in the presence of 200 µM kynurenic acid (see above). Consistent with the first experiment, an almost 2-fold difference in RRP size now became evident (WT: 0.95 ± 0.14 nC; and WT plus kynurenic acid: 0.63 ± 0.1 nC, $P < 0.05$; SFVM18: 1.04 ± 0.10 nC; and SFVM18 plus kynurenic acid: 0.96 ± 0.08, $P = 0.5$; Figure 8C). Third, we directly labeled the RRP by using the styryl dye FM4-64 in combination with 500 mM sucrose application (Pyle et al., 2000; Mozhayeva et al., 2002). This direct presynaptic assessment also showed an ~2-fold

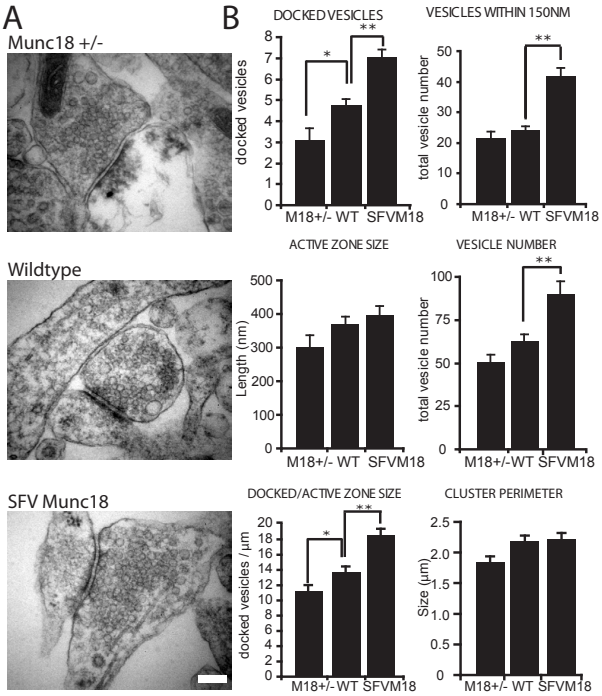

Figure 11. Munc18 protein levels control the number of docked synaptic vesicles.
(A) Electron micrographs of typical asymmetrical glutamatergic synapses from munc18-1$^{+/-}$, WT, and SFVM18-overexpressing autaptic neurons. Hippocampal autaptic neurons were analyzed after 14 days in culture and 6 h after infection with SFV. (Scale bar: 200 nm.) (B) The number of vesicles docked at the active zone increases with increasing amounts of munc18-1 (munc18-1$^{+/-}$: 3.1 ± 0.6, n=26;WT: 4.8 ± 0.3, n = 62; and SFVM18: 7.0 ± 0.4, n = 45; P<0.05 for munc18-1$^{+/-}$ vs. WT and P < 0.001 for WT vs. SFVM18), whereas the size of the active zone and the vesicle cluster perimeter do not significantly change (ANOVA, P> 0.05). The number of vesicles within 150 nm from the active zone (WT: 24.4 ± 0.9; SFVM18: 41.9 ± 2.6, P < 0.001) and total number of vesicles per synapse is higher in SFV Munc18-1-overexpressing synapses compared with WT (WT: 62.6 ± 3.8; SFVM18: 90.1 ± 7.2, P < 0.001) but not in munc18-1$^{+/-}$ neurons.

higher fluorescence intensity on Munc18-1 overexpression (Figure 8D) Together, these independent lines of evidence confirm that Munc18-1 overexpression indeed leads to a larger initial RRP size.

Next, we examined whether Munc18-1 overexpression also resulted in a smaller rundown and faster RRP replenishment. Indeed, synapses overexpressing Munc18-1 showed less synaptic depression during high-frequency stimulation (Figure 8 G and H, EPSC rundown; 40 Hz) and an accelerated refilling of the RRP after high-rate (40-Hz) electrical stimulation (Figure 8E; SFV Munc18-1: τ = 1.8 ± 0.2 s and WT: τ = 2.9 ± 0.4 s, P < 0.05). The same effect was observed in GABAergic neurons infected with either SFVM18 or Lenti virus Munc18-1 (Figure 7 B and C). We ruled out any contribution of postsynaptic receptor desensitization by repeating the experiment in the presence of 50 µM cyclothiazide, a drug that blocks glutamate receptor desensitization (Figure 9). In contrast to the faster RRP replenishment after activity-dependent depletion, paired sucrose application did not reveal an effect of Munc18-1 overexpression on the rate of RRP replenishment when tested in the presence of 200 µM kynurenic acid (Figure 6 C and D). Thus, Munc18-1 overexpression increases the RRP size and its replenishment, probably by activity- and/or Ca^{2+}-dependent mechanisms. As a result, synapses recover faster. Consistent with an increase in RRP size, Munc18-1 overexpression also led to a >2-fold increase in the frequency of spontaneous vesicle release in both glutamatergic and GABAergic

neurons, without affecting postsynaptic receptor sensitivity and/or numbers (Figure 8 I and J, mEPSCs, and Figure 7 D and L, mIPSCs).

Munc18-1-overexpressing mice have enhanced synaptic function in NMJs.

We analyzed diaphragm NMJs of Munc18-1-overexpressing mice (munc18^{OE}, Figure 10). We first assessed RRP size with 500 mM sucrose. The sucrose-induced MEPP frequency was not significantly different between munc18^{OE} and WT NMJs ($P = 0.16$; Figure 5E). Both spontaneous uniquantal acetylcholine release (MEPP frequency) and evoked release (quantal content at 0.3-Hz stimulation) were increased compared with WT controls, by 53% and 14%, respectively ($P < 0.001$ and $P < 0.05$; Figure 5D and E). As in munc18-1$^{+/-}$ mice, no differences were seen in resting membrane potential, quantal size (MEPP amplitude), upward or downward slopes of spontaneous events, and evoked response latency (Figure 5D and data not shown). Hence, in accordance with autaptic neurons and in contrast to the robust decrease of EPP responses in *Drosophila* NMJs on overexpression of Rop (Schulze et al., 1994), increased levels of Munc18-1 lead to an increase in synaptic efficacy of the NMJ without affecting the fusion process.

Munc18-1 proteins levels control the number of docked synaptic vesicles.

In autaptic neurons, the RRP size correlates with the number of docked vesicles (Schikorski and Stevens, 2001). Therefore, we performed quantitative electron microscopy on glutamatergic synapses at 14 days in vitro (DIV). At low magnification, the general appearance of autaptic cultures from munc18-1$^{+/-}$, WT littermates, and WT neurons infected with SFV Munc18-1 was similar, and asymmetrical synapses with a clear active zone and postsynaptic density were present in comparable numbers (Figure 11A). The size of the active zone, postsynaptic density, and synaptic vesicle cluster perimeter did not differ between genotypes (Figure 11B), indicating that Munc18-1 levels do not influence general synapse morphology or size. However, the number of vesicles in immediate contact with the presynaptic active zone membrane increased significantly with increasing Munc18-1 expression levels (munc18-1$^{+/-}$: 3.1 ± 0.6, $n = 26$; WT: 4.8 ± 0.3, $n = 62$; and SFVM18: 7.0 ± 0.4, $n = 45$; $P < 0.05$ for munc18-1$^{+/-}$ versus WT and $P < 0.001$ for WT versus SFVM18). Hence, these morphometric data show that Munc18-1 expression levels correlate with the number of docked synaptic vesicles per active zone area, which parallels the observed physiological changes in RRP size. We also quantified the number of vesicles within 150 nm (approximately three times the synaptic vesicle size) from the active zone. Again, a positive correlation between the number of vesicles present in this pool and Munc18-1 expression levels was found (Figure 11B), which may explain the faster RRP replenishment. Finally, the total number of vesicles present in the synapse also increases when more Munc18-1 is present (Figure 11B).

Discussion

In the present study we show that the efficacy of synaptic transmission at both excitatory and inhibitory synapses depends on Munc18-1 levels, and we identify changes in RRP size and replenishment as the primary underlying mechanism. This mechanism may be related to the way in which protein kinase C (Stevens and Sullivan, 1998; Virmani et al., 2005) and ras GTPases (Kushner et al., 2005) modulate synaptic transmission, but it is distinct from the two other major mechanisms to control synaptic efficacy in nerve terminals, which rely on changes in vesicle-release probability (Geppert et al., 1997; Augustin et al., 1999; Reim et al., 2001) or connectivity changes [changes in the number of synapses that connect two neurons and/or the size of the terminals (Tyler and Pozzo-Miller, 2001)]. Although all three mechanisms can increase presynaptic output, only an increase in RRP size and replenishment warrants a sustained enhancement in synaptic efficacy.

Munc18-1-dependent changes in RRP size can be explained by the observed bidirectional changes in docked vesicles (fewer in munc18-1$^{+/-}$ neurons and more on Munc18-1 overexpression). These observations are in line with our previous observations in Munc18-1 null mutant chromaffin cells (Voets et al., 2001) and neocortex at late embryonic stages (Bouwman et al., 2004) as well as with studies in *C. elegans* (Weimer et al., 2003). Earlier in development, a docking defect was not observed in mouse neocortex (Verhage et al., 2000). The docking phenotype suggests a role for Munc18-1 that is distinct from other presynaptic proteins like Munc13-1, Rab3s, complexins, and Rim1α, which all influence synaptic efficacy through modulation of the release probability without affecting vesicle docking and number or their localization (Augustin et al., 1999; Reim et al., 2001; Calakos et al., 2004). The increase in docked vesicles on Munc18-1 overexpression may be a consequence of the increased total number of vesicles in the terminal. However, in previous studies, changes in total vesicle number did not lead to concomitant changes in the number of docked vesicles (Weimer et al., 2003; Gitler et al., 2004), and Munc18-1 overexpression in chromaffin cells also increased docking but without affecting total vesicle numbers (Toonen et al., 2006). Hence, often docking does not correlate with the total number of available vesicles, presumably because of the limited availability of docking sites. Therefore, we conclude that Munc18-1 specifically regulates the docking step, maybe by establishing such sites. In addition, Munc18-1 overexpression apparently influences the total number of vesicles in the synapse by an unknown mechanism. The increased total number of vesicles may contribute to the faster RRP replenishment, especially the increased number of vesicles within 150 nm from the membrane (Figure 11B). Because the cluster perimeter and active zone area were unchanged (Figure 11B), the vesicle concentration within the cluster must be higher, which may promote faster reloading and greater occupancy of docking sites. The

unaltered responses to paired hypertonic shocks suggest that Munc18-1 overexpression increases replenishment in a calcium-dependent manner.

The conclusion that Munc18-1 regulates the docking step, together with the unaltered kinetics of spontaneous and evoked fusion events, both in autapses and NMJs, argue for a role of Munc18-1 upstream of the synaptic vesicle fusion process itself. A large body of evidence suggests that the interaction of soluble N-ethylmaleimide-sensitive factor attachment protein receptors (SNARE) proteins from vesicular and target membranes drives this fusion reaction (Chen et al., 1999; Schoch et al., 2001; Washbourne et al., 2002). Deletion of SNAP-25 or synaptobrevin, two members of the SNARE complex involved in synaptic-vesicle release, results in a severe impairment of neurotransmission without affecting vesicle docking (Chen et al., 1999; Schoch et al., 2001). Hence, our data suggest that Munc18-1 functions upstream of SNARE complex formation. In vitro, Munc18-1 interacts tightly with the SNARE protein syntaxin 1 (Hata et al., 1993; Pevsner et al., 1994). As Munc18-1 has no membrane interacting domains, the interaction with syntaxin 1 at the plasma membrane may be important for vesicle docking. Therefore, it seems plausible that the Munc18-1/syntaxin 1 dimer is involved in initial steps preceding vesicle fusion, the docking step, and that Munc18-1 subsequently is displaced to allow syntaxin to initiate SNARE complex formation and vesicle fusion.

Most of the effects of altered Munc18-1 expression described here can be explained by changes in the RRP size only (sucrose response, FM-dye loading, and vesicle distribution in electron micrographs). The increase in miniature frequency in Munc18-1 overexpressing neurons and the decrease in the munc18-1$^{+/-}$ NMJ are consistent with this conclusion. However, miniature frequency was not significantly different in munc18-1$^{+/-}$ autaptic neurons, as expected given the smaller RRP size in these cells, which is probably because of the fact that this frequency is rather variable in autapses. There is a trend between the groups (27% difference in group average; Figure 1D), in fact, this is rather similar to the NMJ (29% difference; Figure 5C). Increasing the release rate by using 200 mM sucrose (Figure 8B) did result in the expected Munc18-1-dependent changes. Secondly, single evoked responses were normal in munc18$^{+/-}$ and Munc18-1-overexpressing neurons (Figures 1B and F, 2C, and 7A) despite differences in RRP size. This finding suggests that the release probability of the vesicles released during these single stimuli is altered. The observed differences in synaptic depression upon repetitive stimulation (Figures 3A, 5A, 8G, 2 D and E, and 7F and G) are consistent with such an explanation, although in this case changes in RRP size may still contribute. On the other hand, the fact that, at the monosynaptic NMJ, changes in RRP size do correlate with changes in EPP amplitude and miniature frequency strengthens the explanation that Munc18-1 does not directly control release probability but primarily RRP size. It is becoming evident that synaptic transmission in central synapses cannot be described accurately unless

heterogeneity of vesicular release probability is taken into account. The fact that single evoked responses are unaltered in autapses despite differences in RRP size also may be attributable to such heterogeneous release probability. The initial release probability per synapse may be adjusted to the optimal dynamic range (Burrone and Murthy, 2003) despite differences in RRP size and the release probability of the first vesicle, released on a single stimulus, may be different from other releasable vesicles.

Reference List

Ashery U, Betz A, Xu T, Brose N, Rettig J (1999) An efficient method for infection of adrenal chromaffin cells using the Semliki Forest virus gene expression system. Eur J Cell Biol 78: 525-532.

Augustin I, Rosenmund C, Sudhof TC, Brose N (1999) Munc13-1 is essential for fusion competence of glutamatergic synaptic vesicles. Nature 400: 457-461.

Bouwman J, Maia AS, Camoletto PG, Posthuma G, Roubos EW, Oorschot VM, Klumperman J, Verhage M (2004) Quantification of synapse formation and maintenance in vivo in the absence of synaptic release. Neuroscience 126: 115-126.

Burrone J, Murthy VN (2003) Synaptic gain control and homeostasis. Curr Opin Neurobiol 13: 560-567.

Calakos N, Schoch S, Sudhof TC, Malenka RC (2004) Multiple roles for the active zone protein RIM1alpha in late stages of neurotransmitter release. Neuron 42: 889-896.

Chen YA, Scales SJ, Patel SM, Doung YC, Scheller RH (1999) SNARE complex formation is triggered by Ca^{2+} and drives membrane fusion. Cell 97: 165-174.

Del Castillo J, Katz B (1954) Quantal components of the end-plate potential. J Physiol 124: 560-573.

Dresbach T, Burns ME, O'Connor V, DeBello WM, Betz H, Augustine GJ (1998) A neuronal Sec1 homolog regulates neurotransmitter release at the squid giant synapse. J Neurosci 18: 2923-2932.

Geppert M, Goda Y, Stevens CF, Sudhof TC (1997) The small GTP-binding protein Rab3A regulates a late step in synaptic vesicle fusion. Nature 387: 810-814.

Gitler D, Takagishi Y, Feng J, Ren Y, Rodriguiz RM, Wetsel WC, Greengard P, Augustine GJ (2004) Different presynaptic roles of synapsins at excitatory and inhibitory synapses. J Neurosci 24: 11368-11380.

Harrison SD, Broadie K, van de GJ, Rubin GM (1994) Mutations in the *Drosophila* Rop gene suggest a function in general secretion and synaptic transmission. Neuron 13: 555-566.

Hata Y, Slaughter CA, Sudhof TC (1993) Synaptic vesicle fusion complex contains unc-18 homologue bound to syntaxin. Nature 366: 347-351.

Kushner SA, Elgersma Y, Murphy GG, Jaarsma D, van Woerden GM, Hojjati MR, Cui Y, LeBoutillier JC, Marrone DF, Choi ES, De Zeeuw CI, Petit TL, Pozzo-Miller L, Silva AJ (2005) Modulation of presynaptic plasticity and learning by the H-ras/extracellular signal-regulated kinase/synapsin I signaling pathway. J Neurosci 25: 9721-9734.

Meyer AC, Neher E, Schneggenburger R (2001) Estimation of quantal size and number of functional active zones at the calyx of held synapse by nonstationary EPSC variance analysis. J Neurosci 21: 7889-7900.

Miyamoto MD (1975) Binomial analysis of quantal transmitter release at glycerol treated frog neuromuscular junctions. J Physiol 250: 121-142.

Mozhayeva MG, Sara Y, Liu X, Kavalali ET (2002) Development of vesicle pools during maturation of hippocampal synapses. J Neurosci 22: 654-665.

Naldini L, Blomer U, Gallay P, Ory D, Mulligan R, Gage FH, Verma IM, Trono D (1996) In vivo gene delivery and stable transduction of nondividing cells by a lentiviral vector. Science 272: 263-267.

Pevsner J, Hsu SC, Braun JE, Calakos N, Ting AE, Bennett MK, Scheller RH (1994) Specificity and regulation of a synaptic vesicle docking complex. Neuron 13: 353-361.

Pyle JL, Kavalali ET, Piedras-Renteria ES, Tsien RW (2000) Rapid reuse of readily releasable pool vesicles at hippocampal synapses. Neuron 28: 221-231.

Pyott SJ, Rosenmund C (2002) The effects of temperature on vesicular supply and release in autaptic cultures of rat and mouse hippocampal neurons. J Physiol 539: 523-535.

Reim K, Mansour M, Varoqueaux F, McMahon HT, Sudhof TC, Brose N, Rosenmund C (2001) Complexins regulate a late step in Ca^{2+}-dependent neurotransmitter release. Cell 104: 71-81.

Rhee JS, Betz A, Pyott S, Reim K, Varoqueaux F, Augustin I, Hesse D, Sudhof TC, Takahashi M, Rosenmund C, Brose N (2002) Beta phorbol ester- and diacylglycerol-induced augmentation of transmitter release is mediated by Munc13s and not by PKCs. Cell 108: 121-133.

Rizo J, Sudhof TC (2002) Snares and munc18 in synaptic vesicle fusion. Nat Rev Neurosci 3: 641-653.

Rizzoli SO, Betz WJ (2005) Synaptic vesicle pools. Nat Rev Neurosci 6: 57-69.

Rosenmund C, Sigler A, Augustin I, Reim K, Brose N, Rhee JS (2002) Differential control of vesicle priming and short-term plasticity by Munc13 isoforms. Neuron 33: 411-424.

Rosenmund C, Stevens CF (1996) Definition of the readily releasable pool of vesicles at hippocampal synapses. Neuron 16: 1197-1207.

Schikorski T, Stevens CF (2001) Morphological correlates of functionally defined synaptic vesicle populations. Nat Neurosci 4: 391-395.

Schoch S, Deak F, Konigstorfer A, Mozhayeva M, Sara Y, Sudhof TC, Kavalali ET (2001) SNARE function analyzed in synaptobrevin/VAMP knockout mice. Science 294: 1117-1122.

Schulze KL, Littleton JT, Salzberg A, Halachmi N, Stern M, Lev Z, Bellen HJ (1994) rop, a *Drosophila* homolog of yeast Sec1 and vertebrate n-Sec1/Munc-18 proteins, is a negative regulator of neurotransmitter release in vivo. Neuron 13: 1099-1108.

Scott BL, Van Komen JS, Irshad H, Liu S, Wilson KA, McNew JA (2004) Sec1p directly stimulates SNARE-mediated membrane fusion in vitro. J Cell Biol 167: 75-85.

Sons MS, Plomp JJ (2006) Rab3A deletion selectively reduces spontaneous neurotransmitter release at the mouse neuromuscular synapse. Brain Res 1089: 126-134.

Stevens CF, Sullivan JM (1998) Regulation of the readily releasable vesicle pool by protein kinase C. Neuron 21: 885-893.

Stevens CF, Tsujimoto T (1995) Estimates for the pool size of releasable quanta at a single central synapse and for the time required to refill the pool. Proc Natl Acad Sci U S A 92: 846-849.

Sudhof TC (2004) The synaptic vesicle cycle. Annu Rev Neurosci 27: 509-547.

Toonen RF, de Vries KJ, Zalm R, Sudhof TC, Verhage M (2005) Munc18-1 stabilizes syntaxin 1, but is not essential for syntaxin 1 targeting and SNARE complex formation. J Neurochem 93: 1393-1400.

Toonen RF, Kochubey O, de Wit H, Gulyas-Kovacs A, Konijnenburg B, Sorensen JB, Klingauf J, Verhage M (2006) Dissecting docking and tethering of secretory vesicles at the target membrane. EMBO J 25: 3725-3737.

Toonen RF, Verhage M (2003) Vesicle trafficking: pleasure and pain from SM genes. Trends Cell Biol 13: 177-186.

Tyler WJ, Pozzo-Miller LD (2001) BDNF enhances quantal neurotransmitter release and increases the number of docked vesicles at the active zones of hippocampal excitatory synapses. J Neurosci 21: 4249-4258.

Verhage M, Maia AS, Plomp JJ, Brussaard AB, Heeroma JH, Vermeer H, Toonen RF, Hammer RE, van den Berg TK, Missler M, Geuze HJ, Sudhof TC (2000) Synaptic assembly of the brain in the absence of neurotransmitter secretion. Science 287: 864-869.

Virmani T, Ertunc M, Sara Y, Mozhayeva M, Kavalali ET (2005) Phorbol esters target the activity-dependent recycling pool and spare spontaneous vesicle recycling. J Neurosci 25: 10922-10929.

Voets T, Toonen RF, Brian EC, de Wit H, Moser T, Rettig J, Sudhof TC, Neher E, Verhage M (2001) Munc18-1 promotes large dense-core vesicle docking. Neuron 31: 581-591.

Washbourne P, Thompson PM, Carta M, Costa ET, Mathews JR, Lopez-Bendito G, Molnar Z, Becher MW, Valenzuela CF, Partridge LD, Wilson MC (2002) Genetic ablation of the t-SNARE SNAP-25 distinguishes mechanisms of neuroexocytosis. Nat Neurosci 5: 19-26.

Weimer RM, Richmond JE, Davis WS, Hadwiger G, Nonet ML, Jorgensen EM (2003) Defects in synaptic vesicle docking in unc-18 mutants. Nat Neurosci 6: 1023-1030.

Wu MN, Littleton JT, Bhat MA, Prokop A, Bellen HJ (1998) ROP, the *Drosophila* Sec1 homolog, interacts with syntaxin and regulates neurotransmitter release in a dosage-dependent manner. EMBO J 17: 127-139.

6

Munc18-1 is involved in homeostatic upregulation of transmitter release at the myasthenic mouse neuromuscular synapse

Michèle S. Sons,[1] Ruud F. Toonen,[2] Matthijs Verhage,[2] Jaap J. Plomp[1]

1 Departments of Neurology and MCB-Neurophysiology, Leiden University Medical Centre, Leiden, The Netherlands

2 Center for Neurogenomics and Cognitive Research, Department of Functional Genomics, Vrije Universiteit (VU) and VU Medical Centre, Amsterdam, The Netherlands

Abstract

Homeostatic upregulation of presynaptic neurotransmitter release in response to a reduction of postsynaptic transmitter sensitivity has been observed at brain synapses and neuromuscular junctions (NMJs). This phenomenon allows synapses to adapt to (patho-)physiological changes. Compensatory upregulation of ACh release has been observed at NMJs of patients with myasthenia gravis and in experimental animal models for this paralytic auto-immune disease, in which postsynaptic ACh receptors at NMJs are reduced by autoantibodies. This form of synaptic plasticity presumably involves local retrograde signaling from post- to presynapse. Ultimate targets of such signaling pathway may be the protein components of the neuro-exocytotic machinery or proteins that modulate its function. One candidate is Munc18-1, a presynaptic protein which is essential for neurotransmitter release and presumably acts as positive regulator of transmitter release at mouse NMJs. Munc18-1 is known to interact with the protein complex that regulates membrane fusion of transmitter vesicles. Here, we have investigated Munc18-1 involvement in homeostatic upregulation of transmitter release at NMJs. To this end, we induced an experimental form of myasthenia gravis to Munc18-1 heterozygous null-mutant mice, Munc18-1 overexpressing transgenic mice, and wild type controls. Neurotransmitter release was measured with in vitro electrophysiological methods. Myasthenic Munc18-1 heterozygous null-mutant mice were impaired in their ability to upregulate acetylcholine release at their NMJs. On the other hand, Munc18-1 overexpressing NMJs did not show additional upregulation, compared to wild-type controls. We conclude that Munc18-1 is involved in homeostatic upregulation of transmitter release, and that other factors become limiting when Munc18-1 is present at elevated level.

Acknowledgements
The authors gratefully acknowledge support from the Netherlands Organization for Scientific Research NWO (grants 903-42-073, M.S.S; 903-42-023, R.F.T. and Pionier 900-01-001, M.V.) and the KNAW Van Leersumfonds (J.J.P.).

Introduction

Successful synaptic transmission between a neuron and its target cell relies on mutual tuning of pre- and postsynaptic structure and function. This is of particular importance during embryonic development when the physical properties of cells, e.g. cell input resistance, change drastically as a result of their growth. Throughout later stages in life there are also further (patho-)physiological changes that require structural and/or functional synaptic adaptation to ensure appropriate signal transmission. The molecular mechanisms by which neuronal cells monitor and adapt their synaptic strength are not well understood yet (Davis and Bezprozvanny, 2001; Davis, 2006; for review, see Turrigiano et al., 1998; Regehr et al., 2009).

One form of synaptic adaptation is the increase of presynaptic neurotransmitter release following a reduction in postsynaptic sensitivity for the transmitter. It has been suggested that a retrograde messenger is involved, signaling from the postsynaptic cell to the presynaptic cell. Although synaptic adaptation has been observed at CNS synapses (Bacci et al., 2001), this apparent homeostatic adaptive change has been best characterized at vertebrate and invertebrate neuromuscular junctions (NMJs). For example, increase of glutamate release from motor nerve terminals has been observed at the *Drosophila* NMJ, either upon lowering the number of postsynaptic glutamate receptors or inhibiting their function with transgenetic methods (Davis et al., 1998; Petersen et al., 1997). In transgenic mice with reduced expression of neuregulin and a consequently impairment of acetylcholine receptor (AChR) synthesis, the reduction of functional postsynaptic AChRs leads to compensatory increase in presynaptic ACh release at the NMJ (Sandrock, Jr. et al., 1997).

Similarly, compensatory increase of ACh release has been found at NMJs of patients suffering from myasthenia gravis (MG), in which autoantibodies against the AChR cause a reduction of receptor density resulting in muscle weakness (Vincent et al., 2001). *In vitro* electrophysiological analysis of NMJ function in muscle biopsies from MG patients revealed (partial) compensatory upregulation of ACh release (Cull-Candy et al., 1980; Plomp et al., 1995). MG has been studied using experimental models in rat, where the AChR function has been decreased by the use of antibodies or by chronic *in vivo* application of the AChR blocker α-bungarotoxin. In these models, a similar upregulation of ACh relase was demonstrated (Plomp et al., 1992; Plomp et al., 1995). Detailed electrophysiological studies showed that the amount of this upregulation at each individual (experimental) myasthenic NMJ was depending on the amount of reduction of postsynaptic AChRs at that NMJ (Plomp et al., 1992; Plomp et al., 1995). This strongly suggests that local postsynaptic factors are signaling in a retrograde fashion to the presynaptic cell, as also suggested for *Drosophila* NMJs (Aberle et al., 2002; Davis et al., 1998; McCabe et al., 2003;

Petersen et al., 1997), cricket CNS synapses (Davis and Murphey, 1993) and rat hippocampal synapses (Micheva et al., 2003).

The molecular mechanism underlying retrograde signaling in the homeostatic control of ACh release at myasthenic NMJs is largely unknown. Retrograde signaling is accomplished either by diffusible retrograde messenger or through a transsynaptic protein complex (Regehr et al., 2009). Neurotrophic factors are candidates for diffusible messengers, since *in vitro* pharmacological block of the tyrosine kinases receptors reduces the increased ACh release levels at experimental MG NMJs to normal values (Plomp and Molenaar, 1996). Furthermore, nitric oxide has been shown to act as retrograde messenger in hippocampal synapses (Micheva et al., 2003). Interesting candidates for forming a transsynaptic signalling protein complex are e.g. neuroligins and neurexins (Futai et al., 2007; Scheiffele, 2003).

The ultimate target of the retrograde signaling cascade leading to increased release is likely to be the presynaptic exocytotic machinery, dedicated to fast and precisely timed fusion of synaptic vesicles with the plasma membrane. A vast number of proteins is involved in exocytosis (see for reviews (Rosenmund et al., 2003; Sudhof, 2004; Verhage and Toonen, 2007; Toonen and Verhage, 2007), but the key event in synaptic vesicle fusion is the formation of the so-called SNARE complex (Poirier et al., 1998; Sutton et al., 1998). This is a parallel four-helix bundle formed by the SNARE motifs of the three neuronal SNARE proteins (syntaxin-1 and SNAP25 on the plasma membrane, and vesicle membrane-associated synaptobrevin). The energy released by the formation of this complex catalyzes the fusion reaction that leads to transmitter release (Finley et al., 2002; Hanson et al., 1997; Lin and Scheller, 1997).

The protein family Sec-Munc18 is necessary for exocytosis in yeast (Aalto et al., 1992; Novick et al., 1981), *C. elegans* (Hosono et al., 1992), *Drosophila* (Harrison et al., 1994) and mice (Verhage et al., 2000) and was initially discovered as a binding to syntaxin (Hata et al., 1993). Munc18 can either bind to the to the 'closed' form of syntaxin, or to syntaxin participating in the SNARE complex. In the 'closed' form of syntaxin, the N-terminus folds back onto the Habc domain forming a four helical structure which prevents participation of the protein in the SNARE complex (Dulubova et al., 1999; Misura et al., 2000). The arch-like structure of Munc18 binds as a clasp to the four helical syntaxin structure. The other mode of binding involves association of the N-terminus of Munc18 with the N-terminus of syntaxin while assembled in the SNARE complex, leaving the arch-shape structure of Munc18 free to clasp the four helices of the SNARE complex (Dulubova et al., 2007; Shen et al., 2007; Yamaguchi et al., 2002). How exactly Munc18 is involved in secretion is not clear yet, but most likely Munc18 is a catalyst for SNARE complex formation, which in turn drives membrane fusion (Sudhof and Rothman, 2009; see for reviews Toonen and Verhage, 2007).

Based on fact that Munc18-1 is a key player in exocytosis, the protein could be involved in the release-increasing retrograde signaling cascade at myasthenic NMJs. In a previous paper we have described the effect of varying the levels of Munc18-1 on transmitter release in mice by the use of heterozygous Munc18-1 null-mutant mice (Munc18-$1^{+/-}$) and mice overexpressing Munc18-1 (Munc18-1^{OE}) (Toonen et al., 2006b). A clear positive correlation between release parameters in the NMJ and the level of Munc18-1 was described. In the present study, we investigated the role of Munc18-1 in homeostatic upregulation of transmitter release in the NMJ. Heterozygous Munc18-1 null-mutant mice and mice overexpressing Munc18-1 were subjected to an experimental form of MG involving chronic *in vivo* application of the AChR blocker α-bungarotoxin and it was investigated whether compensatory increase of ACh release occurred at their NMJs. Our results indicate that Munc18-1 is indeed involved in this form of synaptic adaptation.

Materials and Methods

Mice

Munc18-$1^{+/-}$ mice were bred by means of standard mouse husbandry and back-crossed for at least 6 generations to a C57Bl/6 background (Verhage et al., 2000). These mice had 50% reduced Munc18-1 protein level in brain, as determined by Western blot analysis (Toonen et al., 2006b).

Munc18-1^{OE} mice were generated as described (Toonen et al., 2006b). The linearized pNSE-Ex4 minigene containing the promoter of neuron specific enolase from rat (Forss-Petter et al., 1990) and Munc18-1 cDNA was injected into zygotes with a C57Bl/6 x CBA background. The transgenic mice were viable and fertile. Histological analysis of brain and spinal cord sections at C1-C3 level, from which the innervation of the diaphragm muscle originates, showed transgene expression. In the spinal cord, the transgene staining was co-localized with staining for the motor neuronal marker choline-acetyltransferase.

Genotypes were analyzed using Southern blot or polymerase chain reaction methods. The mice were housed under a 12 h light / 12 h dark regime with *ad libitum* food and water. The animals were euthanized by CO_2 inhalation. Hemi-diaphragms with their phrenic nerves were rapidly dissected and pinned out in Ringer's solution (see below) at room temperature.

All animal experiments were carried out according to the Dutch law and local University guidelines (DEC#99029).

Toxin-induced myasthenia gravis

We used an experimental animal model for MG that was originally developed in rats and is termed toxin-induced MG (TIMG) (Molenaar et al., 1991). The model involves repeated injections with small doses of α-bungarotoxin (Biotoxins Incor-

porated, ST. Cloud, FA, USA), a highly potent and selective blocker of AChRs at NMJs. We adjusted and re-evaluated the model for use with mice (data not shown).

During a period of four weeks, mice of about 4 months of age (body weights of about 20 g) were injected intraperitoneally every 48 hour during the work week (i.e. on Mondays, Wednesdays and Fridays) with a low dose of α-bungarotoxin. Control groups received physiological saline (0.9% NaCl) injections. As a first dose, 1.2 μg α–bungarotoxin was injected. Thereafter, doses of 0.8 μg were given. Three hours after an injection the mice showed slightly invaginated flanks, indicating mild muscle weakness. There were no apparent breathing problems. In general, these symptoms had disappeared by the next, toxin-free, day. If the symptoms of weakness (scored in individual mice) were too severe, the dose of α-bungarotoxin was lowered. The mice were well able to feed and drink. At the end of the TIMG treatment, body weights of the TIMG and saline-injected control mice were similar.

Neuromuscular synapse electrophysiology

Measurements were performed on nerve/muscle preparations from right and left hemi-diaphragms of wild type, Munc18-1$^{+/-}$, and Munc18-1^{OE} mice. Upon stimulation of the phrenic nerve, the nerve terminal releases a number of ACh quanta. Part of the transmitter binds postsynaptic ACh receptors and causes them to open. The resulting ion current gives rise to an endplate potential (EPP). Spontaneous release of single quanta results in miniature EPPs (MEPPs). We recorded EPPs and MEPPs by impaling muscle fibers near the NMJ with a 10-20 MΩ glass capillary microelectrode filled with 3 M KCl and standard recording equipment at 26-28°C (Plomp et al., 1994) in Ringer's medium containing (mM): NaCl, 116; KCl, 4.5; $MgCl_2$, 1; $CaCl_2$, 2; NaH_2PO_4, 1; $NaHCO_3$, 23; glucose 11; pH 7.4, gassed with 95 % O_2/5 % CO_2. Hemi-diaphragms were incubated with 3.1 μM μ-Conotoxin GIIIB (Scientific Marketing Associates, Herts, UK), a selective blocker of muscle sodium channels, to prevent action potentials. This allowed for the undisturbed recording of EPPs during electrical nerve stimulation (0.3 and 40 Hz) of the phrenic nerve with a bipolar stimulation electrode. The quantal content (i.e. the number ACh quanta released upon a single nerve impulse) at each NMJ was calculated from EPP and MEPP amplitudes, normalized to -75 mV membrane potential. The EPP amplitude was corrected for non-linear summation, as described before (Plomp et al., 1994). During high-frequent stimulation (1 s, 40 Hz), EPP amplitudes decrease to a plateau level. The rundown level of the EPP amplitude during 40 Hz stimulation for 1 s of the phrenic nerve was determined by averaging the amplitudes of the last 10 EPPs of the train and expressing it as percentage of the amplitude of the first EPP of the train.

A GeneClamp 500B amplifier from Axon Instruments (Union City, CA, USA) was used for amplifying and filtering (10 kHz low-pass) of the signals. The record-

ings were digitized and analyzed using a Digidata 1200 interface, Clampex 8.0 and Clampfit 8.0 programs (Axon Instruments) and routines programmed in Matlab (The MathWorks Inc., Natick, MA, USA).

Statistical analysis

The significance of differences in mean values between genotype groups were tested using Student's *t*-test. Differences in effect of TIMG treatment between genotypes was tested with the multivariate general linear model (interaction parameter) and the post-hoc Tukey test by using SPSS 10.0 for Windows (SPSS Inc., Chicago, IL, USA).

Results

Analysis of basic neuromuscular synaptic function in Munc18$^{+/-}$ mice

We performed intracellular recordings of EPPs from muscle fibers of diaphragm-phrenic nerve-muscle preparations from wild type mice (N=12, 10-15 NMJs sampled per animal) and Munc18-1$^{+/-}$ mice (N=10, 10-15 NMJs sampled per animal). These mice had received repeated injections with saline and served as a control for the TIMG group that was injected with α-bungarotoxin (see below).

The MEPP amplitude was the same in both genotype groups (0.93 ± 0.05 and 0.93 ± 0.05 mV, Figure 1A, G). We did not observe differences in spontaneous quantal ACh release between wild type and Munc18-1$^{+/-}$ NMJs. The mean MEPP frequency was 1.62 ± 0.10 and 1.52 ± 0.10 s^{-1}, respectively (Figure 1B, G). At low-frequency nerve stimulation (0.3 Hz), the mean amplitude of the EPPs was 25.66 ± 1.31 mV in wild type and 25.44 ± 1.17 mV in Munc18-1$^{+/-}$ NMJs. The calculated quantal content was 41.54 ± 2.08 in wild type and 40.57 ± 2.31 in Munc18-1$^{+/-}$ NMJs (Figure 1C). Upon high-frequency (40 Hz) nerve stimulation, Munc18-1$^{+/-}$ NMJs displayed a more pronounced rundown of EPP amplitude, to a level of 74 ± 1.3% of the amplitude of the first EPP of the stimulation train, compared to 83 ± 0.9% at wild type NMJs (Figure 2, $p<0.001$).

Thus, although low-frequency evoked ACh release as well as spontaneous release did not differ between Munc18-1$^{+/-}$ and wild type NMJs, a more pronounced rundown of EPP amplitude was observed at Munc18-1$^{+/-}$ NMJs at high-frequency nerve stimulation. This most likely reflects a decrease in quantal content during the stimulus train.

Myasthenic Munc18-1$^{+/-}$ neuromuscular synapses show impaired compensatory increase of ACh release

Subjection of mice to the TIMG protocol (four weeks α-bungarotoxin treatment) induced a reduction of the mean MEPP amplitude of about 65% at NMJs of both

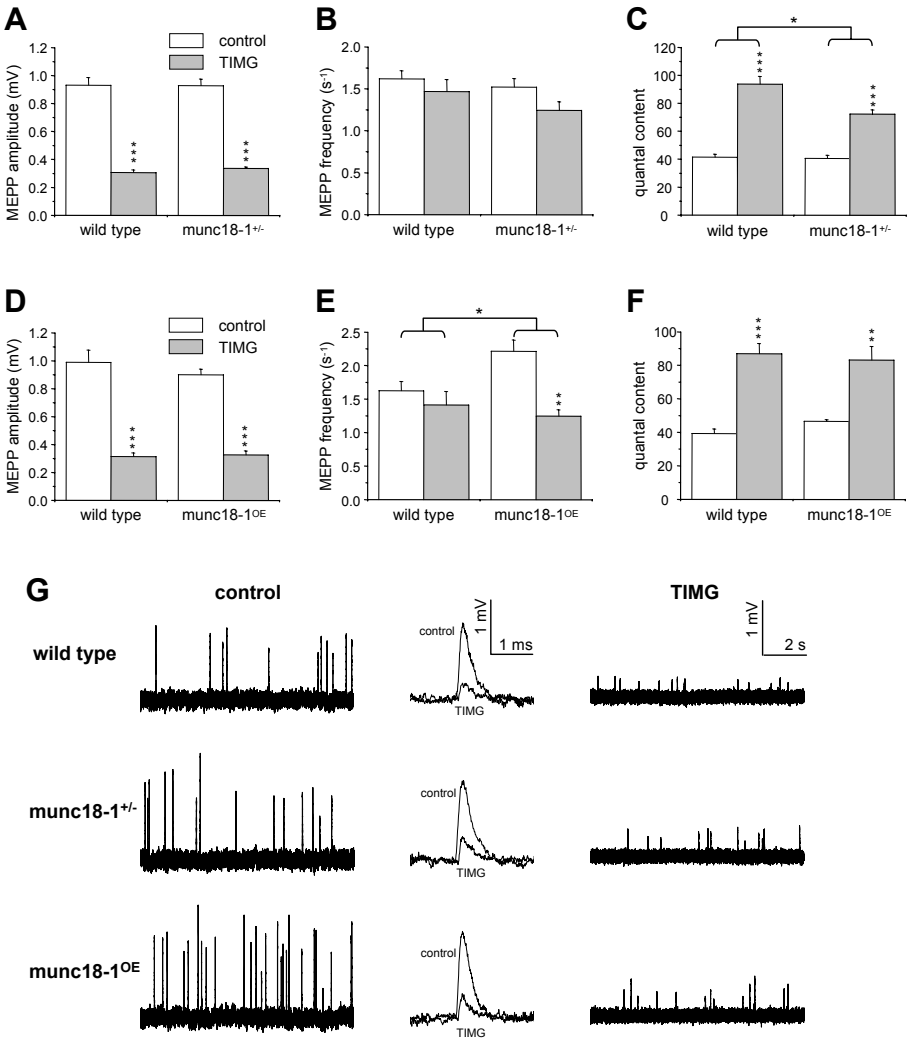

Figure 1. Low-rate evoked and spontaneous acetylcholine release at neuromuscular synapses of wild type, Munc18-1$^{+/-}$ and Munc18-1^{OE} mice with toxin-induced myasthenia gravis.
Effect of TIMG-treatment (shaded bars) on MEPP amplitude, quantal content at 0.3 Hz nerve stimulation and MEPP frequency at NMJs of diaphragms from Munc18-1$^{+/-}$ (A-C), Munc18-1^{OE} (D-F) mice, compared with wild type littermates. N=5-12 mice, 10-15 NMJs sampled per muscle, data represent grand mean group values + S.E.M. TIMG-treatment induced equal reductions of MEPP amplitudes of ~70% in either genotype. The extent of the resulting increase in quantal content in the wild type group was larger than that in the Munc18-1$^{+/-}$ group ($p<0.05$). MEPP frequency at saline-injected control Munc18-1^{OE} NMJs was higher than at wild type NMJs ($p<0.05$). TIMG treatment reduced the MEPP frequency at Munc18-1^{OE} NMJs ($p<0.05$), to a larger extent than at wild type NMJs ($P<0.01$). (G) Typical examples of MEPP recordings at NMJs of the different genotype mice under TIMG- and saline-injected control condition (10s traces, left and right columns). In the middle column, individual MEPPs recorded from control and TIMG-treated NMJs have been superimposed at enlarged time-base. *$p<0.05$, ***$p<0.001$.

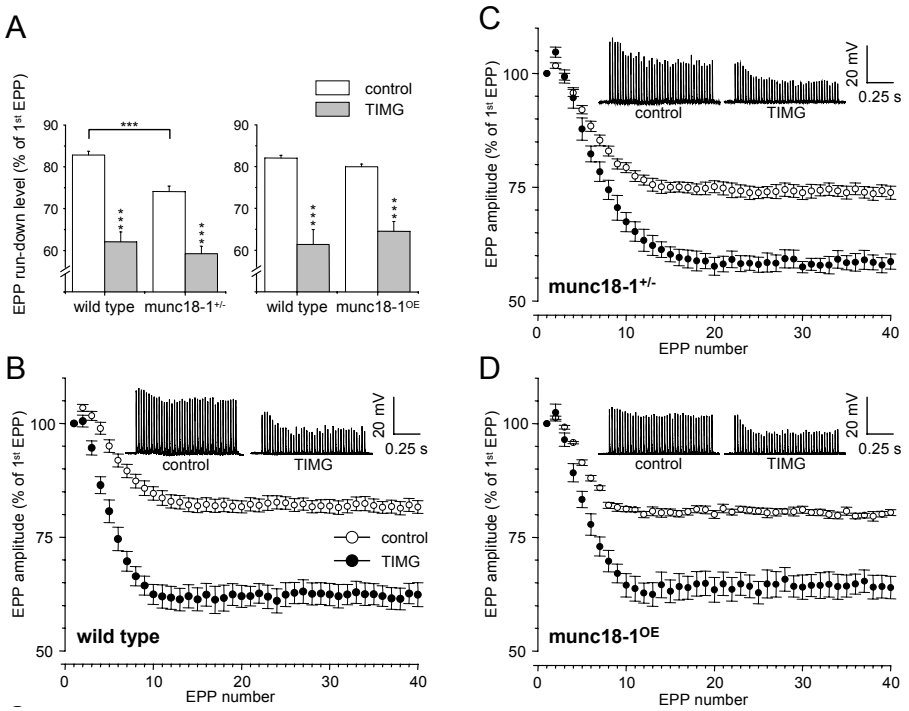

Figure 2. High-rate evoked acetylcholine release at neuromuscular synapses of wild type, Munc18-1$^{+/-}$ and Munc18-1^{OE} mice with toxin-induced myasthenia gravis.
Effect of TIMG-treatment (shaded bars) on EPP amplitude rundown during high-rate (40 Hz) stimulation for 1 s of the phrenic nerve of diaphragms from wild-type, Munc18-1$^{+/-}$ and Munc18-1^{OE} mice (N=5-12 mice, 10-15 NMJs sampled per muscle). (A) Mean rundown level of EPP amplitude. At each NMJ the EPP amplitude rundown level was taken as the calculated mean amplitude of the last 10 EPPs in the train, expressed as a percentage of the first EPP of the train. Data represent grand mean group values ± S.E.M. Average rundown profiles from (B) wild-type, (C) Munc18-1$^{+/-}$ and (D) Munc18-1^{OE} NMJs under saline-injected control condition (filled circles) and TIMG condition (open circles). Insets are typical examples of 40 Hz EPP train recordings. ***p<0.001.

Munc18-1$^{+/-}$ and wild type mice, to 0.34 ± 0.01 mV (n=11) and 0.31 ± 0.02 mV (n=10), respectively (Figure 1A, G). This indicates that the reduction of postsynaptic sensitivity to ACh in the TIMG condition was established at a similar degree in both genotypes. The amplitude of EPPs evoked by low-frequency stimulation (0.3 Hz) after TIMG treatment was 19.5 ± 1.43 mV in wild type and 17.8 ± 0.64 mV in Munc18-1$^{+/-}$ NMJs. At wild type TIMG NMJs the quantal content was increased by 126% ($p<0.001$) compared with the saline-treated controls (Figure 1C). However, the increase of quantal content at Munc18-1$^{+/-}$ TIMG NMJs was only 79% ($p<0.001$), statistically significantly less than the increase at wild type NMJs ($p<0.01$). Thus, although basic neuromuscular synaptic transmission seems largely unaltered at Munc18-1$^{+/-}$ NMJs, presynaptic adaptation in response to reduced postsynaptic transmitter sensitivity is impaired.

In both wild type and Munc18-1$^{+/-}$ groups, rundown of the EPP amplitude at 40 Hz stimulation was more pronounced in TIMG than saline-injected control mice (Figure 2). In wild type TIMG-NMJs the rundown reached a level of 62 ± 2.4% of

the first EPP in the train, which differed from the 83 ± 0.9% observed in controls ($p<0.001$). In Munc18-1$^{+/-}$ TIMG NMJs the rundown of EPPs amplitude increased to 59 ± 1.8%, which was significantly different from control values (74 ± 1.3%, $p<0.001$).

At TIMG-NMJs the mean MEPP frequency tended to be reduced in both wild type (9%) and Munc18-1$^{+/-}$ mice (18%), compared with their saline-injected controls, but this difference was not statistically significant. At NMJs with very small MEPPs, as often encountered under TIMG conditions, the mean frequency may have been underestimated due to loss of MEPPs that were too small to detect, i.e. with amplitudes smaller than about 0.1 mV. In order to substantiate this hypothesis we classified the NMJs with respect to their MEPP amplitude into classes of 0.1 mV bin-width and calculated for each class the mean MEPP frequency. In all overlapping MEPP amplitude classes there was no statistically significant difference between MEPP frequencies measured in TIMG or control NMJs, in either wild type or Munc18-1$^{+/-}$ NMJs (Figure 3). The wild type and Munc18-1$^{+/-}$ TIMG-NMJs in the 0.1-0.2 mV MEPP amplitude class (which were not encountered in saline-treated controls) had clearly lower MEPP frequencies than all the classes of NMJs, with larger MEPP amplitude. This indicates that some loss of MEPPs in the baseline noise had occurred, which may explain the small reduction of overall mean MEPP frequency in the TIMG groups of either genotype compared to their control value obtained in saline-injected mice. As a result the mean MEPP amplitude may have been overestimated at these NMJs and, consequently, the TIMG quantal contents may have been underestimated.

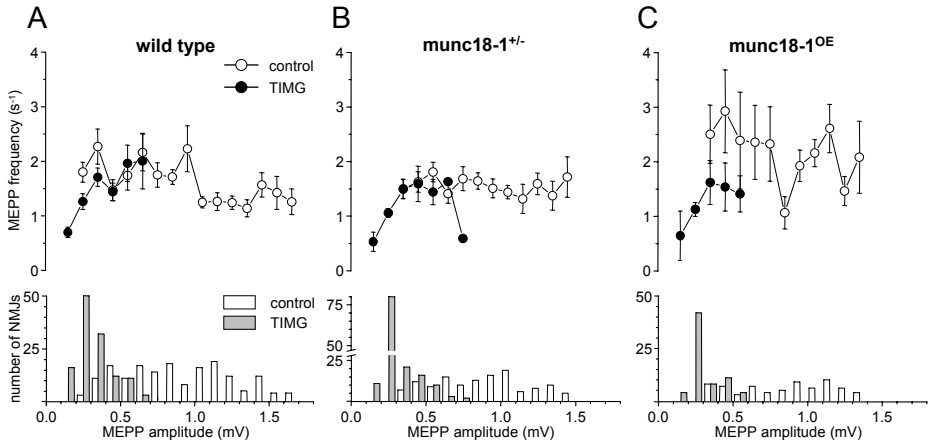

Figure 3. Relation between MEPP amplitude and MEPP frequency at neuromuscular synapses of Munc18-1$^{+/-}$ and Munc18-1^{OE} mice with toxin-induced myasthenia gravis.
NMJs of (A) wild-type, (B) Munc18-1$^{+/-}$ and (C) Munc18-1^{OE} mice were classified with respect to their mean MEPP amplitudes (normalized to -75 mV resting membrane potential) in bins of 0.1 mV width. Data points represent the mean MEPP frequency ± S.E.M. within a bin (open symbols, TIMG; filled symbols, saline-injected controls). In the lower panels of each figure, the numbers of NMJs in each bin are given in a histogram (filled bars, TIMG; open bars, saline-injected control). No statistically significant differences were found between TIMG and controls NMJs, when both present in a bin.

Thus, NMJs from Munc18-1$^{+/-}$ mice showed impaired synaptic plasticity in that they were not able to upregulate their ACh release as much as wild type control NMJs upon reduction of postsynaptic transmitter sensitivity (Figure 4).

Overexpression of Munc18-1 does not further increase the level of homeostatic upregulation of transmitter release in TIMG

The data obtained from Munc18-1$^{+/-}$ mice indicated that a reduced level of Munc18-1 limits the ability of motor nerve terminals to compensate for the reduced postsynaptic ACh sensitivity under myasthenic conditions by an increase of ACh release. Consequently, we hypothesized that increased Munc18-1 protein levels might increase the level of compensatory upregulation of ACh release. To test this hypothesis we subjected Munc18-1^{OE} mice, which overexpress Munc18-1 in motor neurons, to our TIMG protocol and analyzed synaptic transmission at their NMJs.

Under control (i.e. saline-injected) conditions (N=7 wild type mice and N=5 Munc18-1^{OE} mice, 10-15 endplates per muscle), MEPP amplitude was similar at wild-type and Munc18-1^{OE} NMJs (0.99 ± 0.09 mV and 0.90 ± 0.04, respectively, Figure 1E, G). Munc18-1^{OE} NMJs had a 36% increased MEPP frequency compared with wild type (2.21 ± 0.17 s^{-1} and 1.62 ± 0.14 s^{-1}, respectively, $p<0.05$, Figure 1E, G). The mean quantal content of Munc18-1^{OE} NMJs was 46.6 ± 1.05, which is 18% more than the 39.4 ± 2.68 observed at wild type NMJs, although this difference

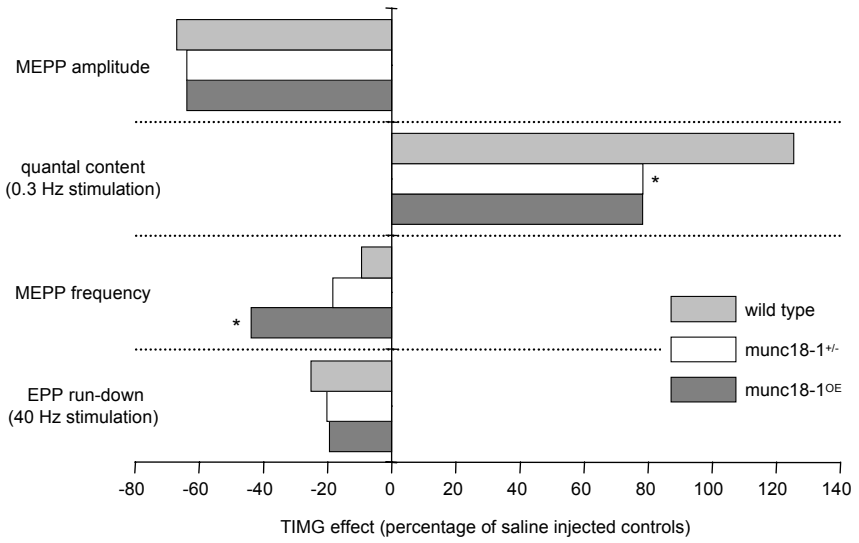

Figure 4. Normalized effects of toxin-induced myasthenia gravis on neuromuscular synapse parameters of wild type, Munc18-1$^{+/-}$ and Munc18-1^{OE} mice.
Overview of the effects of TIMG-treatment on MEPP amplitude, MEPP frequency, quantal content and rundown of 40 Hz EPP amplitude in wild-type, Munc18-1$^{+/-}$ and Munc18-1^{OE} NMJs. TIMG values of the parameters of each genotype group were expressed as a percentage of the mean values obtained in saline-injected control groups. *$p<0.05$, different from wild type group.

did just not reach statistical significance (p=0.05, Figure 1F). Also, there was no significant change in EPP amplitude rundown upon 40 Hz stimulation at Munc18^{OE} NMJs compared to wild type (rundown to 80 ± 0.7% and 82 ± 0.7% of the first EPP, respectively, Figure 2).

At Munc18-1^{OE} NMJs under TIMG conditions there was a tendency to display less compensatory increase of ACh release than at TIMG/wild type NMJs (78% vs. 121% increase, respectively, N=5 TIMG/Munc18-1^{OE} and 5 TIMG/wild type mice, Figure 1F). However, this difference was not statistically significant. Under TIMG conditions, the EPP amplitude rundown became more pronounced, compared to saline-injected controls, to a similar degree in both genotypes (rundown level of 61 ± 3.6% of first EPP at TIMG/wild type and 65 ± 2.4% at TIMG/Munc18-1^{OE} NMJs, Figure 2). We observed a TIMG-induced decrease of the overall mean MEPP-frequency of 44% at Munc18-1^{OE} NMJs, which was larger ($p<0.05$) than the small TIMG-induced decrease of ~10% at wild type NMJs (Figure 1E, G). When we classified the NMJs in MEPP amplitude bins of 0.1 mV it appeared that there was a clear tendency of MEPP frequencies at TIMG/Munc18-1^{OE} NMJs to be about 50% lower than that of NMJs in the similar amplitude class of saline-injected controls. However, these reductions were not statistically significant (Figure 3 and 4).

Thus, overexpression of Munc18-1 did not further augment the level of compensatory increase of ACh release upon a reduction in postsynaptic ACh sensitivity.

Discussion

At myasthenic NMJs, homeostatic upregulation of ACh release partially compensates for the loss of postsynaptic transmitter sensitivity after reduction of AChRs. Most likely, this involves retrograde signaling from muscle fibers to motor nerve terminals. We hypothesized that neuro-exocytotic proteins are the final targets of such a signaling pathway. The data presented here indicate that the key neuro-exocytotic protein Munc18-1 indeed plays a role in the mechanism underlying this form of functional synaptic plasticity.

Role of Munc18-1 in neurotransmitter release at the neuromuscular synapse

Munc18-1$^{+/-}$ saline control group NMJs showed increased rundown of EPP amplitude during high-frequent stimulation, compared to wild-type, and Munc18-1^{OE} NMJs displayed an increased MEPP frequency. This is in agreement with data we reported previously on NMJs and hippocampal autaptic synapses of Munc18-1$^{+/-}$ and Munc18-1^{OE} mice (Toonen et al., 2006b), concluding a role for Munc18-1 in regulation of the vesicle pool size. A smaller vesicle pool size in Munc18-1$^{+/-}$ NMJs explains the reduced MEPP frequency, since vesicle pool size is a factor that de-

termines the level of spontaneous transmitter release (Prange and Murphy, 1999; Stevens and Sullivan, 1998). Rundown of high-rate evoked transmitter release is believed to represent depletion of the readily releasable pool of synaptic vesicles (Kuromi and Kidokoro, 2000), and Munc18-1 also controls the number of docked, release-ready vesicles in chromaffin cells (Toonen et al., 2006a; Voets et al., 2001) and *C. elegans* (Weimer and Jorgensen, 2003). The increased rundown of high-rate evoked release as observed in Munc18-1$^{+/-}$ is consistent with these reports.

Our earlier studies on Munc18-1$^{+/-}$ NMJs showed a decrease in quantal content and MEPP frequency, which we did not find in the present study. In addition we observed an increase in quantal content in Munc18-1^{OE} NMJs and in MEPP frequency in in Munc18-1^{OE} NMJs (Toonen et al., 2006b). Although we did find the increase in MEPP frequeny, the increase in quantal content in this study was not statistically significant.The reason for this discrepancy is not clear but might stem from the difference in age of the mice. The mice used in the present study were older due to the TIMG/saline treatment of six weeks. Possibly, adaptation occurs to the changed Munc18-1 levels during aging.

Role of Munc18-1 in homeostatic transsynaptic upregulation of transmitter release at myasthenic neuromuscular synapses

Subjection of Munc18-1$^{+/-}$ mice to an experimental model for MG showed that these NMJs are less capable of compensatory increase of transmitter release compared to wild-type myasthenic NMJs. This indicates that Munc18-1 is involved in the homeostatic upregulation of ACh release at myasthenic NMJs.

It has been shown that Munc18-1 is involved in all steps leading to neurotransmitter release, from tethering, docking, priming to fusion (Rizo and Rosenmund, 2008; reviewed in: Toonen and Verhage, 2007). Munc18-1 may act as crystallization points for SNARE formation, so recruitment or activation of Munc18-1 may lead to an increased number of ACh quanta released following a presynaptic impulse. This may be the result of an increase of the readily releasable pool (RRP) of vesicles. This is in accordance with the observed more pronounced rundown during high-frequency stimulation in TIMG and MG, since the maintenance of a high vesicle turnover in such a large RRP during high-frequency stimulation will put more strain to the exocytotic machinery. However, one could expect a higher basal MEPP frequency in TIMG NMJs when the RRP is increased, which was not observed.

Munc18-1 is a substrate for cyclin-dependent kinase 5 (Fletcher et al., 1999; Shuang et al., 1998) and protein kinase C (PKC) (Barclay et al., 2003; de Vries et al., 2000; Fujita et al., 1996). Activation of PKC has been shown to underlie enhancement of neurotransmitter secretion in different forms of synaptic plasticity (Brager et al., 2003). Phosphorylation of Munc18-1 might be involved in the upregulation of ACh release at myasthenic NMJs. This would require stimulation of kinases at

motor nerve terminal by the putative retrograde messenger that is released from the myasthenic muscle fiber. Interestingly, stimulation of TrkB membrane receptors by neurotrophins, which are candidate retrograde factors, has been shown to activate PKC (Zirrgiebel et al., 1995). However, other studies did not find an effect of PKC inhibition on upregulated ACh release in rat TIMG NMJs *in vitro* (Plomp and Molenaar, 1996). In addition, PKC phosphorylation of Munc18-1 is known to stimulate release in chromaffin cells (Barclay et al., 2003), without increasing the number of docked vesicles (Wierda et al., 2007).

Another mechanism by which Munc18-1 might be targeted in the signaling cascade is via a transsynaptic protein complex formed by the postsynaptic scaffolding protein PSD-95, and neuroligin and presynaptic β-neurexin (Futai et al., 2007). This signaling route was described for rat hippocampal CA1 pyramidal neurons, and positively influences presynaptic release. Since β-neurexin binds to the scaffolding protein CASK, which in turn is known to bind Mint1, a binding partner of Munc18-1, a role of Munc18-1 could be envisioned here (Futai et al., 2007, and references herein). However, more research is necessary to elucidate the exact signaling pathway that is employed in MG synapses.

Surprisingly, Munc18-1^{OE} NMJs did not show further enhanced levels of upregulation of ACh release upon the loss of postsynaptic ACh sensitivity induced by the TIMG treatment, when compared to the augmented level at wild type TIMG-treated NMJs. Upregulation of ACh release rather tended to be lower in Munc18-1^{OE} TIMG-NMJs, but the difference was not significant. Apparently, Munc18-1 protein at Munc18-1^{OE} NMJs is present at a supramaximal level and under this condition other factors that participate in the mechanism of upregulation of ACh release will become limiting. Alternatively, Munc18-1 at this increased level may exert unknown inhibitory actions on such factors.

TIMG treatment reduced MEPP frequency at Munc18-1^{OE} NMJs but not at wild type controls. The reasons for this difference are not clear. One possible explanation is that a larger proportion of MEPPs remained undetected due to a larger reduction of MEPP amplitude at Munc18-1^{OE} NMJs by the TIMG treatment. However, this was not observed. It is possible that due to the already elevated ACh release level at Munc18-1^{OE} NMJs, compared to wild type controls, a further increase of evoked release induced by the TIMG treatment prevents full replenishment of the transmitter vesicle pool so that MEPP frequency becomes reduced.

TIMG induced a more pronounced rundown of ACh release at high-rate nerve stimulation at NMJs of all three studied Munc18-1 genotypes, compared to that at NMJs of saline-injected control mice. As the quantal content is increased under TIMG conditions, the most likely explanation is that the readily releasable vesicle pool becomes exhausted at a faster rate. A similar association between increased quantal content and a more pronounced rundown at high-rate nerve stimulation

was shown at NMJs of mice overexpressing acetylcholinesterase (Farchi et al., 2003). However, increased exhaustion of the vesicle pool due to the high level of ACh release may not be the only explanation because an increased rundown of release has been observed as soon as 3 hours after the first α-bungarotoxin injection in TIMG rats, when MEPP amplitude is decreased but quantal content not yet increased (J.J. Plomp, unpublished results). Furthermore, it was expected that increased levels of Munc18-1 at Munc18-1^{OE} NMJs would have counteracted more pronounced rundown of ACh release during high-rate nerve stimulation through facilitation of the replenishment rate of the vesicle pool. However, this was not observed; apparently Munc18-1 is not the rate-limiting factor in this process.

In conclusion, we have shown that Munc18-1 is involved in homeostatic upregulation of ACh release at mouse NMJs in response to a lowered postsynaptic sensitivity for ACh. From a clinical point of view, elucidation of the molecular mechanism of upregulation of ACh release at myasthenic NMJs is important. New drug targets can be identified and their activation should boost the process of synaptic adaptation in order to counteract or prevent muscle weakness. Unfortunately, Munc18-1 appears to be a poor candidate in view of the observed lack of enhanced compensatory upregulation of ACh release at myasthenic Munc18-1^{OE} NMJs.

Reference List

Aalto MK, Ruohonen L, Hosono K, Keranen S (1992) Cloning and sequencing of the yeast Saccharomyces cerevisiae SEC1 gene localized on chromosome IV. Yeast 8:587-588.

Aberle H, Haghighi AP, Fetter RD, McCabe BD, Magalhaes TR, Goodman CS (2002) wishful thinking encodes a BMP type II receptor that regulates synaptic growth in *Drosophila*. Neuron 33:545-558.

Bacci A, Coco S, Pravettoni E, Schenk U, Armano S, Frassoni C, Verderio C, De Camilli P, Matteoli M (2001) Chronic blockade of glutamate receptors enhances presynaptic release and downregulates the interaction between synaptophysin-synaptobrevin-vesicle-associated membrane protein 2. J Neurosci 21:6588-6596.

Barclay JW, Craig TJ, Fisher RJ, Ciufo LF, Evans GJ, Morgan A, Burgoyne RD (2003) Phosphorylation of Munc18 by protein kinase C regulates the kinetics of exocytosis. J Biol Chem 278:10538-10545.

Brager DH, Cai X, Thompson SM (2003) Activity-dependent activation of presynaptic protein kinase C mediates post-tetanic potentiation. Nat Neurosci 6:551-552.

Cull-Candy SG, Miledi R, Trautmann A, Uchitel OD (1980) On the release of transmitter at normal, myasthenia gravis and myasthenic syndrome affected human end-plates. J Physiol 299:621-638.

Davis GW (2006) Homeostatic control of neural activity: from phenomenology to molecular design. Annu Rev Neurosci 29:307-323.

Davis GW, Bezprozvanny I (2001) Maintaining the stability of neural function: a homeostatic hypothesis. Annu Rev Physiol 63:847-869.

Davis GW, DiAntonio A, Petersen SA, Goodman CS (1998) Postsynaptic PKA controls quantal size and reveals a retrograde signal that regulates presynaptic transmitter release in *Drosophila*. Neuron 20:305-315.

Davis GW, Murphey RK (1993) A role for postsynaptic neurons in determining presynaptic release properties in the cricket CNS: evidence for retrograde control of facilitation. J Neurosci 13:3827-3838.

de Vries KJ, Geijtenbeek A, Brian EC, de Graan PN, Ghijsen WE, Verhage M (2000) Dynamics of Munc18-1 phosphorylation/dephosphorylation in rat brain nerve terminals. Eur J Neurosci 12:385-390.

Dulubova I, Khvotchev M, Liu S, Huryeva I, Sudhof TC, Rizo J (2007) Munc18-1 binds directly to the neuronal SNARE complex. Proc Natl Acad Sci U S A 104:2697-2702.

Dulubova I, Sugita S, Hill S, Hosaka M, Fernandez I, Sudhof TC, Rizo J (1999) A conformational switch in syntaxin during exocytosis: role of munc18. EMBO J 18:4372-4382.

Farchi N, Soreq H, Hochner B (2003) Chronic acetylcholinesterase overexpression induces multilevelled aberrations in mouse neuromuscular physiology. J Physiol 546:165-173.

Finley MF, Patel SM, Madison DV, Scheller RH (2002) The core membrane fusion complex governs the probability of synaptic vesicle fusion but not transmitter release kinetics. J Neurosci 22:1266-1272.

Fletcher AI, Shuang R, Giovannucci DR, Zhang L, Bittner MA, Stuenkel EL (1999) Regulation of exocytosis by cyclin-dependent kinase 5 via phosphorylation of Munc18. J Biol Chem 274:4027-4035.

Forss-Petter S, Danielson PE, Catsicas S, Battenberg E, Price J, Nerenberg M, Sutcliffe JG (1990) Transgenic mice expressing beta-galactosidase in mature neurons under neuron-specific enolase promoter control. Neuron 5:187-197.

Fujita Y, Sasaki T, Fukui K, Kotani H, Kimura T, Hata Y, Sudhof TC, Scheller RH, Takai Y (1996) Phosphorylation of Munc-18/n-Sec1/rbSec1 by protein kinase C: its implication in regulating the interaction of Munc-18/n-Sec1/rbSec1 with syntaxin. J Biol Chem 271:7265-7268.

Futai K, Kim MJ, Hashikawa T, Scheiffele P, Sheng M, Hayashi Y (2007) Retrograde modulation of presynaptic release probability through signaling mediated by PSD-95-neuroligin. Nat Neurosci 10:186-195.

Hanson PI, Roth R, Morisaki H, Jahn R, Heuser JE (1997) Structure and conformational changes in NSF and its membrane receptor complexes visualized by quick-freeze/deep-etch electron microscopy. Cell 90:523-535.

Harrison SD, Broadie K, van de GJ, Rubin GM (1994) Mutations in the *Drosophila* Rop gene suggest a function in general secretion and synaptic transmission. Neuron 13:555-566.

Hata Y, Slaughter CA, Sudhof TC (1993) Synaptic vesicle fusion complex contains unc-18 homologue bound to syntaxin. Nature 366:347-351.

Hosono R, Hekimi S, Kamiya Y, Sassa T, Murakami S, Nishiwaki K, Miwa J, Taketo A, Kodaira KI (1992) The unc-18 gene encodes a novel protein affecting the kinetics of acetylcholine metabolism in the nematode *Caenorhabditis elegans*. J Neurochem 58:1517-1525.

Kuromi H, Kidokoro Y (2000) Tetanic stimulation recruits vesicles from reserve pool via a cAMP-mediated process in *Drosophila* synapses. Neuron 27:133-143.

Lin RC, Scheller RH (1997) Structural organization of the synaptic exocytosis core complex. Neuron 19:1087-1094.

McCabe BD, Marques G, Haghighi AP, Fetter RD, Crotty ML, Haerry TE, Goodman CS, O'Connor MB (2003) The BMP homolog Gbb provides a retrograde signal that regulates synaptic growth at the *Drosophila* neuromuscular junction. Neuron 39:241-254.

Micheva KD, Buchanan J, Holz RW, Smith SJ (2003) Retrograde regulation of synaptic vesicle endocytosis and recycling. Nat Neurosci 6:925-932.

Misura KM, Scheller RH, Weis WI (2000) Three-dimensional structure of the neuronal-Sec1-syntaxin 1a complex. Nature 404:355-362.

Molenaar PC, Oen BS, Plomp JJ, van Kempen GT, Jennekens FG, Hesselmans LF (1991) A non-immunogenic myasthenia gravis model and its application in a study of transsynaptic regulation at the neuromuscular junction. Eur J Pharmacol 196:93-101.

Novick P, Ferro S, Schekman R (1981) Order of events in the yeast secretory pathway. Cell 25:461-469.

Petersen SA, Fetter RD, Noordermeer JN, Goodman CS, DiAntonio A (1997) Genetic analysis of glutamate receptors in *Drosophila* reveals a retrograde signal regulating presynaptic transmitter release. Neuron 19:1237-1248.

Plomp JJ, Molenaar PC (1996) Involvement of protein kinases in the upregulation of acetylcholine release at endplates of alpha-bungarotoxin-treated rats. J Physiol 493 (Pt 1):175-186.

Plomp JJ, van Kempen GT, De Baets MB, Graus YM, Kuks JB, Molenaar PC (1995) Acetylcholine release in myasthenia gravis: regulation at single end-plate level. Ann Neurol 37:627-636.

Plomp JJ, van Kempen GT, Molenaar PC (1992) Adaptation of quantal content to decreased postsynaptic sensitivity at single endplates in alpha-bungarotoxin-treated rats. J Physiol 458:487-499.

Plomp JJ, van Kempen GT, Molenaar PC (1994) The upregulation of acetylcholine release at endplates of alpha-bungarotoxin-treated rats: its dependency on calcium. J Physiol 478 (Pt 1):125-136.

Poirier MA, Xiao W, Macosko JC, Chan C, Shin YK, Bennett MK (1998) The synaptic SNARE complex is a parallel four-stranded helical bundle. Nat Struct Biol 5:765-769.

Prange O, Murphy TH (1999) Correlation of miniature synaptic activity and evoked release probability in cultures of cortical neurons. J Neurosci 19:6427-6438.

Regehr WG, Carey MR, Best AR (2009) Activity-dependent regulation of synapses by retrograde messengers. Neuron 63:154-170.

Rizo J, Rosenmund C (2008) Synaptic vesicle fusion. Nat Struct Mol Biol 15:665-674.

Rosenmund C, Rettig J, Brose N (2003) Molecular mechanisms of active zone function. Curr Opin Neurobiol 13:509-519.

Sandrock AW, Jr., Dryer SE, Rosen KM, Gozani SN, Kramer R, Theill LE, Fischbach GD (1997) Maintenance of acetylcholine receptor number by neuregulins at the neuromuscular junction in vivo. Science 276:599-603.

Scheiffele P (2003) Cell-cell signaling during synapse formation in the CNS. Annu Rev Neurosci 26:485-508.

Shen J, Tareste DC, Paumet F, Rothman JE, Melia TJ (2007) Selective activation of cognate SNAREpins by Sec1/Munc18 proteins. Cell 128:183-195.

Shuang R, Zhang L, Fletcher A, Groblewski GE, Pevsner J, Stuenkel EL (1998) Regulation of Munc-18/syntaxin 1A interaction by cyclin-dependent kinase 5 in nerve endings. J Biol Chem 273:4957-4966.

Stevens CF, Sullivan JM (1998) Regulation of the readily releasable vesicle pool by protein kinase C. Neuron 21:885-893.

Sudhof TC (2004) The synaptic vesicle cycle. Annu Rev Neurosci 27:509-547.

Sudhof TC, Rothman JE (2009) Membrane fusion: grappling with SNARE and SM proteins. Science 323:474-477.

Sutton RB, Fasshauer D, Jahn R, Brunger AT (1998) Crystal structure of a SNARE complex involved in synaptic exocytosis at 2.4 A resolution. Nature 395:347-353.

Toonen RF, Kochubey O, de Wit H, Gulyas-Kovacs A, Konijnenburg B, Sorensen JB, Klingauf J, Verhage M (2006a) Dissecting docking and tethering of secretory vesicles at the target membrane. EMBO J 25:3725-3737.

Toonen RF, Verhage M (2007) Munc18-1 in secretion: lonely Munc joins SNARE team and takes control. Trends Neurosci 30:564-572.

Toonen RF, Wierda K, Sons MS, de Wit H, Cornelisse LN, Brussaard A, Plomp JJ, Verhage M (2006b) Munc18-1 expression levels control synapse recovery by regulating readily releasable pool size. Proc Natl Acad Sci U S A 103:18332-18337.

Turrigiano GG, Leslie KR, Desai NS, Rutherford LC, Nelson SB (1998) Activity-dependent scaling of quantal amplitude in neocortical neurons. Nature 391:892-896.

Verhage M, Maia AS, Plomp JJ, Brussaard AB, Heeroma JH, Vermeer H, Toonen RF, Hammer RE, van den Berg TK, Missler M, Geuze HJ, Sudhof TC (2000) Synaptic assembly of the brain in the absence of neurotransmitter secretion. Science 287:864-869.

Verhage M, Toonen RF (2007) Regulated exocytosis: merging ideas on fusing membranes. Curr Opin Cell Biol 19:402-408.

Vincent A, Palace J, Hilton-Jones D (2001) Myasthenia gravis. Lancet 357:2122-2128.

Voets T, Toonen RF, Brian EC, de Wit H, Moser T, Rettig J, Sudhof TC, Neher E, Verhage M (2001) Munc18-1 promotes large dense-core vesicle docking. Neuron 31:581-591.

Weimer RM, Jorgensen EM (2003) Controversies in synaptic vesicle exocytosis. J Cell Sci 116:3661-3666.

Wierda KD, Toonen RF, de Wit H, Brussaard AB, Verhage M (2007) Interdependence of PKC-dependent and PKC-independent pathways for presynaptic plasticity. Neuron 54:275-290.

Yamaguchi T, Dulubova I, Min SW, Chen X, Rizo J, Sudhof TC (2002) Sly1 binds to Golgi and ER syntaxins via a conserved N-terminal peptide motif. Dev Cell 2:295-305.

Zirrgiebel U, Ohga Y, Carter B, Berninger B, Inagaki N, Thoenen H, Lindholm D (1995) Characterization of TrkB receptor-mediated signaling pathways in rat cerebellar granule neurons: involvement of protein kinase C in neuronal survival. J Neurochem 65:2241-2250.

7

Redundancy of RIM1α in neuromuscular synapse function

Michèle S. Sons and Jaap J. Plomp

Departments of Neurology and MCB-Neurophysiology, Leiden University Medical Centre, Leiden, The Netherlands

Abstract

Rab interacting molecule 1α (RIM1α) is a large, multidomain protein thought to be implicated in neurotransmitter release and several forms of synaptic plasticity in the central nervous system. We investigated the role of RIM1α at the peripheral neuromuscular junction (NMJ) by performing electrophysiological recordings of synaptic signals at ex vivo NMJs of homozygous RIM1α knockout mice. Furthermore, to assess whether RIM1α plays a role in synaptic plasticity at the NMJ, we induced an experimental form of myasthenia gravis by injecting mice with α-bungarotoxin, a blocker of postsynaptic acetylcholine receptors. This procedure is known to induce compensatory upregulation of acetylcholine release from the presynaptic motor nerve terminal at the NMJ. No effect of the deletion of RIM1α in the NMJ was found, neither on the basic neurotransmitter release parameters, nor on the homeostatic increase of transmitter release under experimental myasthenic condition. This leads to the conclusion that RIM1α is redundant for synaptic function at the mouse NMJ.

Acknowledgements
This study was supported by the Netherlands Organization for Scientific Research (NWO) (#903-42-073 to J.J.P.). We thank Prof. T.C. Südhof and dr. S. Schoch (The University of Texas Southwestern Medical Center, Dallas, USA) for supplying the RIM1α KO mice used in this study.

Introduction

Rab3 Interacting Molecule (RIM) proteins are localized to presynaptic zones and are believed to play a scaffolding role in synaptic vesicle docking or priming (Wang et al., 1997). Originally discovered as a Rab3a interacting protein, it has been established that RIM interacts with other active zone proteins as well (e.g. Munc13, liprin, and calcium channels) (Schoch et al., 2002; Kiyonaka et al., 2007).

In vertebrates, the RIM protein family is encoded by four genes expressed in a variety splice variants. α-RIMs (RIM1α and RIM2α) are full length proteins, consisting of an N-terminal Rab3-binding sequence and a Munc13-binding sequence, a central PDZ-domain and two C-terminal C_2-domains (Wang et al., 2000). In contrast to this, β-RIM (RIM2β) does not contain the Rab3- and Munc13-binding sequence. Furthermore, there are three γ-RIMs (RIM2γ, RIM3γ, and RIM4γ), consisting only of the C-terminal C_2-domains and a short flanking sequence (Wang et al., 2000; Wang and Sudhof, 2003). In *C. elegans* RIM is encoded by one gene, unc10 (Koushika et al., 2001).

RIM1α KO mice are viable and fertile but show alterations in memory and learning and an impairment of vesicle priming (Powell et al., 2004). Several forms of synaptic plasticity (mossy fiber long term potentiation (LTP), short term potentiation (STP)) were shown to be altered (Castillo et al., 2002; Schoch et al., 2002; Calakos et al., 2004). The RIM1α /RIM2α double KO mouse (Schoch et al., 2006a) is not viable, and analysis of E18.5 embryos showed a strongly impaired calcium regulated neurotransmitter release in the NMJ. Deletion of *unc10* in *C. elegans* RIM (Koushika et al., 2001) results in impaired neurotransmitter release with a defect in priming.

RIM1α most likely participates in vesicle priming by its N-terminal interaction with Munc13, a large active zone protein that is crucial for priming (Betz et al., 2001; Dulubova et al., 2005). Munc13 forms homodimers, and α-RIM competes with the Munc13-Munc13 interaction to form Munc13-RIM heterodimers (Lu et al., 2006). The N-terminal of α-RIM can simultaneously bind GTP-bound Rab3A on synaptic vesicles (Dulubova et al., 2005); this Rab3/RIM/Munc13 tripartite complex approximates synaptic vesicles to the priming machinery. RIM1α may also stimulate neurotransmitter release in a more direct way through an interaction with presynaptic voltage-dependent calcium channels which inhibits their inactivation (Kiyonaka et al., 2007), although a recent publication failed to show this (Wong and Stanley, 2010).

Many proteins that have been shown to participate in exocytosis in central synapses are also present at neuromuscular junctions (NMJs), such as the SNARE proteins, and Munc18 (reviewed by Lin and Scheller, 2000; Sudhof, 2004; Sudhof and Rothman, 2009). Previously, we demonstrated an identical silencing effect of Munc18-1 deletion on central synapses and the NMJ (Verhage et al., 2000). Howev-

er, absence of specific presynaptic proteins does not always lead to identical effects at central synapses and the NMJ. Analysis of Munc13-1/2 deficient mice showed severely reduced (but not absent) evoked transmitter release and unaltered spontaneous release at the NMJ (Varoqueaux et al., 2005). In contrast, central synapses of these mice were completely silenced (Varoqueaux et al., 2002).

Here, we evaluated the role of RIM1α in neuromuscular synaptic function. Electrophysiological recordings of postsynaptic response in the muscle fiber from diaphragm nerve-muscle preparations of RIM1α KO mice allow to quantify the acetylcholine (ACh) release at NMJs. Surprisingly, all basic ACh release parameters were unaltered compared to those recorded in the wild-type control NMJs. Since RIM1α has been implicated in synaptic plasticity at CNS synapses (Castillo et al., 2002; Schoch et al., 2002; Calakos et al., 2004), we also tested for a possible role of RIM1α in synaptic homeostasis at the NMJ. In the condition of myasthenia gravis (MG), where auto-antibodies reduce the number of functional postsynaptic ACh receptors (AChRs), NMJs up-regulate presynaptic ACh release to compensate for the loss of postsynaptic sensitivity (Plomp et al., 1995). We investigated this in a toxin-induced myasthenia gravis (TIMG) mouse model, where the functional density of AChRs is reduced by application of α-bungarotoxin (Plomp et al., 1992). In order to elucidate a possible role for RIM1α in this form of synaptic plasticity at the NMJ we subjected both RIM1α KO and wild type mice to the TIMG model. Both groups displayed a similar compensatory increase of neurotransmitter release, implicating that RIM1α is not playing a role in this form of synaptic plasticity.

Taken together, our results indicate that RIM1α is redundant for basal neurotransmitter release and synaptic plasticity at the NMJ.

Materials and Methods

Mice

RIM1α KO mice (Schoch et al., 2002) were housed under a 12 h light / 12 h dark regime with *ad libitum* food and water. The animals were euthanized by CO_2 inhalation. Hemi-diaphragms with their phrenic nerves were rapidly dissected and mounted in Ringer's solution (see below) at room temperature.

All animal experiments were carried out according to the Dutch law and guidelines of the Leiden University.

Toxin-induced myasthenia gravis

We used an experimental animal model for myasthenia gravis that was originally developed in rats and is termed toxin-induced myasthenia gravis (TIMG) (Molenaar et al., 1991). The model involves repeated injections with α-bungarotoxin (Biotoxins Incorporated, FA, USA), a highly potent and selective blocker of AChRs at NMJs. We adjusted and re-evaluated the model for use with mice (data not shown). During

a period of four weeks, mice of about 4 months of age were injected intraperitoneally every 48 hour with α-bungarotoxin. Control groups received physiological saline injections. As a first dose, 1.2 μg α-bungarotoxin was injected. Thereafter, doses of 0.8 μg of the toxin were administered. Three hours after an injection the mice showed slightly invaginated flanks, indicating mild muscle weakness. There were no apparent breathing problems. In general, these symptoms had disappeared by the next, toxin-free, day. If the symptoms of weakness (scored visually in individual mice) were too severe, the following dose of α-bungarotoxin was lowered by 0.2 μg. The mice were well able to feed and drink.

Neuromuscular synapse electrophysiology

Measurements were performed on nerve/muscle preparations from right and left hemi-diaphragms of wild type and RIM1α KO mice. Upon electrical stimulation of the phrenic nerve, the nerve terminal releases a number of ACh quanta. Part of the transmitter binds postsynaptic AChRs and causes them to open. The resulting ion current gives rise to an endplate potential (EPP). Spontaneous release of single quanta results in miniature EPPs (MEPPs). We recorded EPPs and MEPPs by impaling muscle fibers near the NMJ with a 10-20 MΩ glass capillary microelectrode filled with 3 M KCl and standard recording equipment at 26-28° C (Plomp et al., 1994) in Ringer's medium containing (mM): NaCl, 116; KCl, 4.5; $MgCl_2$, 1; $CaCl_2$, 2; NaH_2PO_4, 1; $NaHCO_3$, 23; glucose 11; pH 7.4, gassed with 95 % O_2/5 % CO_2. Hemi-diaphragms were incubated with 3.1 μM μ-Conotoxin GIIIB (Scientific Marketing Associates, Herts, UK), a selective blocker of muscle sodium channels, to prevent action potentials. This allowed for the undisturbed recording of EPPs during electrical nerve stimulation (0.3 and 40 Hz) of the phrenic nerve with a bipolar stimulation electrode. The quantal content (i.e. the number ACh quanta released upon a single nerve impulse) at each NMJ was calculated from EPP and MEPP amplitudes, normalized to -75 mV membrane potential. The EPP amplitude was corrected for non-linear summation. During high-frequency stimulation (1 s, 40 Hz), EPP amplitudes have the tendency to decrease to a plateau level. The degree of run-down of EPP amplitudes was determined by averaging the amplitudes of the last 10 EPPs in the train and has been expressed as percentage of the amplitude of the first EPP in the train.

MEPPs were also recorded shortly after exposure of preparations to hypertonic medium (0.5 M sucrose Ringer), assessing the pool of ACh vesicles ready for immediate release (Stevens and Tsujimoto, 1995).

A GeneClamp 500B amplifier from Axon Instruments (Union City, CA, USA) was used for amplifying and filtering (10 kHz low-pass) of the signals. The recordings were digitized and analyzed using a Digidata 1200 interface, Clampex 8.0 and

Clampfit 8.0 programs (Axon Instruments) and routines programmed in Matlab (The MathWorks Inc., Natick, MA, USA).

Statistical analysis

The significance of differences in grand mean values between genotype groups were tested using Student's *t*-test, and differences in effect of TIMG treatment between genotypes was tested with the multivariate general linear model (interaction parameter) and the post-hoc Tukey test by using SPSS 10.0 for Windows (SPSS Inc., Chicago, IL, USA).

Results

Unaltered basic ACh release properties of RIM1α KO NMJs

To investigate whether deletion of RIM1α had an effect on transmitter release properties we analyzed basic NMJ function in RIM1α KO mice. It appeared that both spontaneous as well as evoked release parameters were indistinguishable between wild-type and KO mice (Figure 1, 2). EPP amplitudes were 26.8 ± 1.17 mV in wild-type NMJs, and 28.5 ± 2.0 mV in RIM1α KO NMJs (n = 6, p = 0.516). MEPP amplitudes were 1.02 ± 0.08 mV in wild-type NMJs and 1.02 ± 0.08 mV in RIM1α KO NJMs (n = 6, p = 0.769), MEPP frequency was 2.30 ± 0.24 MEPP s^{-1} in wild-type, and 2.53 ± 0.39 MEPPs s^{-1} in the RIM1α KO NMJs (n = 6, p = 0.736). In addition,

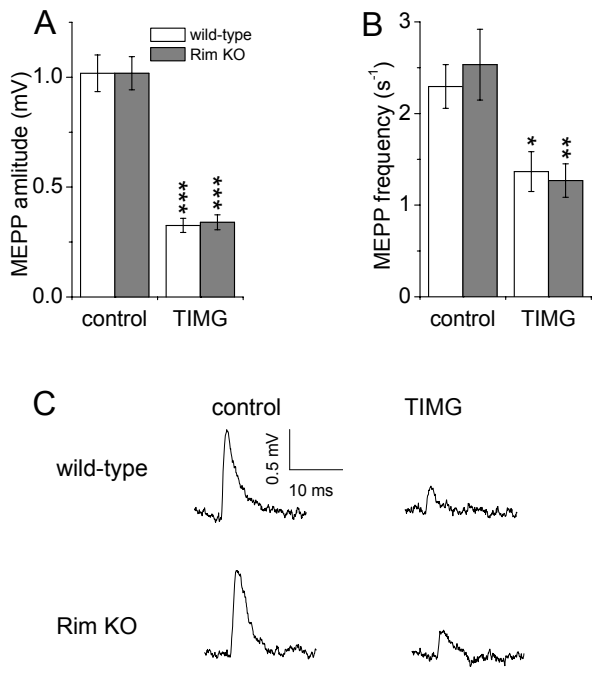

Figure 1. Spontaneous ACh release parameters are unchanged in RIM1α KO and wild-type NMJs.
(A) Mean values of MEPP amplitudes measured in wild-type and RIM1α KO NMJs (n = 6 mice, 10-15 NMJs measured per muscle). In TIMG, the MEPP amplitude was reduced equally (~ 70 %) in both genotypes (n = 7 wild-type mice, n = 8 RIM1α KO mice, 10-15 NMJs measured per muscle). (B) Mean values of MEPP frequency were similar in both genotypes and were similarly decreased in TIMG, presumably due to some loss MEPPs in background noise. (C) Representative examples of MEPPs for both genotypes under control and TIMG conditions.
Data is presented as means ± S.E.M.; * p< 0.05, ** p<0.01, and *** p<0.001, different from control, Student's *t*-test.

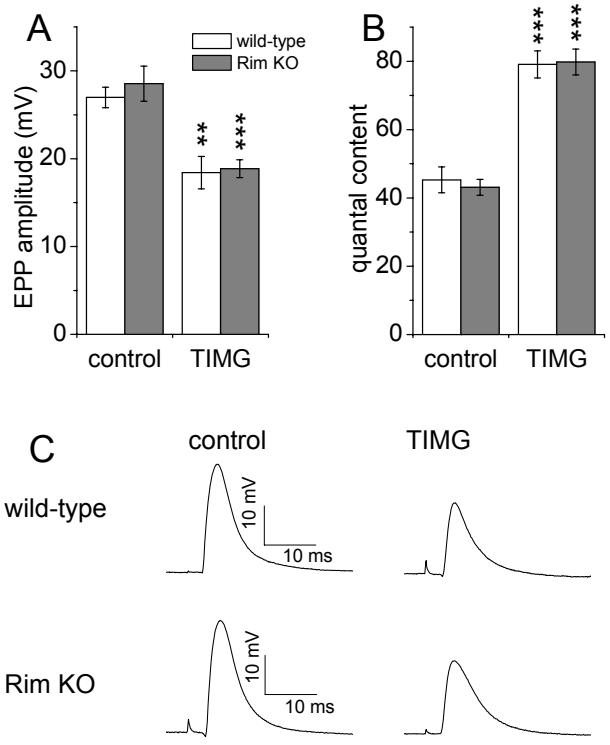

Figure 2 ACh release evoked by 0.3 Hz nerve stimulation is similar in both RIM1α KO and wild-type NMJs.
(A) Mean values of EPP amplitudes in both genotypes in the control and TIMG condition. TIMG treatment induced 32% reduction of the EPP amplitude in wild-type NMJs, and 34% in RIM1α KO NMJs (n = 6 wild-type control and RIM1α KO mice, n = 7 wild-type TIMG mice, n = 8 RIM1α KO mice, 10-15 NMJs measured per muscle). (B) Mean values of quantal content. In both genotypes, the quantal content was increased by ~80 %. (C) Representative examples of EPPs for both genotypes under control and TIMG conditions. Data is presented as means ± S.E.M.; * p< 0.05, ** p<0.01, and *** p<0.001, different from control, Student's *t*-test.

the run-down profiles of EPPs during high-frequency (40 Hz) stimulation were similar as well (Figure 3), 81.8 ± 1.05 %, compared to 82.05 ± 0.63 % in RIM1α KO NMJs (n = 6, p = 0.949). We also found no difference in the number of ready releasable vesicles tested by addition of 0.5 M sucrose solution (Figure 4), in wild-type NMJs 87.6 ± 12.2 MEPPs s^{-1} were recorded, against 75.43 ± 11.4 MEPPs s^{-1} in RIM1α KO NMJs (n = 6, p = 0.488).

Appropriate synaptic homeostasis at RIM1α KO NMJs

Next, we assessed whether RIM1α deficiency impedes or prevents the compensatory mechanism in the NMJ in response to a reduced postsynaptic sensitivity in the TIMG model. In both RIM1α KO as well as wild-type NMJs, the MEPP amplitude was decreased by 68% (Figure 1), to wild-type values of 0.33 ± 0.03 mV, and 0.34 ± 0.03 mV in RIM1α KO NMJs (n = 7 wild-type, n = 8 RIM1α KO mice, p = 0.769). The compensatory up-regulation of the quantal content was similar in both genotypes (Figure 2B), namely 175% of control wild-type NMJ values and 185% of control RIM1α KO values (wild-type 79.1 ± 3.4, n= 7, RIM1α 79.8 ± 3.8, n = 8, p = 0.535). The TIMG treatment caused a more pronounced run-down of EPP

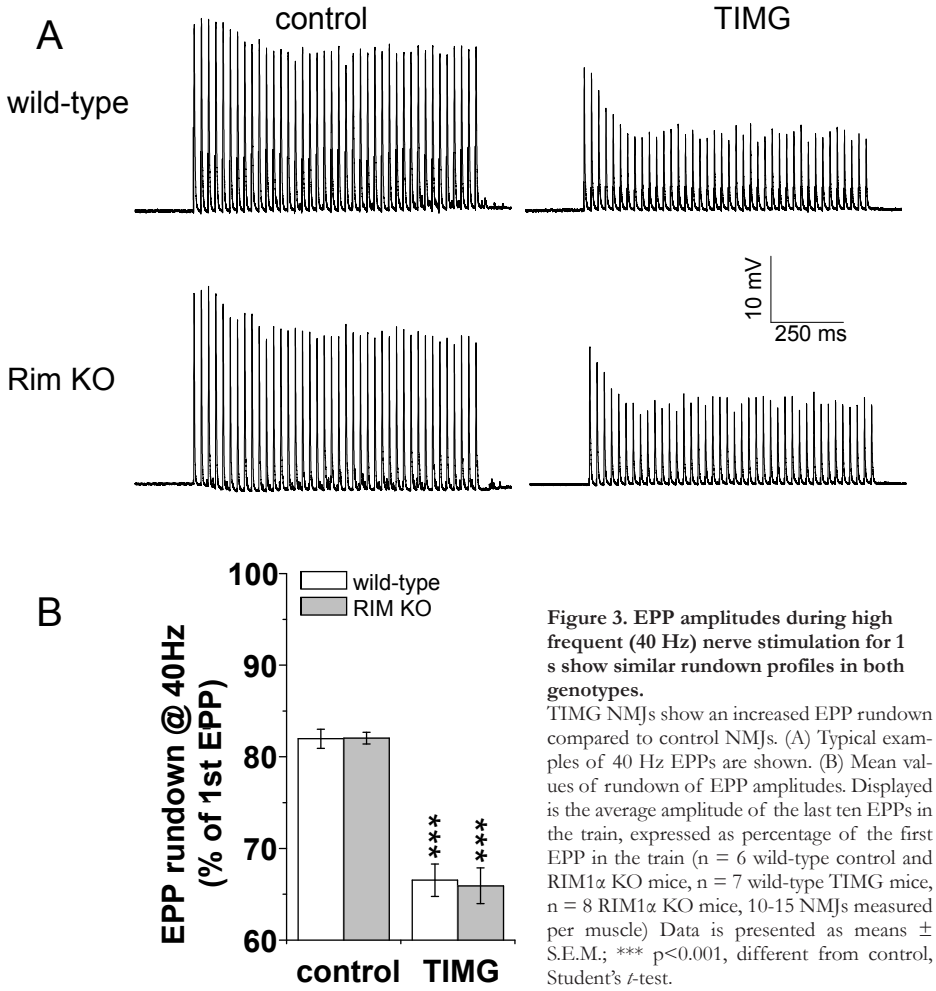

Figure 3. EPP amplitudes during high frequent (40 Hz) nerve stimulation for 1 s show similar rundown profiles in both genotypes.
TIMG NMJs show an increased EPP rundown compared to control NMJs. (A) Typical examples of 40 Hz EPPs are shown. (B) Mean values of rundown of EPP amplitudes. Displayed is the average amplitude of the last ten EPPs in the train, expressed as percentage of the first EPP in the train (n = 6 wild-type control and RIM1α KO mice, n = 7 wild-type TIMG mice, n = 8 RIM1α KO mice, 10-15 NMJs measured per muscle) Data is presented as means ± S.E.M.; *** $p<0.001$, different from control, Student's *t*-test.

amplitudes during high-frequent stimulation, which was comparable in both genotypes (Figure 3; rundown level of 66.5 ± 1.8 %, n = 7 in wild-type, and 65.9 ± 2.0 % in RIM1α KO, n = 8, p = 0.638). We probed for the number of readily releasable vesicles by application of sucrose solution, and found that the induction of TIMG had no statistically significant influence on the resulting increased MEPP frequency (88.7 ± 15 MEPPs s^{-1}, n = 5 in wild-type, and 73.3 ± 14.7 MEPPs s^{-1} in RIM1α KO NMJs, p = 0.492 (Figure 4). Summarizing, RIM1α KO mice do not show any defect in their NMJ functional properties, neither under basal nor TIMG conditions.

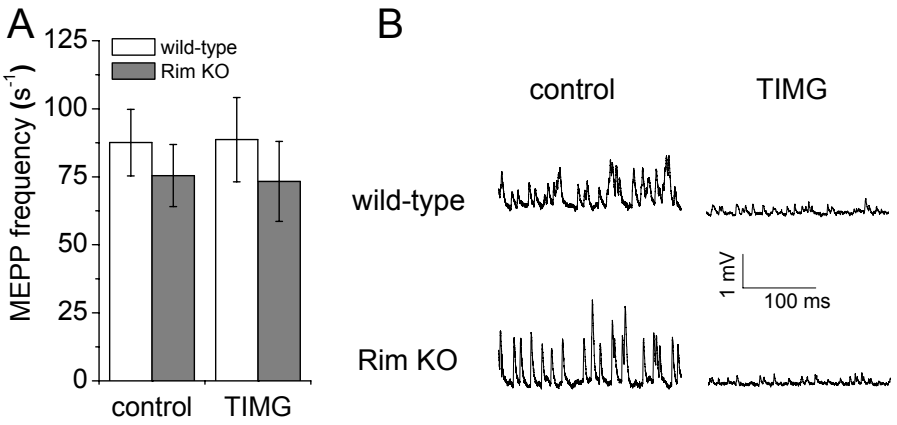

Figure 4. Unaltered size of the readily releasable synaptic vesicle pool.
(A) Mean values of MEPP frequency measured in the presence of hypertonic (0.5 M) sucrose-Ringer's medium (n = 5 wild-type control and RIM1α KO mice, n = 5 wild-type TIMG mice, n = 6 RIM1α KO mice, 10-15 NMJs measured per muscle). (B) Typical examples of 200 ms recordings of MEPPs measured in the presence of 0.5 M sucrose-Ringer's medium. Data is presented as means ± S.E.M.

Discussion

Our experiments performed on NMJs from mice lacking the active zone protein RIM1α did not reveal any synaptic defects. The ACh release evoked by either low- or high-rate electrical stimulation or hypertonic medium was not different from the wild-type control NMJs. Even when challenging the NMJ by subjection of the mice to a model of myasthenia gravis, which causes a compensatory up-regulation of transmitter release, no differences were observed between RIM1α KO NMJs and wild-type. This can be explained in two ways: 1) either RIM does not play a role in NMJ electrophysiology, or 2) the protein is redundant and its absence is functionally compensated for by the highly homologous RIM2α. The presence of RIM1α has been demonstrated in the diaphragm (personal communication, S. Schoch), leaving the latter explanation the most likely one. Indeed, a recent publication on the RIM1α/2α double KO (DKO) mouse (Schoch et al., 2006b) further supported the presumed redundancy of RIM1α in the NMJ. The RIM1α/2α DKO is, in contrast to mice KO for the single genes, not viable and dies immediately after birth due to respiration failure. Analysis of embryonic RIM1α/2α DKO NMJs in diaphragm showed that evoked neurotransmitter release was dramatically impaired. EPPs were 10-fold smaller and exhibited failures during repetitive stimulation. Spontaneous release was unaltered but was no longer calcium dependent. These data show that RIM1α and RIM2α are functionally redundant in the NMJ, thereby explaining the lack of effect we observed here in RIM1α KO NMJs.

NMJs from mice that were subjected to the TIMG model showed a similar response to application of hypertonic medium compared to control NMJs, indicating

that the pool of readily releasable vesicles was not changed in TIMG. This indicates that the compensatory increase of quantal content (by ~80 %) in TIMG is not achieved by increasing the readily releasable pool. The underlying mechanism is still unclear but may involve an increase in Ca^{2+} sensitivity of the release machinery.

The TIMG treatment clearly induced in both RIM1α KO and wild-type mice the phenomenon of compensatory increase of transmitter release at the NMJ. Although we were unable to demonstrate a role for RIM1α in this phenomenon of synaptic homeostasis, it is still likely that α-RIMs are involved since the protein has been implicated in synaptic plasticity in the CNS (Castillo et al., 2002; Schoch et al., 2002; Calakos et al., 2004). In view of this, it would be interesting to investigate NMJ function in mice that are homozygous null-mutant for RIM1α in combination and heterozygous RIM2α null-mutation (one single allele of RIM2 α), since these mice are viable but may be less well able to respond to decreased ACh sensitivity with a compensatory increase of presynaptic transmitter release at the NMJ.

References

Betz A, Thakur P, Junge HJ, Ashery U, Rhee JS, Scheuss V, Rosenmund C, Rettig J, Brose N (2001) Functional interaction of the active zone proteins Munc13-1 and RIM1 in synaptic vesicle priming. Neuron 30:183-196.

Calakos N, Schoch S, Sudhof TC, Malenka RC (2004) Multiple roles for the active zone protein RIM1alpha in late stages of neurotransmitter release. Neuron 42:889-896.

Castillo PE, Schoch S, Schmitz F, Sudhof TC, Malenka RC (2002) RIM1alpha is required for presynaptic long-term potentiation. Nature 415:327-330.

Dulubova I, Lou X, Lu J, Huryeva I, Alam A, Schneggenburger R, Sudhof TC, Rizo J (2005) A Munc13/RIM/Rab3 tripartite complex: from priming to plasticity? EMBO J 24:2839-2850.

Kiyonaka S, Wakamori M, Miki T, Uriu Y, Nonaka M, Bito H, Beedle AM, Mori E, Hara Y, De WM, Kanagawa M, Itakura M, Takahashi M, Campbell KP, Mori Y (2007) RIM1 confers sustained activity and neurotransmitter vesicle anchoring to presynaptic Ca2+ channels. Nat Neurosci 10:691-701.

Koushika SP, Richmond JE, Hadwiger G, Weimer RM, Jorgensen EM, Nonet ML (2001) A post-docking role for active zone protein Rim. Nat Neurosci 4:997-1005.

Lin RC, Scheller RH (2000) Mechanisms of synaptic vesicle exocytosis. Annu Rev Cell Dev Biol 16:19-49.

Lu J, Machius M, Dulubova I, Dai H, Sudhof TC, Tomchick DR, Rizo J (2006) Structural basis for a Munc13-1 homodimer to Munc13-1/RIM heterodimer switch. PLoS Biol 4:e192.

Molenaar PC, Oen BS, Plomp JJ, van Kempen GT, Jennekens FG, Hesselmans LF (1991) A non-immunogenic myasthenia gravis model and its application in a study of transsynaptic regulation at the neuromuscular junction. Eur J Pharmacol 196:93-101.

Plomp JJ, van Kempen GT, De Baets MB, Graus YM, Kuks JB, Molenaar PC (1995) Acetylcholine release in myasthenia gravis: regulation at single end-plate level. Ann Neurol 37:627-636.

Plomp JJ, van Kempen GT, Molenaar PC (1992) Adaptation of quantal content to decreased postsynaptic sensitivity at single endplates in alpha-bungarotoxin-treated rats. J Physiol 458:487-499.

Powell CM, Schoch S, Monteggia L, Barrot M, Matos MF, Feldmann N, Sudhof TC, Nestler EJ (2004) The presynaptic active zone protein RIM1alpha is critical for normal learning and memory. Neuron 42:143-153.

Schoch S, Castillo PE, Jo T, Mukherjee K, Geppert M, Wang Y, Schmitz F, Malenka RC, Sudhof TC (2002) RIM1alpha forms a protein scaffold for regulating neurotransmitter release at the active zone. Nature 415:321-326.

Schoch S, Mittelstaedt T, Kaeser PS, Padgett D, Feldmann N, Chevaleyre V, Castillo PE, Hammer RE, Han W, Schmitz F, Lin W, Sudhof TC (2006a) Redundant functions of RIM1alpha and RIM2alpha in Ca(2+)-triggered neurotransmitter release. EMBO J 25:5852-5863.

Schoch S, Mittelstaedt T, Kaeser PS, Padgett D, Feldmann N, Chevaleyre V, Castillo PE, Hammer RE, Han W, Schmitz F, Lin W, Sudhof TC (2006b) Redundant functions of RIM1alpha and RIM2alpha in Ca(2+)-triggered neurotransmitter release. EMBO J 25:5852-5863.

Stevens CF, Tsujimoto T (1995) Estimates for the pool size of releasable quanta at a single central synapse and for the time required to refill the pool. Proc Natl Acad Sci U S A 92:846-849.

Sudhof TC (2004) The synaptic vesicle cycle. Annu Rev Neurosci 27:509-547.

Sudhof TC, Rothman JE (2009) Membrane fusion: grappling with SNARE and SM proteins. Science 323:474-477.

Varoqueaux F, Sigler A, Rhee JS, Brose N, Enk C, Reim K, Rosenmund C (2002) Total arrest of spontaneous and evoked synaptic transmission but normal synaptogenesis in the absence of Munc13-mediated vesicle priming. Proc Natl Acad Sci U S A 99:9037-9042.

Varoqueaux F, Sons MS, Plomp JJ, Brose N (2005) Aberrant morphology and residual transmitter release at the Munc13-deficient mouse neuromuscular synapse. Mol Cell Biol 25:5973-5984.

Verhage M, Maia AS, Plomp JJ, Brussaard AB, Heeroma JH, Vermeer H, Toonen RF, Hammer RE, van den Berg TK, Missler M, Geuze HJ, Sudhof TC (2000)

Synaptic assembly of the brain in the absence of neurotransmitter secretion. Science 287:864-869.

Wang Y, Okamoto M, Schmitz F, Hofmann K, Sudhof TC (1997) Rim is a putative Rab3 effector in regulating synaptic-vesicle fusion. Nature 388:593-598.

Wang Y, Sudhof TC (2003) Genomic definition of RIM proteins: evolutionary amplification of a family of synaptic regulatory proteins(small star, filled). Genomics 81:126-137.

Wang Y, Sugita S, Sudhof TC (2000) The RIM/NIM family of neuronal C2 domain proteins. Interactions with Rab3 and a new class of Src homology 3 domain proteins. J Biol Chem 275:20033-20044.

Wong FK, Stanley EF (2010) Rab3a interacting molecule (RIM) and the tethering of pre-synaptic transmitter release site-associated $Ca_V2.2$ calcium channels. J Neurochem 112:463-473.

8

Summary and General Discussion

Aim

The aim of the studies described in this thesis was to elucidate the roles of several neuro-exocytotic proteins at the motor nerve terminal in neuromuscular synaptic transmission, making use of genetic knockout (KO) mice, each missing one (or more) neuro-exocytotic proteins. In addition, it was investigated in a pharmacological mouse model for myasthenia gravis (MG) whether some of these proteins play a role in the phenomenon of compensatory upregulation of acetylcholine (ACh) release at the neuromuscular junction (NMJ) in this disease.

This chapter briefly summarizes the major findings of this thesis and addresses some of the remaining questions. In addition, suggestions for future research are made.

Summary of experimental chapters

Chapter 2 describes the electrophysiological and morphological analysis of NMJs from mice lacking Munc13-1 and Munc13-2. Munc13 has been implicated in the priming of synaptic vesicles. In contrast to Munc13-1 and Munc13-2 single KOs, the double KO mice are not viable and die upon birth. Therefore, NMJs of these mice were investigated at embryonic day 18.5. Although evoked release was strongly reduced in the NMJ of Munc13-1/ 2 deficient mice, miniature endplate potentials (MEPPs, i.e. spontaneous ACh release) were observed at more than 2-fold higher frequency, compared to wild-type. This was surprising, because hippocampal synapses in these mice have been reported to be completely silenced. The current finding thus suggests that vesicle priming at the NMJ is partly Munc13 independent. Morphological analysis of the diaphragm showed a highly disorganized muscle fibre orientation and endplates that were no longer organized in the typical mid-line endplate-band as observed in wild-type diaphragms. This phenotype closely resembled that of the choline acetyltransferase KO mice (Brandon et al., 2003), at which NMJs are completely silenced, indicating that action potential evoked ACh release is necessary for normal muscle development. The current findings at Munc13-1/2 double KO mice indicate that the presence of spontaneous ACh release (MEPPs) alone is not sufficient for normal muscle development.

In **chapter 3**, the role of α-neurexins in the NMJ was investigated. There are three isoforms, α-neurexin 1, -2, and -3 (for review, see Missler and Sudhof, 1998). α-Neurexins are transmembrane proteins with an intracellular domain enabling interaction with components of the release machinery, and an extracellular domain that can participate in a transsynaptic protein complex. Deleting α-neurexins in mice results in strongly reduced neurotransmitter release in CNS (Missler et al., 2003). α-Neurexins presumably regulate release through interaction with the $Ca_v2.2$ and $Ca_v2.1$ voltage gated Ca^{2+} channels (Zhang et al., 2005). Mice lacking all three α-neurexin isoforms die at birth, but a subset of mice lacking two isoforms survives to adulthood. We used these mice to analyze NMJ function in two different muscle types (the slow-twitch fiber soleus muscle, and the diaphragm with a mixture of slow and fast twitch fibers). Neuromuscular synapse function in the soleus muscle was slightly impaired, showing a decrease in both MEPP frequency and quantal content of about 30%. In diaphragm NMJs, however, no effect was observed. To investigate the release characteristics of a NMJ without any α-neurexin present, we examined the embryonic diaphragm NMJ of triple KO mice and found undisturbed transmitter release, too. To determine a possible role of α-neurexins in synapse homeostasis, we investigated α-neurexin double KO mice under the condition of toxin-induced MG (TIMG), a model for MG using α-bungarotoxin. This condition normally results in ~2-fold upregulation of evoked ACh release at the NMJ, partially com-

pensating the reduced density of functional ACh receptors. Indeed, compensatory upregulation of quantal content at the α-neurexin double KO NMJ was much less pronounced than in the wild-type controls. These findings show that α-neurexins are important for efficient neurotransmitter release at some types of NMJs and that they play a role in the mechanism of synaptic homeostasis at NMJ under myasthenic condition.

Rab3A is one of a family of small GTP-binding proteins associated with synaptic vesicles, which have been implicated in modulating evoked neurotransmitter release in brain synapses (Fischer von Mollard et al., 1991; Geppert et al., 1994; Fischer et al., 1994; Star et al., 2005). Compound KO mice for Rab3A, Rab3B, Rab3C, and Rab3D are not viable (Schluter et al., 2004). **Chapter 4** describes the NMJ function in soleus and diaphragm of Rab3A deficient mice. We found 20-40% reduction in spontaneous ACh release (MEPP frequency) but unaltered nerve action potential-evoked release and recovery from release induced by high-frequent stimulation. This indicates a selective role of Rab3A in spontaneous transmitter release at the NMJ that cannot or only partially be taken over by the closely related Rab3B, -C, or -D isoforms. It has been hypothesized that Rab3A mutation underlies ACh release deficits in human presynaptic myasthenic syndromes. Our observation of a normal level of evoked ACh release at the Rab3A KO NMJ, however, argues against this hypothesis.

Chapter 5 describes the effect of varying Munc18-1 protein levels in cultures of hippocampal neurons and the NMJ. Munc18-1 is the only protein described in this thesis whose deletion is lethal and causes a total arrest of neurotransmitter release in CNS and PNS (Verhage et al., 2000). Heterozygous Munc18-1 KO ($Munc18^{+/-}$) mice are viable and have a 50% reduction of Munc18-1 protein level in the brain, making them a suitable model to study the effect of decreased Munc18-1 level. In addition, the effect of increased level of the protein on exocytosis was studied in Munc18-1 overexpressing mouse ($Munc18^{OE}$) and in hippocampal cell cultures overexpressing the protein after viral transfection.

NMJ function was analyzed in wild-type mice, $Munc18^{+/-}$, and $Munc18^{OE}$ mice. A clear 'gene-dosage' effect of Munc18-1 was observed on MEPP frequency and quantal content. In $Munc18^{+/-}$ NMJs, increased run-down of ACh release upon high-frequency stimulation was observed as well, and a decreased response to a hypertonic shock, used to probe for the size of the readily releasable pool of synaptic vesicles. Electrophysiological synaptic analysis of hippocampal neuron cultures from $Munc18\text{-}1^{+/-}$ mice showed a similar increased run-down of transmitter release during high-frequency stimulation and decreased response to hypertonic stimulation. Viral overexpression of Munc18-1 in these cultured hipocampal synapses, on the other hand, increased the response to hypertonic shock and resulted in less pronounced run-down during high-frequency stimulation. Electron microscopic analy-

sis showed a clear difference in the number of morphologically docked vesicles. These data led to the conclusion that Munc18-1 is involved in modulating the number of docked, release-ready synaptic vesicles at nerve terminals.

Chapter 6 describes a study where Munc18-1^{OE}, Munc18-1$^{+/-}$, and wild-type mice were subjected to the TIMG model. It appeared that Munc18-1$^{+/-}$ NMJs were less able to increase the quantal content than wild-type NMJs. Overexpression of Munc18-1 on the other hand failed to increase the compensatory response. These results indicate that Munc18-1 is involved in the signaling cascade leading to increased quantal content in TIMG but that other factors may become rate-limiting in the Munc18-1^{OE} NMJ.

RIM1α is a known binding partner of Rab3A (Wang et al., 2000) and has been suggested to play a role in synaptic vesicle priming. Mice in which RIM1α is deleted are viable and show minor behavioral defects (Castillo et al., 2002; Schoch et al., 2002; Powell et al., 2004; Calakos et al., 2004). **Chapter 7** describes that deleting RIM1α in mice does not affect NMJ function, neither under basal conditions, nor in the condition of TIMG. Most likely, RIM1α is redundant and RIM2α assumes its function. Indeed, recent data show that RIM1α/2α double KO mice (Schoch et al., 2006) die upon birth and their embryonic NMJs show strongly impaired evoked ACh release.

Phenotypic differences between central and neuromuscular synapses of neuro-exocytotic protein knockout mice

This thesis has contributed to the knowledge on the role of Munc18-1, Munc13s, Rab3A, Neurexins and RIM1α in neuromuscular synaptic transmission. When comparing the function of these proteins in NMJ and CNS, it is interesting that usually the synaptic phenotype in the NMJ is much milder compared to that in synapses of the CNS. The strongest example is Munc13, deletion of which results in complete ablation of neurotransmitter release in CNS (Varoqueaux et al., 2002) while the NMJ still exhibits MEPPs and even, to some extent, retains nerve-stimulated release. Deleting Rab3A and α-neurexin also has a much milder effect on release properties of the NMJ compared to CNS, while deleting RIM1α failed to elicit any effect. For Munc18-1, the overall similarity between CNS and NMJ phenotype was the strongest. Munc18-1 is the only protein among the ones investigated here whose deletion in mice results in lethality; the two remaining isoforms are apparently not able to take over its functions. Thus, Munc18-1 is essential for neurotransmission at the NMJ, while the other proteins fulfill a more regulatory function, or can be compensated for by isoforms or other proteins.

The NMJ is different from synapses in the CNS both in function and morphology, and therefore it may not be surprising that this is reflected in the molecular organization of the secretion machinery. In contrast to CNS synapses, the post-

synaptic cell is not another neuron, the number of vesicles that is released in an action potential dependent manner is much higher (diaphragm NMJ: around 30; CNS synapses: around 3), the probability of release in the NMJ is approximately 100% and there is only one type of neurotransmitter. In addition, although plasticity is employed to ensure successful muscle contraction, plasticity in the CNS plays a much more crucial role and forms the basis of many of the brain's functions like learning and memory. Concluding, the role of a certain protein in the process of secretion is depending on the cellular context in which it is exerting its role.

Role of the studied neuro-exocytotic proteins in synaptic homeostasis and relevance to myasthenia gravis

One of the goals of this thesis was to investigate the role of specific presynaptic proteins in the homeostatic upregulation of ACh release as observed in NMJs of muscle biopsies from MG patients, by applying the TIMG model in mice genetically lacking these proteins. The phenomenon of compensatory increase of transmitter release has been described in several other experimental systems (see Introduction). The decreased sensitivity to ACh due to a lowered density of postsynaptic ACh receptors leads via a largely unknown mechanism to increased ACh release from the presynaptic nerve terminal. Proteins that are playing a role in transmitter release are likely targets of this signaling mechanism. We investigated the effect of deleting Munc18-1, Neurexins and RIM1α on the homeostatic response at the myasthenic NMJ.

Munc18-1

In NMJs with only 50% Munc18-1 expression level, the compensatory response in TIMG was less pronounced arguing for the implication of this protein somewhere in the signaling pathway. Munc18-1 has been implied in regulating the readily releasable pool of vesicles, which may be the mechanism of increase of ACh release in TIMG. However, when we exposed NMJs from TIMG muscles to high-sucrose medium to probe for the size of the pool we failed to see an increase, rendering it unlikely that it is this specific function of Munc18-1 that is modulated for increase in ACh release. This raises the possibility that instead of being an active player in the signaling cascade, Munc18-1 is present in rate-limiting amounts in the strained exocytotic machinery in NMJs of Munc18-1 heterozygous mice. In line with this, increasing Munc18-1 levels in NMJs had no effect on the homeostatic performance of the synapse under TIMG conditions.

a-Neurexins

Mice lacking two of the three isoforms of α-neurexin showed impaired upregulation of transmitter release at the TIMG NMJ. Interestingly, diaphragm NMJs from

neurexin double KO mice did not differ in ACh release characteristics from wild-type under basal conditions. Even the release properties of NMJs from (embryonic) mice lacking all three isoforms of neurexin were unchanged, indicating that this protein is not involved in basic neurotransmitter exocytosis at the NMJ. The decreased upregulation observed in TIMG neurexin double KO NMJs thus indicates that neurexin is specifically involved in plasticity of the diaphragm NMJ, possibly quite far upstream the exocytotic processes, because neurexin has been suggested to participate in trans-cellular signaling processes. Alternatively, neurexin's role in the homeostatic response may lay in modulation of the coupling of calcium channels with the exocytotic machinery, as observed in central synapses.

RIM1a

Although we did not observe functional changes in NMJs lacking RIM1α (neither under basal nor TIMG conditions) we cannot exclude a role of RIM proteins in homeostasis at the NMJ, because RIM1/2α double KO mice have impaired ACh release at the NMJ, and die perinatally (Schoch et al., 2006). This indicates that Rim2α takes on the role of RIM1α in the RIM1α KO mouse. To further investigate RIM protein involved in synaptic homeostasis at the NMJ, it would be interesting to apply the TIMG model on mice homozygous for RIM1α and heterozygous for RIM2α.

One can wonder whether it is possible to really pinpoint essential factors in the signaling cascade that leads to increased neurotransmitter release in TIMG NMJs. Homeostatic processes are crucial to the survival of the organism, and it is not unthinkable that evolution has produced many parallel pathways and players to ensure NMJ transmission.

The clinical relevance for MG of this rather fundamental neurobiological study is yet unclear. It may be that myasthenic patients exist with a certain polymorphism/splice variant for munc18-1 or neurexin, causing them to have less compensatory upregulation of transmitter release. These patients may have more severe paralytic symptoms. More research into the details of pathways leading to the NMJ's ability to counteract threats to signal transmission may be beneficial for many more diseases in which successful neurotransmission is compromised, like Lambert Eaton myasthenic syndrome and congenital myasthenic syndromes (see for review Boonyapisit et al., 1999). Furthermore, such studies may reveal new pharmacological targets that may be exploited to increase ACh release to overcome or prevent block of neuromuscular transmission.

Considerations on the use of knockout mice

Experiments described in this thesis have been carried out on genetically modified mice (mostly KO mice, and one mouse overexpressing the Munc18-1 gene). Careful

consideration of genetic background, compensatory mechanisms, homeostasis, and developmental differences is necessary when characterizing synaptic transmission in genetically engineered animals.

It is known that genes fulfill different roles during development (in utero and postnatally) and in adulthood (e.g. the dependence of NMJ synaptic transmission on different types of Ca^{2+} channels (Urbano et al., 2003)).

Developmental changes due to the absence of the gene of interest may in itself cause (subtle) changes in the mechanism of synaptic homeostasis. Further activation of synaptic homeostatic mechanisms by the TIMG treatment might show an abnormal result, what could be attributed to a direct functional consequence of the absence of the KO-gene product. However, the mechism of synaptic homeostatis might already have been altered in itself.

Furthermore, the genetic background of the mouse strain can significantly alter a neurological or musculoskeletal phenotype of transgenic animals (Yoshiki and Moriwaki, 2006). For instance, the genetic background alters the outcome of anxiety related tasks, likely due to changes in GABAergic transmission (Robertson, 1979; Chapouthier et al., 1991; Griebel et al., 2000; Rodgers et al., 2002). Genetically deleting proteins participating in synaptic transmission may also have different effects depending on the genetic background of the mouse, as demonstrated with the serotonin-transporter (Holmes et al., 2002; Holmes et al., 2003) and serotonin receptor 5-HT1A deletions (Lesch et al., 2003), when expressed in different inbred mouse strains.

Alternatives for conventional knockout mice

In the studies of this thesis, 'first generation' knockout mice were used, generated by gene targeting through homologous recombination (Capecchi, 1989). One of the disadvantages of this technique is that the gene is deleted in every cell and throughout the development and lifetime of the mouse, as described above. New techniques have become available that enable temporal and spatial control of genetic manipulations: the Cre/LoxP recombinase system (Tsien et al., 1996a; Tsien et al., 1996b), and the tetracycline-inducible system (Gossen and Bujard, 1992; Furth et al., 1994). The Cre-LoxP system uses mice with LoxP sites flanking the gene of interest (floxed mice), which are bred with transgenic mice expressing Cre recombinase under the control of a selected promoter (Cre mice). Once expressed, Cre recombines the floxed gene and produces gene KO (reviewed in Gaveriaux-Ruff and Kieffer, 2007). In this system, the choice of the promoter determines the time and location of Cre expression. One possibly underestimated worry is the potential cellular toxicity of Cre recombinase (Schmidt-Supprian and Rajewsky, 2007). The tetracycline-inducible system is similar to the Cre-LoxP in that both systems make

use of homologous recombination and embryonic stem cells, and both require the generation of two sets of transgenic mice.

Another, fundamentally different approach is RNA interference (RNAi), which can selectively down-regulate gene expression (reviewed in Gao and Zhang, 2007). The silencing of a gene is accomplished posttranscriptionally. Due to variation in the degree of silencing, the term 'knock-down' has been introduced. The method has been used in cell cultures and whole organisms, and the methods of delivery can be as simple as feeding double stranded RNA to worms (Kamath and Ahringer, 2003), and by injecting RNA constructs into pronuclei. Moreover, stable RNAi knock-down mouse have been engineered (Peng et al., 2006) although it is yet to be confirmed that the transgenic RNAi effect is permanent (Gao and Zhang, 2007). One drawback of the RNAi method is that there may be residual expression of RNAi-targeted genes. In addition, there is a difference in the competency of cells to carry out RNAi (Gao and Zhang, 2007).

RNAi has been successfully used in mammalian muscle tissue by Kong and coworkers (Kong et al., 2004), decreasing the levels of MuSK and rapsyn. However, to my knowledge, the method has not been used to target presynaptic proteins in the NMJ as the the small size of the nerve terminal precludes RNAi injection.

Outlook

Future research on elucidating the roles of synaptic proteins in the mammalian NMJ certainly will most likely involve the further analysis of the still growing number of KO mice, both conventional and inducible, like described above. Subjecting these animals to TIMG will help to gain insight into the mechanism of homeostatic increase of transmitter release. It would be very helpful to induce gene KO after establishment of the TIMG situation, to avoid pre-existing homeostatic mechanisms counteracting the effects of the protein's absence.

A publication by Das and coworkers described a co-culture of vertebrate embryonic motoneuron and skeletal muscle cells, which formed neuromuscular synapses (Das et al., 2007). Although the functional aspects of these synapses were not described in much detail in this paper, it may be interesting to use such a system to induce TIMG. This may allow for a controlled, ex vivo experimental set-up in which blockers can be used to investigate the homeostatic signaling cascade in detail.

RNAi sounds like a promising method as soon as it possible to knock down genes in the nerve ending, although this method is only useful for genes that are expressed locally.

References

Boonyapisit K, Kaminski HJ, Ruff RL (1999) Disorders of neuromuscular junction ion channels. Am J Med 106: 97-113.

Brandon EP, Lin W, D'Amour KA, Pizzo DP, Dominguez B, Sugiura Y, Thode S, Ko CP, Thal LJ, Gage FH, Lee KF (2003) Aberrant patterning of neuromuscular synapses in choline acetyltransferase-deficient mice. J Neurosci 23: 539-549.

Calakos N, Schoch S, Sudhof TC, Malenka RC (2004) Multiple roles for the active zone protein RIM1alpha in late stages of neurotransmitter release. Neuron 42: 889-896.

Capecchi MR (1989) Altering the genome by homologous recombination. Science 244: 1288-1292.

Castillo PE, Schoch S, Schmitz F, Sudhof TC, Malenka RC (2002) RIM1alpha is required for presynaptic long-term potentiation. Nature 415: 327-330.

Chapouthier G, Bondoux D, Martin B, Desforges C, Launay JM (1991) Genetic difference in sensitivity to beta-carboline: evidence for the involvement of brain benzodiazepine receptors. Brain Res 553: 342-346.

Das M, Rumsey JW, Gregory CA, Bhargava N, Kang JF, Molnar P, Riedel L, Guo X, Hickman JJ (2007) Embryonic motoneuron-skeletal muscle co-culture in a defined system. Neuroscience 146: 481-488.

Fischer von Mollard G, Sudhof TC, Jahn R (1991) A small GTP-binding protein dissociates from synaptic vesicles during exocytosis. Nature 349: 79-81.

Fischer vM, Stahl B, Khokhlatchev A, Sudhof TC, Jahn R (1994) Rab3C is a synaptic vesicle protein that dissociates from synaptic vesicles after stimulation of exocytosis. J Biol Chem 269: 10971-10974.

Furth PA, St Onge L, Boger H, Gruss P, Gossen M, Kistner A, Bujard H, Hennighausen L (1994) Temporal control of gene expression in transgenic mice by a tetracycline-responsive promoter. Proc Natl Acad Sci U S A 91: 9302-9306.

Gao X, Zhang P (2007) Transgenic RNA interference in mice. Physiology (Bethesda) 22: 161-166.

Gaveriaux-Ruff C, Kieffer BL (2007) Conditional gene targeting in the mouse nervous system: Insights into brain function and diseases. Pharmacol Ther 113: 619-634.

Geppert M, Bolshakov VY, Siegelbaum SA, Takei K, De Camilli P, Hammer RE, Sudhof TC (1994) The role of Rab3A in neurotransmitter release. Nature 369: 493-497.

Gossen M, Bujard H (1992) Tight control of gene expression in mammalian cells by tetracycline-responsive promoters. Proc Natl Acad Sci U S A 89: 5547-5551.

Griebel G, Belzung C, Perrault G, Sanger DJ (2000) Differences in anxiety-related behaviours and in sensitivity to diazepam in inbred and outbred strains of mice. Psychopharmacology (Berl) 148: 164-170.

Holmes A, Lit Q, Murphy DL, Gold E, Crawley JN (2003) Abnormal anxiety-related behavior in serotonin transporter null mutant mice: the influence of genetic background. Genes Brain Behav 2: 365-380.

Holmes A, Yang RJ, Murphy DL, Crawley JN (2002) Evaluation of antidepressant-related behavioral responses in mice lacking the serotonin transporter. Neuropsychopharmacology 27: 914-923.

Kamath RS, Ahringer J (2003) Genome-wide RNAi screening in *Caenorhabditis elegans*. Methods 30: 313-321.

Kong XC, Barzaghi P, Ruegg MA (2004) Inhibition of synapse assembly in mammalian muscle in vivo by RNA interference. EMBO Rep 5: 183-188.

Lesch KP, Zeng Y, Reif A, Gutknecht L (2003) Anxiety-related traits in mice with modified genes of the serotonergic pathway. Eur J Pharmacol 480: 185-204.

Missler M, Sudhof TC (1998) Neurexins: three genes and 1001 products. Trends Genet 14: 20-26.

Missler M, Zhang W, Rohlmann A, Kattenstroth G, Hammer RE, Gottmann K, Sudhof TC (2003) Alpha-neurexins couple Ca^{2+} channels to synaptic vesicle exocytosis. Nature 424: 939-948.

Peng S, York JP, Zhang P (2006) A transgenic approach for RNA interference-based genetic screening in mice. Proc Natl Acad Sci U S A 103: 2252-2256.

Powell CM, Schoch S, Monteggia L, Barrot M, Matos MF, Feldmann N, Sudhof TC, Nestler EJ (2004) The presynaptic active zone protein RIM1alpha is critical for normal learning and memory. Neuron 42: 143-153.

Robertson HA (1979) Benzodiazepine receptors in "emotional" and "non-emotional" mice; comparison of four strains. Eur J Pharmacol 56: 163-166.

Rodgers RJ, Davies B, Shore R (2002) Absence of anxiolytic response to chlordiazepoxide in two common background strains exposed to the elevated plus-maze: importance and implications of behavioural baseline. Genes Brain Behav 1: 242-251.

Schluter OM, Schmitz F, Jahn R, Rosenmund C, Sudhof TC (2004) A complete genetic analysis of neuronal Rab3 function. J Neurosci 24: 6629-6637.

Schmidt-Supprian M, Rajewsky K (2007) Vagaries of conditional gene targeting. Nat Immunol 8: 665-668.

Schoch S, Castillo PE, Jo T, Mukherjee K, Geppert M, Wang Y, Schmitz F, Malenka RC, Sudhof TC (2002) RIM1alpha forms a protein scaffold for regulating neurotransmitter release at the active zone. Nature 415: 321-326.

Schoch S, Mittelstaedt T, Kaeser PS, Padgett D, Feldmann N, Chevaleyre V, Castillo PE, Hammer RE, Han W, Schmitz F, Lin W, Sudhof TC (2006) Redundant functions of RIM1alpha and RIM2alpha in Ca(2+)-triggered neurotransmitter release. EMBO J 25: 5852-5863.

Star EN, Newton AJ, Murthy VN (2005) Real-time imaging of Rab3a and Rab5a reveals differential roles in presynaptic function. J Physiol 569: 103-117.

Tsien JZ, Chen DF, Gerber D, Tom C, Mercer EH, Anderson DJ, Mayford M, Kandel ER, Tonegawa S (1996a) Subregion- and cell type-restricted gene knockout in mouse brain. Cell 87: 1317-1326.

Tsien JZ, Huerta PT, Tonegawa S (1996b) The essential role of hippocampal CA1 NMDA receptor-dependent synaptic plasticity in spatial memory. Cell 87: 1327-1338.

Urbano FJ, Piedras-Renteria ES, Jun K, Shin HS, Uchitel OD, Tsien RW (2003) Altered properties of quantal neurotransmitter release at endplates of mice lacking P/Q-type Ca^{2+} channels. Proc Natl Acad Sci U S A 100: 3491-3496.

Varoqueaux F, Sigler A, Rhee JS, Brose N, Enk C, Reim K, Rosenmund C (2002) Total arrest of spontaneous and evoked synaptic transmission but normal synaptogenesis in the absence of Munc13-mediated vesicle priming. Proc Natl Acad Sci U S A 99: 9037-9042.

Verhage M, Maia AS, Plomp JJ, Brussaard AB, Heeroma JH, Vermeer H, Toonen RF, Hammer RE, van den Berg TK, Missler M, Geuze HJ, Sudhof TC (2000) Synaptic assembly of the brain in the absence of neurotransmitter secretion. Science 287: 864-869.

Wang Y, Sugita S, Sudhof TC (2000) The RIM/NIM family of neuronal C2 domain proteins. Interactions with Rab3 and a new class of Src homology 3 domain proteins. J Biol Chem 275: 20033-20044.

Yoshiki A, Moriwaki K (2006) Mouse phenome research: implications of genetic background. ILAR J 47: 94-102.

Zhang W, Rohlmann A, Sargsyan V, Aramuni G, Hammer RE, Sudhof TC, Missler M (2005) Extracellular domains of alpha-neurexins participate in regulating synaptic transmission by selectively affecting N- and P/Q-type Ca^{2+} channels. J Neurosci 25: 4330-4342.

Samenvatting

Michèle S. Sons

Roles of neuro-exocytotic proteins at the neuromuscular junction

Dit proefschrift heeft als vraagstelling wat de rol van een aantal specifieke eiwitten is bij de afgifte van neurotransmitter in de neuromusculaire junctie (NMJ). Tevens is voor een aantal van deze eiwitten onderzocht of ze een rol spelen in het fenomeen van compensatoire verhoging van neurotransmitter afgifte zoals dat waargenomen wordt in de NMJs van patiënten met de spierziekte myasthenia gravis (MG).

Neuromusculaire junctie

De NMJ vormt het contact tussen de spiervezel en het motorneuron. Het uiteinde van de zenuw maakt hier nauw contact met de spier. De elektrische prikkel die vanuit het cellichaam van het neuron in het ruggenmerg naar het zenuwuiteinde is gereisd, wordt hier overgedragen naar de spiervezel waarna via een aantal stappen de vezel contraheert en er beweging tot stand komt.

Exocytose

In het zenuwuiteinde bevinden zich blaasjes, gevuld met acetylcholine (in het geval van skeletspieren van zoogdieren). Acetylcholine (ACh) is een zgn. neurotransmitter, een stof die gebruikt wordt bij de overdracht van prikkels binnen het zenuwstelsel. Op het moment dat een elektrische prikkel het zenuwuiteinde bereikt, wordt dit waargenomen door calciumdoorlaatbare kanalen in het celmembraan. Deze kanalen gaan kortstondig open, waardoor calcium de cel binnenstroomt. Dit calciumsignaal resulteert via aan aantal stappen in de fusie van een aantal van tevoren klaargelegde synaptische blaasjes met het celmembraan. Hierdoor wordt acetylcholine afgegeven aan de extracellulaire ruimte. De spiercel heeft op de plek van de NMJ ACh receptoren (AChR) in het celmembraan, dit zijn ionkanalen die uitsluitend openen wanneer acetylcholine zich bindt aan het kanaal. Tijdens de korte opening van de AChR loopt er een netto positieve stroom, waardoor de membraanpotentiaal stijgt. Wanneer deze potentiaal een drempel overschrijdt, gaan voltageafhankelijke natriumkanalen in de spiercel open en stijgt de membraanpotentiaal nog verder. Deze potentiaalverandering wordt de 'spier actiepotentiaal' genoemd. Een spier actiepotentiaal leidt tot de opening van voltageafhankelijke calciumkanalen in het membraan van de spiervezel, waarop calciumionen de cel binnenstromen. Deze calcium instroom resulteert in bulk calcium afgifte uit het sarcoplasmatisch reticulum (een onderdeel van de cel), dit zorgt voor contractie van de spiervezel en dus voor de mogelijkheid tot beweging. Naast de hierboven beschreven gestimuleerde afgifte waarbij een aantal blaasjes tegelijkertijd fuseert met het plasmamembraan bestaat spontane afgifte, waarbij ongeveer één keer per seconde één blaasje fuseert met het membraan (afhankelijk van diersoort en spiertype).

Myasthenia gravis

MG is een autoimmuun ziekte. 20-500 op de miljoen mensen krijgen MG, waarbij er in het bloed van de patiënt antilichamen tegen de AChR aangetroffen worden. De ziekte kenmerkt zich door spierzwakte die verergert na inspanning. Tegenwoordig zijn er behandelingen waardoor de ziekte onder controle gehouden kan worden.

Wanneer een spiermonster van een patiënt met MG met behulp van elektrofysiologische technieken (zie hieronder) onderzocht wordt, ziet men dat de gevoeligheid voor ACh van het postsynaptische element sterk verminderd is. Eén van de oorzaken hiervan is dat er, na binding van de auto-antilichamen tegen de AChR een immuunsysteem-aanval op de cel plaatsvindt, waardoor deze cel schade oploopt. Er is gebleken dat de zenuwcel probeert te compenseren voor de verminderde gevoeligheid van ACh van de spiercel, door de afgifte van meer blaasjes ACh dan normaal. Deze (gedeeltelijke) compensatie van het systeem zorgt ervoor dat de drempel van de spier actiepotentiaal iets beter gehaald wordt, maar de zenuwcel houdt het niet lang vol om veel meer blaasjes dan normaal af te geven. Na inspanning neemt de spierzwakte dus sneller toe.

Het fenomeen van de compensatie van neurotransmitterafgifte is heel interessant. De postsynaptische cel geeft kennelijk feedback aan de presynaptische cel over de mate waarin de signaalstofafgifte effectief is, waarop de presynaptische cel het aantal blaasjes met neurotransmitter aanpast aan de gevoeligheid van de postsynaptische cel. Deze feedback wordt 'retrograde signalering' genoemd ('retro' aangezien de postsynaptische cel de presynaptische cel informeert). Waaruit dit signaal precies bestaat is in dit specifieke geval niet bekend, net zo goed als niet bekend is via welke route de toename van neurotransmitterafgifte tot stand komt. Wanneer dit mechanisme opgehelderd wordt, kan dit potentieel belangrijk zijn voor klinisch onderzoek. Voor ziekten waarbij een toename van synaptische 'kracht' wenselijk is (bijvoorbeeld bij spierzwakte) zouden farmaca die een dergelijk mechanisme kunnen stimuleren een onderdeel van de behandeling kunnen uitmaken.

Om het fenomeen van synaptische compensatie zoals gezien in spierbiopten van patiënten met MG te onderzoeken zijn verschillende diermodellen ontwikkeld. Eén model bestaat uit het herhaaldelijk injecteren van muizen met het toxine α-Bungarotoxine (toxin-induced myasthenia gravis, TIMG). Dit toxine wordt opgezuiverd uit het gif van de 'banded krait', een dodelijk giftige slang die o.a. in China en Thailand voorkomt. Het gif bindt specifiek aan de AChR en blokkeert deze. Herhaaldelijk injecteren zorgt ervoor dat een deel van de receptoren in de NMJ van de muizen geblokkeerd wordt. Hiermee wordt het effect dat de antilichamen tegen de ACh in MG patiënten teweeg brengen nagebootst.

Elektrofysiologie

Door gebruik te maken van elektrofysiologische technieken kan het proces van neurotransmitterafgifte in de NMJ onderzocht worden. Voor de experimenten die beschreven staan in dit proefschrift is voornamelijk gebruik gemaakt van een preparaat van het middenrif met de bijbehorende phrenische zenuw. Het preparaat wordt daarbij vastgezet in een schaaltje met fysiologische zoutoplossing en in de opstelling gebracht. Een glaselektrode met een zeer fijn uiteinde (gekoppeld aan een versterker) wordt in de spiervezel gebracht ter hoogte van de NMJ, hiermee wordt de membraanpotentiaal geregistreerd (normaal ligt deze rond de -75 mV). Spontane afgifte van een blaasje met neurotransmitter wordt gezien als een kleine piek met een amplitude van ongeveer 1 mV, de miniatuur eindplaat potentiaal (MEPP). Wanneer de zenuw gestimuleerd wordt fuseren meerdere blaasjes, het signaal dat dit tot gevolg heeft heet de eindplaatpotentiaal (EPP). Normaal gesproken leidt een EPP direct tot een spieractiepotentiaal en dus tot contractie van de spier, dit is niet wenselijk aangezien contractie de meting ernstig verstoort. Door toediening van een specifiek toxine (μ-conotoxine) worden de voltagegevoelige natriumkanalen geblokkeerd en zodoende treedt er geen spieractiepotentiaal en dus contractie op. De EPP bestaat uit de sommatie van MEPPs, wanneer de amplitude van de EPP gedeeld wordt door de amplitude van de MEPP binnen één eindplaat wordt de 'quantal content' verkregen. Dit is het aantal afgegeven blaasjes per zenuwstimulatie. Voor uit uitvoeren van deze berekening worden de amplitudes eerst genormaliseerd naar -75 mV en wordt er gecorrigeerd voor de niet-lineaire sommatie van MEPPs.

Door het bepalen van de EPP amplitude, de MEPP amplitude, de 'quantal content', de frequentie van de MEPPs en nog andere waarden kunnen uitspraken worden gedaan over het functioneren van de NMJ. Wanneer bijvoorbeeld NMJs van muizen die een TIMG behandeling hebben ondergaan geanalyseerd worden, ziet men hele kleine MEPPs. Wanneer de 'quantal content' berekend wordt van deze NMJs ligt deze rond de 100, terwijl in controle dieren de waarde rond de 30 ligt.

Synaptische eiwitten

Het fusieproces van de blaasjes met acetylcholine is complex. Het is van groot belang dat dit strak geregisseerd wordt, er moet op de juiste tijd en op de juiste locatie genoeg (maar niet teveel) ACh vrijkomen. Deze specifieke regulatie wordt verzorgd door een groot aantal eiwitten, de zgn. synaptische eiwitten. De SNARE eiwitfamilie is van cruciaal belang: Syntaxine en Synaptotagmine aan het plasmamembraan en Synaptobrevine aan het blaasje. Deze drie eiwitten binden en vormen zo het SNARE complex. Bij de vorming van dit complex komt de energie vrij die nodig is om het membraan van het blaasje te laten fuseren met het celmembraan. Naast de SNARE eiwitten bestaan er vele andere eiwitten die verschillende functies hebben in synaptische exocytose. Van veel van deze eiwitten is de rol in neurotransmitter afgifte

in synapsen in het brein onderzocht maar nog niet in de NMJ. In dit proefschrift is de rol van vijf eiwitten (Munc13, Munc18, α-Neurexine, Rim1α en Rab3A) in de NMJ onderzocht. Dit is gedaan door het analyseren van NMJs van knock-out (KO) muizen. Een KO muis is een muis die genetisch gemodificeerd is zodat het het gen dat codeert voor een eiwit afwezig is. Om te onderzoeken of een eiwit betrokken is bij het compensatie-effect in MG is bij drie typen KO muizen ook het TIMG model toegepast.

Munc13 is een groot eiwit met verschillende domeinen en lijkt betrokken te zijn bij het primingsproces, waarbij het blaasje klaargemaakt wordt om na het calciumsignaal direct te fuseren met het celmembraan. In **hoofdstuk 2** worden NMJs van muizen geanalyseerd die zowel Munc13-1 en Munc13-2 missen, zgn. dubbel KO muizen. Aangezien deze muizen niet levensvatbaar zijn worden embryonale spieren geanalyseerd. Het blijkt dat gestimuleerde afgifte sterk verminderd is in de dubbel KO NMJs, terwijl de spontane afgifte is verdubbeld. Dit suggereert dat priming in de NMJ niet uitsluitend geregeld wordt door Munc13. Een morfologische analyse laat zien dat de eindplaten niet zoals in controle muizen gerangschikt zijn in één band maar chaotisch verdeeld zijn.

Neurexine1α is transmembraaneiwit, waarvan een deel buiten en een deel binnen de cel uitsteekt. Het is ontdekt als de bindingsplaats van het gif van de zwarte weduwe spin: α-latrotoxine. Dit gif heeft tot gevolg dat er een massieve exocytose plaatsvindt. Eerdere experimenten hebben uitgewezen dat Neurexine interacteert met een calciumkanaal en op deze manier waarschijnlijk een regulerend effect heeft op exocytose. In zoogdieren bestaan drie verschillende vormen van het eiwit. Muizen die alle drie de vormen missen sterven bij de geboorte, van muizen die nog één vorm hebben bereikt een aantal de volwassen leeftijd. In **hoofdstuk 3** beschrijven wij de analyse van muizen die twee vormen van Neurexine missen. Ondanks het feit dat deze dieren duidelijk minder sterk waren dan controle muizen, bleken de NMJs van het diafragma normaal. In een kuitspier, die samengesteld is uit een ander type spiervezels) zagen wij een geringe afname van exocytose. Om de NMJ in totale afwezigheid van Neurexine te onderzoeken, hebben wij embryonale spieren onderzocht van muizen die triple-knock out waren. De kuitspier was te klein om te onderzoeken en in het diafragma bleek de afgifte onveranderd.

We hebben onderzocht of Neurexine een rol speelt in de synaptische homeostase door het TIMG model toe te passen op muizen die twee vormen van Neurexine missen. Het bleek dat deze muizen minder in staat waren tot het compenseren van het verlies van gevoeligheid voor ACh. Neurexine is dus in sommige NMJs van belang voor efficiente neurotransmissie en blijkt een rol te spelen in het mechanisme van synaptische homeostase.

Rab3A is een klein GTP-bindend eiwit dat in de GTP-gebonden vorm bindt aan synaptische blaasjes en na (of tijdens) fusie weer vrijkomt van het blaasje wanneer

GTP tot GDP gehydrolyseerd wordt. De transitie tussen de GTP- en GDP-gebonden vorm kan als een moleculaire schakelaar functioneren waardoor interactie met bindingpartners gereguleerd kan worden. Het eiwit is betrokken bij plasticiteit waardoor een modulatoire rol verondersteld wordt. **Hoofdstuk 4** beschrijft de analyse van NMJs in het diafragma en een kuitspier van de Rab3A KO muis. Het blijkt dat de afwezigheid van Rab3A alleen een effect heeft op de MEPP frequentie, deze is zo'n 20-40% verlaagd. Kennelijk speelt het eiwit een rol bij de spontane afgifte van neurotransmitter, welke niet overgenomen wordt door één van de drie andere Rab3 vormen (Rab3B, -C, en-D).

Munc18-1 is een bindingspartner van het SNARE eiwit Syntaxine en essentieel voor neurotransmitter afgifte. Muizen zonder Munc18-1 gaan dood bij de geboorte en hebben geen exocytose. In **hoofdstuk 5** is gekeken naar het effect van het variëren van de hoeveelheid Munc18-1 in celculturen en in de NMJ. Hierbij is gebruik gemaakt van muizen die heterozygoot KO zijn, deze hebben nog 50% Munc18-1 en zijn levensvatbaar. Tevens is gekeken naar muizen die Munc18-1 tot overexpressie brengen, deze groepen zijn met elkaar vergeleken. Het blijkt dat de MEPP frequentie na een hypertone schok verlaagd is in NMJs van heterozygote muizen, en de NMJs zijn minder goed in staat om tijdens hoogfrequente stimulatie de EPP amplitude op niveau te houden. Deze bevindingen werden ook gezien in celculturen van hippocampusneuronen van deze muizen. Samen met de resultaten van morfologische analyse lijkt het aannemelijk dat Munc18-1 betrokken is in het moduleren van het aantal gedockte en geprimede blaasjes in zenuwuiteinden.

In **hoofdstuk 6** wordt beschreven wat TIMG voor effect heeft op muizen die heterozygoot voor Munc18-1 zijn en muizen die het eiwit tot overexpressie brengen. Het blijkt dat heterozygote muizen minder in staat zijn om te compenseren voor het verlies van ACh gevoeligheid. Muizen die Munc18-1 tot overexpressie brengen bleken niet beter te zijn in het compenseren voor het verlies van ACh gevoeligheid. Munc18-1 is kennelijk betrokken bij de signaalroute die leidt tot de upregulatie van afgifte in TIMG maar andere factoren zijn beperkend zodat extra Munc18-1 ineffectief is.

Rab interacting molecule-1 α (RIM1α) is een groot eiwit dat een belangrijke rol speelt in neurotransmissie, waarschijnlijk bij het klaarmaken van blaasjes voor de fusie. Het eiwit bindt o.a. aan Rab3A en aan Munc13. Naast RIM1α bestaat RIM2α, muizen die beide eiwitten missen zijn niet levensvatbaar. **Hoofdstuk 7** beschrijft de elektrofysiologische analyse van de neurotransmitter afgifte in NMJs van RIM1α KO muizen, zowel onder controle omstandigheden als met TIMG. Het blijkt dat de afwezigheid van RIM1α geen effect heeft op de neurotransmitterafgifte. Waarschijnlijk neemt RIM2α de rol van RIM1α over.

Het werk dat beschreven staat in dit proefschrift heeft bijgedragen aan de kennis die bestaat over de rol die bepaalde synaptische eiwitten (Munc13, Neurexine,

Munc18-1, Rab3A en RIM1α) spelen bij neurotranmsitter afgifte in de NMJ van muizen. Verder is aangetoond dat Munc18-1 en Neurexine naar alle waarschijnlijkheid betrokken zijn de upregulatie van neurotransmitterafgifte in de myasthene NMJ.

List of publications

Toonen R.F.*, Wierda K.*, Sons M.S.*, de Wit H., Cornelisse L.N., Brussaard A., Plomp J.J., Verhage M.
Munc18-1 expression levels control synapse recovery by regulating readily releasable pool size.
Proceedings National Academy of Sciences USA 2006 28; 103(48):18332-7.
* These authors contributed equally to this work

Sons M.S., Plomp J.J.
Rab3A deletion selectively reduces spontaneous neurotransmitter release at the mouse neuromuscular synapse.
Brain Research 2006; 1089:126-134.

Sons M.S.*, Busche N.*, Strenzke N., Moser T., Ernsberger U., Mooren F.C., Zhang W., Ahmad M., Steffens H., Schomburg E.D., Plomp J.J., Missler M.
Alpha-Neurexins are required for efficient transmitter release and synaptic homeostasis at the mouse neuromuscular junction.
Neuroscience 2006; 138:433-446.
* These authors contributed equally to this work

Varoqueaux F.*, Sons M.S.*, Plomp J.J., Brose N.
Aberrant morphology and residual transmitter release at the Munc13-deficient mouse neuromuscular synapse.
Molecular Cell Biology 2005; 25: 5973-5984.
* These authors contributed equally to this work

Sons M.S., Verhage M., Plomp J.J.
Role of Munc18-1 in synaptic plasticity at the myasthenic neuromuscular junction.
Annals New York Academy of Sciences 2003; 998: 404-406.

Mansvelder H.D., Lodder J.C., Sons M.S., Kits K.S.
Dopamine modulates exocytosis independent of Ca^{2+} entry in melanotropic cells.
Journal of Neurophysiology 2002; 87: 793-801.

Acknowledgments

"Ongelofelijk!" is wat ik deze dagen vaak als antwoord krijg op mijn mededeling dat mijn proefschrift daadwerkelijk af is en zelfs binnen korte tijd verdedigd zal gaan worden. Hoewel ik zo mijn ideeën heb over de redenen waarom dit toch wordt gezien als ongelooflijk en mij er zeker ten dele ook in kan vinden, heb ik mij er nog niet aan gewaagd na te vragen wat men nu precies het ongelofelijke eraan vindt..

Ik wil allereerst mijn co-promotor en begeleider Jaap Plomp bedanken, naast het leren van de techniek heb ik veel kennis opgedaan over het opzetten van wetenschappelijke experimenten, de dataverwerking en het uiteindelijke rapporteren. Sommige promovendi kunnen vertraging wijten aan hun begeleider, ik daarentegen had al mijn schrijfwerk dat ik je stuurde zeer snel weer terug, hartelijk dank daarvoor. Ik wil Jan Verschuuren, mijn promotor, bedanken dat hij bereid wil zijn om als mijn promotor op te treden.

Mathijs Verhage wil ik bedanken, hij heeft mij als stagestudent in zijn groep attent gemaakt op het bestaan van dit project, tijdens de werkbesprekingen met zijn groep heb ik veel opgestoken van de wereld van de synaptische eiwitten.

I would like to thank Markus Missler for giving me the opportunity to work in Göttingen, and Weiqi Zhang for using his lab space. My fellow PhD students Vardanush, Lila and Gayane made me feel at home and have become good friends.

Mijn toenmalige collega's Roland Bullens, Jeroen Beekwilder en Trudy van Kempen wil ik bedanken voor de gezellige, bemoedigende en inspirerende momenten.

Tussen de afloop van mijn AIO-contract en mijn daadwerkelijke promotie ligt een aanzienlijke periode waarin een aantal van mijn vrienden de twijfelachtige eer heeft gehad om de (onbetaalde) functie van Proefschriftmanager te bekleden: Alwin, Brenda, Mathijs: bedankt voor jullie bemoedigende, soms licht bedreigende maar nimmer aflatende steun. Simon wil ik ook graag hartelijk danken voor zijn steun en hulp bij het doorgronden van InDesign. Esther, Jelena, Vanja, Maaike, Shandra, Esther, Naomi, Wanda: hartelijk dank voor alle bemoedigende woorden, ook als ik het even niet meer zag zitten, leden van de "VU-groep", hartelijk dank! Mijn dank gaat ook uit naar mijn huidige werkgever Gerard van der Laan, het is een moedige stap een bioloog aan te nemen voor een commerciële functie, dank voor de ruimte die ik heb gekregen om aan de afronding van promotie te werken.

Papa en Mama, hier ligt het resultaat van al die jaren, bedankt voor het vertrouwen dat het af zou komen.

Lieve Stephan, ongelofelijk, het is af! Bedankt voor je ondersteuning en liefde.

Curriculum Vitae

Michèle Sons werd geboren op 10 maart 1976 te Amsterdam. In 1994 behaalde zij haar Atheneum diploma aan het Hermann Wesselink College te Amstelveen, waarna zij begon met haar studie Biologie aan de Vrije Universiteit in Amsterdam. Als onderdeel van haar studie heeft zij een onderzoeksstage gevolgd bij de afdeling Membraanfysiologie van de Vrije Universiteit, daarna heeft zij een onderzoeksstage gevolgd bij het Rudolf Magnus Instituut, afdeling molecular neuroscience in de groep van Mathijs Verhage. In 1999 behaalde zij haar doctoraal diploma Biologie en startte zij haar promotieonderzoek binnen een project dat een samenwerkingsverband was tussen Mathijs Verhage en Jaap Plomp (afdeling Neurologie en Klinische Neurobiologie van het LUMC). Het onderzoek vond plaats in Leiden onder leiding van Jaap Plomp. In 2004 heeft zij een lange reis door Nieuw Zeeland gemaakt en in 2005 is zij in dienst getreden bij MS Vision waar zij momenteel werkzaam is als produktspecialist.